UNIVERSIDAD NACIONAL AUTÓNOMA DE MÉXICO

INSTITUTO DE INVESTIGACIONES BIOMÉDICAS

DOCTORADO EN CIENCIAS BIOMÉDICAS

RELACIÓN ESTRUCTURA FUNCIÓN EN EL COTRANSPORTADOR Na$^+$:Cl$^-$ SENSIBLE A TIAZIDAS

T E S I S

QUE PARA OBTENER EL GRADO DE
DOCTORA EN CIENCIAS PRESENTA:

REYNA ERIKA MORENO MARTÍNEZ

DIRECTOR DE TESIS: DR. GERARDO GAMBA AYALA.

MÉXICO, D.F.   2007

"RELACION ESTRUCTURA FUNCIÓN EN EL COTRANSPORTADOR DE Na$^+$:Cl$^-$ SENSIBLE A TIAZIDAS"

El presente trabajo se realizó bajo la dirección del Dr. Gerardo Gamba Ayala, en la Unidad de Fisiología Molecular del Instituto de Investigaciones Biomédicas de la UNAM, localizada en el Departamento de Nefrología y Metabolismo Mineral del Instituto Nacional de Ciencias Médicas y Nutrición Salvador Zubirán.

RECONOCIMIENTOS

Al jurado de Examen de Doctorado, por sus comentarios y sugerencias, el cuál estuvo formado por:

Presidente: Dra. Herminia Pasantes Ordóñez.
Secretario: Dr. Gerardo Gamba Ayala.
Vocal: Dr. Ataulfo Martínez Torres.
Vocal: Dra. Norma Araceli Bobadilla Sandoval.
Vocal: Dra. Lorenza González Mariscal.
Suplente: Dr. Luis Alfonso Vaca Domínguez.
Suplente: Dr. Armando Roberto Tovar Palacio.

A G R A D E C I M I E N T O S

A mi mamá
Por impulsar mis deseos de superación, por alentarme y quererme
...daría todo por que estuvieras conmigo, te amo.

A mis Luises
Por amarme, por creer en mí y apoyarme, por alegrar mis días
y hacer de mi la persona más afortunada del mundo.
A ustedes dedicó este trabajo, el cuál representa un esfuerzo de equipo.
Los amo…

A mi Papá, Tío, Yola, Chuchín, Martha y Lic. Gutiérrez
Por estar conmigo siempre, por su cariño
y apoyo incondicional, pero sobre todo por hacer feliz mi vida.

A las familias Cano Moreno y Mejía Moreno
Por compartir conmigo grandes momentos.

A mi tutor
Dr. Gerardo Gamba
A quién agradezco el permitirme ser parte de su laboratorio, por sus enseñanzas y amistad, pero sobre todo por su invaluable apoyo.

A la Dra. Norma Bobadilla
Por sus enseñanzas, consejos y amistad.

A Norma Vázquez
Por enseñarme el trabajo en el laboratorio y por su amistad.

A mis compañeros y amigos del laboratorio
Sería muy difícil mencionar a cada uno de ustedes, pero a todos les agradezco el compartir conmigo este tiempo, su amistad y todas las sugerencias realizadas a esta tesis.

A Jose, Blanquita, Vero, Zenaida, Chela y Estelita.
Gracias por facilitarme todo, por su ayuda y su paciencia.

A la Universidad Autónoma del Estado del Estado de Hidalgo
Al Instituto de Ciencias de la Salud
Al Área Académica de Medicina
Al Dr. Humberto Verás Godoy
Por permitirme ser parte de la Universidad y darme todas las facilidades para
concluir mis estudios.

A la Universidad Nacional Autónoma de México
Al Programa del Doctorado en Ciencias Biomédicas

ÍNDICE

RESUMEN

El cotransportador de Na$^+$:Cl$^-$ sensible a tiazidas (CST), es una proteína de membrana que constituye la principal vía de reabsorción de sal en el túbulo distal de la nefrona. El CST es el sitio de acción de los diuréticos tipo tiazida, fármacos ampliamente utilizados en la práctica clínica por su utilidad en el tratamiento de la hipertensión arterial. Mutaciones inactivantes sobre el gen del CST ocasionan el síndrome de Gitelman, una enfermedad autosómica recesiva caracterizada clínicamente por hipotensión arterial, hipocalemia, alcalosis metabólica e hipocalciuria.

Trabajos previos en donde se analizaron las características funcionales del CST de rata (CSTr) y del CST del pez lenguado de invierno (CSTfl), reportaron diferencias importantes desde el punto de vista cinético, farmacológico y de regulación. Análisis cinéticos mostraron que el CSTr y el CSTfl presentan diferente afinidad por los iones que transportan, así como distinto perfil de inhibición por tiazidas y respuesta ante la osmolaridad extracelular. El CSTr y el CSTfl guardan un porcentaje de homología de ~ 60%.

En este trabajo estudiamos proteínas quiméricas entre el CSTr y el CSTfl, con la finalidad de encontrar dominios estructurales involucrados en el transporte de Na$^+$ y Cl$^-$, así como dominios involucrados en la afinidad por tiazidas. Simultáneamente analizamos el papel de la N-glucosilación sobre las propiedades funcionales del CSTfl, ya que previamente fue reportado, que la ausencia de este evento, determina la expresión del CSTr sobre la superficie celular, así como la afinidad del transportador por las tiazidas. Sumado a estos resultados, reportamos aminoácidos específicos involucrados en la regulación de la expresión y/o función del CST.

Mediante mutagénesis puntual fueron eliminados los tres sitios potenciales para N-glucosilación del CSTfl. Se generaron mutantes simples, donde fue eliminado solo un sitio, mutantes dobles y una mutante triple que carecía de los tres sitios; diversos análisis cinéticos mostraron que la N-glucosilación no es un evento involucrado en la afinidad por los iones ni tiazidas en el CSTfl.

En un segundo paso, construimos proteínas quiméricas entre el CSTr y el CSTfl. La nomenclatura para las quimeras generadas, constó de cinco letras, en donde cada letra corresponde a uno de los 5 fragmentos en los que se dividió la proteína. Estos son: NH$_2$ (1), TM1-7 (2), asa conectora TM7-8 (3), TM8-12 (4) y región COOH$^-$ (5); siendo utilizadas las letras R o F para determinar si el fragmento pertenecía al CSTr o al CSTfl. Fueron construidas 18 proteínas quiméricas. Se realizaron análisis cinéticos para el transporte de Na$^+$, Cl$^-$ y de afinidad por tiazidas, en cada una de las construcciones quiméricas.
Los primeros resultados mostraron que las regiones TM del CST son las que determinan el transporte de iones y afinidad por las tiazidas. Las quimeras que conservaron las regiones TM tanto del CSTr como del CSTfl tuvieron un comportamiento cinético similar al del transportador nativo. Por ejemplo, en la quimera FRRRR se observó una Km para el transporte de Na$^+$ de 8.1 ± 1.1 mM; mientras que la quimera RRFRR presentó un Km para el transporte del mismo ión de 5.0 ± 0.6 mM. (CSTr Km Na$^+$ de 5.5 ± 1.0 mM). Un comportamiento similar mostraron las quimeras formadas por las regiones TM de CSTfl, en donde las quimeras RFFFR y FFRFF presentaron una Km para Na$^+$ de 28 ± 6.0 y de 87 ± 45 mM respectivamente, la cual es similar al del CSTfl nativo (30 ± 6.0 mM). La afinidad por el diurético fue similar entre los transportadores nativos y las quimeras en las cuales los dominios TM no fueron modificados.
Para evaluar el papel de las regiones TM sobre las propiedades funcionales del CST, se estudiaron las quimeras, en las que únicamente se intercambiaron los segmentos TM 1-7 y TM 8-12 (RFRRR, FRFFF, RRRFR y FFFRF), de las cuales FRFFF no mostró actividad. Los análisis funcionales de las quimeras RFRRR, RRRFR y FFFRF realizados en ovocitos de *X.*

laevis, permitieron determinar dominios involucrados en la afinidad para iones y tiazidas en el CST.

El IC_{50} para metolazona observado en las quimeras RFRRR y FFFRF (0.4 ± 0.002 y 0.6 ± 0.006 µM respectivamente) fue similar al de CSTr nativo (0.3 ± 0.005 µM) y diferente al que fue observado en CSTfl (12.5 ± 1.8 µM). Mientras que el IC_{50} observado en la quimera RRRFR fue semejante al del CSTfl nativo. Estos resultados sugieren que la afinidad para el diurético esta determinada por las regiones TM8-12 del CST.

Los análisis cinéticos realizados para determinar la afinidad por Na^+ en las quimeras RFRRR, RRRFR y FFFRF (Km de 22 ± 2.8, 14.5 ± 0.7 y 43 ± 12.6 mM respectivamente), mostraron valores intermedios a los que presentaron los transportadores nativos: CSTfl Km de 30 ± 6.0 mM y CSTr 5.5 ± 1.0 mM.

Las cinéticas de transporte para Cl^-, revelaron que las quimeras RFRRR y FFFRF (Km de 17 ± 4.6 y 12.8 ± 3.0 mM) presentan un comportamiento similar al del CSTfl nativo (Km de 15 ± 2.0 mM); mientras que la quimera RRRFR mostró un Km similar al de CSTr nativo (2.4 ± 0.7 vs 2.6 ± 0.6 mM respectivamente). Estos resultados sugieren que la afinidad que muestra el CST por el Cl^- está determinada por las regiones TM1-7, mientras que la afinidad al Na^+ esta determinada tanto por las regiones TM1-7como por las TM8-12.

En este trabajo también reportamos el estudio de polimorfismos de nucleótidos individuales (SNPs) en el CST. El SNP G264A esta localizado en la cuarta región TM del transportador; a diferencia de otros SNPs reportados, la sustitución del residuo glicina por un residuo alanina, se lleva a cabo en un aminoácido altamente conservado en todos los miembros de la familia SLC12.

Los análisis cinéticos para la afinidad por el transporte de Cl^-, mostraron que el SNP G264A incrementa drásticamente la Km para este ión cuando se compara con el CST nativo $^-$(Km 0.89 ± 0.2 vs 6.3 ± 1.1 mM). Este polimorfismo no afectó la afinidad para Na^+ ni la afinidad por tiazidas. Sumado a esto, en la región TM4 del CST, se encontraron tres residuos altamente conservados en todos los miembros de esta familia de transportadores adicionales al G264; estos residuos corresponden a la asparagina 258, arginina 261 y glicina 278. Las sustituciones de estos aminoácidos por residuos con características estructurales similares mostraron, que cuando se sustituye la asparagina 258 por un residuo de glutamina, el CST aumenta significativamente la afinidad por el Cl^- (3.2 ± 0.7 mM) en comparación con el CST nativo (6.3 ± 1.1 mM). Con el estudio del polimorfismo G264A y del residuo asparagina 258 nuevamente mostramos que la afinidad para el Cl^- en el CST está determinada por los dominios TM 1-7, en donde la región TM-4 juega un papel importante.

Así mismo realizamos un estudio de mutaciones tipo Gitelman (G627V, R935Q, V995M, G610S y A585V; ninguna interfiere en la glucosilación de la proteína), que nos permitió detectar aminoácidos puntuales involucrados en el tráfico del CST a la membrana celular. Análisis funcional en ovocitos de *X.laevis*, mostró que las 5 mutaciones son capaces de disminuir significativamente la función del CST. A través de microscopia confocal se pudo establecer que la baja en la función del CST, esta asociada con menor expresión de la proteína sobre la superficie celular. Con este estudio se pudo observar que no solo es necesaria la adecuada glucosilación del CST sino la presencia de aminoácidos específicos que permiten la llegada del transportador a la membrana celular para su adecuada función.

Finalmente reportamos aminoácidos puntuales involucrados en la fosforilación del CST y por lo tanto su regulación.

II. <u>INTRODUCCIÓN</u>

El riñón juega un papel esencial en el mantenimiento del volumen y de la composición del líquido corporal.[1] Estas funciones las realiza por la combinación de los mecanismos de filtración glomerular y de reabsorción tubular. El primer mecanismo depende de la integridad anatómica del glomérulo y de la presión de perfusión renal. La función tubular por su parte, es un proceso mas activo, con alto consumo de energía, el cual depende de los mecanismos de transporte de iones y moléculas a través del epitelio tubular.

Varios mecanismos suceden a lo largo de los túbulos renales, que permiten que diariamente el epitelio tubular reabsorba 180 litros de agua y 1.3 Kg de cloruro de sodio así como otras moléculas y excrete diariamente de 1-2 litros de agua con pequeñas cantidades de sal (50-130 meq). De esta manera se evita la perdida de nutrimentos importantes para el organismo como glucosa, aminoácidos y proteínas.[2,3]

El mecanismo general por el cual los túbulos reabsorben el NaCl del filtrado glomerular es el siguiente:

- En el epitelio de los túbulos renales, la bomba sodio-potasio se expresa en forma polarizada en la membrana basolateral de las células,

- esto genera la formación de un gradiente electroquímico, que permite el transporte vectorial de sodio, de la luz tubular hacia el intersticio renal;

- en la membrana apical el sodio puede transportarse por difusión facilitada a través de canales conductivos, lo cual sucede en la parte final de la nefrona (túbulo colector), o se ve favorecido por el gradiente generado para el sodio con el fin de transportar otros iones o moléculas en contra de su gradiente.

A las proteínas que realizan esta última función se les conoce como *cotransportadores secundarios*. Existen varios tipos de transportadores secundarios y su distribución en la membrana apical del epitelio de la nefrona, es la que determina, al menos en parte, las funciones particulares de cada

segmento tubular. Además de este mecanismo general, existen proteínas transportadoras para iones específicos, entre ellos Ca^{2+}, Mg^{2+}, HCO^{3-} y K^+.[4]

A. <u>MECANISMOS DE REABSORCION DE SAL EN EL TÚBULO RENAL</u>

TÚBULO RENAL

El túbulo renal está formado por un epitelio simple, en donde las sustancias que se reabsorben deben atravesar a las células por vía transcelular o por vía paracelular.

En la *reabsorción transcelular*, las sustancias atraviesan dos membranas diferentes, primero la apical o luminal, que es la membrana que ve hacia la luz del túbulo y después la membrana basolateral, que ve hacia el intersticio renal.

En la *reabsorción paracelular,* los iones o moléculas deben atravesar sólo el sitio de unión paracelular, para encontrarse en el intersticio renal.

El túbulo renal tiene la capacidad de reabsorber agua y diferentes solutos de forma heterogénea, debido a que está formado por diferentes tipos de células. La organización y localización de éstas, divide al túbulo renal en varias porciones que presentan morfología y funciones diferentes.

Para fines prácticos el túbulo renal se divide en cuatro partes: 1) túbulo proximal; 2) asa de Henle, que a su vez se subdivide en tres secciones a) asa descendente delgada, b) asa ascendente delgada, c) asa ascendente gruesa; 3) túbulo distal y 4) túbulo colector.[5]

Diversas proteínas para el transporte NaCl han sido identificadas en los diferentes segmentos tubulares. A continuación se describen algunos mecanismos de reabsorción de sal en la nefrona.

TÚBULO PROXIMAL

Es el sitio de la nefrona donde se reabsorbe alrededor del 65% del filtrado glomerular. En este segmento se reabsorben los iones o moléculas que no deben perderse en la orina como la glucosa y los aminoácidos.

El epitelio del túbulo proximal tiene una enorme capacidad de reabsorción, debido a varios factores, entre los que destacan: sus células grandes que poseen un número importante de mitocondrias y en consecuencia hay gran producción de ATP, por lo tanto el metabolismo es muy alto, sumado a esto la membrana apical de las células es del tipo de borde en cepillo, lo cual incrementa en forma importante la superficie de absorción.[4]

La intensa reabsorción en este segmento del túbulo renal, se debe también a la abundante expresión de la Na^+-K^+-ATPasa en la membrana basolateral de las células, lo cual genera el gradiente de concentración para el transporte de Na^+, que a la vez es aprovechado en la membrana apical para hacer recircular a este ion.

Diferentes mecanismos para *el transporte de sodio* pueden observarse en el túbulo proximal.[6,7,8] En la primera mitad del túbulo, la mayor parte de Na^+ se reabsorbe junto con glucosa, aminoácidos, fosfato y lactato, por medio de los cotransportadores de Na^+:glucosa, Na^+:aminoácidos, Na^+:Pi y Na^+:lactato.[9] En la segunda mitad del túbulo, prácticamente ha desaparecido la glucosa y los aminoácidos. Por lo tanto, la reabsorción de Na^+ se realiza junto con Cl^-, por mecanismos que incluyen la operación simultánea del intercambiador de Na^+-H^+ y del cotransportador de Cl^-HCO^3.

El intercambiador de Na^+-H^+, esta ubicado en la cara apical de las células, en donde extrae H^+ del interior e introduce iones Na^+. Mientras que el intercambiador Cl^-HCO^3- intercambia iones Cl^- por HCO^3-. El Cl^- es llevado de la luz, hacia el interior de la célula, mientras que el HCO^3- es transportado del interior hacia la luz tubular. El HCO^3- al combinarse con el H^+ forma ácido carbónico que es deshidratado a CO_2 por medio de la enzima anhidrasa carbónica. [10]

La figura 1 muestra los distintos segmentos tubulares de la nefrona.
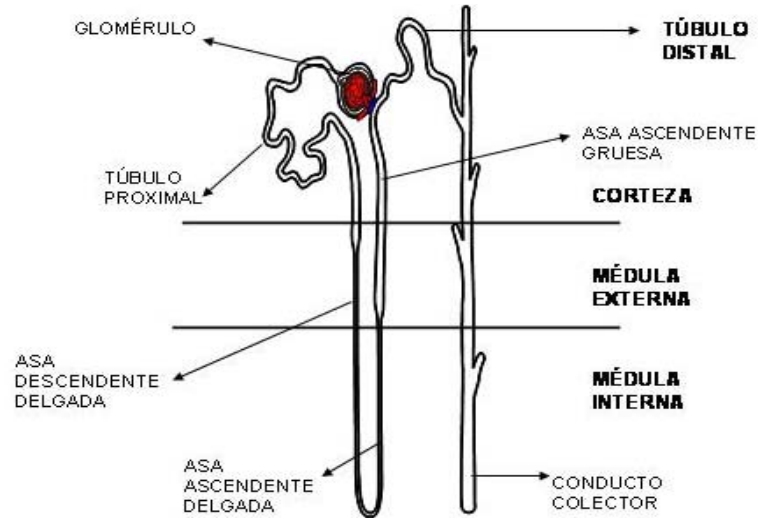
Figura 1. Segmentos tubulares renales.

ASA DE HENLE

En el asa de Henle se reabsorbe aproximadamente el 20% del filtrado glomerular.

Se divide en tres partes para su estudio: 1) asa descendente delgada, 2) asa ascendente delgada, 3) asa ascendente gruesa.

El asa de Henle tiene la capacidad de reabsorber grandes cantidades de sal y solamente el asa delgada, muestra gran permeabilidad al agua. La función del asa es crítica para diluir o concentrar la orina, ya que la reabsorción de sal en la porción ascendente gruesa es la responsable de mantener la hipertonicidad de la médula renal, gracias a la cual, en presencia de la hormona antidiurética se puede reabsorber agua en el conducto colector.[1]

Como ya se mencionó *el transporte de NaCl* se lleva a cabo en el asa ascendente gruesa, a través del cotransportador Na^+:K^+:$2Cl^-$ sensible a bumetanida (CSB1 o NKCC2). [39]

El CSB1 introduce iones Na^+ a la célula, que posteriormente son sacados a través de la Na^+-K^+-ATPasa, mientras que Cl^- introducido a la célula por CSB1 es llevado al insterticio renal por canales localizados en la membrana basolateral denominados ClC-Kb.[13] El K^+ que ingresa a la célula junto con el Na^+ y Cl^-, es reciclado hacia la membrana luminar a través de los canales de potasio

conocidos como ROMK, produciendo un voltaje luminar positivo que favorece la reabsorción de Na^{+} por vía paracelular.[11,12,14]

Se han identificado dos genes distintos para el cotransportador Na^{+}:K^{+}:2Cl[-], el CSB1/NKCC2 que codifica para una proteína específica del riñón, y CSB2/NKCC1, el cual se expresa en la membrana basolateral en diferentes tipos celulares incluyendo el riñón mamífero.[37,19]

TÚBULO DISTAL

El túbulo distal es la región comprendida entre la mácula densa y el conducto colector; en este segmento se reabsorbe del 5 al 7% del filtrado glomerular.[15]

Este segmento tubular está formado por un epitelio cuboidal alto homogéneo, con membrana plasmática basolateral extensa, intercalada con mitocondrias arregladas verticalmente, un núcleo en posición apical y microproyecciones de la membrana plasmática apical abundantes. [17]

En el túbulo distal *el transporte de NaCl* se lleva a cabo por dos mecanismos: por transporte electroneutro de NaCl y por transporte electrogénico de Na^{+}; este último se observa predominante en la porción final del túbulo y se debe a la presencia de canales de sodio sensibles a amilorida.[16]

El transporte electroneutro esta dado por el *cotransportador de Na^{+}:Cl^{-} (CST)* que es el sitio de acción de los diuréticos tipo tiazida (metolazona, politiazida, bendroflumetiazida, triclorometiazida y clortalidona) y constituye la principal vía de reabsorción de sal en este segmento de la nefrona.[15]

TÚBULO COLECTOR

En este segmento se reabsorbe alrededor del 3% del filtrado glomerular. En el túbulo colector se reabsorben iones, moléculas o agua antes de drenar a la orina final.

Anatómicamente el túbulo colector es muy parecido al túbulo distal; ambos están formados por dos clases distintas de células, las células principales y las células intercaladas. Las células principales reabsorben sodio y agua de la luz tubular y

secretan iones potasio. Las células intercaladas reabsorben iones potasio y secretan iones hidrógeno hacia la luz tubular.

En este segmento *el transporte de Na$^+$* se realiza a través de canales de sodio sensibles a amilorida, mientras que el agua se reabsorbe por canales de agua (acuaporina-2). [3]

B. <u>FISIOLOGÍA MOLECULAR DE LAS CÉLULAS DEL TÚBULO DISTAL</u>
EL COTRANSPORTADOR DE SODIO-CLORO SENSIBLE A TIAZIDAS (CST).

Como se menciono, *el CST constituye la principal vía de reabsorción de NaCl en el túbulo distal de la nefrona*. Se localiza en la membrana apical de las células en donde transporta sodio y cloro al interior con una estequiometría 1:1.

En la figura 2, se puede observar la fisiología molecular de las células del túbulo distal. El CST introduce Na$^+$ a la célula, el cual es intercambiado por K$^+$ en la cara basolateral, a través de la Na$^+$:K$^+$-ATPasa. El Cl$^-$ que ingresa a la célula acoplado al Na$^+$, sale por canales de Cl$^-$ situados en la membrana basolateral hacia el intersticio renal. El K$^+$ que fue intercambiado por Na$^+$ vía la Na$^+$:K$^+$ATPasa, es secretado hacia la luz tubular por canales conductivos específicos.[15]

La función de este transportador puede ser inhibida con diuréticos tipo tiazida; se ha observado que cuando esto sucede, la reabsorción de Ca^{2+} aumenta significativamente.[26] Hasta el momento no se ha determinado con precisión el mecanismo por el cual la reabsorción de Ca^{2+} se ve favorecida. Friedman y col.[27], han sugerido que las tiazidas bloquean la entrada de Na$^+$ y Cl$^-$ en la membrana apical; ante esto, el Na$^+$ continúa saliendo en forma activa vía la Na$^+$:K$^+$-ATPasa en la membrana basolateral, lo que resulta en hiperpolarización de la célula tubular distal, que tiene como consecuencia la apertura de canales catiónicos en la membrana apical, de los cuales los más abundantes son los de Ca^{2+}. De esta forma, los diuréticos tiazida, producen aumento en la reabsorción de Ca^{2+}, con disminución en su excreción urinaria, siendo este el fundamento clínico por el cual las tiazidas son utilizadas en el tratamiento de la osteoporosis.

Los pacientes tratados con tiazidas, muestran un efecto benéfico en su masa ósea. [28] La tiazidas han sido fármacos utilizados desde 1957, en el tratamiento del edema, la insuficiencia renal y hepática entre otras enfermedades. Pero sin duda, el mayor beneficio que ha traído el uso de estos compuestos, ha sido en el tratamiento de la hipertensión arterial.

En el 2003 la Asociación Médica Americana, publicó un algoritmo que se debe seguir para el tratamiento del paciente hipertenso. Esta asociación señala que ante un paciente con hipertensión arterial se debe modificar su estilo de vida, en donde una dieta adecuada y el ejercicio continuo son parte del tratamiento. Pero cuando la presión arterial no mejora, es decir el paciente mantiene cifras de presión arterial mayores a 140/90 mm Hg o tiene enfermedad renal crónica o diabetes, entonces se debe comenzar el tratamiento farmacológico. Ante una hipertensión arterial sin complicaciones, el fármaco de primera elección es un diurético tipo tiazida. Si la presión arterial no mejora, el tratamiento de elección es la combinación de fármacos, donde usualmente se mantiene el diurético tiazida y se combina con otros diuréticos, inhibidores de la enzima convertidora de angiotensina o beta-bloqueadores. Como se puede apreciar la utilidad de este fármaco es una potente herramienta para el tratamiento de distintas enfermedades.[34]
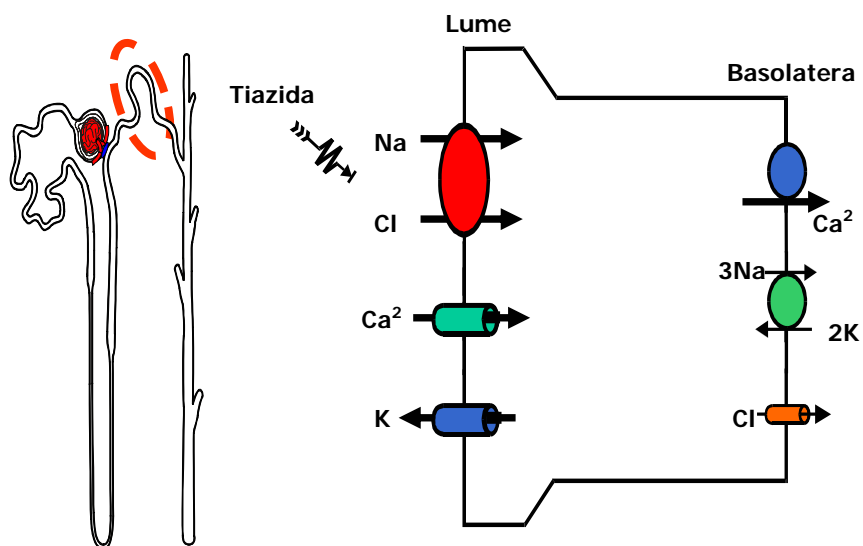
Figura 2. Fisiología del transporte de Na^+ en el túbulo distal.

REGULACIÓN DE LA REABSORCIÓN DE NaCl EN EL TÚBULO DISTAL.

Los cambios en la carga de sal y la velocidad del flujo parecen ser factores suficientes para regular el transporte de sal en el túbulo distal. Sin embargo, existen múltiples mecanismos involucrados en el control de la reabsorción de sal y/o en la abundancia del CST. Como se mencionó anteriormente, en el túbulo distal se reabsorbe el 5% del filtrado glomerular y los primeros estudios sugirieron que tanto la carga tubular de sal, así como la tasa del flujo que llegan a éste, controlan directamente la reabsorción de sodio en este punto de la nefrona. [112] También se ha observado que la furosemida (inhibidor del transporte de NaCl en el asa de Henle) [98] y el aumento de Na^+ en la dieta [15] incrementan la carga de NaCl e inducen hipertrofia e hiperplasia del túbulo distal, con proliferación de la membrana basolateral, aumento en el volumen de las mitocondrias, [96] así como en la actividad de la Na^+:K^+-ATPasa basolateral [95] y en el número de receptores para tiazida en la membrana apical, [94] lo que incrementa la capacidad de reabsorción de Na^+. [99]

EFECTO HORMONAL SOBRE LA REGULACIÓN LA REABSORCIÓN DE NaCl EN EL TUBULO DISTAL.

Diversos estudios han demostrado la participación de distintas hormonas en la regulación de la reabsorción de NaCl en el túbulo distal; brevemente describiremos algunos de ellos.

Es conocido que la hormona aldosterona regula la excreción de Na^+ del organismo al incrementar la reabsorción de este ión. En un principio se describió que el sitio de acción para aldosterona eran los canales de sodio sensibles a amilorida en el conducto colector. Sin embargo ahora conocemos la participación de la aldosterona sobre la regulación de la reabsorción de Na^+ en el túbulo distal. Trabajos de Chen y col. [93] demostraron que la adrenalectomía en ratas disminuye la densidad del CST y observaron un incremento en la unión a [^{3}H]metolazona en homogenados de riñón después de aplicar aldosterona exógena. En 1996 Velázquez y col.[89] observaron que la baja actividad en el transporte electroneutro de sodio, medida *in vivo* en el túbulo distal de ratas adrenalectomizadas, puede ser recuperada a niveles normales e incluso

incrementada con la administración de aldosterona y/o altas dosis de glucorticoides. En 1998 Kim y col.[25] demostraron con estudios de inmunoblot e inmunohistoquímica, que el aumento en las concentraciones séricas de mineralocorticoides y la dieta baja en sal, aumentan la expresión del CST. Por lo tanto este transportador es un blanco importante para la aldosterona.

Estos resultados son consistentes con la presencia de receptores para mineralocorticoides y la enzima 11β-hidroxiesteroidea en el túbulo contorneado distal de rata, conejo y humano, [88] necesarios para que las hormonas esteroideas pueden llevar a cabo su función.

No solo se ha demostrado la presencia de receptores para mineralocorticoides en el túbulo distal, sino también se ha demostrado indirectamente la presencia de receptores para hormonas peptídicas como la calcitonina, la PTH y el isoproterenol. Trabajos de Blakely y col., [85] reportaron un aumento en la unión a [^{3}H]metolazona en homogenados de riñón de ratas tratadas con calcitonina.

Otra hormona involucrada en la reabsorción de Na$^+$ a nivel tubular distal es la hormona Angiotensina II, la cual es un potente vasoconstrictor que juega un papel importante en la reabsorción de sodio y en la regulación de la presión sanguínea. Diversos trabajos han tratado de determinar el mecanismo por el cual la Angiotensina II regula la expresión del CST. Desde 1997 se reportó la presencia de receptores de Angiotensina II (AT1) en la membrana apical de las células del túbulo distal, lo que hizo suponer que esta enzima estaba involucrada directamente en la regulación de Na$^+$ a este nivel.[82] Recientemente Sandberg y col. demostraron que Angiotensina II está involucrada en regular el tráfico del CST a la membrana apical de las células, provocando internalización del CST en vesículas subapicales. [55]

Como se puede apreciar, distintos factores están involucrados en la regulación de la función del CST, en los que podemos incluir eventos de fosforilación/defosforilación del transportador, mutaciones puntuales y polimorfismos de nucleótidos individuales (SNPs), estos factores serán discutidos más adelante.

C. <u>IDENTIFICACION MOLECULAR Y ESTUDIO DEL CST</u>

La identificación molecular del CST [29] fue posible por el descubrimiento de un sistema similar descrito en la vejiga urinaria del pez lenguado de invierno "Winter flounder".[20]

En la década de los años 60´s, se observo que ciertos peces (teleósteos) tienen la capacidad de concentrar o diluir la orina en la vejiga urinaria [30,31] También se observó que este órgano en los peces, es embriológicamente una prolongación del mesonefro renal, por lo tanto las características epiteliales de la vejiga urinaria de estos peces, son similares a las características epiteliales del túbulo distal y del túbulo colector del riñón mamífero.[32]

Renfro [20,21] observó que en la vejiga urinaria del lenguado de invierno, la reabsorción de Na^+ y Cl^- mostraba interdependencia y que para llevarse a cabo, era necesaria la presencia de la $Na^+:K^+$-ATPasa en la membrana basolateral. Stokes y col. [22] demostraron que la reabsorción de Na^+ en la vejiga urinaria de estos peces, era sensible a los diuréticos tipo tiazida. Kunau y col. [23] en 1975, fueron los primeros en sugerir que las tiazidas ejercen su efecto diurético inhibiendo la reabsorción de sal en el túbulo distal. Posteriormente, Ellison [15] describió que la reabsorción de NaCl sensible a tiazidas se llevaba a cabo en la primera porción del túbulo distal.

Beaumont y col. [24] en 1988, realizaron estudios de afinidad de metolazona, un diurético tipo tiazida marcado radioactivamente con tritio ([^{3}H]metolazona), en corteza renal de rata y demostraron que este compuesto se fija en dos sitios, uno de alta afinidad (Kd= 4.27 nM) y otro de baja afinidad (Kd=289 nM). El sitio de alta afinidad correspondería al cotransportador de $Na^+:Cl^-$. La unión de [^{3}H]metolazona puede ser alterada únicamente con otras tiazidas, y no con cualquier otro tipo de droga.

En 1990 Tran y col. [33] observaron que al incrementar la concentración extracelular de sodio (50 mM en forma de Na_2SO_4) se aumentaba la afinidad de la metolazona tritiada unida a membranas de corteza renal de rata aproximadamente 2.6 veces, mientras que al aumentar de las concentraciones extracelulares de cloro (50 Mm de NaCl) la afinidad disminuía ~ 2.6 veces.

La figura 3 muestra el modelo propuesto de unión de iones y diuréticos. Este modelo propone que el CST cuenta con dos sitios de unión, uno que es selectivo para sodio y el otro capaz de reconocer al cloro y a la tiazida, originando competencia entre estos dos últimos por el sitio de unión. Cuando el sodio se une a uno de los dos sitios, la afinidad del segundo sitio aumenta por cloro o metolazona. Normalmente con el transporte de Na^+ del fluido tubular a la célula, se incrementa la afinidad del CST por el Cl^-, transportando ambos iones al interior de la célula. Por otro lado, en este modelo se propone que cuando se administra cualquier tipo de tiazida, este diurético compite con el cloro y al unirse al transportador, impide el transporte de NaCl a la célula.
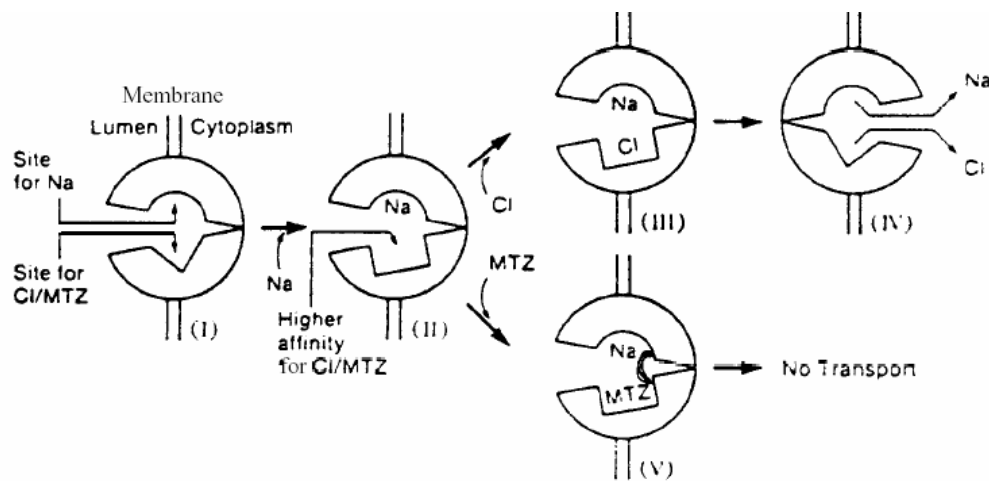
Figura 3. Modelo de unión de iones y tiazidas al CST.

En 1993 Gamba y col. identificaron molecularmente y clonaron al CST a partir de la vejiga urinaria del pez lenguado de invierno (CSTfl), mediante una estrategia de expresión funcional en ovocitos de Xenopus laevis.

Fue obtenido un ARNm de 3.7 kb, cuya secuenciación reveló un marco abierto de lectura de 3,069 pb, en la que se obtuvo una proteína de 1,023 aminoácidos.[29]

El análisis de hidropatía de esta secuencia mediante el método de Kyte and Doolitle [35], reveló un patrón hidrofóbico central, con doce posibles segmentos transmembrana (TM) y una larga asa extracelular entre los segmentos TM 7 y 8 con sitios potenciales para N-glucosilación. Los segmentos TM están

flanqueados por dos asas de localización intracelular que corresponderían a los dominios aminoterminal (NH_2) y carboxiterminal ($COOH^-$) de la proteína, siendo mas largo el extremo $COOH^-$, que esta compuesto aproximadamente de 450 aminoácidos. La figura 4 muestra la topología propuesta para el CST.
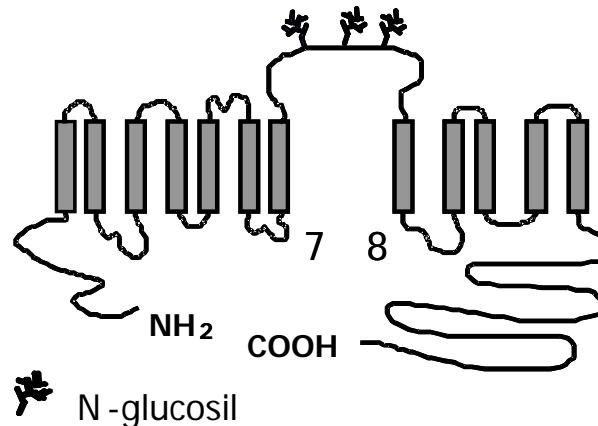
Figura 4. Topología básica del cotransportador de Na^+:Cl^- sensible a tiazidas.

La identificación molecular del CSTfl dio la pauta para la identificación y aislamiento de otros transportadores de NaCl en diferentes especies animales, con metodologías basadas en la homología de secuencias. De esta manera Gamba y col. sintetizaron una sonda del CSTfl marcada con ^{32}P del DNAc para analizar una genoteca de RNAc del riñón de rata, del cual aislaron dos clonas, una de ~4.4 Kb que codifica para el cotransportador Na^+:Cl^- sensible a tiazidas de la corteza renal de rata (CSTr) y otra de ~4.7 Kb que codifica para el cotransportador Na^+:K^+:$2Cl^-$ sensible a bumetanida de la membrana apical de rata (CSBr).[37]

La secuenciación del CSTr reveló una proteína similar a la del pez lenguado de invierno, con un segmento codificante de 3006 pb, que predice una proteína de 1002 aminoácidos. El análisis de hidropatía de esta secuencia mediante el método de Kyte and Doolitle [35], reveló un patrón semejante al del CSTfl.

En 1996 se reportó la identificación molecular del CST de humano (CSTh) por dos grupos de investigadores. Mastroianni y col. [40] reportaron la clonación,

secuenciación y localización cromosómica del CST de humano (CSTh). El análisis de esta secuencia revelo una proteína de 1021 aminoácidos con un peso de de 112 kDa. La topología del CSTh fué similar a la descrita para el CSTr y el CSTfl. Análisis de FISH demostraron que el gen del CST se localiza en la región cromosómica 16q13, mientras que en la rata se localiza en el cromosoma 2. Simon y col. [41] identificaron la secuencia primaria del CSTh con la finalidad de establecer la relación que existe entre este gen y el Síndrome de Gitelman. Análisis de ligamiento y mutaciones puntuales revelaron que el CST está involucrado en una enfermedad conocida como Síndrome de Gitelman, que será descrita más adelante. [41, 43]

En 1998 Velazquez y col. clonaron al CST de la corteza renal de conejo. En ese mismo año, Schultheis y col. reportaron la secuencia del CST de ratón (CSTm); mediante análisis de alineación de secuencia mostraron que existe 92% de identidad entre el CSTh y el CSTm.[39]

Mediante estudios de Northern blot se mostró que transcritos de RNAm del CST se localizaban en tejidos renales.[37] Con hibridación *in situ,* utilizando una sonda del CST marcada radiactivamente con ^{35}S-UTP, se mostró que el RNAm del CST se expresa predominantemente en el túbulo distal. La identificación molecular del CST ha permitido desarrollar estrategias metodológicas que han facilitado su estudio. En 1998 Knepper sintetizó y caracterizó anticuerpos policlonales de conejo que son capaces de reconocer al CST. El péptido sintetizado corresponde a 24 aminoácidos de la región aminoterminal de la proteína. Estudios de inmunoblot e inmunohistoquímica permitieron detectar y localizar al CST. [25]

Actualmente diversas técnicas de biología molecular permiten el estudio del CST, tal es el caso de la fusión de proteínas al CST (proteína verde-fluorescente-EGFP) [78] que permiten detectar la expresión de la proteína en la superficie celular así como su cuantificación y la unión de epítopes al CST (FLAG) que permiten la detección de este transportador.

CST PERTENECE A UNA FAMILIA DE COTRANSPORTADORES CLORO-CATIONICOS.

El CST pertenece a una familia de transportadores electroneutros cloro-catiónicos denominada SLC12 según la *Human Genome Organization* (HUGO).[36] Esta compuesta por nueve genes claramente identificados que codifican para transportadores de membrana, de los cuales tres utilizan sodio (con o sin potasio), como el catión acoplado al transporte de cloro, mientras que los otros cuatro utilizan potasio como el único catión acoplado al cloro.

La figura 5 muestra un árbol filogenético de los diferentes integrantes de la familia, así como el porcentaje de identidad que existe entre ellos.

En el árbol se observan 2 ramas principales: una de los transportadores que acoplan Na^+ (CST, CSB1, CSB2) y otra rama de los que acoplan K^+ (KCC1, KCC2, KCC3 y KCC4). 20% de identidad existe entre los miembros de estas 2 ramas.

Dos integrantes de esta familia, CIP y CCC9, guardan 20% de identidad con respecto a los transportadores que acoplan Na^+ y K^+, la función de estas proteínas aún no ha sido determinada.

Es interesante notar que entre las secuencias de los diferentes integrantes de cada grupo de cotransportadores el porcentaje de identidad es elevado. Por ejemplo, entre el CST, el CSB1 y el CSB2 existe 50% de identidad en la secuencia de aminoácidos; mientras que en los KCCs el porcentaje de identidad es mayor del 65%.

Por otro lado, las diferencias que se pueden observar entre los miembros de la familia son: el número y el tipo de iones que transportan, su localización en la membrana (cara apical o basolateral), así como la sensibilidad a los diuréticos.

Todos los miembros de la familia presentan sitios potenciales para N-glucosilación y altos pesos moleculares en los análisis de Western blots, realizados con anticuerpos específicos para cada transportador, lo que sugiere que todos los transportadores son proteínas glucosiladas. [92-94]
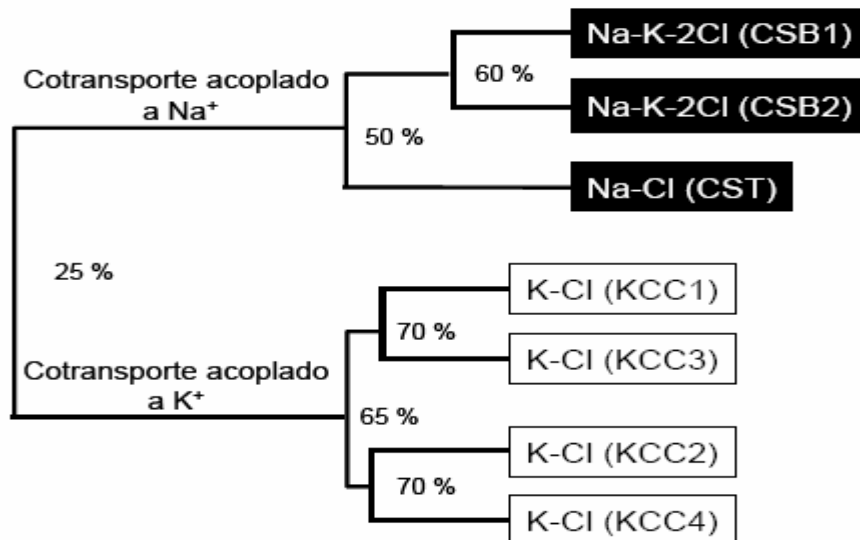
Figura 5. Árbol filogenético de la familia de cotransportadores cloro-catiónicos SLC12.

D. <u>CARACTERIZACIÓN FUNCIONAL DEL CST</u>

La clonación del CST ha permitido determinar y estudiar las propiedades funcionales de este transportador. El sistema de expresión heterólogo de ovocitos de *Xenopus laevis* ha mostrado ser de gran utilidad en estos estudios, ya que hasta el momento se carece de cultivos de células de túbulo distal de riñones mamíferos.[29,37,44,45]

La caracterización funcional del CST se inició con los estudios de Renfro y Stokes, [20-22] en los cuales se describió que el transporte de Na^+ y Cl^- es interdependiente e inhibido específicamente con diuréticos tipo tiazida.

Hace algunos años, trabajos realizados en nuestro laboratorio por Monroy y col. permitieron determinar las propiedades funcionales del CST de rata (CSTr) mediante análisis funcional en ovocitos de *X. laevis.*[44] Brevemente describiremos los resultados más relevantes de este estudio.

Previamente se había demostrado que los ovocitos de *X. laevis* no expresan un transportador endógeno de Na-Cl sensible a tiazidas [29, 37] y como se puede apreciar en la figura 6, la inyección de ovocitos con el RNAc del CSTr

incrementó significativamente de la captación de Na$^+$, la cuál fue dependiente de Cl$^-$ y sensible a las tiazidas.
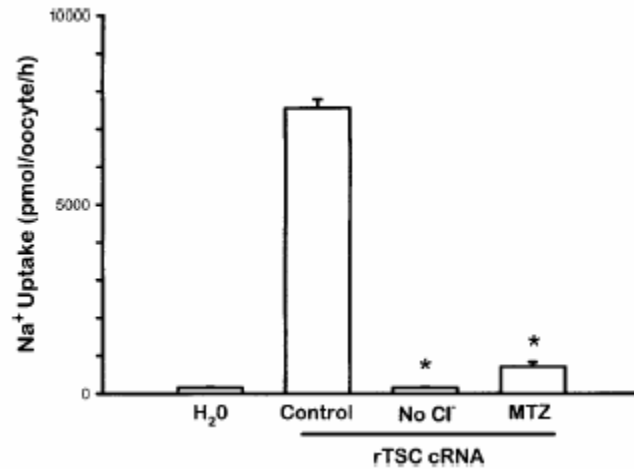
Figura 6. Expresión funcional del CSTr (RNAc) en ovocitos de *X. laevis*

Para determinar la cinética de transporte de iones, Monroy y col. realizaron experimentos en los cuáles se mantuvieron concentraciones fijas de Na$^+$ o Cl$^-$ (40 mM), con modificaciones en las concentraciones del contra-ión (0 a 40 mM). La figura 7 muestra los análisis cinéticos de captación de Na$^+$ en ovocitos inyectados con el RNAc del CSTr. En la gráfica A se muestra la dependencia de Na$^+$ de la captación de ^{22}Na$^+$ y la gráfica B se muestra la dependencia de Cl$^-$ de la captación de ^{22}Na$^+$. La Km calculada para la concentración de Na$^+$ extracelular fue de 7.29 ± 2.1 mM, mientras que la Km calculada para la concentración de Cl$^-$ extracelular fue de 6.48 ± 1.54 mM.
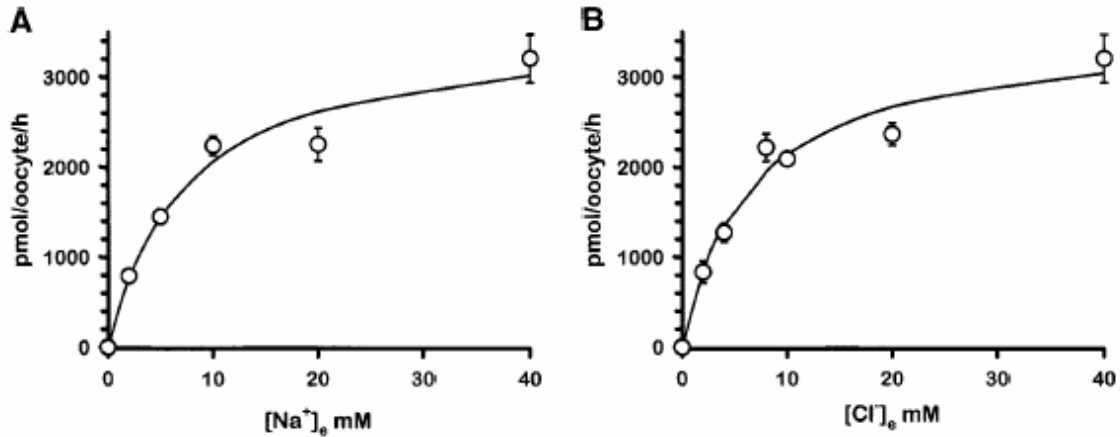
Figura 7. Expresión funcional del CSTr (RNAc) en ovocitos de X. laevis

Con respecto a la función inhibitoria que desempeñan las tiazidas sobre el CSTr, se demostró que el transportador interrumpe su función ante los diferentes tipos de tiazidas (politiazida, metolazona, bendroflumetiazida, hidroclorotiazida, clortalidona y triclorometiazida) y que la función de éste no se ve afectada por la furosemida o la acetazolamina.

Como se describió previamente, Tran y col. [33] observaron que la unión de [³H] metolazona a su receptor se inhibía al incrementar la concentración de Cl⁻ extracelular y se estimulaba por el aumento en la concentración de Na⁺, sugiriendo que las tiazidas y el Cl⁻ compiten por el sitio de unión. En el trabajo de Monroy y col. se evaluó el efecto de la concentración del Cl⁻ extracelular sobre la cinética de inhibición de diferentes tiazidas; en estos experimentos se utilizaron concentraciones de 2 o 100 mM de Cl⁻ extracelular. Los resultados de estos estudios se muestran en la figura 8, en donde diferentes tipos de tiazidas desplazaron la curva de inhibición hacia la izquierda en presencia de concentraciones bajas de Cl⁻ extracelular, indicando que el Cl⁻ afecta la unión de tiazidas al CSTr.
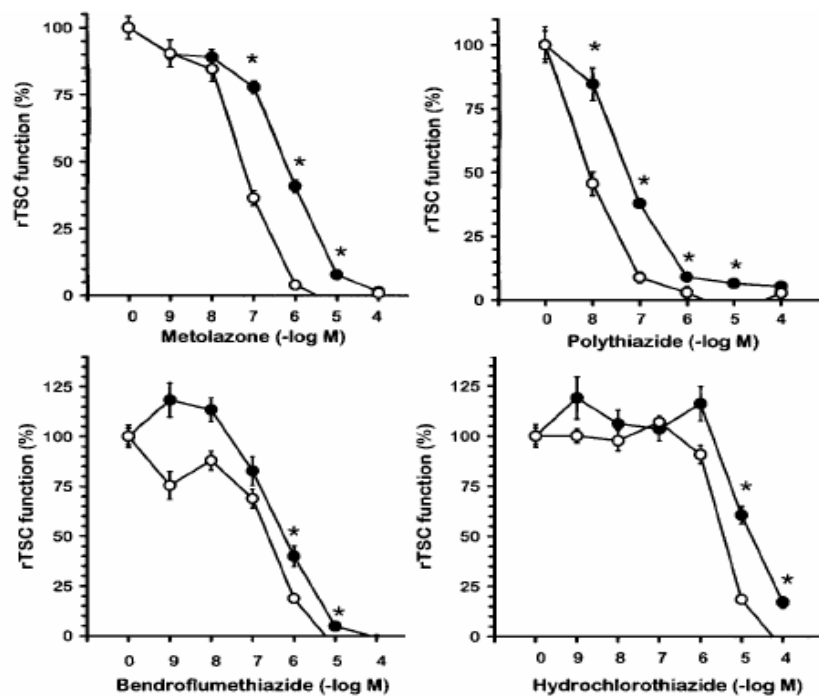
Figura 8. Cinéticas de inhibición del CSTr por diferentes tiazidas en presencia de • 100 mM ó ○ 2 mM de CIP^{-P} extracelular.

También fue evaluado el efecto de la concentración de Na^+ extracelular sobre la inhibición del CSTr por metolazona; en estos experimentos utilizaron concentraciones de 2 o 100 mM de Na^+. La figura 9 muestra que el IC50 de metolazona fue desplazado hacia la izquierda en presencia de concentraciones bajas de Na^+. Con estos resultados demostraron que la concentración de Na^+ extracelular tiene influencia
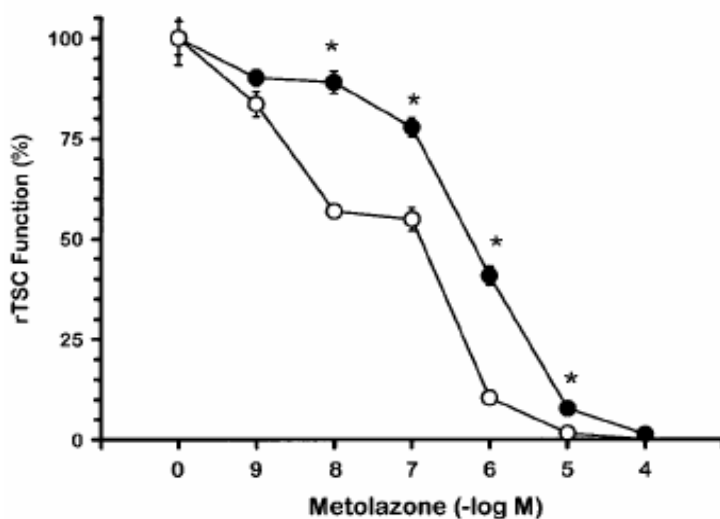
Figura 9. Cinéticas de inhibición del CSTr por metolazona en presencia de • 100 mM ó ○ 2 mM de NaP^{+P} extracelular.

en la inhibición del CSTr por metolazona.

Para determinar la influencia de los iones sobre la inhibición del CSTr por tiazidas, se midió el efecto que produce el incremento en la concentración extracelular de Na^+ o Cl^- sobre el efecto inhibitorio de metolazona a concentraciones de 5×10^{-7} M, la cual es el IC50 de este diurético. El resultado de estos experimentos se muestra en la figura 10, en donde se puede apreciar una correlación negativa entre la concentración de Na^+ o Cl^- extracelular con respecto al porcentaje de inhibición del CSTr.
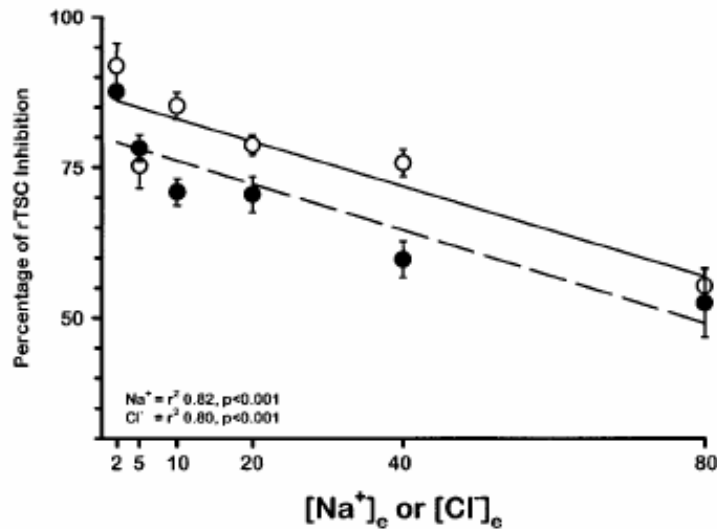
Figura 10. Correlación entre • Na^+ ó ○ CIP^{-P} extracelular con respecto al % de inhibición del CSTr por metolazona ($5 \times 10 P^{-7P}$ M)

Con base en estos resultados los autores propusieron que la unión de los iones al transportador se realiza en forma aleatoria y que la afinidad que muestra el CSTr para Na^+ o para Cl^- depende de la concentración del contra-ión presente en el medio extracelular, mientras que la unión del diurético al CST se ve afectada por la concentración de iones Na^+ y Cl^- presentes en el medio extracelular.

En el 2002 se reportó la caracterización funcional del CST del pez lenguado de invierno (CSTfl); este estudio fue realizado en nuestro laboratorio por Vázquez y col., [45] en el cuál también se describe un análisis detallado de las propiedades funcionales tanto del CSTfl como del CSTr; este estudio permitió establecer

características semejantes y diferencias importantes entre estos dos transportadores que a continuación se describen y se resumen en la tabla 1.

Vázquez y col. realizaron análisis cinéticos para determinar el transporte de iones en CSTfl, los cuáles revelaron que este transportador tiene un Km para Na^+ de 58.2 ± 7.1 mM y un Km para Cl^- de 22.1 ± 4.2 mM. Como puede observarse, el CSTfl mostró menor afinidad por los iones que transporta, en comparación con el CSTr (Km para Na^+ de 7.29 ± 2.1 y una Km para Cl^- de 6.48 ± 1.54 mM). También puede notarse que los valores en el CSTr son similares para ambos iones, mientras que en el CSTfl existe mayor afinidad por el Cl^-.

Con respecto a la inhibición que presenta el CSTfl ante las diferentes tiazidas, se observó un efecto inhibitorio bifásico en este transportador, es decir, bajas concentraciones del fármaco incrementaron la captación de Na^+ (10^{-6} a 10^{-9}M), mientras que altas concentraciones del fármaco (10^{-6} a 10^{-4}M) reducen su función. Este efecto no se observó sobre el CSTr. Se piensa que este comportamiento inhibitorio, puede deberse a la activación de alguna vía de señalización que afecta únicamente al CSTfl. [46] Comparativamente, el CSTr y el CSTfl presentan distinta respuesta que ante los diuréticos tipo tiazida. Concentraciones de 10^{-4} M de clortalidona o triclorometiazida son suficientes para inhibir el 95% de la función del CSTr, mientras que esta concentración de diurético solo reduce parcialmente la función del CSTfl (68 y 46% respectivamente).
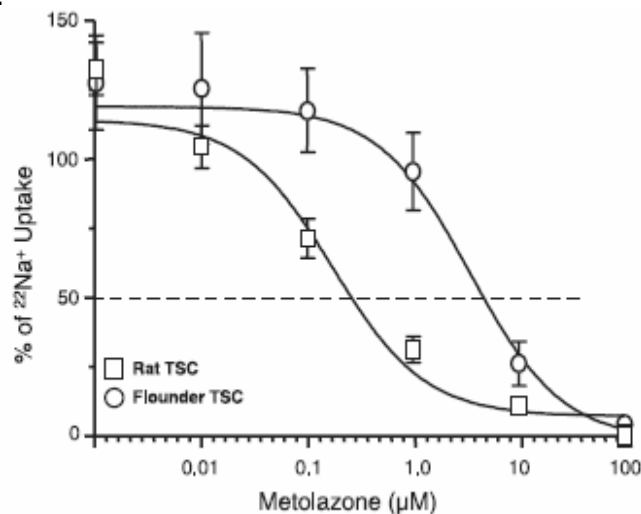
Figura 11. Cinética de inhibición por metolazona en el CSTr y en el CSTfl.

Un ejemplo de la diferente respuesta que presentan el CSTr y el CSTfl a las tiazidas, lo muestra la figura 11, en donde se puede apreciar el perfil de inhibición por metolazona en ambos transportadores.

Una característica semejante observada en el CSTr y en el CSTfl, es que ambos son inhibidos con Hg^{2+}. A mediados del siglo veinte el Hg^{2+} fue usado como un potente diurético en la medicina clínica, pero años mas tarde fue descontinuado por la toxicidad que originaba en los pacientes; aunado a esto se comenzaron a desarrollar nuevos fármacos con mayor eficacia y menor toxicidad.[47] Es conocido que el sitio de acción del Hg^{2+}, es el asa de Henle y en el túbulo distal, aunque no se ha determinado con precisión el mecanismo por el que actúa.[48] El efecto inhibitorio del Hg^{2+} sobre el CST ya había sido observado por Wilkinson y col.[49] en la vejiga urinaria del pez lenguado de invierno. Jacoby y col.[50] también observaron efectos de inhibitorios del Hg^{2+} sobre la isoforma basolateral del cotransportador Na-K-2Cl y efectos similares fueron observados por Plata y col. en la isoforma apical del mismo (datos no publicados).

Una diferencia importante observada entre estos transportadores, es su sensibilidad al volumen celular. La función del CSTr disminuyó parcialmente por la hipotonicidad del medio extracelular, sin ser afectada por la hipertonicidad. Un efecto contrario se observo en el CSTfl, en donde la hipertonicidad redujo significativamente la función del transportador sin que ésta fuera afectada por la hipotonicidad o isotonicidad.

	Na^+ (mM)	Cl^- (mM)	BFTZ IC50 (µM)	$HgCl_2$	Resp. A Tonicidad
CSTr	7.2± 2.1	6.4 ± 1.5	1	↓↓	↓ en hipotonicidad
CSTfl	58.2 ± 7.1	22.1 ± 4.2	10	↓	↓ en hipertonicidad

Tabla 1. Diferencias funcionales entre el CSTr y el CSTfl.

Ante estos hallazgos, Vázquez y col. analizaron la estructura primaria del CSTr y del CSTfl, en donde se observó que estos transportadores guardan un 62% de homología en su estructura primaria. En la figura 12, se puede observar el porcentaje de identidad que existe entre los distintos segmentos de la proteína en ambos transportadores. Las regiones TM muestran un 80% de homología, es decir son las regiones mas parecidas entre ellos. El porcentaje de identidad en la región NH_2 y $COOH^-$ es menor, en el extremo NH_2 presentan 20% de identidad mientras que el $COOH^-$ muestra un 55% de identidad.

Tres sitios potenciales para N-glucosilación se encontraron en la estructura del CSTfl, mientras que en el CSTr solo se observaron dos sitios. También fueron descritos distintos sitios potenciales para fosforilación vía proteína cinasa A o C en estas estructuras. En la figura 12 se pueden observar en círculo verde los sitios potenciales para fosforilación vía PKC que exclusivamente se presentan en la estructura del CSTfl, mientras que en círculo rojo los sitios que pueden ser activados por esta misma vía en el CSTr. Con símbolos de + y – en color verde y en color rojo se representaron aminoácidos con carga presentes únicamente en la estructura del CSTfl o del CSTr. [45]

En este trabajo los autores concluyeron que las diferencias funcionales, farmacológicas y de regulación encontradas entre el CST de rata y del pez, posiblemente se debían a cambios estructurales presentes en la secuencia de estos transportadores.
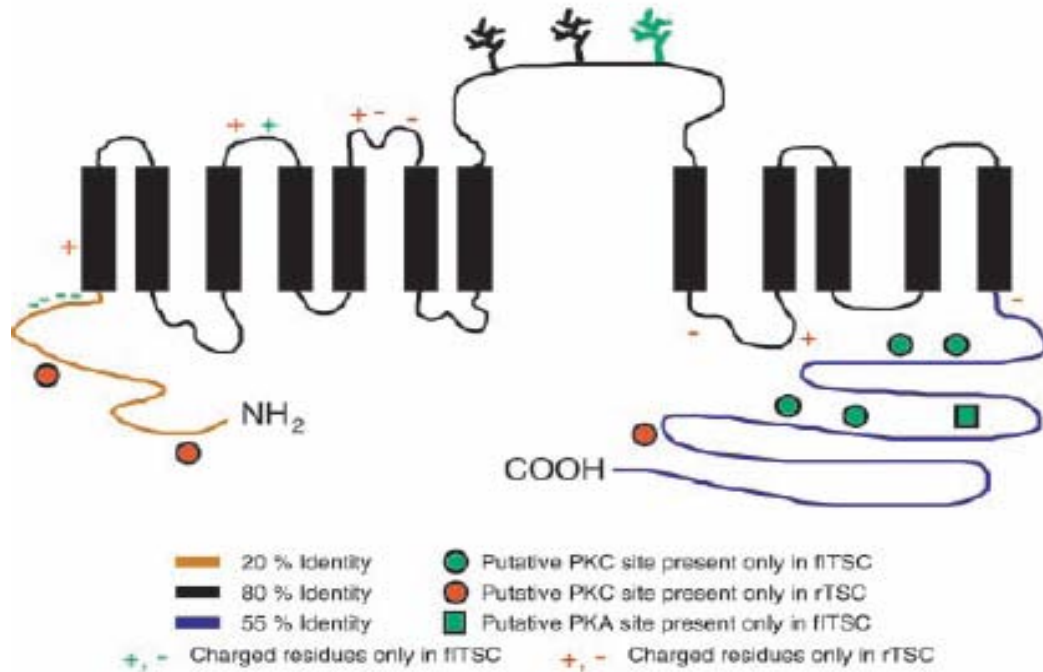
Figura 12. Diferencias estructurales entre el CSTr y el CSTfl.

E. RELACIÓN ESTRUCTURA FUNCIÓN EN LA FAMILIA DE TRANSPORTADORES CLORO-CATIÓNICOS

La identificación molecular y la caracterización funcional de los transportadores cloro-catiónicos, han permitido la realización de estudios de relación estructura-función, en donde el principal objetivo es encontrar dominios estructurales involucrados en determinar las propiedades funcionales de estos transportadores. A continuación se describen diferentes estudios de relación estructura-función realizados en algunos miembros esta familia.

RELACIÓN ESTRUCTURA FUNCIÓN EN EL CSB2/NKCC1.

En el 2001 se publicaron los primeros estudios de relación estructura función en esta familia de transportadores cloro-catiónicos. Estos reportes fueron hechos por Insenring y Forbush en el cotransportador basolateral Na:K:2Cl (CSB2 o NKCC1).[51]

Desde la clonación del CSB2/NKCC1 de humano y de tiburón, se describieron diferencias importantes entre ellos. El CSB2/NKCC1 de humano presenta mayor afinidad a los iones que transporta en comparación con el CSB2/NKCC1 de tiburón, así como mayor inhibición por el diurético (bumetanida).[52]

Al analizar la estructura primaria de estos transportadores se encontró que guardan un 74% de homología entre ellos.

Con la construcción de proteínas quiméricas y la mutagénesis puntual como estrategias metodológicas, en un primer estudio los autores analizaron el papel que desempeñan la región NH$_2$, TM y COOH$^-$ sobre las propiedades funcionales del transportador.

Las construcciones quiméricas entre el CSB2/NKCC1 de humano y de tiburón, fueron posibles al introducir sitios de restricción silenciosos (no modifican la secuencia de aminoácidos), que les permitieron intercambiar regiones de la proteína.

Como se puede observar en la figura 13, se obtuvieron seis quimeras, dos en las que únicamente se intercambió la región NH$_2$, dos quimeras en las que se intercambió en extremo COOH$^-$ y dos en donde las regiones TM del CSB2/NKCC1 de humano estaban flanqueadas por las regiones NH$_2$ y COOH$^-$ del CSB2/NKCC1 de tiburón y viceversa. Tanto los cDNAs de las quimeras como los de los transportadores nativos, fueron transfectados en células HEK para su estudio.[51] En la figura 13 se pueden observar esquemáticamente, las construcciones quiméricas entre el CSB2/NKCC1 de humano y de tiburón.
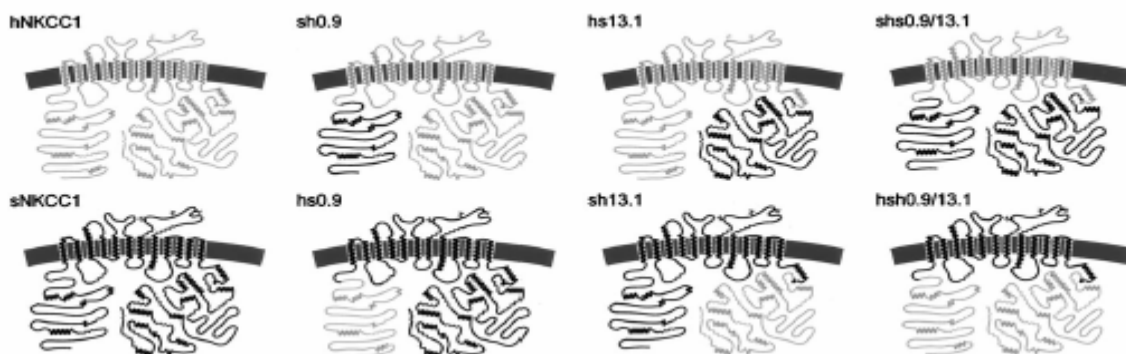
Figura 13. Quimeras obtenidas entre el CSB2/NKCC1 de humano y tiburón.

La figura 14 muestra las constantes de afinidad obtenidas para Na^+, K^+ y Cl^- así como la inhibición por bumetanida tanto para los transportadores nativos como para las quimeras. Se puede observar como el CSB2/NKCC1 de humano presenta mayor afinidad a los iones y muestra gran inhibición por el diurético. Las quimeras mostraron un comportamiento similar a los CSB2/NKCC1 nativos, es decir en ambos casos, las Kms para iones y diuréticos no se vieron afectadas en caso de tener la región NH_2, $COOH^-$ e incluso en ambas regiones, de la proteína contraria. En este estudio se demostró que las regiones TM están involucradas en la afinidad a iones y en la sensibilidad a la bumetanida en el CSB2/NKCC1. [51]
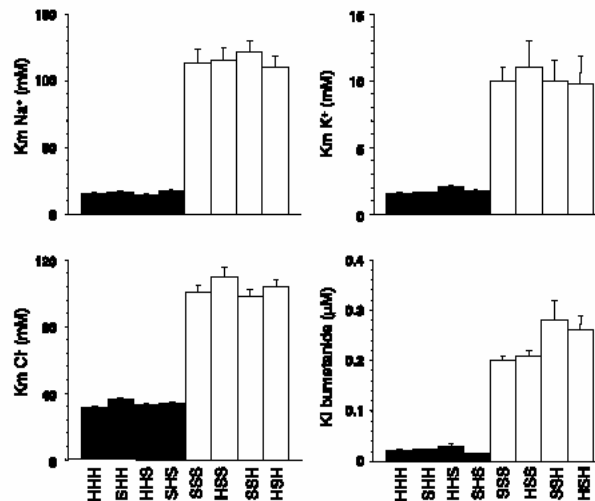
Figura 14. Constantes de afinidad para Na^+, K^+, Cl^- y bumetanida en el CSB2/NKCC1 y en las diferentes quimeras.

En un siguiente estudio, estos mismos autores realizaron un análisis detallado sobre la estructura de las regiones TM en este mismo transportador.

Observaron que las regiones TM 1 y TM3 del CSB2/NKCC1 de humano y de tiburón son idénticas. El análisis de la región TM2 reveló cambios estructurales entre estos transportadores. Por lo tanto, decidieron construir dos nuevas quimeras en las que se intercambio la región TM2 entre el CSB2/NKCC1 de humano y de tiburón, con la finalidad de evaluar el papel que desempeña esta región sobre las propiedades del CSB2/NKCC1. Los análisis funcionales en

células HEK mostraron cambios de afinidad para Na$^+$ y K$^+$ sin encontrar cambios en la afinidad a Cl$^-$, sugiriendo que esta región esta involucrada con el transporte de los cationes.[53]

Con la quimera formada por la región TM2 del tiburón en el CSB2/NKCC1 de humano, se observo una constante de afinidad a bumetanida semejante a la observada en el CSB2/NKCC1 de tiburón, lo que sugirió que la bumetanida se une a la región TM2 y que posiblemente lo realice en un sitio diferente al Cl$^-$

Un nuevo análisis estructural fue realizado sobre la región TM2. Como se puede observar en la figura 15, la región TM2 de CSB2/NKCC1 de humano y de tiburón, muestra 4 aminoácidos diferentes entre estos transportadores.

Los aminoácidos Alanina (A), Leucina (L), Glicina (G) y Treonina (T) presentes en la secuencia del CSB2/NKCC1 de tiburón fueron sustituidos por los aminoácidos Serina (S), Valina (V) y Metionina (M) del CSB2/NKCC1 de humano. Los análisis cinéticos realizados para evaluar el papel que desempeñan estos residuos, mostraron que los aminoácidos A y L de la región TM2 del CSB2/NKCC1 de tiburón y los aminoácidos S y V de la región TM2 de CSB2/NKCC1 de humano son los que están involucrados en el transporte de Na$^+$, mientras que los residuos G y T del CSB2/NKCC1 de tiburón y las 2 Metioninas del CSB2/NKCC1 de humano están involucrados en el transporte de K$^+$. [53]

Figura15. Aminoácidos de la región TM2 en CSB2/NKCC1 de humano y tiburón.

En estudios posteriores de este mismo grupo de investigación, se reportaron las construcciones de otras proteínas quiméricas entre el CSB2/NKCC1 de humano y de tiburón. Fueron generadas nuevas quimeras en las que se intercambiaron

las regiones TM 8 a 12, en las cuales no se observaron cambios con respecto a los transportadores nativos.

También generaron quimeras en las que se intercambio exclusivamente la región TM7, estas mostraron cambios en la constante de afinidad para Na^+, K^+ y Cl^- con valores intermedios entre el CSB2/NKCC1 de humano y de tiburón.

Simultáneamente realizaron un análisis estructural entre las regiones TM4 y TM5 de estos transportadores. Se encontraron algunos aminoácidos diferentes entre ambas secuencias, los cuales fueron intercambiados a través de mutagénesis puntual. Estos aminoácidos no mostraron cambios en las constantes de afinidad para de Na^+, K^+ y Cl^-

En resumen, los autores determinaron diferentes regiones TM involucradas en la translocación de iones en el CSB2/NKCC1. Las regiones TM2 y TM7 en el transporte de Na^+; las regiones TM2, TM4 y TM7 en el transporte de K^+ y las regiones TM4 y TM7 en el transporte de Cl^-. Se consideró que el diurético se une al transportador en la región TM2. En la figura 16 se muestran esquemáticamente estos resultados.[54]
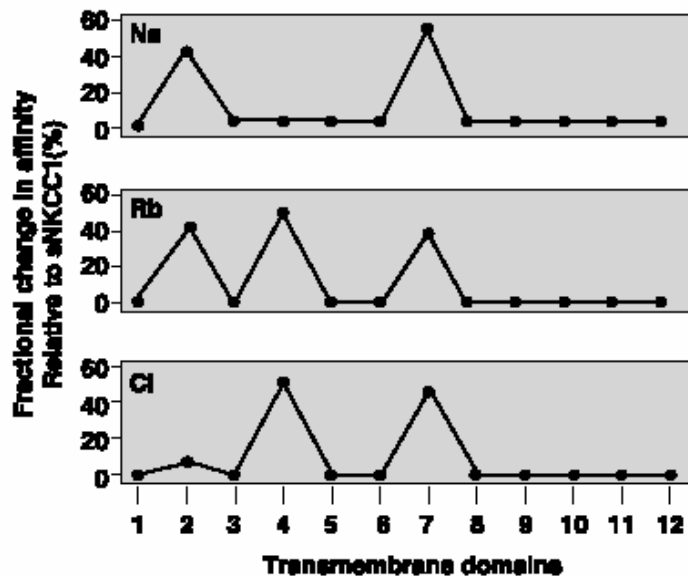
Figura 16. Representación esquemática de las regiones TM del CSB2/NKCC1 involucradas en el transporte de Na^+, K^+ y Cl^-.

RELACIÓN ESTRUCTURA FUNCIÓN EN EL CSB1/NKCC2.

Estudios de relación estructura-función también han sido realizados en la isoforma apical del cotransportador Na^+:K^+:$2Cl^-$ (CSB1/NKCC2). El gen SLC12A1 codifica para este transportador generando por empalme alternativo tres isoformas denominadas A, B y F. Trabajos realizados en nuestro laboratorio por Plata y col. [56] mostraron cambios en la cinética de transporte para iones y sensibilidad al diurético en estas tres proteínas. Los análisis de las propiedades funcionales se realizaron en ovocitos de *X. laevis*, mediante la captación de $^{86}Rb^+$ dependiente de bumetanida. En estos estudios se observó que las isoformas A y B tienen propiedades cinéticas similares, que difieren a las de la isoforma F. La isoforma F tiene la menor afinidad por los iones transportados. A pesar de que la expresión de las tres isoformas en la membrana plasmática de los ovocitos fue similar, la captación de $^{86}Rb^+$ fue significativamente mayor en la isoforma A, lo cuál sugiere que esta proteína tienen una mayor capacidad de transporte. La isoforma B mostró alta afinidad por los iones pero baja capacidad de transporte, mientras que la isoforma F mostró ser un cotransportador de baja afinidad y baja capacidad de transporte. Por otro lado la isoforma B mostró mayor sensibilidad la bumetanida.

Previamente se reporto la existencia de tres casetes de exones mutuamente excluyentes en el CSB1/NKCC2 como los responsables de generar estas tres isoformas. Estos casetes codifican para la región TM2 y para el asa que conecta a las regiones TM2-TM3.[57]

Los análisis estructurales realizados sobre las isoformas A, B y F revelaron cambios mínimos en la secuencia de los aminoácidos que forman la región TM2 y en el asa conectora de la TM2-TM3, por lo que se considero que estos residuos fueran los responsables de generar las diferencias funcionales encontradas en las tres isoformas . La figura 17 muestra las diferencias de residuos entre las tres isoformas. En el esquema, las cajas de color rojo resaltan a los aminoácidos diferentes en las tres secuencias. En color naranja, se marcan a los aminoácidos únicos en la isoforma A; en color azul, se marcan a los

residuos únicos en la isoforma B y en color verde, se marcan a los residuos exclusivos de la isoforma F.[57]
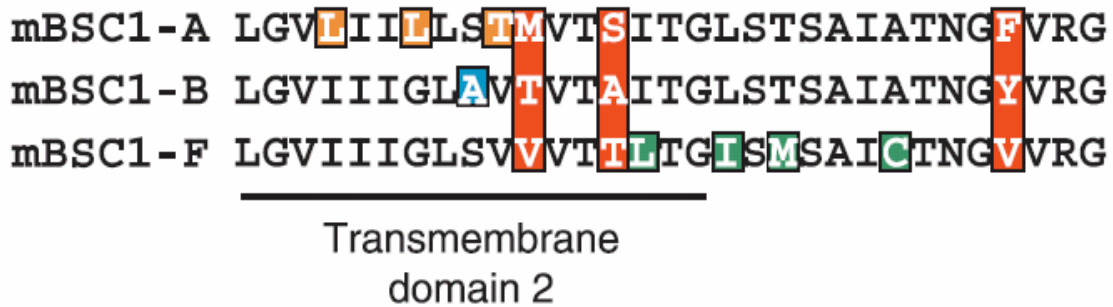
Figura 17. Aminoácidos de la región TM2 y del asa conectora que une a la TM2-3, en las tres isoformas del CSB1/NKCC2

Gagnon y col. reportaron la construcción de proteínas quiméricas entre la isoforma A y la isoforma F del CSB1/NKCC2. Generaron dos quimeras denominadas A/F y F/A. La quimera A/F, fue formada con la región TM2 de la isoforma A y con la región conectora TM2-3 de la isoforma F, mientras que la quimera F/A fue construida con los segmentos contrarios a los de la quimera A/F Los análisis cinéticos demostraron que tanto la TM2 como el asa conectora entre la TM2-3 son importantes para definir la alta o baja afinidad que tienen estas isoformas a los cationes.

En cuanto a la afinidad por Cl⁻, la quimera F/A mostró una Km similar a la de la isoforma A, mientras que la quimera A/F mostró valores similares a los de la isoforma F, sugiriendo que los residuos del asa conectora TM2-3 son los responsables de determinar la afinidad por Cl- en las diferentes isoformas del CSB1/NKCC2.

Recientemente Giménez y Forbush [59] reportaron residuos específicos de la región TM2 involucrados en la translocación de iones Cl⁻ en el CSB1/NKCC2. A través de mutagénesis puntual, sustituyeron los diferentes aminoácidos de la isoforma B por los aminoácidos de la isoforma F; igualmente fueron sustituidos las aminoácidos diferentes de la isoforma B por los aminoácidos de la isoforma A. Los análisis cinéticos realizados para las diferentes sustituciones revelaron

que las Treoninas 240 y 249 de la isoforma B, localizadas en la TM2, son de gran importancia para el transporte de Cl⁻. Como se puede observar estos resultados difieren a los observados por Gagnon y col. [58] quienes propusieron que eran los residuos del asa conectora TM2-3 los que estaban involucrados en el transporte de este ión.

Tovar–Palacio y col.[60] realizaron estudios de relación estructura función entre dos miembros de la familia de transportadores cloro-catiónicos, el CSB1/NKCC2 y el CST. Con la construcción de proteínas quiméricas entre el CSB1/NKCC2 y el CST (ver figura 19) , así como la realización de diversos análisis cinéticos en ovocitos de *Xenopus laevis*, mostraron que las regiones TM de CSB1/NKCC2 presentan un comportamiento similar al del CSB1/NKCC2 nativo, así como sensibilidad a la bumetanida y resistencia al diurético tiazida, con lo que demostró que son las regiones TM las involucradas en el transporte de iones y en la sensibilidad al diurético en el CSB1/NKCC2.

RELACIÓN ESTRUCTURA FUNCIÓN EN EL CST

Pocos estudios de relación estructura-función se han realizado sobre el CST; algunos de estos están basados en determinar únicamente el papel que juegan aminoácidos específicos. A continuación se describen algunos trabajos de investigación donde el principal objetivo fue determinar el efecto de algunos residuos sobre la función de este transportador.

F. EFECTO DE LA GLUCOSILACIÓN SOBRE LAS PROPIEDADES FUNCIONALES DEL CST.

Como ya se mencionó anteriormente, se ha considerado que todos los miembros de la familia de transportadores cloro-catiónicos se encuentran glucosilados ya que en la secuencia de estos, se presentan sitios potenciales para N-glucosilación; además, diversos análisis de Western blots realizados con

anticuerpos específicos para cada transportador revelan pesos moleculares altos en estas proteínas. [92-94]

Una diferencia estructural importante encontrada en dos CSTs de esta familia (el CSTr y el CSTfl), es que presentan diferentes sitios consenso para la N-glucosilación en su estructura primaria. Se ha considerado de gran interés evaluar el papel que juegan los aminoácidos involucrados en este evento ya que podrían determinar algunas de las propiedades funcionales del transportador.

Previamente, se reportaron dos sitios potenciales para N-glucosilación en la secuencia del CSTr y tres en la secuencia del CSTfl, desconociéndose si esta diferencia estructural estaba involucrada en determinar las propiedades funcionales de estos transportadores. [45]

La N-glucosilación se describe como un evento co-transduccional, en el cuál una cadena de oligosacaridos es transferida a un polipéptido naciente en un residuo Asparagina, el residuo Asparagina debe estar localizado dentro de una secuencia consenso específica (Asn-Xaa-Ser/Thr,Xaa≠Pro). [77]

En un estudio realizado en nuestro laboratorio por Hoover y col.[78] se reportó el efecto de la glucosilación sobre las propiedades funcionales del CSTr. Se realizó un análisis estructural detallado sobre la secuencia de este transportador, encontrando seis sitios consenso para N-Glucosilación, pero solo dos de ellos susceptibles de glucosilación in vivo. Los sitios de glucosilación en el CSTr reportados fueron: N404 y N424. Estos sitios están localizados en el asa extracelular que une a la región TM7 a la TM8.

Mediante mutagénesis puntual, los aminoácidos Asparagina fueron sustituidos por residuos de Glutamina en cada una de las secuencias consenso, con el objetivo de prevenir la glucosilación. Se obtuvieron tres proteínas mutadas N404Q, N424Q y una proteína con los dos sitios mutados, la N404-424Q.

A través de ensayos de expresión de proteínas en ovocitos de *X. laevis*, se encontró que la función del CSTr disminuyo hasta un 50% cuando se elimino alguno de los dos sitios, mientras que la función disminuyo hasta un 95% en ausencia de los dos sitios. La afinidad por Na^+ y Cl^- no se vio afectada, sin

embargo, se encontró una tendencia hacia velocidades máximas menores para ambos iones entre el CSTr nativo y las mutantes de glucosilación. En cuanto a la sensibilidad a tiazidas, las mutantes de glucosilación aumentaron la afinidad del CSTr por el diurético (CSTr (2×10^{-6} M), N404 (7×10^{-7} M), N424 (9×10^{-8} M) y N404-424 (1×10^{-8} M)). La expresión sobre la superficie celular fue cuantificada a través de microscopía confocal, la proteína verde fluorescente (EGFP) fue unida al CSTr y a las tres mutantes. El análisis reveló que la ausencia de la glucosilación disminuye la expresión del CST sobre la superficie celular.

Estos estudios demostraron que la eliminación de los sitios de glucosilación, previenen este evento, ocasionando disminución en la expresión del CSTr sobre la superficie celular y aumentando su sensibilidad por el diurético.

El efecto de la glucosilación solo ha sido estudiado en el CSTr. No se conocen los efectos de este evento sobre la función en otros miembros de la familia, por lo que no ha sido posible determinar si estos residuos están involucrados sobre la función del transportador.

G. EFECTO DE MUTACIONES-GITELMAN SOBRE LA FUNCION DEL CST

En los últimos años se han descrito diversas mutaciones en el gen que codifica para el CST; cuando éstas suceden producen una enfermedad conocida como Síndrome de Gitelman (SG).

El SG es un trastorno autosómico recesivo, descrito por primera vez en 1966 por Gitelman, Graham y Welt, [61] que se caracteriza clínicamente por hipotensión arterial, hipocalemia, alcalosis metabólica e hipocalciuria y que se presenta usualmente en la segunda década de la vida.[41, 62, 63]

Más de 100 mutaciones que suceden en el gen que codifica para el CST han sido reportadas hasta el momento; éstas se encuentran disponibles en la base de datos de mutaciones del genoma humano.[18,62-74] Mas del 70% son mutaciones sin sentido (en las que se sustituye una base por otra) o no codificantes (estas introducen un codon de paro produciéndose una proteína truncada). Este tipo de mutaciones suelen ocurrir en aminoácidos conservados.

Aproximadamente el 10% de las mutaciones en este gen, corresponden a pequeñas deleciones y menos del 7%, ocurren en sitios de empalme de la proteína en donde suceden inserciones o deleciones de codones.

Algunas mutaciones-Gitelman dan como resultado un bloqueo total de la función del CST;[39,75] en este caso, el papel que juegan los aminoácidos mutados sobre la función del transportador no puede ser evaluado, ya que se ha observado que las proteínas mutadas no se sintetizan adecuadamente y por lo tanto no se expresan sobre la superficie celular

Se han descrito mutaciones-Gitelman que dan como resultado un transportador parcialmente funcional [39] Se considera de gran importancia el estudio de estos residuos ya que pueden estar involucrados en determinar las propiedades funcionales del CST.

Kunchaparty y col.[39] analizaron varias mutaciones reportadas en pacientes con SG; éstas al ser expresadas en ovocitos de *X. laevis*, no mostraron funcionalidad. Para entender estas observaciones, los autores realizaron varios estudios sobre las proteínas mutadas, encontrando que estas se sintetizaban adecuadamente pero no se glucosilaban, lo que eliminaba su expresión sobre la superficie celular. Estos estudios hacen sentido con los trabajos de Hoover y col.[78] que se describieron anteriormente, en donde se demostró que la eliminación de la glucosilación disminuye la expresión del CST de la superficie celular.

De Jong y col.[76] estudiaron el efecto de cuatro mutaciones sin sentido reportadas en pacientes con SG, encontraron que estas proteínas no presentan anomalías en su glucosilación. Con análisis inmunocitoquímicos detectaron la presencia de las proteínas mutadas tanto en el citoplasma como en la membrana plasmática. Los autores no estudiaron las propiedades funcionales de éstas mutantes, por lo que no se precisó si el efecto que causaban era debido a su inapropiada inserción en la membrana plasmática o a defectos que modificaran las propiedades funcionales del transportador.

Se considera que el estudio de mutaciones-Gitelman es de gran ayuda para entender aspectos de relación estructura-función en el CST, ya que algunos de

los residuos mutados podrían estar involucrados sobre las propiedades funcionales de este transportador.

H. DEFINIENDO DOMINIOS ESTRUCTURALES INVOLUCRADOS EN EL TRASNPORTE DE IONES Y DIURÉTICOS AL CST

En el 2004, trabajos realizados en nuestro laboratorio por Tovar–Palacio y col.[60] reportaron la construcción de proteínas quiméricas entre el CST y el CSB1/NKCC2; estos transportadores guardan un 52% de homología. Como se puede observar en la figura 18, distintos porcentajes de identidad fueron observados entre los diferentes segmentos de la proteína. >85% de homología mostraron las regiones TM 1, 2, 3, 6, 8 y 10, las regiones TM 4 y 9 presentaron del 55 al 75% de homología, así como un porcentaje <50% se encontró entre las regiones TM 5, 7, 11 y 12. La región NH_2 de estos transportadores presentaron un porcentaje menor al 15% de identidad, mientras que las regiones $COOH^-$ presentaron un porcentaje entre el 55 y 75% de identidad.
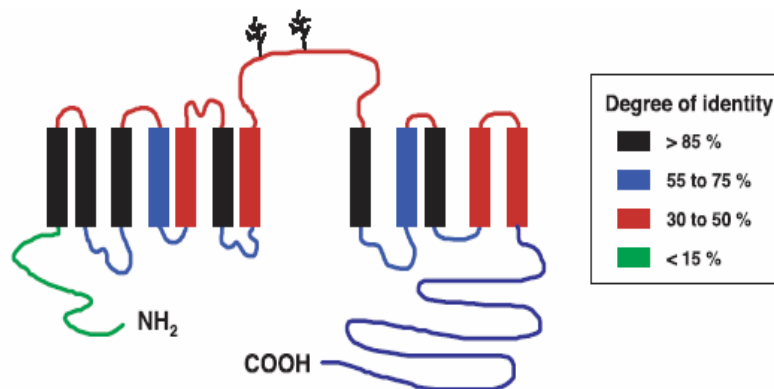
Figura 18. Porcentaje de identidad entre el CST y el CSB1/NKCC2.

Mediante la generación de sitios de restricción silenciosos se intercambiaron regiones de la proteína entre el CST y el CSB1/NKCC2. Como se puede observar en la figura 19, se obtuvieron seis quimeras, dos en las que se intercambio la región NH_2, dos quimeras en las que se intercambio el extremo $COOH^-$ y dos en donde las regiones TM del CST estaban flanqueadas por las

regiones NH_2 y $COOH^-$ del CSB1/NKCC2 y viceversa .Tanto los cRNAs de las quimeras como los de los transportadores nativos, fueron microinyectados en ovocitos de *X. laevis* para su estudio. Para la nomenclatura de las quimeras se utilizaron las letras T (CST) y B (CSB1/NKCC2) para identificar el fragmento de la proteína que había sido utilizado para la construcción de las nuevas proteínas. En la figura 19 también se pueden notar motivos de color negro, estos representan el sitio donde se realiza el emplame alternativo en CSB1/NKCC2 , así como ~70 aminoácidos que se presentan exclusivamente en la región COOH de este transportador.
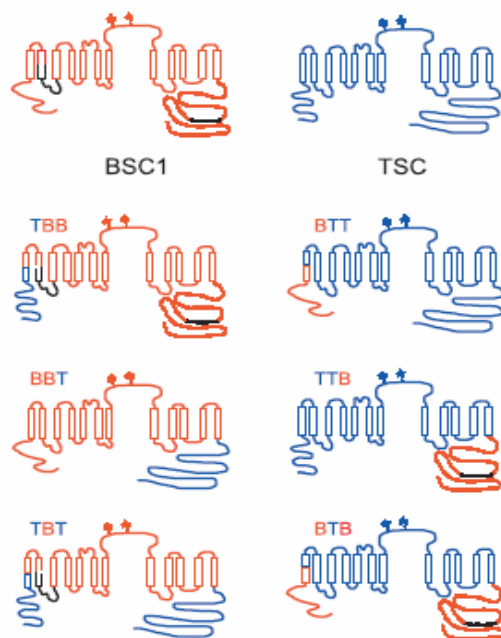
Figura 19. Representación esquemática   de proteínas quiméricas entre el CST y el CSB1/NKCC2.

La expresión funcional de las tres quimeras en las cuales las regiones NH_2 y/o COOH de CSB1/NKCC2 estaban fusionadas con las regiones TM del CST, solo la quimera BTT mostró actividad.

La figura 20 muestra la captación de $^{22}Na^+$ en ovocitos inyectados con el RNAc de BTT, donde se aprecia el aumento significativo en la captación de Na^+ la cuál

es dependiente de Cl^-, sensible a metolazona, independiente de K^+ y resistente a la bumetanida.
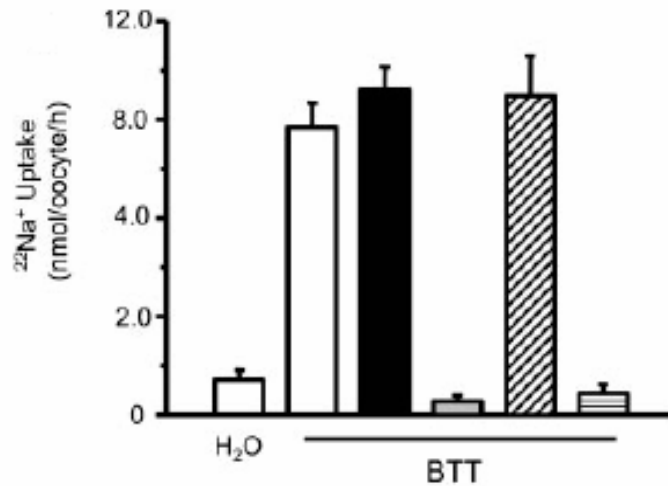
Figura 20. Captación de $^{22}Na^+$ en ovocitos inyectados con el RNAc de la quimera BTT. La barra blanca representa condiciones de ausencia de K^+ extracelular, la barra gris indica ausencia de Cl^- extracelular, la barrra llena y la barra rayada horizontalmente indican concentraciones de 10^{-4} M de bumetanida y metolazona respectivamente.

Con estos resultados Tovar-Palacio y col. sugirieron que son las regiones TM del CST en donde se lleva a cabo en el transporte de iones así como sensibilidad al diurético. Sin embargo es necesario realizar estudios que determinen dominios estructurales involucrados con las propiedades funcionales del CST.

El trabajo que reportamos en esta tesis, tiene como objetivo principal determinar dominios estructurales y/o aminoácidos puntuales en el CST involucrados en el transporte de iones y en la sensibilidad a los diuréticos tipo tiazida.

Hemos descrito que proteínas estructuralmente parecidas como el CSTr y el CSTfl, en donde se observan diferentes propiedades funcionales, constituyen un excelente modelo de estudio para establecer las propiedades de transporte e inhibición de esta proteína.

III. <u>HIPÓTESIS</u>

- Si las diferencias en la cinética de transporte y en la interacción entre iones y tiazidas entre el CSTr y el CSTfl están determinadas por dominios específicos en la secuencia en las regiones transmembrana, entonces la construcción proteínas quiméricas y/o mutaciones puntuales revelaran dominios involucrados en la función del CST.

- Si la N-glucosilación del CSTfl es un evento que interfiere con la unión del diurético al transportador, entonces la eliminación de esta aumentará la inhibición del CSTfl por las tiazidas.

- Si algunas mutaciones tipo-Gitelman resultan en un transportador parcialmente funcional, entonces el estudio de éstas podrá revelar aminoácidos importantes para la función del CST.

IV. <u>OBJETIVO GENERAL</u>

Determinar dominios estructurales y/o aminoácidos puntuales en el cotransportador de Na$^+$:Cl$^-$ sensible a tiazidas involucrados en el transporte de iones y en la sensibilidad a los diuréticos tipo tiazida.

<u>OBJETIVOS ESPECÍFICOS</u>

1.- Conocer el efecto de la N-glucosilación sobre las propiedades funcionales del CSTfl.
1.a. Eliminar los tres sitios consenso para N-glucosilación en el CSTfl.
1.b. Determinar las propiedades funcionales de las clonas construidas en el punto 1.a.

2.- Definir el papel de los dominios aminoterminal, hidrofóbico central y carboxiterminal del CSTr y del CSTfl sobre las diversas propiedades funcionales.
2.a. Generar quimeras entre el CSTr y el CSTfl en las que se intercambien los dominios NH$_2$, TM y COOH$^-$.
2.b. Determinar las propiedades funcionales de las quimeras y compararlas con el CSTr y el CSTfl nativos.

3.- Guiados en los resultados del objetivo 2, determinar el papel de dominios más pequeños y/o aminoácidos puntuales sobre las propiedades funcionales del CST.
3.a. Diseñar y generar la construcción de nuevas quimeras y/o de mutaciones puntuales.
3.b. Determinar las propiedades funcionales de las clonas construidas en el punto 3.a.

4.- Identificar Polimorfismos de Nucleótidos Individuales (SNPs) en el CST y determinar su participación sobre las propiedades funcionales del CST.

5.- Estudiar el efecto que causan mutaciones-Gitelman sobre la función del CST.

5.a. Generar las mutaciones G627V, R935Q, V995M, G610S, A585V sobre la secuencia nativa del CST.

5.b. Determinar las propiedades funcionales de las clonas construidas en el punto 5.a.

METODOLOGÌA Y RESULTADOS.

La metodología utilizada en este trabajo y los resultados obtenidos están descritos en los artículos publicados.

ARTÍCULOS PUBLICADOS.

1.- Affinity defining domains in the Na-Cl cotransporter: different location for Cl- and thiazide binding.
Erika Moreno, Pedro San Cristóbal, Manuel Rivera, Norma Vázquez, Norma A. Bobadilla y Gerardo Gamba. **The Journal of Biological Chemistry. 281:17266-17275.2006.**

2.- A single nucleotide polymorphism alters the activity of the renal Na+:Cl-cotransporter and reveals a role transmembrane segment 4 in chloride and thiazide affinity.
Erika Moreno, Claudia Tovar-Palacio, Paola de los Heros, Blanca Guzmán, Norma A. Bobadilla, Norma Vázquez, Daniela Riccardi, Esteban Poch y Gerardo Gamba. **The Journal of Biological Chemistry. 279:16553-16560.2004.**

3.- The activity of the renal Na+:K+:2Cl- cotransporter is reduced by mutagenesis of the N-glycosylation sites: role for protein surface charge in Cl- transport.
Anahí PAredes, Consuelo Plata, Manuel Rivera, Erika Moreno, Norma Vázquez, Rosario Muñoz-Clares, Steven C. Hebert y Gerardo Gamba. **Am J Physiol. Renal Physiol. 290:F1094-F1102.2006.**

4.- Pathophysiology of functional mutations of the thiazide-sensitive Na-Cl cotransporter in Gitelman disease.
Ernesto Sabath, Patricia Meade, Jennifer Berkman, Paola,de los Heros Erika Moreno, Norma A. Bobadilla, Norma Vázquez, David H. Ellison y Gamba Gerardo. **Am J Physiol. Renal Physiol. 290:F1094-F1102.2004.**

5.-The Na+:Cl- cotransporter is activated and phosphorylated at the amino-terminal domain upon intracellular chloride depletion.
Diana Pacheco-Alvarez, Pedro San Cristóbal, Patricia Meade, Erika Moreno, Norma Vázquez, Abigail Díaz, María Eugenia Juárez, Ignacio Giménez y Gerardo Gamba. **The Journal of Biological Chemistry. 281:28755-28763.2006**

Affinity-defining Domains in the Na-Cl Cotransporter
A DIFFERENT LOCATION FOR Cl⁻ AND THIAZIDE BINDING*

Erika Moreno[‡§1], Pedro San Cristóbal[‡1], Manuel Rivera[‡], Norma Vázquez[‡], Norma A. Bobadilla[‡]
and Gerardo Gamba[‡2]

From the ‡Molecular Physiology Unit, Instituto Nacional de Ciencias Médicas y Nutrición Salvador Zubirán, Instituto de
Investigaciones Biomédicas, Universidad Nacional Autónoma de México Tlalpan 14000, Mexico City, Mexico and §Instituto de
Ciencias de la Salud, Universidad Autónoma del Estado de Hidalgo, Pachuca, Hidalgo 42160, México

The thiazide-sensitive Na⁺-Cl⁻ cotransporter (NCC) is the major pathway for salt reabsorption in the distal convoluted tubule, serves as a receptor for thiazide-type diuretics, and is involved in inherited diseases associated with abnormal blood pressure. Little is known regarding the structure-function relationship in this cotransporter. Previous studies from our group reveal that mammalian NCC exhibits higher affinity for ions and thiazides than teleost NCC and suggest a role for glycosylation upon thiazide affinity. Here we have constructed a series of chimeric and mutant cDNAs between rat and flounder NCC to define the role of glycosylation status, the amino-terminal domain, the carboxyl-terminal domain, the extracellular glycosylated loop, and the transmembrane segments upon affinity for Na⁺, Cl⁻, and metolazone. Xenopus laevis oocytes were used as the heterologous expression system. We observed that elimination of glycosylation sites in flounder NCC did not affect the affinity of the cotransporter for metolazone. Also, swapping the amino-terminal domain, the carboxyl-terminal domain, the glycosylation sites, or the entire extracellular glycosylation loop between rat and flounder NCC had no effect upon ions or metolazone affinity. In contrast, interchanging transmembrane regions between rat and flounder NCC revealed that affinity-modifying residues for chloride are located within the transmembrane 1–7 region and for thiazides are located within the transmembrane 8–12 region, whereas both segments seem to be implicated in defining sodium affinity. These observations strongly suggest that binding sites for chloride and thiazide in NCC are different.

In the mammalian kidney, the apical thiazide-sensitive Na⁺-Cl⁻ cotransporter (NCC)[3] is the major pathway for salt reabsorption in the luminal membrane of the distal convoluted tubule (1, 2). NCC also serves as the target for the thiazide-type diuretics that are currently recommended by the Joint National Committee for the detection, evaluation, and treatment of high blood pressure as the first line pharmaco-logical treatment of hypertension, either as the unique drug in patients with stage I hypertension or in combination with other anti-hypertensive agents for patients with stage II hypertension (3). The fundamental role for NCC in preserving the extracellular fluid volume and blood pressure homeostasis has been firmly established by the identification that Gitelman disease (4–6) (an inherited disorder featuring arterial hypotension, renal salt wasting, hypokalemic metabolic alkalosis, hypocalciuria, and hypomagnesemia) is caused by inactivating mutations of the *SLC12A3* gene that encodes NCC. In addition, a loss of the negative effect of the serine/threonine kinases WNK1 and WNK4 upon NCC activity has been implicated in the pathogenesis of a salt-dependent form of human hypertension known as pseudohypoaldosteronism type II (7, 8), which features a clinical picture that is a mirror image of Gitelman disease (9), with striking sensitivity to hydrochlorothiazide.

NCC belongs to the electroneutral cation Cl⁻-coupled cotransporter gene family (solute carrier family 12 (SLC12)) (10) and exhibits ~50% identity with the Na⁺-K⁺-2Cl⁻ cotransporters NKCC1 and NKCC2 and ~25% identity with the KCl cotransporters KCC1 to KCC4 (for review see Ref. 11). Mammalian NCC is a protein of 1,002 amino acid residues featuring a central hydrophobic domain, which is flanked by a short amino- and a long carboxyl-terminal hydrophilic loops located within the cell (12)(Fig. 1). In the central hydrophobic domain, there are twelve putative transmembrane-spanning segments (TM 1–12) interconnected by six extracellular and five intracellular hydrophilic loops. The extracellular loop 4 (ECL4) is the longest one and exhibits two putative N-linked glycosylation sites. The proposed topology shown in Fig. 1 has been experimentally confirmed for NKCC1 (13), and glycosylation of the ECL4 has been confirmed for rat NCC (14) and rat NKCC2 (15).

Little is known about the structural requirements for ion translocation and thiazide binding in NCC. Tovar-Palacio *et al.* (16) provide evidence that the critical domains and/or residues that define the specificity for ion translocation and thiazide inhibition reside within the central hydrophobic domain. Hoover *et al.* (14) have observed that rNCC glycosylation status markedly affected NCC activity and the affinity for metolazone. Elimination of the ECL4 glycosylation sites reduce the cotransporter activity by 90% and increase the affinity for metolazone. Interestingly, NCC from flounder urinary bladder (fNCC) contains three putative N-linked glycosylation sites in ECL4 instead of two, and compared with rNCC, exhibits lower affinity for thiazide, as well as for both Na⁺ and Cl⁻ ions (17).

The major goal of the present study was to determine the role of glycosylation sites and the different domains of the renal-specific apical sodium-chloride coupled cotransporter in defining the affinity of the transport process and diuretic interaction. We exploited the fact that rNCC and fNCC exhibit distinct affinities for the transported ions and thiazide diuretics together with extensive protein sequence similarities

and differences. Accordingly, we constructed several point-mutated clones as well as chimeric proteins between rNCC and flNCC. The functional properties of the resultant proteins were determined by functional expression in *Xenopus laevis* oocytes. Our results show that affinity-defining regions for Cl^- and thiazides are different, suggesting that Cl^- and thiazide may bind to different regions of the cotransporter.

EXPERIMENTAL PROCEDURES

Mutagenesis and Construction of Chimeric Cotransporters—For the present study, we used the rat and flounder NCC cDNAs that we previously cloned from rat kidney (rNCC) [12] and flounder urinary bladder (flNCC) [18], respectively. The wild-type rNCC cDNA contains a unique NsiI site on the base pairs 444–449 that encodes residues located at the middle of the first TM segment. To exchange regions or domains between rNCC and flNCC, we have engineered both cDNAs by introducing several silent restriction sites in exactly the same location. In flNCC, a silent NsiI site was introduced at the middle of the first TM segment, and in both rNCC and flNCC, silent MunI, SacII, and HpaI sites were created. MunI and SacII at the beginning and at the end of ECL4, respectively, and HpaI at the beginning of the carboxyl-terminal domain. Thereafter, the unique EcoRI (in the 5′ side of the polylinker) and NotI (in the 3′ side of the polylinker) together with the unique NsiI, MunI, SacII, and HpaI sites were used to exchange domains between rNCC and flNCC by gel purification and ligation of the appropriate cDNA bands. In addition, site-directed mutagenesis was used to add and/or eliminate *N*-glycosylation sites from rNCC, flNCC, and chimeric clones (see "Results"). The double mutant rNCC cDNA used in this study, in which both *N*-glycosylation sites were eliminated, was previously described [14]. For flNCC, the oligonucleotides 5′-CTCTG-GTGAGTTGCAAGACACCCTGTCTTAC-3′, 5′CTCATCCAGCG-AGCAATGTTCGGGATTAGCTTG-3′, and 5′CGAGTGTATAAAG-CAAAACACATGCAAACAC-3′, were used to mutate the asparagines at positions 403 (N403Q), 414 (N414Q), and 432 (N432Q), respectively, to glutamine. Thereafter, double or triple mutants were constructed using the same primers upon the previously mutated clones. Finally, by means of double-step PCR, the epitope FLAG sequence DYKDDDDK was added in-frame to flNCC following the first methionine. All silent or site-directed mutations were introduced using the QuikChange site-directed mutagenesis system (Stratagene) following the manufacturer's recommendations. Restriction analysis and automatic DNA sequencing was used to corroborate all of the mutations and in the switching place of each chimera. All primers used for mutagenesis were custom made (Sigma).

In Vitro cRNA Translation—To prepare cRNA for microinjection, each wild-type, mutant, or chimeric cDNA was digested at the 3′-end using NotI from New England Biolabs (Carlsbad, CA), and cRNA was transcribed *in vitro* using the T7 RNA polymerase mMESSAGE mMACHINE™ (Ambion) transcription system. cRNA product integrity was confirmed on agarose gels and concentration was determined by absorbance reading at 260 nm (DU 640, Beckman Instruments). cRNA was stored frozen in aliquots at −80 °C until used.

X. laevis Oocyte Preparation—Oocytes were harvested by surgery from adult female *X. laevis* frogs (Nasco) under 0.17% tricaine anesthesia and incubated in frog Ringer ND96 ((in mM) 96 NaCl, 2 KCl, 1.8 $CaCl_2$, 1 $MgCl$, and 5 Hepes/Tris, pH 7.4) in the presence of collagenase B (2 mg/ml) for 1 h. The oocytes were washed four times in ND96, defolliculated, and incubated overnight at 18 °C in ND96 supplemented with 2.5 mM sodium pyruvate and 5 mg/100 ml of gentamicin. Next day, mature oocytes [19] were injected with 50 nl of water alone or containing cRNA at 0.2–0.75 μg/μl (10–37.5 ng of cRNA/oocyte). Thereafter,

the oocytes were incubated 4–6 days in ND96 with sodium pyruvate and gentamicin that was changed every 24 h. The night before the uptake experiments were performed, the oocytes were incubated in Cl^--free ND96 ((in mM) 96 Na isethionate, 2 K⁺-gluconate, 1.8 Ca^{2+} gluconate, 1.0 Mg^{2+}-gluconate, 5 mM Hepes, 2.5 sodium pyruvate, and 5 mg/100 ml gentamicin, pH 7.4) [18].

Transport Assays—The function of the Na^+-Cl^- cotransporter was determined by assessing tracer $^{22}Na^+$ uptake (PerkinElmer Life Sciences) in groups of 10–15 oocytes following our protocol [20] of 30 min of incubation in a Cl^--free ND96 medium containing 1 mM ouabain, 0.1 mM amiloride, and 0.1 mM bumetanide followed by a 60-min uptake period in a K⁺-free, NaCl medium ((in mM) 40 NaCl, 56 sodium-gluconate, 4.0 $CaCl_2$, 1.0 $MgCl_2$, and 5.0 Hepes/Tris, pH 7.4) containing ouabain, amiloride, bumetanide, and 2 μCi of $^{22}Na^+$/ml). We have previously demonstrated that *X. laevis* oocytes do not express a thiazide-sensitive Na^+-Cl^- cotransporter [18, 20]. Thus, in all experiments along the study, only one group of water-injected oocytes was included to determine the basal, unspecific tracer $^{22}Na^+$ uptake. The sensitivity and kinetics for metolazone diuretics was assessed by exposing groups of cRNA-injected oocytes to metolazone at concentrations varying from 10^{-9} to 10^{-4} M. For these experiments, the desired concentration of the diuretic was present in both the incubation and uptake periods. All metolazone dependence curves were assessed twice for each clone. To determine the ion transport kinetics of the wild-type, mutant, or chimeric cotransporter, we performed experiments varying the concentrations of Na^+ and Cl^-. To maintain osmolarity and ionic strength, gluconate was used as a Cl^- substitute and *N*-methyl-D-glucamine as a Na^+ substitute. To minimize variations along the study due to ion concentrations, two sets of solutions for Na^+ transport kinetic analysis and two sets for Cl^- transport kinetic analysis were made. Thereafter, all clones were subjected to at least two different ion transport kinetic experiments with each set of solution.

All uptakes were performed at 32 °C. At the end of the uptake period, oocytes were washed five times in ice-cold uptake solution without isotope to remove extracellular fluid tracer. After the oocytes were dissolved in 10% sodium dodecyl sulfate, tracer activity was determined for each oocyte by β-scintillation counting.

Western Blotting—Western blot analysis was used to analyze wild-type or *N*-glycosylation-mutant FLAG-flNCC proteins in corresponding cRNA-injected oocytes following our standard protocol [21]. First, proteins extracted from 50 oocytes were immunoprecipitated using the FLAG-tagged protein immunoprecipitation kit following the manufacturer's recommendations. Subsequently, proteins from 10 oocytes/lane were heated in sample buffer containing 6% SDS, 15% glycerol, 0.3% bromphenol blue, 150 mM Tris, pH 7.6, and 2% β-mercaptoethanol, resolved by Laemmli SDS-polyacrylamide (7.5%) gel electrophoresis, and transferred to a polyvinylidene difluoride membrane. Immunodetection was performed using an anti-FLAG monoclonal antibody (Sigma). Membranes were exposed to the anti-FLAG antibody overnight at 4 °C, washed, incubated for 60 min at room temperature with alkaline phosphatase-conjugated secondary (anti-mouse) antibody (BIO-RAD) diluted 1:2000 in blocking buffer, and then washed again. Bands were detected by using the Immun-Star chemiluminescent protein detection system (Bio-Rad).

Data Analysis—All results presented are based on a minimum of two different experiments with at least 12 oocytes/group in each experiment. The significance of the differences between groups was evaluated by one-way analysis of variance, with multiple comparisons using Dunnett or Bonferroni correction as required. Results are presented as mean ± S.E.

FIGURE 1. Topology and alignment analysis between mammalian and flounder NCC. A, NCC-proposed topology of a central hydrophobic domain containing 12 putative transmembrane segments with a large extracellular glycosylated loop between TM segments 7 and 8. Numbers of some residues are shown by arrows. A comparison between mammalian and flounder NCC reveals identity degree >80% in the white TM segments; between 50 and 80% in black TM segments; most of the interconnecting segments, and the carboxyl-terminal domain; and below 50% in the regions in gray. Putative glycosylation sites are shown in ECL4. R and F denote sites present in rat and/or flounder, respectively. B, sequence alignment of the ECL4 from all known NCC sequences, as stated. The N-glycosylation sites that fulfill the algorithm NX(S/T), X ≠ Pro are highlighted in boxes. The first site, corresponding to Asn-403 of flNCC is conserved among all NCC sequences. The second site, Asn-414 is unique in flNCC. The third site in flNCC, corresponding to Asn-432, is present only in teleost NCC (flounder and zebrafish). Finally, a second site in mammalian NCC is absent in flNCC but present in all other NCCs, including zebrafish. * denotes second site of mammalian NCCs (NFT)

Extracellular loop
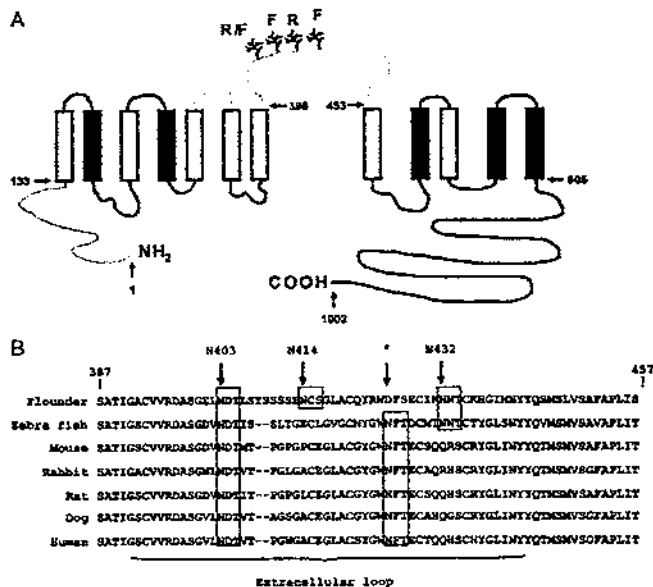
RESULTS

Topology and Putative N-Glycosylation Site Comparison in the Na⁺-Cl⁻ Cotransporter—Fig. 1A depicts the proposed topology of the Na⁺-Cl⁻ cotransporter in which a *gray-black scale* is used to highlight similarities and differences between rat and flounder NCC. The identity of the TMs -1, -3, -5, -6, -7, -8, and -10 is >80%, whereas TMs -2, -4, -9, -11, and -12 are shown in *black* and the carboxyl-terminal domain identity degree is between 60 and 80%. The more divergent segments are the amino-terminal domain and the extracellular connecting segments ECL3 and ECL4, *highlighted in gray* (Fig. 1). Because Hoover *et al.* (14) suggest that the glycosylation status of the ECL4 affects affinity for metolazone in rNCC, we studied ECL4 in greater detail. Fig. 1B shows an alignment of ECL4 among species from which NCC cDNA has been cloned and sequenced or deduced by genomic analysis. In all mammalian NCCs, two N-glycosylation consensus sequences are present (Asn-Xaa-(Ser/Thr), Xaa ≠ Pro (22)). We have previously shown in rNCC that both sites are glycosylated (14). In contrast, using the same algorithm, three N-glycosylation motifs can be found in flNCC ECL4. The first site, Asn-403, was conserved among all NCCs. The second site, Asn-414, was present only in flNCC. This second site in flNCC is unique among all known NCC sequences. The third N-glycosylation site in flNCC, Asn-432, was absent in all mammalian NCCs but present in the deduced zebrafish NCC sequence. Interestingly, the second site of mammalian NCCs (NFT) (shown by an *asterisk* in Fig. 1B) that was absent in flNCC was present in zebrafish. Thus, the teleost NCC sequences known so far (flounder or zebrafish) exhibited three potential N-glycosylation sites in the loop, although only two of them were conserved.

Mammalian and Flounder NCC Exhibit Different Affinity for Metolazone—We have previously shown that affinity for ions and thiazides is higher in rNCC than in flNCC (17, 20). However, these transport affinity analyses and thiazide inhibition curves were obtained from independent experiments in which rNCC and flNCC were expressed separately. Thus, for the present study, we first confirmed that differences in the affinity for ions and thiazide diuretics between mammalian and fish NCC were reproducible in simultaneous experiments in which *X. laevis* oocytes where microinjected with rNCC or flNCC cRNA, and 4 days later, the ion transport kinetics and metolazone dose-responses were determined using the same uptake solutions and metolazone dilutions. Therefore, the only difference between the rNCC and flNCC groups was the injected cRNA. The combined results of three different ion transport kinetic analyses and five curves for thiazide affinity are shown in Fig. 2. The K_m value for Na⁺ transport in rNCC was 5.5 ± 1.0 mM, whereas in flNCC it was 30 ± 6.0 mM ($p < 0.05$). Similarly, the Cl⁻ transport kinetic analysis showed that apparent Cl⁻ K_m for rNCC was 2.6 ± 0.6 mM, whereas for flNCC it was 15 ± 2.0 mM ($p < 0.05$). A similar situation was observed for thiazide affinity. As shown in Fig. 2C, the calculated IC₅₀ for metolazone inhibition in rNCC was 0.3 ± 0.005 μM, whereas in flNCC it was 4.0 ± 0.08 μM ($p < 0.01$). Thus, confirming our previous proposal, results in Fig. 2 show that rNCC exhibits a significantly higher affinity for ions as well as for metolazone than flNCC.
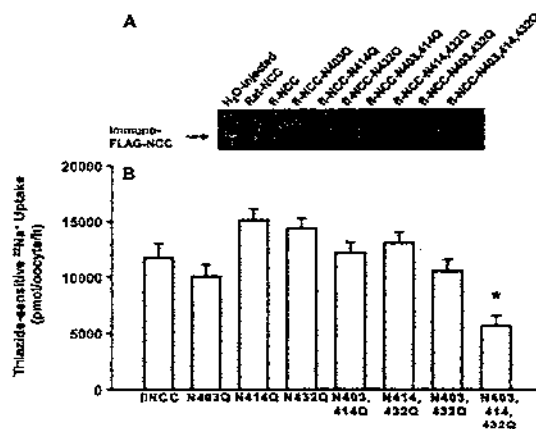
Effect of Elimination of N-Glycosylation Sites in flNCC—We have previously shown that elimination of the N-glycosylation sites in rat NCC is associated with a dramatic increase in affinity for metolazone (14) and a smaller, although significant, increase in Cl⁻ affinity. Because flNCC exhibits lower affinity for metolazone and contains three

N-linked glycosylation sites, we reasoned that the presence of three sites in flNCC could be responsible, at least in part, for the difference in metolazone affinity between mammalian and teleost NCC. Thus, to define the effect of N-glycosylation on the flounder Na^+-Cl^- cotransporter functional properties, single, double, and triple N-glycosylation
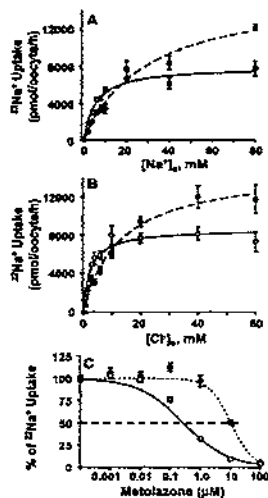
FIGURE 2. **Functional properties of rat and flounder NCC using the heterologous expression system of *X. laevis* oocytes.** *A*, Na^+-dependent $^{22}Na^+$ uptake. Groups of oocytes were injected with rNCC cRNA (white circles and continuous line) or with flNCC cRNA (black circles and dashed line). *B*, Cl^--dependent $^{22}Na^+$ uptake. *C*, metolazone dose-response. In *A* and *B*, each point represents the mean ± S.E. of 20–24 oocytes from two different experiments. In *C*, each point represents the mean ± S.E. of 50–60 oocytes from five different experiments. Curves were fitted by nonlinear regression using Graph Pad Prisma software. In all single experiments, both rfCC- and flNCC-cRNA injected oocytes were studied simultaneously using the same solutions and/or metolazone dilutions.

FIGURE 3. **Effect of N-glycosylation site elimination in FLAG-flNCC upon glycosylation and activity.** *A*, Western blot analysis with monoclonal anti-FLAG antibodies of proteins extracted from oocytes injected with each clone cRNA as stated. The proteins were immunoprecipitated with the anti-FLAG immunoprecipitation system (Sigma), resolved in polyacrylamide gels, transferred into polyvinylidene difluoride membranes, and probed with anti-FLAG antibody. *B*, thiazide-sensitive $^{22}Na^+$ uptake in groups of oocytes injected with cRNA from wild-type flNCC or mutants, as stated. Oocytes were injected with the same amount of cRNA from the corresponding clone (10 ng/oocyte). Uptake in water-injected oocytes was 245 ± 31 pmol/oocyte/h. Each bar represents the mean ± S.E. of 15 oocytes from a single experiment. Uptake was assessed for all groups the same day, using the same solutions. *, $p < 0.0001$ versus Control flNCC.

mutants were constructed by site-directed mutagenesis. The mutations were performed upon the FLAG-flNCC cDNA to allow immunodetection of the cotransporter in proteins extracted from injected oocytes using monoclonal anti-FLAG antibodies (Sigma). Oocytes were injected with water or with similar amounts of wild-type FLAG-rNCC cRNA, FLAG-flNCC cRNA, or with cRNA from each of the single, double, and triple FLAG-flNCC N-glycosylation mutants. Proteins were extracted from oocytes and immunoprecipitated by means of anti-FLAG antibodies. As shown in Fig. 3*A*, rNCC and flNCC resulted in the expression of a thick band of ~110 kDa with a broad smear *above* it. This band is not present in proteins extracted from water-injected oocytes. The smear was not changed or was slightly reduced by the elimination of one or two N-glycosylation sites. However, the triple mutation in which the asparagines 403, 414, and 432 were changed to glutamine resulted in a clear reduction of the smear. These observations suggest that in flNCC, as occurred with rNCC (14) and rat NKCC2 (15), elimination of all of the ECL4 N-glycosylation sites is required to affect glycosylation of the protein. Fig. 3*B* shows the effect of the elimination of one, two, or the three N-glycosylation sites upon the activity of flNCC. *X. laevis* oocytes were injected with similar amounts of cRNA from each clone. Four days later, the tracer $^{22}Na^+$ uptake was assessed in groups injected with water, wild-type flNCC cRNA, or with any of the single, double, or triple mutant cRNAs. Elimination of one or two N-glycosylation sites had no effect upon the flounder cotransporter activity. In contrast, although $^{22}Na^+$ uptake in wild-type flNCC-injected oocytes was 11,738 ± 1,293 pmol/oocyte/h, $^{22}Na^+$ uptake in the triple mutant-injected oocytes was 6576 ± 919 pmol/oocyte/h ($p < 0.01$). Thus, elimination of the three N-glycosylation sites resulted in a significant reduction of flNCC activity. We have shown previously that elimination of ECL4 glycosylation sites in rNCC or rNKCC2 results in the reduction of the cotransporter activity by 90 and 80%, respectively, whereas the observed reduction in transport activity of the triple mutant flNCC was ~50%. Thus, although the effect is qualitatively similar to our previous results, with rNCC (14) or rNKCC2 (15), the effect is quantitatively different.

As discussed above, the elimination of N-glycosylation sites in rNCC resulted in a significant increase in metolazone affinity (14), whereas in rat, NKCC2 resulted in a slight decrease in bumetanide affinity (15).
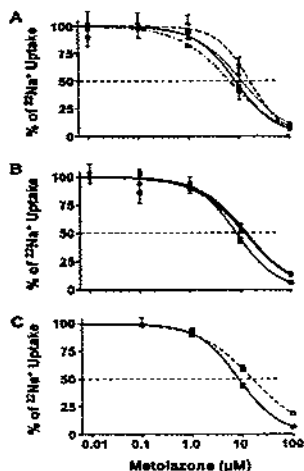
FIGURE 4. Effect of N-glycosylation sites elimination in fNCC upon affinity for metolazone. Metolazone dose-response analysis was assessed in all groups the same day, using the same metolazone dilutions and uptake solutions. A, dose-response curves in wild-type fNCC (continuous line and closed squares) and single mutants N403Q, N414Q, and N432Q (dashed lines and closed circles, triangles, and inverted triangles, respectively). B, dose-response curves in wild-type fNCC (continuous line and closed squares) and double mutants N403Q/N414Q, N403Q/N432Q, and N414Q/N432Q (continuous lines and closed circles, triangles, and inverted triangles, respectively). C, dose-response curves in wild-type fNCC (continuous line and closed squares) and the triple mutant N403Q/N414Q/N432Q (dashed lines and open squares).

Thus, it was of interest to define the metolazone dose-response behavior in the wild-type and mutant fNCC cotransporters. The metolazone dose-response for fNCC single mutants N403Q, N414Q, and N432Q are shown in Fig. 4A, for the fNCC double mutants N403Q/N414Q, N403Q/N432Q, and N414Q/N432Q, Fig. 4B, and for the triple mutant, Fig. 4C. For comparison purposes, in all graphs, the dose-response observed for the wild-type fNCC is included. In striking contrast to our previous observations in rNCC, elimination of one, two, or all three N-glycosylation sites resulted in no significant changes in the fNCC affinity for metolazone. Thus, the effect of elimination of ECL4 N-glycosylation sites upon diuretic affinity in fNCC resembles what was observed in mammalian NKCC2 (15) rather than in mammalian NCC (14). This observation indicated that the difference in glycosylation sites cannot explain the differences in affinity for ions or metolazone between rNCC and fNCC.

Because rat and flounder exhibit such strikingly different effects of glycosylation upon thiazide affinity, together with the fact that the long extracellular loop is one of the most divergent domains between these proteins (Fig. 1B), we decided to construct and analyze the functional properties of several mutant and chimeric proteins between rat and flounder NCC to explore the role of ECL4, the amino- and carboxyl-terminal domains, TM regions, and glycosylation sites upon NCC activity and metolazone affinity.

Nomenclature and Construction of Mutant and Chimeric Proteins— We used the silent restriction sites described under "Experimental Procedures" to cut the cotransporters into five different pieces, the amino-terminal domain, TM segment 1–7, the ECL4, TM segments 8–12, and the carboxyl-terminal domain. Thereafter, cDNA fragments were ligated to obtain several chimeric proteins. All chimeras are denoted by

five letters. The first corresponds to the amino-terminal, the second to the TM segment 1–7, the third to ECL4, the fourth to the TM segment 8–12, and the fifth to the entire carboxyl-terminal domain. In addition, color is used to denote the origin of each fragment. Thus, the letter R and blue color denote when the domain belongs to the RAT NCC, and the letter F and red color denote when domains belong to flounder NCC. The nomenclature of the studied constructs is as follows (see Fig. 5): (i) rNCC without glycosylation sites (RG⁻) and fNCC without glycosylation sites (FG⁻), (ii) six chimeras in which the amino-terminal, the carboxyl-terminal, or both domains were interchanged between rNCC and fNCC (FRRRR, RRRRF, FRRRF, RFFFF, FFFFR, and RFFFR), (iii) four chimeras in which ECL4 was swapped between rNCC and fNCC, with or without glycosylation sites (RRFRR, FFRFF, RRFRR/G⁻, and FFRFF/G⁻), (iv) rNCC containing the three flounder glycosylation sites (rNCC-fl-G-like) and fNCC containing the two rat glycosylation sites (fNCC-r-G-like), (v) RRFRR with the rat glycosylation site (RRFRR-r-G-like), (vi) FFRFF with the flounder glycosylation site (FFRFF-fl-G-like), and (vii) four chimeras in which the TM segments 1–7 or 8–12 were swapped between rat and flounder NCC (RRRFR, RFRRR, FRFFF, and FFFRF).

Effect of Glycosylation Sites upon Thiazide Affinity— The results of several experiments in which the activity and the metolazone affinity were assessed in *X. laevis* oocytes microinjected with cRNA, transcribed from the different clones described above, are depicted in Figs. 6 and 7. Most of the constructs described in Fig. 5 exhibited enough activity to allow us to perform consistent metolazone dose-response curves and ion transport kinetic analyses. The exceptions were RRFRR/G⁻, RRFRR-r-G-like, RRRRF, FRRRF, and FRFFF, which were considered non-functional.

Fig. 6 shows the metolazone dose curves of each functional construct. For comparison purposes, in all cases, the average dose-response curves for rNCC (IC₅₀ = 0.3 ± 0.005 μM) and fNCC IC₅₀ = 12.5 ± 1.8 μM) are shown in blue and red, respectively. The observed curve for each construct is shown in black. The graphs in Fig. 6, A–D, depict the dose-response curve in four constructs based upon rNCC backbone, whereas Fig. 6, E–I, shows the curves in constructs based upon fNCC. When compared with rNCC, the IC₅₀ for metolazone was shifted to the *left* in the clones RRFRR and RG⁻ (IC₅₀ = 0.01 ± 0.0008 and 0.03 ± 0.003 μM, respectively) and was not changed in clones rNCC-fl-G-like and FRRRR (IC₅₀ = 0.28 ± 0.003 and 0.3 ± 0.005 μM, respectively). This observation in the RG⁻ clone confirmed our previous report of increased affinity for metolazone when both N-glycosylation sites of rNCC were eliminated (14) and suggested that RRFRR protein is probably not properly glycosylated. When contrasted with fNCC, no change in metolazone IC₅₀ was observed in RFFFF, FFRFF, FFRFF-fl-G-like, and FG (IC₅₀ = 12.5 ± 2.0, 12.6 ± 1.9, 20 ± 0.42, and 20 ± 0.4 μM, respectively), and a small shift to *right* was observed in FFRFF/G⁻ and fNCC-r-G-like (IC₅₀ = 25 ± 4.9 and 50 ± 2.9 μM, respectively). Fig. 7 shows both the activity and mean IC₅₀ observed in each construct. The groups are ordered from the construct that exhibited the highest to the one with the lowest affinity (from *left* to *right*). The level of uptake observed in wild-type rNCC and fNCC was 18873 ± 722 and 15825 ± 1171 pmol/oocyte/h, respectively. Most of the mutant and chimeric proteins were functional and exhibited activity that was at least 50% of that shown in the corresponding wild type. The constructs that induced the lowest degree of activity were RG⁻ and RRFRR, with uptake values of 2177 ± 393 and 2710 ± 285 pmol/oocyte/h, respectively. This level of uptake was ~10-fold higher than the uptake observed in water-injected oocytes (204 ± 31 pmol/oocyte/h; p < 0.01). Because the level of activity in the studied clones varied from 2,177 ± 393 to
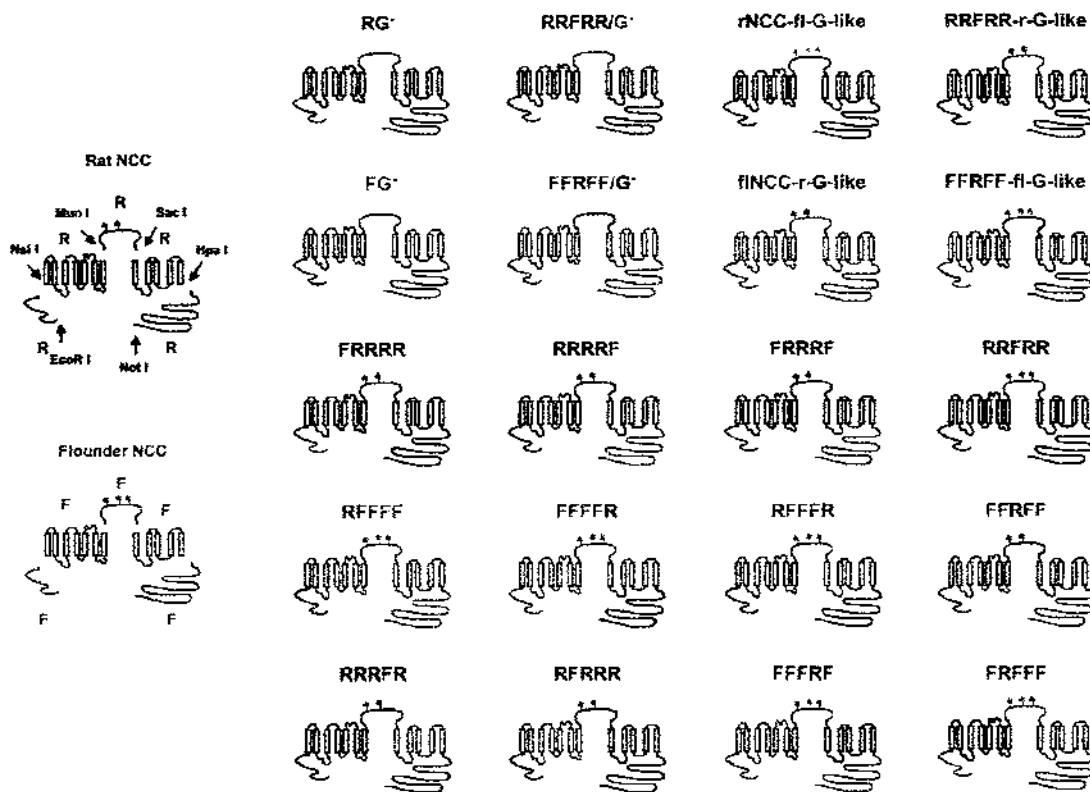
FIGURE 5. **Topological models of the mutant and chimeric constructs.** The *left panel* shows wild-type rat NCC in *blue* and flounder NCC in *red*. The restriction sites used to make the constructs are depicted in *black* over the rNCC sequence. These silent restriction sites were also introduced into fNCC at the same locations. Subsequently, "cut and paste" of cDNA fragments was used to construct the chimeras shown in the *right panel*. *Blue* fragments are from rat NCC and *red* from flounder NCC. N-glycosylation sites were added or eliminated by site-directed mutagenesis, as stated. G^- = "glycosylation minus," that is, when glycosylation sites were eliminated from rat NCC (RG^-), flounder NCC (FG^-), chimera RRFRR ($RRFRR/G^-$), and chimera FFRFF ($FFRFF/G^-$). R-G-like, glycosylation sites as in the flounder sequence; R-G-like, glycosylation sites as in the rat sequence.

31,052 ± 1,021 pmol/oocyte/h, we wanted to know whether the metolazone IC_{50} could be affected by the level of expression observed in each clone. In a single experiment, several groups of *X. laevis* oocytes were injected with increased concentrations of rNCC cRNA that are known to increase rNCC activity, either alone or together with cRNA *in vitro* transcribed from the serine/threonine kinase WNK3 (23). Subsequently, a metolazone dose-response curve for each group was assessed. As expected and shown in Fig. 8A, the more rNCC cRNA injected, the greater the thiazide-sensitive tracer $^{22}Na^+$ uptake. The activity in all groups was increased by the presence of WNK3. However, as shown in Fig. 8B, dose-response curves to metolazone were similar among all groups. In addition, we have previously shown, in rNCC-injected oocytes, metolazone IC_{50} of ~1 μM with $^{22}Na^+$ uptakes of ~3,000 pmol/oocyte/h (20), similar to that shown for RG^- or RRFRR in the present study. Thus, the metolazone IC_{50} was not affected by different levels of activity, suggesting that differences observed in metolazone affinity in chimeric and mutant constructs are not due to the different degree of activity.

Role of Amino- or Carboxyl-terminal Domain and ECL4 upon Ion and Metolazone Affinity—Fig. 9 shows the K_m values for sodium and chloride of the chimeras FRRRR, RRFRR, RFFFR, and FFRFF. The K_m values for Na^+ in the chimeras containing the central hydrophobic domain from rNCC were 8.1 ± 1.1 and 5.0 ± 0.6 mM for FRRRR and RRFRR, respectively, whereas in the chimeras containing the central hydrophobic domain from fNCC, the K_m values for Na^+ were 28 ± 6.0 and 87 ± 45 mM for RFFFR and FFRFF, respectively (Fig. 9A). The apparent Cl^- K_m values in the same chimeras were 2.1 ± 1.1, 1.8 ± 0.5, 17 ± 2.8, and 11 ± 4.1 mM, respectively (Fig. 9B). Thus, ion transport kinetics in these chimeras followed the central hydrophobic domain. Taken together, the results shown in Figs. 6–9 strongly suggest that ion transport kinetics and metolazone affinity-modifying residues are not located in the amino-terminal domain, the carboxyl-terminal domain, or in ECL4.

Role of Transmembrane Segments 1–7 and 8–12 in Ion and Metolazone Affinity—We then constructed four chimeric proteins in which the TM 1–7 or TM 8–12 regions were swapped between rNCC and fNCC to
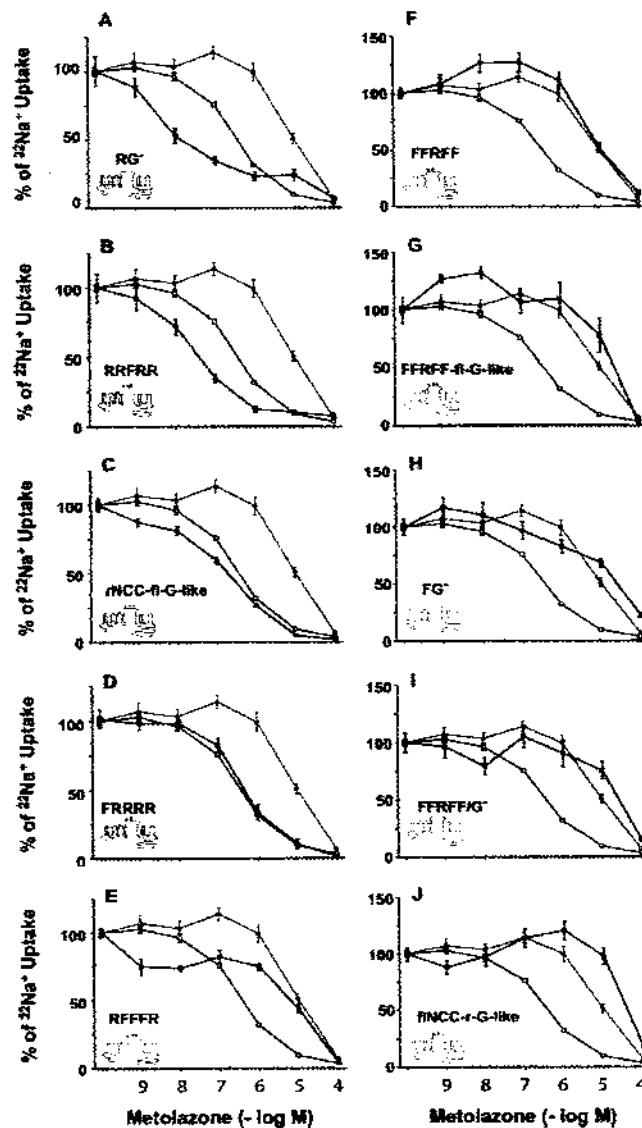
FIGURE 6. **Kinetic analyses of inhibition of cotransporter function by metolazone.** Each graph shows the dose-response curves of the mutant or chimeric protein in *black*, as stated. Each point represents the mean ± S.E. of 20 oocytes from two different experiments. For comparison purposes, in all panels, the results of rNCC and flNCC are shown in *blue* and *red lines*, respectively. For rNCC and flNCC, each point represents the mean ± S.E. of ~50 oocytes from five different experiments.

create the chimeras RFRRR, RRRFR, FFFRF, and FRFFF (Fig. 6, *lower panel*). As shown in Fig. 10A, microinjection of *X. laevis* oocytes with 25 ng of cRNA from wild-type rNCC, flNCC, or each chimera revealed transport activity in the first three chimeras. FRFFF chimera was not functional. Fig. 10B shows the metolazone dose-response curves obtained simultaneously in groups of oocytes injected with each construct. The IC_{50} values in chimeras RFRRR and FFFRF were 0.4 ± 0.002 and 0.6 ± 0.006 μM, respectively. These values are similar to that of rNCC (0.3 ± 0.005; $p = NS$) but different from flNCC (12.5 ± 1.8 μM; $p < 0.05$). In contrast, the RRRFR IC_{50} was 4.0 ± 0.08 μM. This value was different from that shown in rNCC ($p < 0.05$) but similar to flNCC ($p = NS$). Thus, metolazone affinity in chimeras containing the rNCC TM 8–12 region was similar to rNCC,

whereas the chimera with the same region from flNCC behaved as flNCC. These observations suggest that the metolazone affinity modifier residues are located within the TM 8–12 region.

The results of Na^+ and Cl^- transport kinetic analysis of these chimeras are shown in Fig. 10, *C* and *D*, respectively. The K_m values for Na^+ transport were (in mM) 22 ± 2.8 in RFRRR, 14.5 ± 0.7 in RRRFR, and 42.3 ± 12.6 in FFFRF. These values are significantly different from the Na^+ K_m value of 5.5 ± 1.0 mM observed in rNCC ($p < 0.05$) but similar to the K_m value of 30 ± 6.0 mM flNCC ($p = NS$). A different situation occurred for Cl^- transport kinetics. The apparent K_m value for Cl^- transport was 17 ± 4.6 mM in RFRRR and 12.8 ± 3.0 mM in FFFRF. These values are significantly different from rNCC K_m values for Cl^-

FIGURE 7. **Activity and metolazone affinity in wild-type rNCC and fNCC, as well as in mutant and/or chimeric cotransporters, as stated.** The level of activity of each clone is shown in the *green bars* and expressed as thiazide-sensitive $^{22}Na^+$ uptake in pmol/oocyte/h in the *left y-axes*. The affinity for metolazone is shown in the *yellow bars* and expressed as K_{50} in μM in the *right y-axes*. The uptake in cRNA-injected oocytes is ordered from the clone with higher metolazone affinity (RRFRR) to that with the lowest affinity (fNCC-r-G-like).
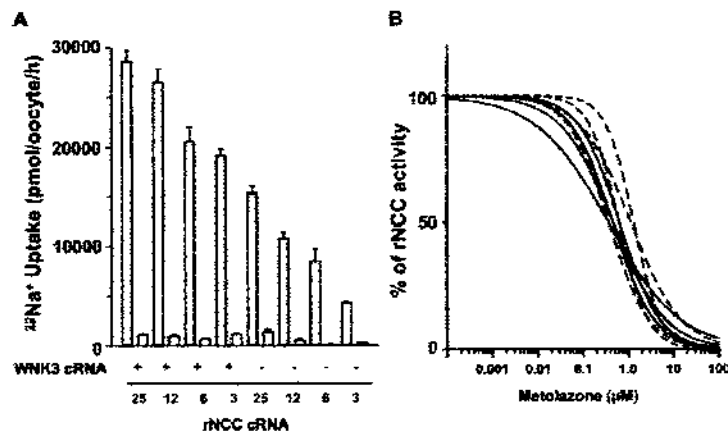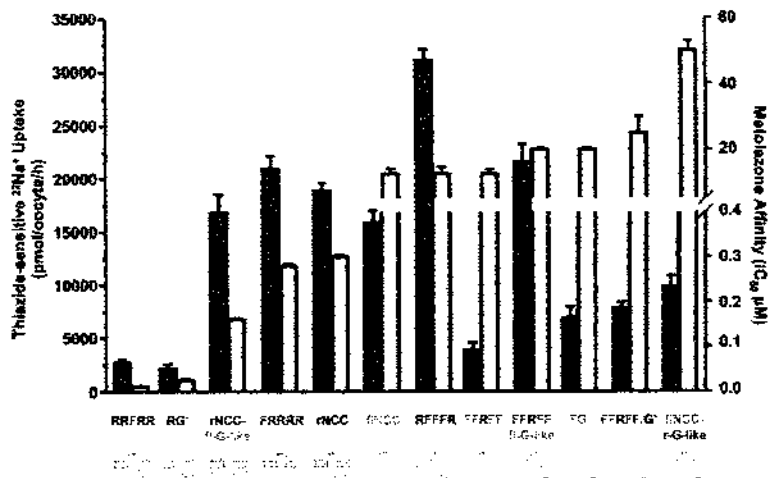
FIGURE 8. **Absence of relationship between wild-type rNCC activity and metolazone affinity.** *A*, $^{22}Na^+$ uptake in groups of oocytes injected with rNCC cRNA at 25, 12, 6, and 3 ng/oocyte in the absence (−) or presence (+) of 5 ng/oocyte of WNK3 cRNA. Uptakes were performed in the absence (*open bars*) or presence (*dashed bars*) of 100 μM metolazone. Each bar represents the mean ± S.E. of 15 oocytes/group. Uptake in water-injected oocytes was 272 ± 27 pmol/oocyte/h. *B*, kinetic analyses of the inhibition of each rNCC group by metolazone. rNCC groups are depicted by *continuous lines* and rNCC + WNK3 groups by *dashed lines*. All dose-response curves were performed the same day using the same uptake solutions and metolazone dilutions. There was no correlation between the level of activity and the IC_{50} values ($R^2 = 0.04$).
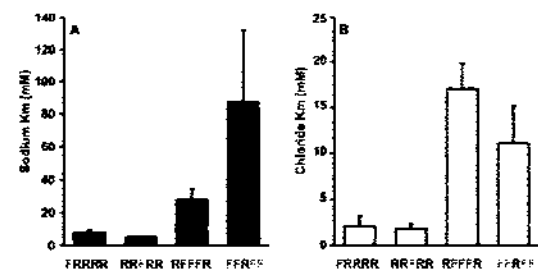
FIGURE 9. K_m **values for Na$^+$ (A) and Cl$^−$ (B) observed in oocytes injected with cRNA from chimeras FRRRR, RRFRR, RFFFR, and FFRFF, as stated.** *X. laevis* oocytes were injected with 25 ng/oocyte of each chimera cRNA, and 4–6 days later, the Na$^+$- and Cl$^−$-dependent $^{22}Na^+$ uptakes were assessed in groups of 10 oocytes/point. All experiments were done in duplicate. Curves were fitted by nonlinear regression using GraphPad Prisma software.

transport (2.6 ± 0.7 mM; $p < 0.05$) but similar to fNCC (15 ± 2.0 mM; $p =$ NS). In contrast, the apparent Cl$^−$ K_m value in RRFRR was 2.4 ± 0.7 mM. This value was similar to rNCC (2.6 ± 0.6 mM; $p =$ NS) but different from fNCC (15 ± 2.0 mM; $p > 0.05$). Thus, Cl$^−$ affinity in chimeras containing the fNCC TM 1–7 region was similar to fNCC, whereas the chimera with the same region from rNCC behaved as rNCC. These observations suggest that chloride affinity-modifying residues are located within the TM 1–7 region.

## DISCUSSION

In the present study, chimeric proteins between rNCC and fNCC were used to define ions and diuretic affinity-modifying regions. A similar approach has been successfully used by Isenring *et al.* (24–26) (for a review, see Ref. 27) between the human and shark basolateral isoform of the Na$^+$-K$^+$-2Cl$^−$ cotransporter NKCC1.

Hoover *et al.* (14) make the striking observation that elimination of N-glycosylation sites in the rat Na$^+$-Cl$^−$ cotransporter is associated with increased affinity for thiazide-type diuretics. rNCC contains two N-glycosylation sites in ECL4. Elimination of one site only (Asn 404

FIGURE 10. **Functional properties of the chimeras RFRRR, RRRFR, and FFFRF in which the TM 1–7 and 8–12 regions were swapped between fNCC and rNCC.** *X. laevis* oocytes were injected with 25 ng/oocyte of each chimera cRNA, and 4–6 days later, the functional properties were determined. *A*, level of activity is shown as ^{22}Na$^+$ uptake in the absence (*open bars*) or presence (*dashed bars*) of metolazone in water, wild-type rNCC (*blue*), fNCC (*red*), or chimeric protein-injected oocytes, as shown. *B*, kinetic analyses of inhibition of ^{22}Na$^+$ uptake by metolazone in oocytes injected with wild-type rNCC cRNA (*blue*), fNCC cRNA (*red*), and chimeric cotransporters cRNA (*black lines* and chimeric *drawn*, as shown). *C* and *D*, mean ± S.E. of the K_m values for the Na$^+$ and Cl$^-$ transport kinetic analysis, respectively, of wild-type rNCC, fNCC, and chimeric clones RFRRR, RRRFR, and FFFRF, as stated.
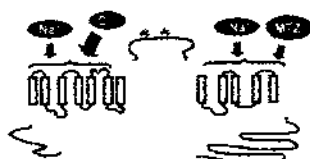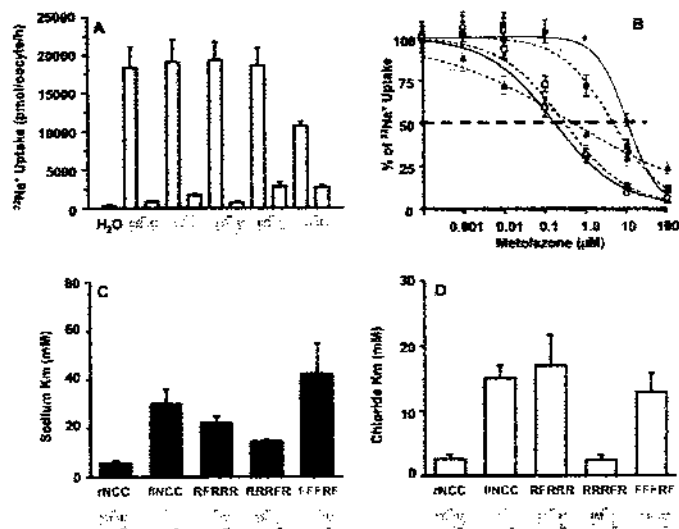
FIGURE 11. **Affinity-modifying domains in the thiazide-sensitive Na$^+$-Cl$^-$ cotransporter.**

or −424) reduced the activity of the cotransporter by ~50% and increased the affinity for metolazone in one order of magnitude from IC$_{50}$ ~1 to ~100 nM. Elimination of both sites reduces the activity by 90–95% and increases the affinity for metolazone to an IC$_{50}$ of ~10 nM. Confocal image analysis of an enhanced green fluorescent protein-tagged NCC has revealed that most of the reduction in rNCC activity, when both N-glycosylation sites were eliminated, is because of decreased surface expression of the cotransporter. In the present study, however, we observed that the consequences of N-glycosylation site elimination from fNCC were not similar to rNCC (14). Elimination of one or two N-glycosylation sites had no effect on fNCC activity, and elimination of the three sites reduced the activity of the cotransporter but only by ~50% (Fig. 3). Thiazide affinity was not affected in single, double, or triple fNCC mutants (Fig. 4). Therefore, the consequences of the N-glycosylation site elimination are different between rNCC and fNCC. In rNCC, the activity was critically reduced, and the affinity for thiazides was increased, whereas in fNCC, the activity was mildly reduced and the affinity for thiazide was not affected. In addition, any change of ECL4 in fNCC had no critical functional effects (Fig. 6). Thus, increased affinity for thiazides in rNCC, when the N-glycosylation sites are eliminated, is a unique feature of rNCC. The mechanism is not clear and will need further studies to be clarified.

In the present study, we also showed (Figs. 6 and 7) that swapping the amino- or carboxyl-terminal domains also had no effect upon thiazide affinity. In this regard, we have previously shown that interchanging these domains between NKCC2 and NCC had no effect upon bumetanide or thiazide sensitivity (16). All of these data together suggest that affinity-modifying residues for thiazide are unlikely to be located within

ECL4 or the intracellular amino- or carboxyl-terminal domain. Instead, these residues must be located within the TM segments. The same conclusion can be reached for ion transport affinity-defining domains following our observations, shown in Fig. 9, that interchanging ECL4 or the amino- or carboxyl-terminal domains between rNCC and fNCC had no significant effect upon the K_m values for Na$^+$ or Cl$^-$ transport.

Following our observations in the present study, we propose the model shown in Fig. 11. There is no role for amino-terminal, carboxyl-terminal, and ECL4 in defining ions or thiazide affinity constants. The affinity-modifying regions for Cl$^-$ are probably located within TM segments 1–7, whereas for thiazides, within TM segments 8–12. Both regions contain affinity-modifying residues for Na$^+$. These conclusions are inconsistent with a previous proposal by Tran *et al.* (28) that thiazide and chloride ions may bind to the same site on the cotransporter. These investigators observed in membrane preparations from rat renal cortex that increased concentrations of chloride in the extracellular medium decreased the affinity binding for [^{3}H]metolazone. In a study in which the functional properties of rNCC expressed in *X. laevis* oocytes were analyzed with certain detail (20), we have also observed a relationship between ion concentrations and thiazide affinity, not only for chloride ions, but also for sodium ions. We observed that the lower the sodium or chloride concentration in the uptake medium, the higher the affinity for metolazone. Thus, it is possible that ion binding to the cotransporter may induce a conformational change on the protein that reduces the affinity for thiazides. This, however, does not imply that ions and diuretics share the same binding site.

In the basolateral isoform of the Na$^+$-K$^+$-2Cl$^-$ cotransporter NKCC1, Isenring *et al.* (27) took advantage of the kinetic differences in apparent affinity for ions and bumetanide between the shark and human isoforms to reveal that the TM 1–7 segment was the only segment defining ion transport kinetics and bumetanide affinity. No role was observed for the TM 8–12 region. Specifically, they observed that TM 2 is implicated in Na$^+$, K$^+$, and bumetanide affinity (24, 25), TM 4 in K$^+$ and Cl$^-$ affinity (26), and TM 7 in Na$^+$, K$^+$, and Cl$^-$ affinity (26). The role of TM 2 in defining kinetic properties has also been studied in NKCC2. Three alternative spliced variants known as A, B, and F, which differ in the sequence of TM 2 and the interconnecting segment

between TMs 2 and 3 exhibit different kinetic properties for Na^+, K^+, and Cl^-, as well as affinity for bumetanide (29–31). Therefore, no role for Cl^- or bumetanide affinity was observed in TM 2 from NKCC1, whereas a clear role was observed in NKCC2. Here we have shown, for the thiazide-sensitive Na^+-Cl^- cotransporter, that Cl^- affinity-modifying residues reside only in the TM 1–7 region, whereas Na^+ affinity-modifying residues reside in both the TM 1–7 and 8–12 regions. Supporting this conclusion, we have previously shown that a single nucleotide polymorphism changing the glycine residue 264 within the fourth TM segment for alanine affected the affinity of the cotransporter for Cl^- but not for Na^+ transport (32). Thus, it is likely that, among NCC, NKCC1, and NKCC2, the affinity-modifying domains are different. Further experiments will help to define shorter fragments or individual residues involved in defining NCC kinetic properties.

In summary, the present study shows that, in rat and flounder NCC, the amino-terminal domain, the carboxyl-terminal domain, and the long glycosylated loop (ECL4) are not involved in defining affinity for ions and thiazides. Affinity-modifying residues for chloride are located within TM segments 1–7 and for thiazides within TM segments 8–12, whereas both segments seem to be implicated in defining sodium affinity.

REFERENCES

1. Ellison, D. H., Velazquez, H., and Wright, F. S. (1987) *Am. J. Physiol. (Renal Fluid Electrolyte Physiol.)* 253, F546–F554
2. Plotkin, M. D., Kaplan, M. R., Verlander, J. M., Lee, W.-S., Brown, D., Poch, E., Gullans, S. R., and Hebert, S. C. (1996) *Kidney Int.* 50, 174–183
3. Chobanian, A. V., Bakris, G. L., Black, H. R., Cushman, W. C., Green, L. A., Izzo, J. L., Jr., Jones, D. W., Materson, B. J., Oparil, S., Wright, J. T., Jr., and Roccella, E. J. (2003) *JAMA* 289, 2560–2571
4. Simon, D. B., Nelson-Williams, C., Johnson-Bia, M., Ellison, D., Karet, F. E., Morey-Molina, A., Vaara, I., Iwata, F., Cushner, H. M., Koolen, M., Gainza, F. J., Gitelman, H. J., and Lifton, R. P. (1996) *Nature Genetics* 12, 24–30
5. Mastroianni, N., Defusco, M., Zollo, M., Arrigo, G., Zuffardi, O., Bettinelli, A., Ballabio, A., and Casari, G. (1996) *Genomics* 35, 486–493
6. Mastroianni, N., Bettinelli, A., Bianchetti, M., Colussi, G., de Fusco, M., Sereni, F., Ballabio, A., and Casari, G. (1996) *Am. J. Hum. Genet.* 59, 1019–1026
7. Wilson, F. H., Kahle, K. T., Sabath, E., Lalioti, M. D., Rapson, A. K., Hoover, R. S., Hebert, S. C., Gamba, G., and Lifton, R. P. (2003) *Proc. Natl. Acad. Sci. U. S. A.* 100, 680–684
8. Yang, C. L., Angell, J., Mitchell, R., and Ellison, D. H. (2003) *J. Clin. Invest.* 111, 1039–1045
9. Mayan, H., Vered, I., Mouallem, M., Tzadok-Witkon, M., Pauzner, R., and Farfel, Z. (2002) *J. Clin. Endocrinol. Metab.* 87, 3248–3254
10. Gamba, G. (2000) *Curr. Opin. Nephrol. Hypertens.* 9, 535–540
11. Gamba, G. (2005) *Physiol. Rev.* 85, 423–493
12. Gamba, G., Miyanoshita, A., Lombardi, M., Lytton, J., Lee, W. S., Hediger, M. A., and Hebert, S. C. (1994) *J. Biol. Chem.* 269, 17713–17722
13. Gerelsaikhan, T., and Turner, R. J. (2000) *J. Biol. Chem.* 275, 40471–40477
14. Hoover, R. S., Poch, E., Monroy, A., Vazquez, N., Nishio, T., Gamba, G., and Hebert, S. C. (2003) *J. Am. Soc. Nephrol.* 14, 271–282
15. Paredes, A., Plata, C., Rivera, M., Moreno, E., Vazquez, N., Munoz-Clares, R., Hebert, S. C., and Gamba, G. (2006) *Am. J. Physiol. Renal Physiol.* 290, F1094–F1102
16. Tovar-Palacio, C., Bobadilla, N. A., Cortes, P., Plata, C., De Los, H. P., Vazquez, N., and Gamba, G. (2004) *Am. J. Physiol. Renal Physiol.* 287, F570–F577
17. Vazquez, N., Monroy, A., Dorantes, E., Munoz-Clares, R. A., and Gamba, G. (2002) *Am. J. Physiol. Renal Physiol.* 282, F599–F607
18. Gamba, G., Saltzberg, S. N., Lombardi, M., Miyanoshita, A., Lytton, J., Hediger, M. A., Brenner, B. M., and Hebert, S. C. (1993) *Proc. Natl. Acad. Sci. U. S. A.* 90, 2749–2753
19. Dumont, J. N. (1970) *J. Morph.* 136, 153–180
20. Monroy, A., Plata, C., Hebert, S. C., and Gamba, G. (2000) *Am. J. Physiol. Renal Physiol.* 279, F161–F169
21. Meade, P., Hoover, R. S., Plata, C., Vazquez, N., Bobadilla, N. A., Gamba, G., and Hebert, S. C. (2003) *Am. J. Physiol. Renal Physiol.* 284, F1145–F1154
22. Landfear-Marticorena, C., and Reithmeier, R. A. F. (1994) *Biochem. J.* 302, 253–260
23. Riazhari, J., Kahle, K. T., De Los, H. P., Vazquez, N., Meade, P., Wilson, F. H., Hebert, S. C., Gimenez, I., Gamba, G., and Lifton, R. P. (2006) *Proc. Natl. Acad. Sci. U. S. A.* 102, 16777–16782
24. Isenring, P., and Forbush, III B. (1997) *J. Biol. Chem.* 272, 24556–24562
25. Isenring, P., Jacoby, S. C., and Forbush, III B. (1998) *Proc. Natl. Acad. Sci. U. S. A.* 95, 7179–7184
26. Isenring, P., Jacoby, S. C., Chang, J., and Forbush, III B. (1998) *J. Gen. Physiol.* 112, 549–558
27. Isenring, P., and Forbush, B. (2001) *Comp. Biochem. Physiol. A. Mol. Integr. Physiol.* 130, 487–497
28. Tran, J. M., Farrell, M. A., and Fanestil, D. D. (1990) *Am. J. Physiol. (Renal Fluid Electrolyte Physiol.)* 258, F908–F915
29. Plata, C., Mount, D. B., Rubio, V., Hebert, S. C., and Gamba, G. (1999) *Am. J. Physiol. (Renal Physiol.)* 276, F359–F366
30. Plata, C., Meade, P., Vazquez, N., Hebert, S. C., and Gamba, G. (2002) *J. Biol. Chem.* 277, 11004–11012
31. Gimenez, I., Isenring, P., and Forbush, B. III (2002) *J. Biol. Chem.* 277, 8767–8770
32. Moreno, E., Tovar-Palacio, C., De Los, H. P., Guzman, B., Bobadilla, N. A., Vazquez, N., Riccardi, D., Poch, E., and Gamba, G. (2004) *J. Biol. Chem.* 279, 16553–16560

A Single Nucleotide Polymorphism Alters the Activity of the Renal Na+:Cl- Cotransporter and Reveals a Role for Transmembrane Segment 4 in Chloride and Thiazide Affinity*

Erika Moreno‡, Claudia Tovar-Palacio‡, Paola de los Heros‡, Blanca Guzmán§,
Norma A. Bobadilla‡, Norma Vázquez‡, Daniela Riccardi¶, Esteban Poch§, and Gerardo Gamba‡||

From the ‡Molecular Physiology Unit, Instituto de Investigaciones Biomédicas, Universidad Nacional Autónoma de México and Instituto Nacional de Ciencias Médicas y Nutrición Salvador Zubirán, Tlalpan 14000, Mexico City, Mexico, §Servicio de Nefrología, IDIBAPS, Hospital Clínic, 08036 Barcelona, Spain, and ¶School of Biological Sciences, University of Manchester, Manchester M13 9PT, United Kingdom

The thiazide-sensitive Na+:Cl- cotransporter is the major salt transport pathway in the distal convoluted tubule of the kidney, and a role of this cotransporter in blood pressure homeostasis has been defined by physiological studies on pressure natriuresis and by its involvement in monogenic diseases that feature arterial hypotension or hypertension. Data base analysis revealed that 135 single nucleotide polymorphisms along the human SLC12A3 gene that encodes the Na+:Cl- cotransporter have been reported. Eight are located within the coding region, and one results in a single amino acid change; the residue glycine at the position 264 is changed to alanine (G264A). This residue is located within the fourth transmembrane domain of the predicted structure. Because Gly-264 is a highly conserved residue, we studied the functional properties of this polymorphism by using in vitro mutagenesis and the heterologous expression system in Xenopus laevis oocytes. G264A resulted in a significant and reproducible reduction (~50%) in ^{22}Na+ uptake when compared with the wild type cotransporter. The affinity for extracellular Cl- and for thiazide diuretics was increased in G264A. Western blot analysis showed similar immunoreactive bands between the wild type and the G264A cotransporters, and confocal images of oocytes injected with enhanced green fluorescent protein-tagged wild type and G264A cotransporter showed no differences in the protein surface expression level. These observations suggest that the G264A polymorphism is associated with reduction in the substrate translocation rate of the cotransporter, due to a decrease in the intrinsic activity. Our study also reveals a role of the transmembrane segment 4 in defining the affinity for extracellular Cl- and thiazide diuretics.

The thiazide-sensitive Na+:Cl- cotransporter (TSC,[1] gene symbol, SLC12A3; locus ID 6559) is the major NaCl transport

pathway in the apical membrane of the mammalian distal convoluted tubule and the teleost urinary bladder (1–7). The fundamental role of the Na+:Cl- cotransporter encoded by the SLC12A3 gene in preserving the extracellular fluid volume and divalent cation homeostasis has been firmly established by the identification of inactivating mutations of this gene as the cause of Gitelman's disease (8–10), an inherited disorder featuring arterial hypotension, hypokalemic metabolic alkalosis with hypocalciuria, hypomagnesemia, and renal salt wasting. TSC also serves as the target for the thiazide-type diuretics that are currently recommended as the drug of choice for treatment of hypertension (11). Finally, a defect in TSC regulation by the WNK1 and WNK4 kinases has been implicated in the pathogenesis of a salt-dependent form of human hypertension known as pseudohyopaldosteronism type II (12, 13), which features marked sensitivity to hydrochlorothiazide and a clinical picture that is a mirror image of Gitelman's disease (hypertension, hyperkalemia, and metabolic acidosis) (14). Taken together, all these observations suggest that TSC molecular variants, resulting from single nucleotide polymorphisms (SNPs), could contribute to the normal variations in blood pressure in the population at large, to the inherited predisposition toward essential hypertension, and/or to the differential response to diuretic therapy.

Despite the important role of TSC in cardiovascular physiology, pharmacology, and pathophysiology, little is currently known about the structure-function relationships in this cotransporter. By using [³H]metolazone binding to membrane preparations from rat renal cortex, Tran et al. (15) proposed that thiazides and Cl- share the same binding site. Recent studies in which the functional properties of the cloned cotransporter were determined, however, provided evidence that metolazone competes with both Na+ and Cl- ions (16), suggesting that the thiazide-binding site may be shared by both ions and not only by Cl-, as suggested by Tran et al. (15). In addition, nothing is known regarding domains or amino acid residues defining the TSC ion transport kinetics or thiazide affinity. So far, within the family of electroneutral cotransporters, some aspects of the structure-function relationships have been investigated only in the two isoforms of the Na+:K+:2Cl- cotransporter, BSC1/NKCC2 and BSC2/NKCC1. Results between both isoforms, however, have shown important differences suggesting that conclusions reached in one member of the family cannot be extended to the other members. For example, in BSC2/NKCC1, Isenring et al. (17, 18) have implicated transmembrane domains 4 and 7 in defining Cl- transport affinity, whereas recent studies (19–21) in BSC1/NKCC2

[1] The abbreviations used are: TSC, thiazide-sensitive Na+:Cl- cotransporter; EGFP, enhanced green fluorescent protein; SNPs, single nucleotide polymorphisms; WT, wild type.

clearly showed that transmembrane domain 2 contains affinity modifier residues for extracellular Cl⁻.

In the present study we show that an SNP that changes one amino acid residue in TSC results in a dramatic decrease in TSC function, apparently secondary to a decrease in the intrinsic activity of the cotransporter, and reveals a role of transmembrane segment 4 in TSC affinity for extracellular Cl⁻ and for thiazide diuretics.

MATERIALS AND METHODS

An extensive search of genome data bases (lpgws.nci.nih.gov/cgi-bin/GeneViewer.cgi; ncbi.nlm.nih.gov/SNP) was performed to find the SNPs that have been informed within the *SLC12A3* gene. The SNPs within the coding regions that were considered as potentially important were incorporated into the rat TSC cDNA by using the QuickChange site-directed mutagenesis system (Stratagene) following the manufacturer's recommendations. Automatic DNA sequencing was used to corroborate all the mutations. All primers used for mutagenesis were custom-made (Sigma).

Genotyping of the G264A Polymorphism—A restriction fragment length polymorphism method was created for the G264A polymorphism to confirm it and to simplify its detection in 200 normal subjects. Total genomic DNA was extracted from whole blood according to standard procedures. PCR was conducted using 125 ng of genomic DNA using the primer pair sense 5′-AGACCGTGCGGGACCTGCTC-3′ and antisense 5′-CCTCCTCCATGGCCTCCTCACCTT-3′. PCR was conducted for 34 cycles with denaturation at 96 °C for 30 s, annealing at 60 °C for 30 s, and extension at 72 °C for 30 s, with a final extension step at 72 °C for 5 min. The G264A variant was recognized by restriction fragment length polymorphism by using Btg1 (New England Biolabs), and the restriction fragments were separated on 7.5% PAGE, and visualized under ultraviolet light after staining with ethidium bromide. The polymorphism was confirmed by automatic sequencing (AbiPrism®) in all positive cases.

Assessment of the Na⁺:Cl⁻ Cotransporter Function—Oocytes were harvested from anesthetized adult female *Xenopus laevis* frogs, defolliculated, and prepared for microinjection following our standard procedure (16, 19). The next day mature oocytes were injected with 50 nl of water or cRNA transcribed *in vitro*, using the T7 RNA polymerase mMESSAGE kit (Ambion), at a concentration of 0.5 μg/μl. Oocytes were then incubated for 3 days in ND96 with sodium pyruvate and gentamicin and 1 day in Cl⁻-free ND96 (16). The function of the Na⁺:Cl⁻ cotransporter was determined by assessing tracer ²²Na⁺ uptake (PerkinElmer Life Sciences) in groups of at least 15 oocytes following our standard protocol (16): 30 min of incubation in a Cl⁻-free ND96 medium containing 1 mM ouabain, 0.1 mM amiloride, and 0.1 mM bumetanide, followed by a 60-min uptake period in a K⁺-free, NaCl medium containing some drugs plus 2 μCi of ²²Na⁺ per ml. Gluconate was used as a Cl⁻ substitute and N-methyl-D-glucamine as a Na⁺ substitute. At the end of the uptake period tracer activity was determined for each dissolved oocyte by β-scintillation counting.

Western Blotting—Western blot analysis was used to compare WT with mutant protein in cRNA-injected oocytes following our standard protocol (22). In brief, groups of 15 oocytes injected with water or cRNA were homogenized in 2 μl/oocyte of homogenization buffer and centrifuged twice at 100 × g for 10 min at 4 °C, and the supernatant was collected. Protein extracts from oocytes (four oocytes per lane) were heated in sample buffer containing 6% SDS, 15% glycerol, 0.3% bromphenol blue, 150 mM Tris, pH 7.6, and 2% β-mercaptoethanol, resolved by Laemmli SDS- 7.5% PAGE, and transferred to a polyvinylidene difluoride membrane. For immunodetection we used a rabbit polyclonal anti-rat TSC antibody (generously provided by Dr. Mark Knepper, National Institutes of Health), diluted 1:1000 (23). The membrane was exposed to anti-TSC antibody diluted in blocking buffer (TTBS, 0.2% Tween 20) overnight at 4 °C, subsequently washed in TTBS, and incubated for 60 min at room temperature with alkaline phosphatase-conjugated secondary (anti-rabbit) antibody (Bio-Rad) diluted 1:2000 in blocking buffer and washed again. Immunoreactive species were detected using Immun-Star Chemiluminescent Protein Detection Systems (Bio-Rad).

Assessment of the TSC Expression at the Oocytes Plasma Membrane—The surface expression of wild type or mutant TSC (see below) was determined by assessing the fluorescence in the *Xenopus* oocytes using a TSC fusion construct that we have previously validated (12, 24). In this construct, the EGFP was fused to the amino-terminal domain of TSC. *Xenopus* oocytes were then microinjected with water as control or
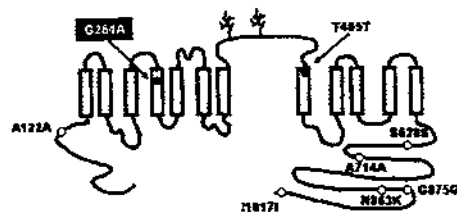
FIG. 1. **Topological model of the thiazide-sensitive Na⁺:Cl⁻ cotransporter and the localization of the eight SNPs located within the coding region.**

with EGFP-WT-TSC or EGFP-mutant-TSC cRNA. After 4 days of incubation, oocytes were monitored for EGFP fluorescence in the oocytes surface using a Zeiss laser-scanning confocal microscope (objective lens ×10, Nikon). Excitation and emission wavelengths used to visualize EGFP fluorescence were 488 and 515-565 nm, respectively. We have shown previously that EGFP-TSC fluorescence in the oocytes surface colocalizes with the F-404 specific plasma membrane dye and that oocytes injected with EGFP-TSC exhibit significant thiazide-sensitive ²²Na⁺ uptake, indicating the EGFP-TSC fluorescence is located in the plasma membrane (24). For densitometry analysis, the plasma membrane fluorescence was quantified by determining the pixel intensity around the entire oocytes circumference using SigmaScan Pro image analysis software.

Statistical Analysis—Statistical significance is defined as two-tailed $p < 0.05$, and the results are presented as mean ± S.E. The significance of the differences between means was tested with the Student's t test.

RESULTS

Single Nucleotide Polymorphisms in the SLC12A3 Gene—Up to 135 SNPs have been informed within the *SLC12A3* gene. 127 SNPs are located within intronic sequences and only eight are within exonic sequences. Fig. 1 depicts the proposed TSC topology (25) and the localization of the eight SNPs within the coding sequence. Six SNPs result in no change of the amino acid sequence. These are the SNPs A122A, T465T, S628S, A714A, G875G, and I1017I corresponding to the NCBI SNP cluster IDs rs2304479, rs5801, rs55802, rs5803, rs5804, and rs2289113, respectively. Two SNPs result in a single amino acid change. One is the R863K SNP (cluster ID rs8060046) that was considered as irrelevant because this SNP located within the carboxyl-terminal domain results in a conserved substitution of the positively charged amino acid arginine, which is present in the human cotransporter (8), for the positively charged residue lysine, which is present in the TSC from rabbit, rat, mouse, and fish (2, 25–27). In contrast, the other SNP that alter the primary sequence of human TSC (ID number rs1529927) predicts a change of the nonpolar amino acid glycine at the position 264 for the residue alanine. The residue glycine is located within the fourth transmembrane domain and is a conserved amino acid residue, not only in the available TSC sequences from rat (25), mouse (27), rabbit (26), human (8), and flounder (2), but also in all members of SLC12 family that include two genes encoding Na⁺:K⁺:2Cl⁻ cotransporters (25, 28) and four genes encoding K⁺:Cl⁻ cotransporters (29–31). Thus, the G264A SNP was considered as potentially important and therefore was introduced into TSC by *in vitro* mutagenesis.

Allele Frequency of the G264A Polymorphism—A restriction fragment length polymorphism strategy was used to assess the presence of G264A SNP by PCR. The PCR product (510 bp) contained a constant Btg1 restriction site, and therefore, when digested, two bands of 461 and 49 bp, respectively, are observed in GG genotype (encoding glycine at position 264 in both alleles). In contrast, in GA genotype heterozygotes (that is one allele encoding glycine and the other encoding alanine at posi-

tion 264), a new specific Btg1 restriction site was used, and then four bands of 461, 390, 71, and 49 bp were observed. To test the allele frequency of the G264A polymorphism, 200 Caucasian subjects were genotyped. The sample included 119 males and 81 females with the following characteristics (mean ± S.D.): age 52 ± 16 years, systolic blood pressure 117 ± 11 mmHg, diastolic blood pressure 69 ± 7 mmHg, and body mass index of 24 ± 4 kg/m². None of the subjects had present or past cardiovascular conditions including hypertension, coronary heart disease, stroke, or diabetes. The frequency of the GA genotype was 2% in the sample studied. No subjects with AA phenotype were detected (that is homozygotes encoding alanine

at position 264 in both alleles). Shown in Fig. 2A is a representative gel containing the Btg1-digested PCR fragment from a normal subject and one heterozygous for the GA genotype. Fig. 2, *B* and *C*, illustrates sequencing of this region in a GG and a GA phenotype (codons GGC and GCC, respectively). Thus, our results suggest that G264A is a true SNP.

Functional Consequences of the TSC G264A Polymorphism— The functional consequences of the G264A SNP were assessed using a heterologous expression system in *X. laevis* oocytes. This expression system has been shown to be an excellent tool for a robust and reproducible expression of TSC in our hands (2, 12, 16, 24, 25, 32) and also in other laboratories (13, 27, 33, 34). In contrast, TSC expression in transfected eukaryotic cells has not been successful in many laboratories, including our own. The best expression so far observed in stably transfected eukaryotic cells (MDCK cells) with human TSC cDNA consists of small increase (~25%) over background (35). Thus, *X. laevis* oocytes were microinjected with cRNA transcribed from wild type TSC (WT) or from TSC harboring the G264A SNP (G264A). As shown in Fig. 3, WT or G264A cRNA injection induced a significant increase in $^{22}Na^+$ uptake in *X. laevis* oocytes. However, the increase in G264A-injected oocytes was of a significantly lower magnitude than the increase observed in WT oocytes. Uptake in WT-injected oocytes was 3448 ± 234 pmol oocyte^{-1} h^{-1}, whereas in G264A-injected oocytes was 1712 ± 366 pmol oocyte^{-1} h^{-1} ($p < 0.01$, $n = 20$). As shown in Fig. 3, the uptake was due to the TSC activity because a complete inhibition of uptake was observed in the absence of extracellular chloride or in the presence of the thiazide-type diuretic, metolazone. A reduction of a similar magnitude in the G264A activity was consistently observed in every single ex-

FIG. 2. *A*, example of a genotyping result for the Gly-264 → Ala (G264A) polymorphism. The polymorphism consists in a G to C transversion at codon 264 that changed the glycine-encoding codon GGC to the alanine-encoding codon, GCC. The PCR products were digested with Btg1 and resolved on SDS-PAGE: *lane 1*, molecular weight marker, *lane 2*, GA heterozygous (codon GCC); *lane 3*, GG homozygous (codon GGC), and *lane 4* (undigested PCR product). *B*, sequence of wild type and *C*, polymorphic variant G264A PCR products were excised from the gel and fully sequenced.

FIG. 3. **Functional expression of WT and G264A cotransporters in *X. laevis* oocytes.** *A*, $^{22}Na^+$ uptake in oocytes that were injected with water, with 25 ng of cRNA from WT, or from G264A. Uptake was assessed in control conditions (*open bars*), in the absence of extracellular Cl (*hatched bars*), or in the presence of 10^{-4} M of the inhibitor metolazone (*closed bars*). The absence of endogenous thiazide-inhibitable $^{22}Na^+$ uptake in *X. laevis* oocytes has been shown before (2, 16, 25). *, $p < 0.01$ *versus* WT cRNA oocytes in control conditions. $n = 20$ oocytes per bar. *B*, ethidium bromide-stained agarose gel showing 2 μl of 0.5 μg/μl of WT and G264A cRNA as stated. *C*, autoradiograms of Western blot analysis of proteins extracted from WT or G264A cRNA-injected oocytes, as stated. The analysis was performed using rabbit polyclonal anti-TSC antibodies. Comparable immunoreactivities are observed in both lanes.

periment. In order to ensure that the reduction in $^{22}Na^+$ uptake was not due to differences in the amount of cRNA injected or in the transcription rate of the protein, cRNA concentration was determined by densitometry of the corresponding bands in the ethidium bromide-stained agarose gel, and the transcribed protein was assessed by Western blot analysis of the injected oocytes. No differences were found between WT and G264A in the amount of cRNA injected (Fig. 3B), as well as in the TSC protein produced by the oocytes (Fig. 3C).

Surface Expression Analysis in EGFP-WT or EGFP-G264A— Because *X. laevis* oocytes injected with WT or G264A exhibited similar immunoreactive proteins in the Western blot, we reasoned that potential explanations for the reduction in functional expression of the TSC containing the G264A could be a decrease in the amount of the transporter that reaches the plasma membrane, a decrease in the affinity for the cotransported ions, or a decrease in the intrinsic activity of the cotransporter. To study the first possibility, we assessed the surface expression of the WT and G264A proteins by injecting *X. laevis* oocytes with the cRNA encoding the WT or G264A cotransporters that had been tagged previously with the EGFP. To perform these experiments, we used the EGFP-tagged TSC construct that we have characterized previously (24) in which the EGFP was fused to the amino-terminal domain of TSC. Then the EGFP cDNA was subcloned into the G264A TSC. The cRNA encoding the EGFP-WT or EGFP-G264A was injected into *X. laevis* oocytes. As shown in Fig. 4A, densitometry of the corresponding cRNA bands in an ethidium bromide-agarose gel ensured that similar amounts of cRNA were injected. Four days after injection, the surface expression was assessed by monitoring the EGFP fluorescence with a confocal microscope. After oocytes were analyzed in the microscope, half of them were used for protein extraction to assess the EGFP-tagged proteins by Western blot, using a rabbit polyclonal antibody against TSC, and the other half was used in a functional expression assay to determine the thiazide-sensitive $^{22}Na^+$ uptake. Western blot revealed similar immunoreactive bands

in proteins extracted from EGFP-WT- or EGFP-G264A-injected oocytes (Fig. 4B), and surface expression analysis revealed similar fluorescence intensity at the surface of oocytes injected with EGFP-WT or EGFP-G264A, respectively (representative images are shown in Fig. 4, *C* and *D*). Fig. 4, *E* and *F,* illustrates the plasma membrane fluorescence intensity analysis in 30 EGFP-WT- or 30 EGFP-G264A-injected oocytes, and the functional activity was expressed as $^{22}Na^+$ uptake in the same oocytes, respectively. Although the surface expression of both clones was comparable, the ^{22}Na uptake was reduced in G264A-injected oocytes. Thus, the G264A substitution results in a reduction in the cotransporter activity, which does not appear to be due to a decrease in the surface expression rate.

*Ion Transport Kinetics—*One potential source of reduction in the functional activity of a membrane transporter is a reduction of the affinity for the transported ions or molecules, preventing the cotransporter from reaching maximal transport capacity when incubated in regular uptake solutions. Thus, we assessed the Na$^+$ and Cl$^-$ transport kinetics in *X. laevis* oocytes injected with WT or G264A cRNA. Shown in Fig. 5, *A* and *C,* are the Na$^+$ transport kinetics analyses in WT and G264A, respectively. The K_m values for Na$^+$ transport kinetics were 7.6 ± 1.6 and 5.7 ± 1.1 mM in WT and G264A, respectively, with no significant difference between them. Shown in Fig. 5, *B* and *D,* are the Cl transport kinetic analyses. The apparent K_m value for extracellular Cl$^-$ uptake in WT (Fig. 5B) was 6.3 ± 1.1 mM. This value is similar to that reported previously for the wild type TSC (16). In contrast, the apparent K_m value in G264A-injected oocytes was 0.89 ± 0.2 mM ($p < 0.001$, $n = 3$). We repeated the same analysis in triplicate using three different batches of oocytes, and the results were similar. Thus, the G264A resulted in a significant increase in Cl$^-$ affinity on the cotransporter. This increase in ion transport affinity, however, does not explain the reduction in the cotransporter activity.

*Diuretic Inhibitory Kinetics—*Studies in which the kinetic analyses of [^3H]metolazone to renal cortex plasma membranes were assessed suggested that chloride and thiazides may com-

FIG. 5. Kinetic analysis of $^{22}Na^+$ uptake in oocytes injected with cRNA from WT (*A* and *B*) or G264A (*C* and *D*). *A* and *C*, Na^+ dependence of $^{22}Na^+$ uptake. *B* and *D*, Cl^- dependence of $^{22}Na^+$ uptake. Uptakes were performed with Na^+ or Cl^- fixed at 96 mM, varying the concentration of the appropriate counterion from 0 to 40 mM, as indicated. Uptakes were also measured in water-injected oocytes (data not shown), and the mean values for the corresponding water groups were subtracted to analyze only the $^{22}Na^+$ uptake due to each injected cotransporter. Curve fitting was performed using the Michaelis-Menten equation. Data are expressed as uptakes in pmol oocyte^{-1} h^{-1}, each point represents the mean of at least 15 oocytes.
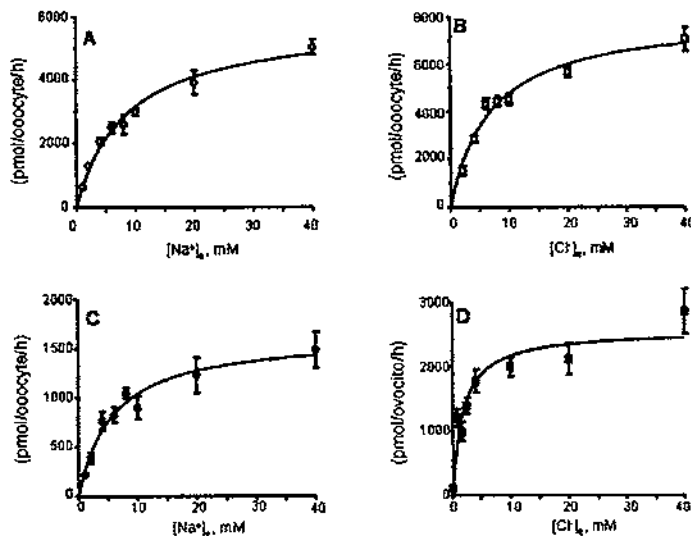
pete for the same site in the cotransporter (15). By supporting this possibility we have shown that thiazide affinity in TSC is increased when oocytes are incubated in uptake solutions containing low Cl^- concentration (16). Because an increase in Cl^- affinity in the G264A cotransporter was observed, we assessed the dose-response simultaneously on TSC and G264A for the thiazide-type diuretic metolazone in order to determine the thiazide affinity on each cotransporter. As shown in Fig. 6, when uptakes were performed in 96 mM NaCl (*closed symbols and solid lines*), the IC_{50} value for metolazone-induced reduction in $^{22}Na^+$ uptake was similar between WT and G264A. The IC_{50} value in both was ~1 × 10^{-6} M, which is similar to the IC_{50} value that we have reported previously for rat TSC (16). However, because the K_m for extracellular Cl^- in WT TSC is below 10 mM and in G264A below 1 mM, it is possible that competition between chloride and thiazides does not become apparent by using 96 mM of extracellular Cl^-. Thus, we performed the metolazone dose-response inhibitory curve in the same experiment, but using another group of oocytes in which uptake was done using an extracellular Cl^- concentration around the K_m values for this ion, that is ~6 mM for TSC and 1 mM for G264A (*open symbols* and *dashed lines*). As we have shown before (16), the metolazone IC_{50} value in the oocytes injected with WT-TSC changed from −1 × 10^{-6} to ~3 × 10^{-7} M, suggesting that metolazone binding to the cotransporter is enhanced when extracellular chloride is lower. In oocytes injected with G264A cRNA, the shift to the left was more dramatic than in WT-TSC because metolazone IC_{50} changed from ~8 × 10^{-7} M in the presence of 96 mM Cl to ~1 × 10^{-8} M when extracellular Cl^- concentration was 1 mM. To test the possibility that the G264A SNP not only affects the affinity for thiazides, but also the diuretic inhibitory profile, we also assessed the dose-response to several thiazides. This experiment was performed simultaneously in WT and G264A-injected oocytes. Therefore, each of the thiazide dilutions that were used was the same for both WT and G264A oocytes. As shown in Fig. 7, the thiazide inhibitory profile of polythiazide > bendroflumethiazide = trichloromethiazide = benzthiazide > hydrochlorothiazide = chlortalidone was similar between WT and G264A TSC cotransporters, suggesting that the G264A substitution increases the affinity of
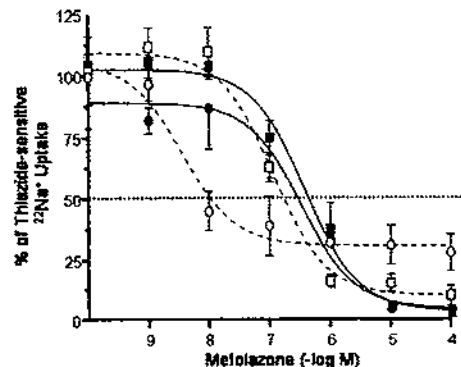
FIG. 6. Concentration-response for inhibition of WT (*squares*) and G264A (*circles*) by metolazone. Groups of 15 oocytes microinjected with WT or G264A were exposed to increased concentrations of metolazone in the preincubation and uptake mediums, from 10^{-9} to 10^{-4} M. Uptakes were performed in the presence of 96 mM of extracellular Cl^- in both WT and G264A (*solid lines* and *closed symbols*) or in the presence of 6 mM of extracellular Cl^- for WT (*open squares* and *dashed lines*), or 1 mM of extracellular Cl^- for G264A (*open circles* and *dashed line*). Data were normalized as the percentage of influx, taking 100% as the value observed in oocytes in which uptake was performed in the absence of metolazone. Each point represents the mean ± S.E. of at least 15 oocytes.

the cotransporter for thiazides but does not affect the inhibitory profile.

Role of the Conserved Residues in the Transmembrane Segment 4—As shown in Fig. 8, the alignment analysis of the transmembrane domain 4 in the electroneutral cotransporter family members revealed that Gly-264 is not the only residue that is conserved in all cotransporters. In addition to Gly-264, the residues Asn-258, Arg-261, and Gly-278 are also conserved in all members of the family. Thus we performed similar substitutions of these residues and analyzed the effects upon the functional properties of the cotransporter. As shown in Fig. 9,
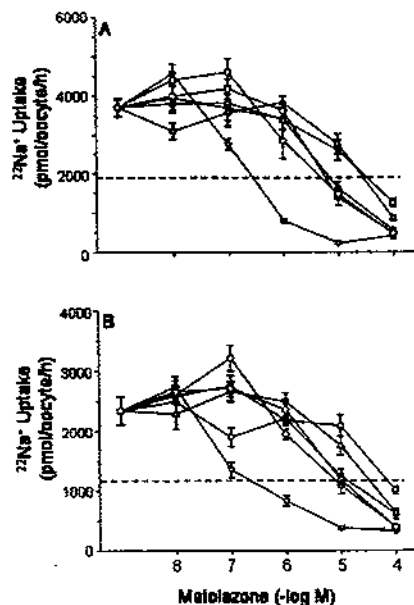
FIG. 7. **Kinetic analyses of the inhibition of WT (A) or G264A (B) function by several thiazide-type diuretics.** All Na^+ uptakes were preformed during 60 min with thiazides tested at concentrations from 10^{-8} to 10^{-4} M in uptake solution containing 40 mM Na^+ and 96 mM Cl^-. Each point represents the mean ± S.E. of at least 15 oocytes. The inhibitory profile polythiazide (▽) > metolazone (not shown) > bendroflumethiazide (◇) = trichloromethiazide (○) = benzthiazide (·) > hydrochlorothiazide (□) = chlortalidone (△) is similar between WT and G264A.

FIG. 8. **Alignment of the amino acid residues that in the electroneutral cation-chloride cotransporters correspond to the transmembrane domain 4, according with the topology analysis that has been performed for BSC2 (53).** Amino acid numbers correspond to the TSC sequence.

substitution of these residues resulted in different magnitudes of reduction in the TSC activity. The effect was similar between G264A and N258Q (~50% reduction). Further reduction in the activity was observed in the R261L transporter, whereas the G278A substitution resulted in a complete block of the cotransporter activity. To find out if the decrease in activity was associated or not with a decrease in the surface expression of the cotransporters, *X. laevis* oocytes were injected with similar amounts of cRNA transcribed from the EGFP-tagged wild type TSC or the EGFP-tagged TSC containing the substitutions, and confocal microscopy analysis of the oocytes was performed 4 days later for assessing the fluorescence intensity at the surface. Most interesting, as shown in Fig. 10, there were no significant differences among all groups. Thus, mutations in TSC on any of the conserved residues in the transmembrane segment 4 produce cotransporters in which the intrinsic activ-

ity is reduced. Finally, the ion transport kinetics analysis revealed that in TSC harboring the N258Q and R261L substitutions, the K_m values for extracellular Na^- were 7.3 ± 0.7 and 8.9 ± 2.3 mM, respectively, and for extracellular Cl^- were 3.2 ± 0.7 ($p < 0.05$, $n = 4$) and 3.2 ± 1.6 mM ($p =$ not significant, $n = 4$), respectively. Thus, no change was observed in the affinity for extracellular Na^+, whereas a slight increase was observed in the affinity for Cl^-.

DISCUSSION

One hundred and thirty five SNPs have been informed along the *SLC12A3* gene that encodes the thiazide-sensitive Na^-:Cl^- cotransporter of the renal distal convoluted tubule. Only eight of the 135 SNPs are located within exonic sequences, and one of them, the SNP G264A, results in a significant change of a single amino acid residue. We showed that in our population the distribution of this SNP is 98% homozygous for G264G and 2% for heterozygous G264A. This frequency is different from that shown previously by Melander *et al.* (36) to be ~91% for homozygous G264G, ~8% for heterozygous G264A, and ~1% for homozygous A264A. When expressed in the heterologous system of *X. laevis* oocytes, G264A exhibited a reduced maximal transport capacity to about 50% that shown in simultaneous experiments with WT-TSC. As shown by Western blot analysis, the lower activity of the TSC harboring the G264A substitution does not appear to be due to reduced translation of the protein because densitometric analysis demonstrated no differences in the amount of TSC protein produced with or without the G264A substitution. The surface image analysis that was assessed by confocal microscopy in *X. laevis* oocytes injected with EGFP-tagged WT or G264A cRNA revealed that reduced translocation of the cotransporter to the cell surface is not responsible for the lower activity in G264A, because surface expression in the plasma membrane was comparable between EGFP-WT and EGFP-G264A, whereas the $^{22}Na^-$ uptake experiments performed with the EGFP-WT- or EGFP-G264A-injected oocytes revealed a significant reduction in TSC activity in the presence of the G264A substitution. Thus, by taking all these data together; we propose that the lower activity in TSC harboring the G264A substitution is due to a reduced ion translocation rate; *i.e.* due to a decrease in the intrinsic activity of the cotransporter. A similar negative effect on the intrinsic activity or on the receptor signaling capacity has been documented for the SNP I89V and the SNP S268P that occur in the human high affinity choline transporter (37) and in the human μ-opioid receptor (38), respectively.

The observation in the present study of one SNP in the renal Na^+:Cl^- cotransporter that results in reduction of the cotransporter intrinsic activity suggests a number of testable hypotheses. For example, this SNP may be probably less prevalent in hypertensive patients than in normal subjects, or individuals harboring this SNP probably are less sensitive to treatment with thiazide drugs. In addition, it is well known that TSC activity inversely correlates with calcium reabsorption in the distal tubule (39) and that chronic thiazide treatment is associated with increased bone density (40), which is a protective factor against osteoporosis (41, 42). Therefore, another hypothesis could be that SNP G264A is less prevalent in patients with osteoporosis than the general population.

One study addressed the genotype frequency distribution on this G264A SNP in 264 normal and 292 hypertensive subjects from Sweden (36), and no difference was observed between normotensive and hypertensive subjects. It is possible, however, that more hypertensive patients will need to be studied in order to reveal the association between hypertension and certain SNPs. For example, Baker *et al.* (43) have shown that the T594M mutation in the β-subunit of the epithelial sodium

FIG. 9. **Functional expression of WT and TSC harboring the substitutions G264A, N258Q, R261L, or G278A.** The $^{22}Na^+$ uptake was determined in groups of oocytes that were injected with water or with 25 ng of cRNA from the WT or substituted mutants (as stated). Uptake was assessed in control conditions (*open bars*) or in the presence of 10^{-4} M of the inhibitor metolazone (*closed bars*). *, $p < 0.01$ *versus* WT cRNA oocytes in control conditions. $n = 20$ oocytes per bar.
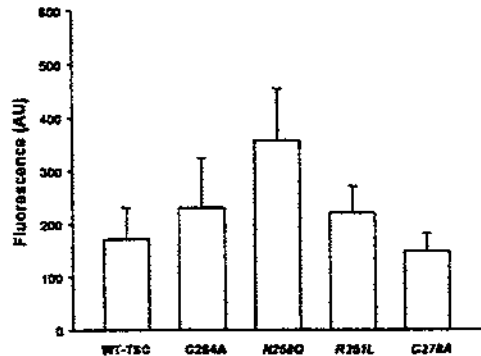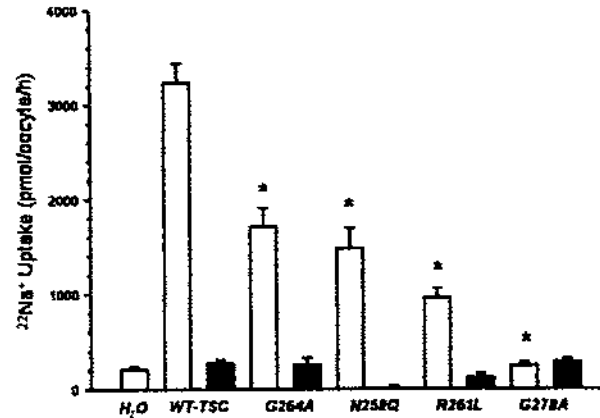
FIG. 10. **Surface abundance of EGFP-tagged WT or EGFP-tagged TSC harboring the substitutions G264A, N258Q, R261L, or G278A, as stated.** Oocytes were injected with corresponding cRNA, and green fluorescence was assessed by confocal microscopy as described under "Materials and Methods." The mean and standard error of fluorescence is shown for each set of eight oocytes per injection in arbitrary units.

channel correlates with the development of hypertension only in black patients with low renin hypertension, and Zhu *et al.* (44) observed that in white patients, but not in black hypertensive subjects, there is a significant association between the intron 2 conversion allele of the aldosterone synthase gene and the development of essential hypertension.

Regardless of the potential role in the disease discussed above, the G264A SNP reveals a role of the transmembrane domain 4 in the affinity for extracellular Cl^- and also for thiazides. We observed that TSC harboring the G264A exhibits an increase in the affinity for extracellular Cl^-, because the apparent K_m value for extracellular Cl^- in G264A was almost 10 times lower than in WT. This increase in affinity for Cl^- was specific for this ion because no change was observed in the affinity for extracellular Na^+. Glycine is a non-hydrophobic residue at position 264, which is predicted to be located in the TSC putative transmembrane domain 4 and is conserved in all species in which TSC has been sequenced, including human (8), rat (25), mouse (27), rabbit (26), and flounder (2), as well as among all members of the SLC12 family including TSC, two $Na^+:K^+:2Cl^-$, and four $K^+:Cl^-$ cotransporter isoforms. Previous studies in the basolateral isoform of the $Na^+:K^+:2Cl$

cotransporter (18, 45) indicated that transmembrane helix 4 contains affinity-modifying residues for Cl^- translocation. In addition to Gly-264, there are three other residues within the transmembrane domain 4 that are conserved among all members of the SLC12 family (Fig. 8). We observed that substitution of each of these residues resulted in $Na^-:Cl^-$ cotransporters with reduced intrinsic activity, and one of them also exhibited increased affinity for extracellular Cl^-. Thus, as has been suggested by Isenring *et al.* (18) in the $Na^-:K^-:2Cl^-$ cotransporter BSC2/NKCC1, it is possible that transmembrane segment 4 in TSC also plays a role in defining the affinity for extracellular chloride. The G278A substitution resulted in a non-functional protein, without affecting the surface expression rate, suggesting that this glycine is completely necessary for the cotransporter to reach its functional conformation state.

The structural mechanisms by which glycine substitution in the TSC fourth transmembrane domain produces the observed changes in its functional properties are not clear, but some hypotheses can be proposed. Glycine is an amino acid residue that plays an important structural role, because this residue allows unusual main chain conformations in proteins. This is probably why glycine is one of the amino acid residues that show high proportion of conservation among homologous protein sequences (46). Although not yet studied in cotransporters, it has been shown in several enzymes that some glycine residues can be important to define the protein flexibility because this residue can be part of a hinge (47-50), and the extent of rigidity or flexibility in a given hinge has been proposed to play a role in the affinity of the protein for its ligand (51). Thus, one possibility is that the presence of glycine at position 264 provides certain flexibility that in TSC might affect both rates of transport and anion binding. Alternatively, because the four residues that we studied, conserved among all members of the SLC12 family, are hydrophilic (two glycines, one asparagine and one arginine), it is possible that these amino acids mainly face the putative translocation pocket in the cotransporter, and the conformational change that results when these residues were substituted could render the putative translocation pocket more accessible to Cl^- ions but with reduced rates of transport. Further studies will be necessary to clarify these issues

Previous studies using the binding of tracer [^3H]metolazone suggested that Cl^- ions and thiazide diuretics compete for the same site on the cotransporter (15). Supporting this hypothesis, we have shown that in TSC the higher affinity for chloride

is accompanied by a higher affinity for thiazide diuretics. On one hand, the affinity for thiazides is shifted to the left when dose-response curves are performed in low extracellular Cl^- concentrations (16, 32), and on the other hand, the prevention of glycosylation in rat TSC increases the affinity for both extracellular Cl^- and thiazides (24). In the present study, we observed that G264A substitution produces a dramatic increase in Cl^- affinity, together with an increase in the affinity for the thiazide-type diuretic metolazone. This observation also supports the hypothesis that in TSC, the affinity-modifying residues for Cl^- may also be involved in defining thiazide affinity, increasing the data supporting that anions and diuretics compete for the same site on the cotransporter. Most interesting, while a similar type of competence between Cl^- and loop diuretics was proposed for the $Na^+:K^+:2Cl^-$ cotransporter based on studies using [^3H]bumetanide (52), the functional analysis of chimeras between the shark and human basolateral BSC2/NKCC1 revealed that changes in Cl^- transport kinetics are not accompanied by similar changes in bumetanide affinity (45).

In summary, we report here the functional characterization of a single nucleotide polymorphism in the *SLC12A3* gene that encodes the thiazide-sensitive $Na^+:Cl^-$ cotransporter. This membrane protein has been implicated in human diseases such as arterial hypertension and osteoporosis, and the pharmacological modulations of its function are currently used for treating or preventing these disorders. The studied SNP is a substitution of a glycine for alanine in the fourth transmembrane domain, which caused a significant reduction in the $Na^+:Cl^-$ transport rate, suggesting that people with this SNP could have an allele with reduced function of the cotransporter. In addition to the effect of the SNP upon the TSC activity, the G264A substitution produced an increase in the affinity of the cotransporter for extracellular Cl^-, but not for Na^+, that was accompanied by an increase in the affinity for thiazide diuretics. Thus, our study represents the first detailed examination of genetic polymorphism in the *SLC12A3* gene and reveals a role of the TSC transmembrane segment 4 in anion and thiazide affinity.

REFERENCES

1. Stokes, J. B., Lee, I., and D'Amico, M. (1984) *J. Clin. Invest.* **74,** 7–16
2. Gamba, G., Saltzberg, S. N., Lombardi, M., Miyanoshita, A., Lytton, J., Hediger, M. A., Brenner, B. M., and Hebert, S. C. (1993) *Proc. Natl. Acad. Sci. U. S. A.* **90,** 2749–2753
3. Kunau, R. T., Weller, D. R., and Webb, H. L. (1975) *J. Clin. Invest.* **56,** 401–407
4. Velazquez, H., Good, D. W., and Wright, F. S. (1984) *Am. J. Physiol.* **247,** F904–F911
5. Costanza, L. S. (1985) *Am. J. Physiol.* **248,** F527–F535
6. Ellison, D. H., Velazquez, H., and Wright, F. S. (1987) *Am. J. Physiol.* **253,** F546–F554
7. Plotkin, M. D., Kaplan, M. R., Verlander, J. M., Lee, W.-S., Brown, D., Poch, E., Gullans, S. R., and Hebert, S. C. (1996) *Kidney Int.* **50,** 174–183
8. Simon, D. B., Nelson-Williams, C., Johnson-Bia, M., Ellison, D., Karet, F. E., Morey-Molina, A., Vaara, I., Iwata, F., Cushner, H. M., Koolen, M., Gainza, F. J., Gitelman, H. J., and Lifton, R. P. (1996) *Nat. Genet.* **12,** 24–30
9. Mastroianni, N., DeFusco, M., Zollo, M., Arrigo, G., Zuffardi, O., Bettinelli, A., Ballabio, A., and Casari, G. (1996) *Genomics* **35,** 486–493
10. Mastroianni, N., Bettinelli, A., Bianchetti, M., Colussi, G., de Fusco, M., Sereni, F., Ballabio, A., and Casari, G. (1996) *Am. J. Hum. Genet.* **59,** 1019–1026
11. Chobanian, A. V., Bakris, G. L., Black, H. R., Cushman, W. C., Green, L. A., Izzo, J. L., Jr., Jones, D. W., Materson, B. J., Oparil, S., Wright, J. T., Jr., and Roccella, E. J. (2003) *J. Am. Med. Assoc.* **289,** 2560–2571
12. Wilson, F. H., Kahle, K. T., Sabath, E., Lalioti, M. D., Rapson, A. K., Hoover, R. S., Hebert, S. C., Gamba, G., and Lifton, R. P. (2003) *Proc. Natl. Acad. Sci. U. S. A.* **100,** 680–684
13. Yang, C. L., Angell, J., Mitchell, R., and Ellison, D. H. (2003) *J. Clin. Invest.* **111,** 1039–1045
14. Mayan, H., Vered, I., Mouallem, M., Tzadok-Witkon, M., Pauzner, R., and Farfel, Z. (2002) *J. Clin. Endocrinol. Metab.* **87,** 3248–3254
15. Tran, J. M., Farrell, M. A., and Fanestil, D. D. (1990) *Am. J. Physiol.* **258,** F908–F915
16. Monroy, A., Plata, C., Hebert, S. C., and Gamba, G. (2000) *Am. J. Physiol.* **279,** F161–F169
17. Isenring, P., and Forbush, B., III (1997) *J. Biol. Chem.* **272,** 24556–24562
18. Isenring, P., Jacoby, S. C., Chang, J., and Forbush, B., III (1998) *J. Gen. Physiol.* **112,** 549–558
19. Plata, C., Meade, P., Vazquez, N., Hebert, S. C., and Gamba, G. (2002) *J. Biol. Chem.* **277,** 11004–11012
20. Gimenez, I., Isenring, P., and Forbush, B., III (2002) *J. Biol. Chem.* **277,** 8767–8770
21. Gagnon, E., Bergeron, M. J., Brunet, G. M., Daigle, N. D., Simard, C. F., and Isenring, P. (2003) *J. Biol. Chem.* **278,** 5648–5654
22. Meade, P., Hoover, R. S., Plata, C., Vazquez, N., Bobadilla, N. A., Gamba, G., and Hebert, S. C. (2003) *Am. J. Physiol.* **284,** F1145–F1154
23. Wang, X. Y., Masilamani, S., Nielsen, J., Kwon, T. H., Brooks, H. L., Nielsen, S., and Knepper, M. A. (2001) *J. Clin. Invest.* **108,** 215–222
24. Hoover, R. S., Poch, E., Monroy, A., Vazquez, N., Nishio, T., Gamba, G., and Hebert, S. C. (2003) *J. Am. Soc. Nephrol.* **14,** 271–282
25. Gamba, G., Miyanoshita, A., Lombardi, M., Lytton, J., Lee, W. S., Hediger, M. A., and Hebert, S. C. (1994) *J. Biol. Chem.* **269,** 17713–17722
26. Velazquez, H., Naray-Fejes-Toth, A., Silva, T., Andujar, E., Reilly, R. F., Desir, G. V., and Ellison, D. H. (1998) *Kidney Int.* **54,** 464–472
27. Kunchaparty, S., Palcso, M., Berkman, J., Zquez, H., Desir, G. V., Bernstein, P., Reilly, R. F., and Ellison, D. H. (1999) *Am. J. Physiol.* **277,** F643–F649
28. Delpire, E., Rauchman, M. I., Beier, D. R., Hebert, S. C., and Gullans, S. R. (1994) *J. Biol. Chem.* **269,** 25677–25683
29. Gillen, C. M., Brill, S., Payne, J. A., and Forbush, B., III (1996) *J. Biol. Chem.* **271,** 16237–16244
30. Payne, J. A., Stevenson, T. J., and Donaldson, L. F. (1996) *J. Biol. Chem.* **271,** 16245–16252
31. Mount, D. B., Mercado, A., Song, L., Xu, J., George, A. L., Jr., Delpire, E., and Gamba, G. (1999) *J. Biol. Chem.* **274,** 16355–16362
32. Vazquez, N., Monroy, A., Dorantes, E., Munoz-Clares, R. A., and Gamba, G. (2002) *Am. J. Physiol.* **282,** F599–F607
33. De Jong, J. C., Willems, P. H., Mooren, F. J., van den Heuvel, L. P., Knoers, N. V., and Bindels, R. J. (2003) *J. Biol. Chem.* **278,** 24302–24307
34. De Jong, J. C., Van Der Vliet, W. A., van den Heuvel, L. P., Willems, P. H., Knoers, N. V., and Bindels, R. J. (2002) *J. Am. Soc. Nephrol.* **13,** 1442–1448
35. De Jong, J. C., Willems, P. H., van den Heuvel, L. P., Knoers, N. V., and Bindels, R. J. (2003) *J. Am. Soc. Nephrol.* **14,** 2428–2435
36. Melander, O., Orho-Melander, M., Bengtsson, K., Lindblad, U., Rastam, L., Groop, L., and Hulthen, U. L. (2000) *Hypertension* **36,** 389–394
37. Okuda, T., Okamura, M., Koitabu, C., Haga, T., and Gurwitz, D. (2002) *J. Biol. Chem.* **277,** 45315–45322
38. Befort, K., Filliol, D., Decaillot, F. M., Gaveriaux-Ruff, C., Hoehe, M. R., and Kieffer, B. L. (2001) *J. Biol. Chem.* **276,** 3130–3137
39. Gesek, F. A., and Friedman, P. A. (1995) *Am. J. Physiol.* **268,** F89–F98
40. Feskanich, D., Willett, W. C., Stampfer, M. J., and Colditz, G. A. (1997) *Osteoporos. Int.* **7,** 79–84
41. Jones, G., Nguyen, T., Sambrook, P. N., and Eisman, J. A. (1995) *J. Bone Miner. Res.* **10,** 106–111
42. Schoofs, M. W., van der, K. M., Hofman, A., de Laet, C. E., Herings, R. M., Stijnen, T., Pols, H. A., and Stricker, B. H. (2003) *Ann. Intern. Med.* **139,** 476–482
43. Baker, E. H., Dong, Y. B., Sagnella, G. A., Rothwell, M., Onipinla, A. K., Markandu, N. D., Cappuccio, F. P., Cook, D. G., Persu, A., Corvol, P., Jeunemaitre, X., Carter, N. D., and MacGregor, G. A. (1998) *Lancet* **351,** 1388–1392
44. Zhu, H., Sagnella, G. A., Dong, Y., Miller, M. A., Onipinla, A., Markandu, N. D., and MacGregor, G. A. (2003) *J. Hypertens.* **21,** 87–95
45. Isenring, P., and Forbush, B. (2001) *Comp. Biochem. Physiol. A Mol. Integr. Physiol.* **130,** 487–497
46. Branden, C., and Tooze, J. (1991) *Introduction to Protein Structure*, pp. 1–302, 1st Ed., Garland Publishing Inc., New York
47. Cheng, B., Feng, J., Gadgil, S., and Tse-Dinh, Y. C. (2004) *J. Biol. Chem.* **279,** 8648–8654
48. Grant, G. A., Hu, Z., and Xu, X. L. (2001) *J. Biol. Chem.* **276,** 17844–17850
49. Zhao, G. P., and Somerville, R. L. (1993) *J. Biol. Chem.* **268,** 14921–14931
50. Rafferty, J. A., Wibley, J. E., Speers, P., Hickson, I., Margison, G. P., Moody, P. C., and Douglas, K. T. (1997) *Biochim. Biophys. Acta* **1342,** 90–102
51. Vermersch, P. S., Tesmer, J. J., Lemon, D. D., and Quiocho, F. A. (1990) *J. Biol. Chem.* **265,** 16592–16603
52. Haas, M., and McManus, T. J. (1983) *Am. J. Physiol.* **245,** C235–C240
53. Gerelsaikhan, T., and Turner, R. J. (2000) *J. Biol. Chem.* **275,** 40471–40477

Activity of the renal Na+-K+-2Cl− cotransporter is reduced by mutagenesis of N-glycosylation sites: role for protein surface charge in Cl− transport

Anahí Paredes,[1] Consuelo Plata,[1] Manuel Rivera,[1] Erika Moreno,[1] Norma Vázquez,[1]
Rosario Muñoz-Clares,[2] Steven C. Hebert,[3] and Gerardo Gamba[1]

[1]Molecular Physiology Unit, Instituto de Investigaciones Biomédicas, Universidad Nacional Autónoma de México,
and Instituto Nacional de Ciencias Médicas y Nutrición Salvador Zubirán, [2]Departamento de Bioquímica,
Facultad de Química, Universidad Nacional Autónoma de México, Mexico City, Mexico; and [3]Department
of Cellular and Molecular Physiology, Yale University Medical School, New Haven, Connecticut

Paredes, Anahí, Consuelo Plata, Manuel Rivera, Erika Moreno, Norma Vázquez, Rosario Muñoz-Clares, Steven C. Hebert, and Gerardo Gamba. Activity of the renal Na+-K+-2Cl− cotransporter is reduced by mutagenesis of N-glycosylation sites: role for protein surface charge in Cl− transport. Am J Physiol Renal Physiol 290: F1094–F1102, 2006. First published November 15, 2005; doi:10.1152/ajprenal.00071.2005.—The renal-specific Na+-K+-2Cl− cotransporter NKCC2 belongs to the SLC12 gene family; it is the target for loop diuretics and the cause of type I Bartter's syndrome. Because the NKCC2 sequence contains two putative N-linked glycosylation sites, one of which is conserved with the renal Na+-Cl− cotransporter in which glycosylation affects thiazide affinity, we assessed the role of glycosylation on NKCC2 functional properties. One (N442Q or N452Q) or both (N442,452Q) N-glycosylation sites were eliminated by site-directed mutagenesis. Wild-type NKCC2 and mutant clones were expressed in Xenopus laevis oocytes and analyzed by 86Rb+ influx, Western blotting, and confocal microscopy. Inhibition of glycosylation with tunicamycin in wild-type NKCC2-injected oocytes resulted in an 80% reduction of NKCC2 activity. Immunoblot of injected oocytes revealed that glycosylation of NKCC2 was completely prevented in N442,452Q-injected oocytes. Functional activity was reduced by 50% in N442Q- and N452Q-injected oocytes and by 80% in oocytes injected with N442,452Q, whereas confocal microscopy of oocytes injected with wild-type or mutant enhanced green fluorescent protein-tagged NKCC2 clones revealed that surface fluorescence intensity was reduced ~20% in single mutants and 50% in the double mutant. Ion transport kinetic analyses revealed no changes in cation affinity and a small increase in Cl− affinity by N442Q and N442,452Q. However, a slight decrease in bumetanide affinity was observed. Our data demonstrate that NKCC2 is glycosylated and suggest that prevention of glycosylation reduces its functional expression by affecting insertion into the plasma membrane and the intrinsic activity of the cotransporter.

bumetanide; thick ascending limb; isoforms; salt reabsorption

THE APICAL BUMETANIDE-SENSITIVE Na+-K+-2Cl− cotransporter is the most important salt transport pathway in the mammalian thick ascending limb of Henle's loop (TALH). This cotransporter is critical for salt reabsorption, countercurrent multiplication, acid-base regulation, and divalent mineral cation metabolism (10). The Na+-K+-2Cl− cotransporter protein in the TALH is the main pharmacological target of loop diuretics (19), which are extensively used in the treatment of edematous states. In addition, inactivating mutations of the Na+-K+-2Cl−

cotransporter gene in humans (36) and targeted disruption in mice (39) produce severe renal salt wasting or Bartter's syndrome, an autosomal recessive disease that is characterized by metabolic alkalosis, hypokalemia, hypercalciuria, and severe volume depletion accompanied by reduction in arterial blood pressure.

The primary structure of the kidney-specific, bumetanide-sensitive Na+-K+-2Cl− cotransporter, known as BSC1 or NKCC2, was elucidated by cloning corresponding cDNAs from rat (13), rabbit (32), mouse (21), and human kidney (36). NKCC2 belongs to the superfamily of electroneutral cation-coupled Cl− cotransporters (SLC12A), for which 9 genes have been identified, two of which encode for Na+-K+-2Cl− cotransporters: NKCC2 is the kidney-specific cotransporter that is expressed only at the apical membrane of the TALH, and NKCC1 is expressed in all tissues, either at the basolateral membrane of epithelial cells or in nonepithelial cells (11, 12). The degree of identity between both Na+-K+-2Cl− cotransporter genes is ~60 and 50% between these genes and the thiazide-sensitive Na+-Cl− cotransporter (NCC), the other Na+-coupled-to-Cl− transporter of the SLC12 family. The basic topology of the Na+-K+-2Cl− and Na+-Cl− cotransporters has been deduced from hydropathy analysis and features a central hydrophobic domain containing 12 transmembrane (TM)-spanning regions that are flanked by short NH2- and long COOH-terminal domains, presumably located within the cell. A long loop between TM *segments 7 and 8* faces the extracellular side of the protein. This topology has been experimentally confirmed only in NKCC1 (15).

NKCC1 and NKCC2 form dimers, although each monomer is thought to be fully functional (28, 38). The predicted core molecular size of the NKCC2 monomer is ~120 kDa, whereas Western blot analysis of proteins extracted from rat kidney has shown an apparent molecular size of ~160 kDa (1, 6, 23, 24). In vitro translation experiments of rat NKCC2 protein revealed an increase in apparent molecular size in the presence of canine pancreatic microsomes, which are known to express functional oligosaccharyl transferase activity, and this effect was prevented by addition of the deglycosylating enzyme endoglycosidase H (13). Thus in vivo and in vitro observations suggest that the bumetanide-sensitive cotransporter BSC1/NKCC2 is a glycosylated protein. In addition, we recently showed that the rat NCC protein is glycosylated at two sites and that elimina-

tion of the *N*-glycosylation sites produced *1*) a decrease in activity of the cotransporter secondary to a decrease in surface expression, *2*) a slight increase in affinity for extracellular Cl^-, and *3*) a large increase in affinity for the thiazide-like diuretic metolazone (20). One of the sites at which NCC is glycosylated is conserved in NKCC2. Thus the present study was carried out to elucidate the specific glycosylation sites in the renal-specific Na^+-K^+-$2Cl^-$ cotransporter NKCC2 and to determine the effects of glycosylation on transporter function.

METHODS

Extraction of crude membranes from renal kidney and Xenopus laevis oocytes. Total proteins were extracted from pooled rat renal medullas by homogenization using a Polytron homogenizer (Kinematica) in four volumes of lysis buffer (200 mM sucrose, 0.5 mM EDTA, 5 mM Tris·HCl, pH 7.0, and complete inhibitor protease cocktail). The homogenates were centrifuged at 4,000 *g* for 4 min at 4°C to remove tissue debris without precipitating plasma membrane fragments. For *N*-glycosidase F digestion, 100 μg (20 μl) of protein from kidney membranes were denatured in 0.5% SDS, 50 mM β-mercaptoethanol, 0.55 M Tris·HCl (pH 8.6), and 1 mM EDTA for 1–2 h at 4°C and diluted with Nonidet P-40 to a final concentration of 1.5% in the presence of 1 μg/ml leupeptin and 0.2 mM PMSF. After the samples were split into two aliquots, 2 U of *N*-glycanase or water (control) were added and the samples were incubated for 12–15 h at 37°C. For analysis of proteins from oocytes (see below), groups of 15 oocytes injected with water or cRNA from wild-type or mutant clones were homogenized in homogenization buffer at 2 μl/oocyte and centrifuged twice at 100 *g* for 10 min at 4°C, the supernatant was collected and centrifuged again at 14,000 rpm for 20 min, and the pellet was resuspended in loading buffer (6% SDS, 15% glycerol, 150 mM Tris, 3% bromphenol blue, and 5% β-mercaptoethanol, pH 7.6). Protein concentrations were assessed in duplicate using the DC protein assay (Bio-Rad, Hercules CA).

Immunoblotting. For Western blot analysis, 50 μg of medulla protein or protein extracts from 1–10 oocytes, with or without *N*-glycosidase F or endoglycosidase digestion, were diluted in 10 μl of loading buffer and subsequently denatured by boiling for 5 min. Proteins were resolved by SDS-PAGE and then transferred to polyvinylidene difluoride membranes (Amersham Pharmacia Biotech; 2 h at 400 mA). Prestained Rainbow markers (Amersham) were used as molecular size standards. Nonspecific binding sites were blocked for 60 min at 37°C in 500 mM NaCl-20 mM Tris-buffered saline containing 0.4% nonfat dry milk. Thereafter, membranes were incubated with 1:1,000 dilutions of the specific rabbit polyclonal antibody L320 diluted in blocking buffer (Tris-buffered saline + 0.1% Tween 20) overnight at 4°C. L320 antibody, which was raised against a peptide corresponding to residues 33–55 of the NH₂-terminal domain of rat NKCC2, was generously provided by Mark Knepper (24) and Javier Alvarez-Leefmans. Membranes were subsequently washed three times in Tris-buffered saline + 0.1% Tween 20 for 10 min and incubated for 60 min at room temperature with alkaline phosphatase-conjugated secondary (anti-rabbit) antibody (Bio-Rad) diluted 1:2,000 in blocking buffer and washed again. Immunoreactive species were detected using Immun-Star chemiluminescent protein detection systems (Bio-Rad).

Site-directed mutagenesis. Sequence analysis of the rat NKCC2 protein (Lasargene protean) revealed six asparagine residues that fit the consensus sequence for an *N*-glycosylation motif: Asn-Xaa-Ser/Thr,Xaa ≠ Pro (Fig. 1) (25). Only two (N442 and N452) were considered putative *N*-glycosylation sites, because they are located within an extracellular loop of the protein that has been shown to be glycosylated in NCC (20). The consensus sites N395 and N579 are located within TM domains, and the consensus sites N868 and N875 are located within the cytoplasmic COOH-terminal domain. One of
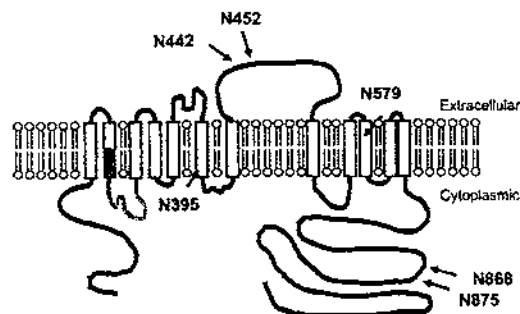
Fig. 1. NKCC2 topology and location of consensus *N*-glycosylation motifs in rat orthologs. First and 4th motifs (N395 and N579) are predicted to be located within transmembrane domains 6 and 10, respectively. Two distal motifs (N868 and N875) are predicted to be in cytoplasmic COOH-terminal domain. Only N442 and N452 are located within a putative extracellular loop and, thus, are potential *N*-glycosylation sites. N442 is a conserved site that is present in all orthologs that have been isolated from thiazide-sensitive Na^+-Cl^- cotransporter and both genes encoding Na^+-K^+-$2Cl^-$ cotransporters, NKCC1 and NKCC2 (14). Gray-shaded region is location of mutually exclusive cassette exons A, B, and F.

both *N*-glycosylation sites located at the extracellular loop was eliminated by site-directed mutagenesis (Quickchange, Stratagene) according to the manufacturer's recommendations. The custom-made (Sigma) oligonucleotides 5'-CACTGGGAGCATGCAAGACACTGTCGTTTCTG-3' and 5'-GGGATGAATTGCCAAGGGTCCG-CAGCCTGCG-3' were used to mutate the asparagine at positions 442 (N442Q) and 452 (N452Q), respectively, to glutamine in wild-type and enhanced green fluorescent protein (EGFP)-tagged NKCC2 clones. The latter primer was also used to create double mutants (N442,452Q). Automatic DNA sequencing was used to corroborate all mutations.

Heterologous expression in X. laevis oocytes. Stage V–VI oocytes were harvested from adult female *X. laevis* (Nasco, Fort Atkinson, MI) by surgery under anesthesia with 0.17% tricaine. All protocols were approved by the Institutional Animal Care and Use Committee. Oocytes were incubated for 1 h in frog Ringer ND96 (in mM: 96 NaCl, 2 KCl, 1.8 $CaCl_2$, 1 $MgCl_2$, and 5 HEPES-Tris, pH 7.4) in the presence of collagenase B (2 mg/ml), washed four times in ND96, manually defolliculated, and incubated overnight at 18°C in the same medium supplemented with 2.5 mM sodium pyruvate and gentamicin (5 mg/100 ml). Oocytes (5) were injected with 50 nl of water (control) or cRNA from wild-type or mutant clones at 0.5 μg/μl (25 ng cRNA per oocyte). cRNA was in vitro transcribed from corresponding clones using the T7 RNA polymerase mMESSAGE kit (Ambion). After injection, oocytes were incubated for 3–4 days in ND96 with sodium pyruvate and gentamicin. The incubation medium was changed every 24 h. On the night before the uptake experiments were performed, oocytes were incubated in Cl^--free ND96 (in mM: 96 sodium isethionate, 2 potassium gluconate, 1.8 calcium gluconate, 1.0 magnesium gluconate, 5 mM HEPES, 2.5 sodium pyruvate, and 5 mg/100 ml gentamicin, pH 7.4) (14).

Assessment of Na^+-K^+-$2Cl^-$ *cotransporter function.* The function of the Na^+-K^+-$2Cl^-$ cotransporter was assessed by measurement of tracer $^{86}Rb^+$ uptake (New England Nuclear) in groups of ≥15 oocytes following our general protocol (27, 33, 34): 30 min of incubation in isotonic K^+- and Cl^--free medium (mM: 96 sodium gluconate, 6.0 calcium gluconate, 1.0 magnesium gluconate, and 5 HEPES-Tris, pH 7.4) with 1 mM ouabain followed by a 60-min uptake period in the presence of Na^+, K^+, and Cl^-. For most experiments, the isotonic medium contained (mM) 96 NaCl, 10 KCl, 1.8 $CaCl_2$, 1 $MgCl_2$, and 5 HEPES, pH 7.4, and was supplemented with 1 mM ouabain and 2.0
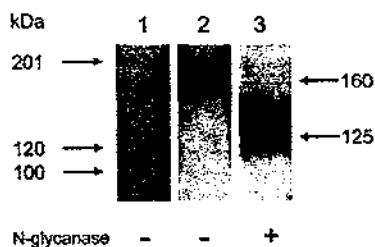
Fig. 2. Western blot analysis of proteins from liver and rat renal medulla and effect of enzymatic deglycosylation. Membrane proteins extracted from liver and rat renal medulla were isolated and exposed to N-glycosidase F (0.25 U) digestion. Proteins were separated by SDS-PAGE (6% polyacrylamide gel), transferred to polyvinylidene membranes, and incubated with polyclonal anti-NKCC2 antibody (1:1,000 dilution). *Lane 1*, liver untreated proteins. *Lane 2*, renal medulla untreated proteins. *Lane 3*, renal medulla proteins treated with N-glycanase for 15 h at 37°C. Molecular size markers (in kDa) are shown by arrows at *left*; calculated mass of NKCC2 proteins with or without N-glycanase treatment are shown by arrows at *right*.

μCi of ^{86}Rb$^-$. Because *X. laevis* oocytes express an endogenous NKCC1-type Na$^+$-K$^+$-2Cl$^-$ cotransporter (13), every experiment included control water-injected oocytes.

To analyze the ion transport kinetics of the wild-type NKCC2 or glycosylation mutants, the concentrations of each ion were varied: for Na$^+$ kinetics, the extracellular K$^+$ and Cl$^-$ concentrations were fixed at 10 and 90 mM, respectively; for K$^+$ kinetics, Na$^+$ and Cl$^-$ concentrations were fixed at 90 mM; and for Cl$^-$ kinetics, Na$^+$ and K$^+$ concentrations were fixed at 90 and 10 mM, respectively. Ionic strength and osmolarity were maintained by substitution of N-methyl-D-glucamine for Na$^+$ and K$^+$ and substitution of gluconate for Cl$^-$. The transport kinetics for a single ion (Na$^+$, K$^+$, or Cl$^-$) for water-injected control, wild-type NKCC2, N442Q, N452Q, and double-mutant groups were assessed at the same time with the same batch of oocytes and solutions. Mean values for the water-injected groups were subtracted from values for the corresponding wild-type NKCC2 or mutant groups to analyze ^{86}Rb$^+$ uptake due to the injected cRNA. The sensitivity and kinetics for bumetanide were assessed by exposure of groups of wild-type NKCC2 or mutant cRNA-injected oocytes to 10^{-9}–10^{-4} M bumetanide. The loop diuretic was present in the incubation and uptake periods.

All uptake studies were performed at 32°C. At the end of the uptake period, oocytes were washed five times in ice-cold uptake solution without isotope and dissolved in 10% SDS, and tracer activity was determined for each oocyte by β-scintillation counting.

Assessment of NKCC2 expression in oocyte plasma membrane. The surface expression of wild-type and mutant NKCC2 in the oocyte plasma membrane was measured by fluorescence microscopy using EGFP-tagged NKCC2 fusion constructs, as we previously described (27, 34). Briefly, N-glycosylation sites were eliminated in the EGFP-tagged NKCC2/pSPORT1 cDNA as described above, and cRNA from EGFP-tagged wild-type and mutant NKCC2 was transcribed in vitro and microinjected into *X. laevis* oocytes (25 ng/oocyte). After 4 days of incubation in regular ND96, EGFP fluorescence in oocytes was monitored using a Zeiss laser scanning confocal microscope (×10 objective lens, Nikon). Light of excitation wavelength at 488 nm and emission at 515-565 nm was used to visualize EGFP fluorescence. Plasma membrane fluorescence was quantified by determination of the pixel intensity around the entire oocyte circumference using SigmaScan Pro image analysis software. We previously demonstrated that this methodology can be used to quantify green fluorescent proteins in the plasma membrane of *X. laevis* oocytes (20, 27, 30).

Statistical analysis. The significance of the differences between groups was tested by one-way ANOVA or Kruskal-Wallis one-way

ANOVA on ranks, with Dunn's method for multiple comparison procedures as needed. Values are means ± SE.

RESULTS

Western blot analysis of proteins extracted from renal medulla. Immunodetection of rat NKCC2 protein from renal medulla membrane proteins revealed a broad band at ~160 kDa, similar to our previous observations and those of others with anti-NKCC2 antibodies raised against different epitopes in the NH$_2$- or COOH-terminal domain (Fig. 2) (1, 6, 23). After enzymatic deglycosylation with N-glycosidase F, the broad band was reduced to a lower band of ~120 kDa, which represents the expected core molecular size of rat NKCC2. Thus the rat renal-specific Na$^+$-K$^+$-2Cl$^-$ cotransporter is an N-glycosylated protein.

Effect of tunicamycin on glycosylation and functional expression of NKCC2. To begin to define the role of glycosylation on Na$^+$-K$^+$-2Cl$^-$ cotransporter function, NKCC2 cRNA-microinjected *X. laevis* oocytes were coinjected with vehicle or the N-glycosylation inhibitor tunicamycin (50 μg/ml) (3, 7). After 4 days, the glycosylation status and functional expression were assessed by immunoblotting and ^{86}Rb$^+$ uptake, respectively, and the results are depicted in Fig. 3. As we showed previously (13, 27, 34), microinjection of *X. laevis* oocytes with 25 ng of NKCC2 cRNA resulted in a significant increase in ^{86}Rb$^+$ uptake over that of water-injected oocytes (14,336 ±
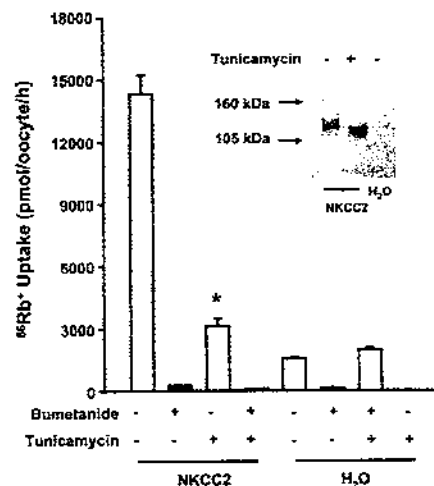
Fig. 3. Effect of tunicamycin on rat NKCC2 expression and activity in oocytes. *Xenopus laevis* oocytes were injected with water or NKCC2 cRNA alone or coinjected with tunicamycin (dissolved in DMSO). At 4 days after incubation, functional expression was determined by assessment of ^{86}Rb$^+$ uptake in the absence (open bars) or presence (solid bars) of 10^{-4} M bumetanide in groups of 15 oocytes each. *P < 0.01 vs. absence of tunicamycin. *Inset*: results from 10 oocytes used for protein extraction and immunoblot with anti-NKCC2 antibodies. *Lane 1*, protein from NKCC2-injected control oocytes: ~120-kDa band, which represents molecular core size of NKCC2 protein, and ~160-kDa band, which represents glycosylated fraction of NKCC2 protein. *Lane 2*, protein from tunicamycin-coinjected oocytes in which only 120-kDa band was expressed. *Lane 3*, protein from water-injected control oocytes.

910 vs. 1,528 ± 44 pmol·oocyte^{-1}·h^{-1}, $P < 0.01$), and the increased ^{86}Rb$^+$ uptake was completely inhibited by 10^{-4} M bumetanide. Coinjection of tunicamycin resulted in an 80% reduction in ^{86}Rb$^+$ uptake to 3,125 ± 367 pmol·oocyte^{-1}·h^{-1} ($P < 0.01$ vs. NKCC2 alone). The reduction in ^{86}Rb' uptake by tunicamycin was associated with prevention of NKCC2 N-glycosylation (Fig. 3, *inset*). Thus exposure of NKCC2-injected oocytes to the N-glycosylation inhibitor tunicamycin resulted in prevention of NKCC2 glycosylation, together with reduction of the NKCC2 functional expression, indicating that glycosylation is important for full transporter activity and/or plasma membrane expression of the renal Na$^+$-K$^+$-2Cl$^-$ cotransporter.

Characterization of wild-type and mutant NKCC2 glycosylation. To confirm that NKCC2 expressed in oocytes is also glycosylated, proteins were extracted from oocytes injected with wild-type NKCC2 cRNA and treated with N-glycosidase F. Similar to observations with renal medulla proteins (Fig. 2), the upper broad band observed in the absence of N-glycanase was reduced to a lower band of ~120 kDa, which correspond with NKCC2 core molecular size (Fig. 4A). Thus NKCC2 expressed in oocytes is also glycosylated. As shown in Fig. 3, treatment of NKCC2-injected oocytes with tunicamycin not only prevented the N-glycosylation of the cotransporter but also decreased the core molecular size by ~1–3 kDa. This slight decrease was also observed after N-glycanase treatment of proteins extracted from NKCC2-injected oocytes (Fig. 4A). The reduction in the molecular size with tunicamycin treatment suggested that the lower band may represent a high-mannose glycoprotein. It is known that N-glycosidase F removes core and N-oligosaccharide side chains of high-mannose and complex glycoproteins, whereas endoglycosidase H hydrolyzes only the high-mannose glycoproteins. Therefore to confirm that the lower band is indeed a high-mannose glycoprotein, we exposed NKCC2-injected oocyte proteins to endoglycosidase

H. Endoglycosidase treatment resulted in a similar small decrease in the size of the lower band without a change in the upper band (Fig. 4B), confirming that the upper band is a complex glycoprotein and the lower band is a high-mannose glycoprotein.

Because N-glycosylation on one site can account for 4–20 kDa (25), the 40-kDa reduction in NKCC2 migration with deglycosylation (Figs. 2 and 3) requires participation of at least two different glycosylation sites. Of the six asparagines in NKCC2 that are contained within a glycosylation motif (Fig. 1), only N442 and N452 fit the requirements known to be associated with true glycosylation; i.e., the motif is located in a loop longer than 30 amino acid residues and is exposed to the extracellular side of the protein. To determine the effects of these two predicted glycosylation sites, N442 and N452 were mutated to glutamine, and the effects of these mutations on NKCC2 protein abundance and glycosylation in *X. laevis* oocytes were assessed by Western blotting. Oocytes were injected with similar amounts of wild-type NKCC2 cRNA or with cRNA from N442Q or N452Q mutants or the double mutant N442,452Q cRNA. Mutation of N442 or N452 resulted in expression of only the lower 120-kDa band, with a faint broad band midway between the two bands shown for wild-type NKCC2 (Fig. 4C). Elimination of N442 and N452 resulted in complete loss of the upper band, with only the lower 120-kDa band remaining. No difference was observed in the amount of NKCC2 protein among the four groups. Thus elimination of both sites located in the extracellular loop between TM *segments 7* and *8* (Fig. 1) completely prevented glycosylation of the NKCC2 protein, apparently without affecting the synthesis or degradation rate of the protein, suggesting that the other N-glycosylation sites observed in the computational analysis of NKCC2 (N395, N579, N868, and N875) are not functional glycosylation sites. Because in the present study we analyzed the cell surface expression of the
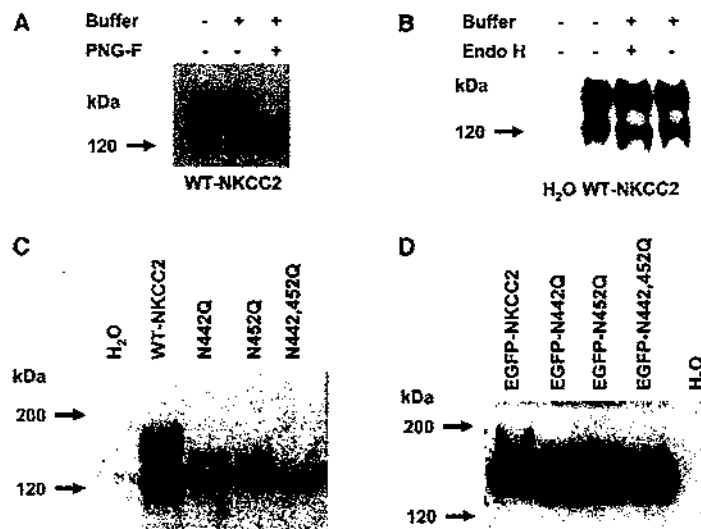
Fig. 4. Western blot analysis of membranes from oocytes injected with water, wild-type (WT) NKCC2 cRNA, N442Q cRNA, N452Q cRNA, or N442/N452Q cRNA, with or without enhanced green fluorescent protein (EGFP) tag. Oocytes were injected with water or 25 ng of cRNA in vitro transcribed from regular or EGFP-tagged wild-type NKCC2 and mutant cDNA. At 4 days after injection, proteins were isolated and separated by SDS-PAGE (7% polyacrylamide gel), transferred to polyvinylidene membranes, and incubated with anti-NKCC2 immune serum (1:500 dilution), and immunoreactive bands were visualized. A: effect of N-glycosidase F (PNG-F) treatment of proteins extracted from oocytes injected with wild-type NKCC2. B: effect of endoglycosidase (Endo H) treatment of proteins extracted from oocytes injected with wild-type NKCC2. C: immunoblot of proteins extracted from oocytes injected with wild-type or mutant NKCC2 cRNA. D: immunoblot of proteins extracted from oocytes injected with EGFP-tagged wild-type or mutant NKCC2 cRNA.

EGFP-tagged wild-type and mutant NKCC2 proteins (see below), we also assessed whether the amount of EGFP-tagged proteins was also similar among the wild-type and mutant constructs. After injection of similar concentrations of EGFP-tagged wild-type and mutant NKCC2 cRNA, we detected similar amounts of proteins by Western blot of oocyte proteins using the anti-NKCC2 antibody (Fig. 4D) or the anti-EGFP monoclonal antibody (data not shown).

To define the effect of *N*-glycosylation on $Na^+-K^+-2Cl^-$ cotransporter functional properties, we assessed $^{86}Rb^+$ uptake in *X. laevis* oocytes microinjected with wild-type NKCC2 cRNA or with N442Q, N452Q, or N442,452Q cRNA. Wild-type NKCC2-injected oocytes exhibited the expected 13-fold increase in $^{86}Rb^+$ uptake over water-injected oocytes: $17,314 \pm 814$ pmol·oocyte^{-1}·h^{-1} (Fig. 5). Whereas bumetanide-sensitive $^{86}Rb^+$ uptake was also observed in oocytes injected with cRNA from each mutant clone, transport activity was significantly lower than in wild-type NKCC2; uptake was $7,294 \pm 308$, $8,140 \pm 331$, and $3,777 \pm 150$ pmol·oocyte^{-1}·h^{-1} (all $P < 0.01$) in N442Q-, N452Q-, and double mutant-injected oocytes, respectively. The reduction in $^{86}Rb^+$ uptake in mutant clones was 58%, 53%, and 80%, respectively. Figure 5 depicts the results of a representative experiment; however, similar observations were obtained in ≥ 10 different experiments involving different batches of oocytes. In all experiments, activity of each single mutant and activity of the double mutant were ~50 and 20%, respectively, of that shown for the wild-type NKCC2-injected oocytes. Thus elimination of the *N*-glycosylation sites in NKCC2 cDNA results in a reduction of the $Na^+-K^+-2Cl^-$ cotransporter activity.

Role of glycosylation in kinetic properties of NKCC2. One mechanism for the reduction in NKCC2 functional activity in mutant clones is the effect of elimination of *N*-glycosylation sites on affinity for the cotransported ions. In a previous study, we observed that elimination of one of the *N*-glycosylation sites in the renal thiazide-sensitive Na^+-Cl^- cotransporter resulted in a slight, but significant, increase in affinity for Cl^- (20), suggesting a role for glycosylation in Cl^- transport kinetics. Thus we assessed the kinetic properties of Na^+, K^+, and Cl^- transport simultaneously in wild-type NKCC2 and mutant clones. The renal $Na^+-K^+-2Cl^-$ cotransporter gene

encodes for three alternatively spliced variants (A, B, and F), exhibiting different affinities for the three ions (34). Because the F isoform has the lowest Cl^- affinity, we used this isoform to study the effects of glycosylation on ion affinities. Results from two different experiments are shown in Table 1. The K_m values for Na^+ and K^+ uptakes in oocytes injected with mutant clones were not altered. Thus a reduced affinity for these ions cannot explain the reduced activity of the cotransporters in which the *N*-glycosylation sites were eliminated. Interestingly, however, the K_m for Cl^- significantly decreased when the N442 site was eliminated by itself or in the context of the double mutant (Table 1). In contrast, elimination of the second *N*-glycosylation site, N452, had no effect on Cl^- affinity. This finding is similar to our observation of the thiazide-sensitive Na^+-Cl^- cotransporter (20), in which elimination of the first *N*-glycosylation site also marginally increased the affinity for extracellular Cl^-. Thus changes in ion affinities cannot account for the reduction in transport activity of the *N*-glycosylation mutants.

We had also observed that elimination of the *N*-glycosylation sites in the thiazide-sensitive Na^+-Cl^- cotransporter increased affinity for the thiazide diuretic metolazone (20). Thus we also assessed the affinity of the wild-type NKCC2 and mutant clones for bumetanide. The experiment was performed in duplicate, and the dose response to bumetanide was assessed simultaneously for all control and experimental groups to obtain the kinetics of bumetanide inhibition with use of the

Table 1. *Ion transport and bumetanide-inhibitory kinetic analysis in wild-type NKCC2 and glycosylation mutants*

	WT-NKCC2	N442Q	N452Q	DM
K_m, mM				
Na$^+$	16.5±3.8	34.1±12	23.8±3.1	31.1±6.4
K$^+$	2.9±0.8	2.3±1.1	1.8±0.3	3.7±0.96
Cl$^-$	98±22	35±18*	37±18	37.8±19*
IC$_{50}$, μM				
Bumetanide	0.7±0.3	1.8±0.4*	0.9±0.2	1.9±0.3*

Values are means ± SE. WT, wild type; DM, double mutant. *$P < 0.05$ vs. WT-NKCC2.
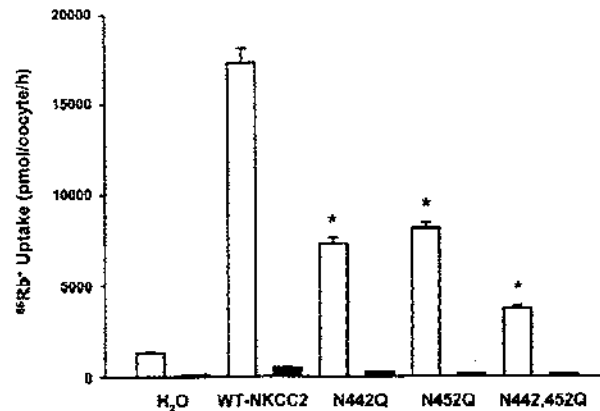
Fig. 5. Functional expression of wild-type NKCC2 and mutant cotransporters in *X. laevis* oocytes. Oocytes were injected with 25 ng of wild-type NKCC2 cRNA, N442Q cRNA, N452Q cRNA, or N442,N452Q cRNA and analyzed for $^{86}Rb^+$ uptake after 4 days of incubation. Water-injected oocytes were used as controls. Uptake was assessed in the absence (open bars) or presence (solid bars) of 10^{-4} M bumetanide in uptake medium. Values are means ± SE of 15 oocytes. *$P < 0.01$ vs. WT-NKCC2 and H$_2$O.
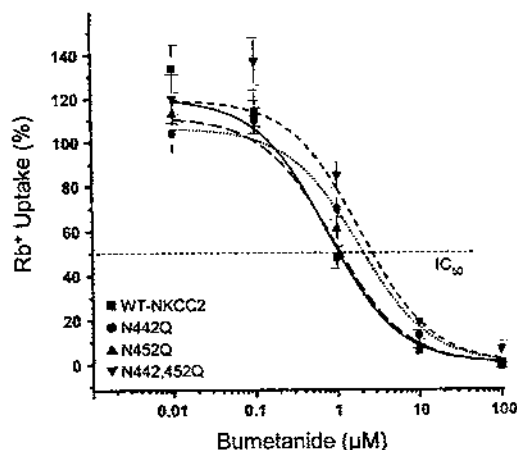
Fig. 6. Kinetics of bumetanide inhibition of wild-type NKCC2 and glycosylation mutants. Sensitivity of cotransporters to bumetanide was determined by exposure of groups of cRNA-injected oocytes to 10^{-8}–10^{-4} M bumetanide. Diuretic was present in incubation and uptake periods, and all groups were studied at the same time. Uptake in water control group was subtracted at each point from all groups to analyze only $^{86}Rb^+$ uptake due to injected cRNA. Data points represent means of percent changes in function, with uptake of each clone in the absence of bumetanide taken as 100%. Values are means ± SE of 25 oocytes from 2 different experiments.

same batch of oocytes, solutions, and bumetanide dilutions. As shown in Fig. 6 and Table 1, the affinity for bumetanide was not increased but, rather, reduced by elimination of the *N*-glycosylation sites.

Surface expression of wild-type and mutant EGFP-NKCC2 constructs in X. laevis oocytes. Another potential mechanism accounting for a reduction in the NKCC2 activity of *N*-glycosylation site mutants is a reduction in the steady-state expression of protein in the plasma membrane. Thus, to quantitatively compare the plasma membrane expression of wild-type NKCC2 vs. N442Q, N452Q, and N442,452Q NKCC2 mutants, we assessed NKCC2 surface expression by confocal fluorescence microscopy using the EGFP-tagged wild-type and mutant constructs. We previously showed (27) surface colocalization of the EGFP-NKCC2 fusion construct with plasma membrane marker FM 4-64 fluorescence in all tested oocytes, indicating that the EGFP-NKCC2 fluorescence measured at equatorial confocal sections in oocytes is indicative of expression on the plasma membrane. Images from oocytes injected with wild-type EGFP-NKCC2 or each of the EGFP-NKCC2 *N*-glycosylation mutant clones are shown in Fig. 7A, and the results of densitometric analyses are shown in Fig. 7B. Control oocytes injected with water or NKCC2 cRNA showed no significant fluorescence at the emission and excitation wavelengths for EGFP (data not shown). Fluorescence intensity in the single mutants EGFP-N442Q and EGFP-N452Q was 86 and 81%, respectively, of that observed in wild-type EGFP-NKCC2 oocytes. The difference, however, was not statistically significant. In contrast, in the double-mutant-injected oocytes, fluorescence intensity was 48% of that shown for the wild-type EGFP-NKCC2 group ($P < 0.05$).

DISCUSSION

In the present study, we show that the renal-specific Na^+-K^+-$2Cl^-$ cotransporter NKCC2 is a glycosylated protein in vivo and that N442 and N452, located in the putative extracellular domain between TM *segments 7* and *8*, are used as the

Fig. 7. Surface expression of EGFP-tagged NKCC2 and EGFP-tagged glycosylation mutants in oocytes determined by confocal microscopic fluorescence analysis. Oocytes were injected with water or 25 ng of wild-type EGFP-NKCC2 cRNA, EGFP-N442Q cRNA, EGFP-N452Q, or the double mutant EGFP-N442Q/N452Q-EGFP. Fluorescence of oocytes was visualized through a laser scanning confocal microscope and measured. *A*: confocal images of 9 oocytes in each group. *B*: fluorescence intensity. Values are means ± SE of 10 oocytes. *$P < 0.05$ vs. WT-NKCC2.

N-glycosylation sites. This observation verifies that the loop between TM *segments* 7 and 8 in NKCC2 is indeed extracellular, as has been observed in NCC (20) and in the basolateral $Na^+-K^+-2Cl^-$ cotransporter NKCCI (15). We also demonstrate that glycosylation at N442 and N452 in NKCC2 is essential for normal activity, such that elimination of one site reduces the activity of the cotransporter by ~50%, whereas elimination of both sites reduces activity by 80%. This lowered cotransporter activity in the mutant constructs was not due to nonspecific effects of the N → Q mutations per se, because prevention of glycosylation with the inhibitor tunicamycin also decreased the activity of the wild-type NKCC2.

The possible mechanisms to explain a reduction in $^{86}Rb^+$ uptake in glycosylation mutant clones include a change in the ion affinities, a decrease in the protein synthesis and/or protein expression in the plasma membrane, or a defect in the turnover rate of the cotransporter. For example, elimination of glycosylation sites reduced the activity of the GLUT-1 transporter by increasing the K_m for glucose (2). However, ion transport kinetic analyses of NKCC2 revealed no significant increases in K_m values for Na^+, K^+, or Cl^-, suggesting that a decrease in ion affinity is not responsible for the reduction of activity in glycosylation mutant proteins. Western blot analysis revealed that, when constructs with and without EGFP were used, elimination of the N-glycosylation sites had no effect on the amount of detected proteins, suggesting that protein synthesis and degradation rates were not affected. In contrast, confocal image analysis of *X. laevis* oocytes injected with cRNA transcribed from EGFP-tagged wild-type and mutant clones revealed a decrease in surface expression of the $Na^+-K^+-2Cl^-$ cotransporter only when both N-glycosylation sites were eliminated. No significant decrease in plasma membrane fluorescence signal was seen for the single N442Q and N452Q mutants, nor can the signal account for the 50% reduction in $^{86}Rb^+$ uptake observed for these mutant constructs. Moreover, the 50% reduction in surface expression of the double mutant (N442,452Q) is less than the 80% decrease in $^{86}Rb^+$ uptake (Fig. 5). Thus elimination of glycosylation sites on NKCC2 appears to reduce the intrinsic activity or turnover rate of this cotransporter. This latter possibility was also suggested for the Na^+-Cl^- cotransporter NCC, because surface expression of the double mutant was reduced 67%, whereas functional activity was decreased 92% (20). In this regard, prevention of glycosylation reduces the activity of the glycine transporter GLYT-1 (31) and the renal NaPi-2 transporter (18) because of a defect in the protein targeting the plasma membrane, whereas decrease of the Na^+-H^+ antiporter (42) and the NaSi-1 (26) cotransporter activity is due solely to reduction of the intrinsic activity of the transporters, without an effect on the surface expression. Thus it is possible that, in NKCC2, glycosylation is required not only for proper folding and intracellular trafficking of NKCC2, but also for maintaining a fully active cotransporter.

Kinetic analysis of wild-type NKCC2 and glycosylation mutants showed that prevention of glycosylation had no effect on cation transport kinetics, because no significant changes in K_m values of Na^+ or K^+ were observed. However, there was a significant decrease in the apparent K_m for Cl^- in the single mutant N442Q and in the double mutant. This increase in Cl^- affinity with elimination of the N442 site is specific for Cl^-, because it was not observed for Na^+ or K^+ and is consistent

with a similar observation in NCC (20), in which elimination of the N404 site was also associated with increased affinity for Cl^-. Interestingly, this N-glycosylation site is conserved in NKCC2, NKCC1, and NCC. Although reductions in V_{max} can increase the apparent affinity for transported ions, it seems unlikely that this is the cause for the observed change in Cl^- affinity in NKCC2 for several reasons: 1) We did not see comparable changes in the affinities for cations, which would be expected for an effect related to a reduction in V_{max}. 2) The increase in Cl^- affinity was proportionally greater than the reduction in V_{max}. 3) Although the N452Q mutant also reduced $^{86}Rb^+$ uptake by 50%, there was no effect on the affinities for cations or anions. Given these arguments, our results suggest that the Cl^- binding site is near or associated with the glycosylation site N442 or that glycosylation partially restricts the access of Cl^- to its binding site. Because complex oligosaccharides can contain sialic acid, glycosylation can contribute to the net negative external surface charge of proteins. For example, Cronin et al. (4) recently demonstrated that the shift of the conductance-voltage curves observed in deglycosylated voltage-gated Na^+ channels appears to be secondary to a change in the electrostatic charge that occurs with loss of a large negative charge, rather than a conformational change in the protein. Thus a decrease in the net negative charge at the external face of NKCC2 due to the absence or reduction of N442 glycosylation could potentially enhance access of Cl^- to one of its binding sites.

In the present study, the affinity for the loop diuretic bumetanide was decreased in N442Q and the double mutant N442,452Q. This finding is opposed to our observations in NCC, in which a large increase in the affinity for thiazides was observed (20). In this regard, on the basis of the competition between Cl^- and tracer $[^3H]$bumetanide or $[^3H]$metolazone in membrane preparations from renal medulla (17) or renal cortex (41), respectively, it has been proposed that in the electroneutral cotransporters the diuretic binding site could be the same as, or part of, the Cl^- binding site. Site-directed mutagenesis used to substitute single amino acid residues in NCC to eliminate one or two glycosylation sites (20), to introduce a single nucleotide polymorphism that switches glycine 264 to alanine (29), or to introduce a partially functional Gitelman-type mutation (35) have shown that an increase in affinity for Cl^- was accompanied in all cases by a simultaneous increase in affinity for metolazone. In contrast, chimera studies between the human colonic and shark rectal gland NKCC1 cotransporter revealed that chimeras exhibiting changes in affinity for Cl^- do not exhibit changes in affinity for bumetanide, and vice versa (22). In the present study, we observed that elimination of the N442 glycosylation site resulted in an NKCC2 cotransporter with increased affinity for Cl^-, but with decreased affinity for bumetanide. In other words, elimination of the N442 glycosylation site has an opposite effect on Cl^- and bumetanide affinity. Thus functional analyses of native, chimeric, or mutant cotransporters in heterologous expression systems have provided evidence supporting the hypothesis of Cl^- and diuretic competition in NCC, but not NKCC1 or NKCC2, cotransporters.

In the present study, the functional characteristics of wild-type and glycosylation mutant NKCC2 were assessed using the heterologous expression system in *X. laevis* oocytes. This expression system has been shown to be an excellent tool for

a robust and reproducible expression of NKCC2 in our hands (13, 27, 33, 34, 40) and in other laboratories (8, 9, 16, 37). Although pharmacology determined in oocytes may not be completely applicable to proteins in mammalian systems and NKCC2 functional analysis in mammalian cells will be preferred, NKCC2 expression in transfected mammalian cells has not been successful in any laboratories, including our own.

In summary, the present study demonstrates that the renal apical bumetanide-sensitive Na^+-K^+-$2Cl^-$ cotransporter NKCC2 is a glycosylated protein and that N442 and N452, located in the extracellular loop between TM *segments 7* and *8*, are the sites used for glycosylation. This finding provides compelling evidence that the loop between TM *segments 7* and *8* in NKCC2 is indeed extracellular. Glycosylation appears to be important for normal surface expression and maximal turnover of the transporter. In addition, the change in surface charge due to glycosylation may modulate Cl^- affinity but only slightly affect the affinity for bumetanide. Thus our results provide further evidence of a role for glycosylation in transport kinetics.

REFERENCES

1. **Amlal H and Wilke C.** Resistance of mTAL Na$^+$-dependent transporters and collecting duct aquaporins to dehydration in 7-month-old rats. *Kidney Int* 64: 544–554, 2003.
2. **Asano T, Takata K, Katagiri H, Ishihara H, Inukai K, Anai M, Hirano H, Yazaki Y, and Oka Y.** The role of *N*-glycosylation in the targeting and stability of GLUT1 glucose transporter. *FEBS Lett* 324: 258–261, 1993.
3. **Chang JY and Korolev VV.** Specific toxicity of tunicamycin in induction of programmed cell death of sympathetic neurons. *Exp Neurol* 137: 201–211, 1996.
4. **Cronin NB, O'Reilly A, Duclohier H, and Wallace BA.** Effects of deglycosylation of sodium channels on their structure and function. *Biochemistry* 44: 441–449, 2005.
5. **Dumont JN.** Oogenesis in *Xenopus laevis* (Daudin). Stages of oocyte development in laboratory-maintained animals. *J Morphol* 136: 153–180, 1970.
6. **Ecelbarger CA, Terris J, Hoyer JR, Nielsen A, Wade JB, and Knepper MA.** Localization and regulation of the rat renal Na$^+$-K$^+$-2Cl$^-$ cotransporter, BSC1. *Am J Physiol Renal Fluid Electrolyte Physiol* 271: F619–F628, 1996.
7. **Elbein AD.** Inhibitors of the biosynthesis and processing of *N*-linked oligosaccharide chains. *Annu Rev Biochem* 56: 497–534, 1987.
8. **Gagnon E, Bergeron MJ, Brunet GM, Daigle ND, Simard CF, and Isenring P.** Molecular mechanisms of Cl transport by the renal Na-K-Cl cotransporter: identification of an intracellular locus that may form part of a high affinity Cl-binding site. *J Biol Chem* 279: 5648–5654, 2003.
9. **Gagnon E, Forbush B, Flemmer AW, Gimenez I, Caron L, and Isenring P.** Functional and molecular characterization of the shark renal Na-K-Cl cotransporter: novel aspects. *Am J Physiol Renal Physiol* 283: F1046–F1055, 2002.
10. **Gamba G.** Molecular biology of distal nephron sodium transport mechanisms. *Kidney Int* 56: 1606–1622, 1999.
11. **Gamba G.** Electroneutral chloride-coupled co-transporters. *Curr Opin Nephrol Hypertens* 9: 535–540, 2000.
12. **Gamba G.** Molecular physiology and pathophysiology of electroneutral cation-chloride cotransporters. *Physiol Rev* 85: 423–493, 2005.
13. **Gamba G, Miyanoshita A, Lombardi M, Lytton J, Lee WS, Hediger MA, and Hebert SC.** Molecular cloning, primary structure and characterization of two members of the mammalian electroneutral sodium-(potassium)-chloride cotransporter family expressed in kidney. *J Biol Chem* 269: 17713–17722, 1994.
14. **Gamba G, Saltzberg SN, Lombardi M, Miyanoshita A, Lytton J, Hediger MA, Brenner BM, and Hebert SC.** Primary structure and functional expression of a cDNA encoding the thiazide-sensitive, electroneutral sodium-chloride cotransporter. *Proc Natl Acad Sci USA* 90: 2749–2753, 1993.
15. **Gerelsaikhan T and Turner RJ.** Transmembrane topology of the secretory Na$^+$-K$^+$-2Cl$^-$ cotransporter (NKCC1) studied by in vitro translation. *J Biol Chem* 275: 40471–40477, 2000.
16. **Gimenez I, Isenring P, and Forbush B III.** Spatially distributed alternative splice variants of the renal Na-K-Cl cotransporter exhibit dramatically different affinities for the transported ions. *J Biol Chem* 277: 8767–8770, 2002.
17. **Haas M and McManus TJ.** Bumetanide inhibits (Na⁺ K⁺ Cl) co-transport at a chloride site. *Am J Physiol Cell Physiol* 245: C235–C240, 1983.
18. **Hayes G, Busch A, Lotscher M, Waldegger S, Lang F, Verrey F, Biber J, and Murer H.** Role of *N*-linked glycosylation in rat renal Na/Pi-cotransport. *J Biol Chem* 269: 24143–24149, 1994.
19. **Hebert SC.** Nephron heterogeneity. In: *Handbook of Physiology. Renal Physiology.* Bethesda, MD: Am. Physiol. Soc., 1992, sect. 8, vol. 1, chapt. 20, p. 875–925.
20. **Hoover RS, Poch E, Monroy A, Vazquez N, Nishio T, Gamba G, and Hebert SC.** *N*-glycosylation at two sites critically alters thiazide binding and activity of the rat thiazide-sensitive Na$^-$:Cl$^-$ cotransporter. *J Am Soc Nephrol* 14: 271–282, 2003.
21. **Igarashi P, Vanden Heuver GB, Payne JA, and Forbush B III.** Cloning, embryonic expression, and alternative splicing of a murine kidney-specific Na-K-Cl cotransporter. *Am J Physiol Renal Fluid Electrolyte Physiol* 269: F406–F418, 1995.
22. **Isenring P and Forbush B.** Ion transport and ligand binding by the Na-K-Cl cotransporter, structure-function studies. *Comp Biochem Physiol A* 130: 487–497, 2001.
23. **Kaplan MR, Plotkin MD, Lee WS, Xu ZC, Lytton J, and Hebert SC.** Apical localization of the Na-K-Cl cotransporter, rBSC1, on rat thick ascending limbs. *Kidney Int* 49: 40–47, 1996.
24. **Kim GH, Ecelbarger CA, Mitchell C, Packer RK, Wade JB, and Knepper MA.** Vasopressin increases Na-K-2Cl cotransporter expression in thick ascending limb of Henle's loop. *Am J Physiol Renal Physiol* 276: F96–F103, 1999.
25. **Landiot-Marticorena C and Reithmeier RAF.** Asparagine-linked oligosaccharides are localized to single extracytosolic segments in multi-span membrane glycoproteins. *Biochem J* 302: 253–260, 1994.
26. **Li H and Pajor AM.** Mutagenesis of the *N*-glycosylation site of hNaSi-1 reduces transport activity. *Am J Physiol Cell Physiol* 285: C1188–C1196, 2003.
27. **Meade P, Hoover RS, Plata C, Vazquez N, Bobadilla NA, Gamba G, and Hebert SC.** cAMP-dependent activation of the renal-specific Na$^+$-K$^+$-2Cl$^-$ cotransporter is mediated by regulation of cotransporter trafficking. *Am J Physiol Renal Physiol* 284: F1145–F1154, 2003.
28. **Moore-Hoon ML and Turner RJ.** The structural unit of the secretory Na$^+$-K$^+$-2Cl$^-$ cotransporter (NKCC1) is a homodimer. *Biochemistry* 39: 3718–3724, 2000.
29. **Moreno E, Tovar-Palacio C, De Los HP, Guzman B, Bobadilla NA, Vazquez N, Riccardi D, Poch E, and Gamba G.** A single nucleotide polymorphism alters the activity of the renal Na$^+$:Cl$^-$ cotransporter and reveals a role for transmembrane segment 4 in chloride and thiazide affinity. *J Biol Chem* 279: 16553–16560, 2004.
30. **O'Connell AD, Leng Q, Dong K, MacGregor GG, Giebisch G, and Hebert SC.** Phosphorylation-regulated endoplasmic reticulum retention signal in the renal outer-medullary K$^+$ channel (ROMK). *Proc Natl Acad Sci USA* 102: 9954–9959, 2005.
31. **Olivares L, Aragón C, Giménez C, and Zafra FX.** The role of *N*-glycosylation in the targeting and activity of the GLYT1 glycine transporter. *J Biol Chem* 270: 9437–9442, 1995.
32. **Payne JA and Forbush B III.** Alternatively spliced isoforms of the putative renal Na-K-Cl cotransporter are differentially distributed within the rabbit kidney. *Proc Natl Acad Sci USA* 91: 4544–4548, 1994.
33. **Plata C, Mount DB, Rubio V, Hebert SC, and Gamba G.** Isoforms of the Na-K-2Cl cotransporter in murine TAL. II. Functional characterization

and activation by cAMP. *Am J Physiol Renal Physiol* 276: F359–F366. 1999.

34. Plata C, Meade P, Vazquez N, Hebert SC, and Gamba G. Functional properties of the apical Na⁺-K⁺-2Cl⁻ cotransporter isoforms. *J Biol Chem* 277: 11004–11012, 2002.

35. Sabath E, Meade P, Berkman J, De Los HP, Moreno E, Bobadilla NA, Vazquez N, Ellison DH, and Gamba G. Pathophysiology of functional mutations of the thiazide-sensitive Na-Cl cotransporter in Gitelman disease. *Am J Physiol Renal Physiol* 287: F195–F203, 2004.

36. Simon DB, Karet FE, Hamdan JM, Di Pietro A, Sanjad SA, and Lifton RP. Bartter's syndrome, hypokalaemic alkalosis with hypercalciuria, is caused by mutations in the Na-K-2Cl cotransporter NKCC2. *Nat Genet* 13: 183–188, 1996.

37. Starremans PG, Kersten FF, Knoers NV, van den Heuvel LP, and Bindels RJ. Mutations in the human Na-K-2Cl cotransporter (NKCC2) identified in Bartter syndrome type I consistently result in nonfunctional transporters. *J Am Soc Nephrol* 14: 1419–1426, 2003.

38. Starremans PG, Kersten FF, van den Heuvel LP, Knoers NV, and Bindels RJ. Dimeric architecture of the human bumetanide-sensitive Na-K-Cl co-transporter. *J Am Soc Nephrol* 14: 3039–3046, 2003.

39. Takahashi N, Chernavvsky DR, Gomez RA, Igarashi P, Gitelman HJ, and Smithies O. Uncompensated polyuria in a mouse model of Bartter's syndrome. *Proc Natl Acad Sci USA* 97: 5434–5439, 2000.

40. Tovar-Palacio C, Bobadilla NA, Cortes P, Plata C, De Los HP, Vazquez N, and Gamba G. Ion and diuretic specificity of chimeric proteins between apical Na⁺:K⁺:2Cl⁻ and Na⁺:Cl⁻ cotransporters. *Am J Physiol Renal Physiol* 287: F570–F577, 2004.

41. Tran JM, Farrell MA, and Fanestil DD. Effect of ions on binding of the thiazide-type diuretic metolazone to kidney membrane. *Am J Physiol Renal Fluid Electrolyte Physiol* 258: F908–F915, 1990.

42. Yusufi ANK, Szczepanska-Konkel MX, and Dousa TP. Role of *N*-linked oligosaccharides in the transport activity of the Na⁺/H⁺ antiporter in rat renal brush-border membrane. *J Biol Chem* 263: 13683–13691, 1988.

Pathophysiology of functional mutations of the thiazide-sensitive Na-Cl cotransporter in Gitelman disease

Ernesto Sabath,[1] Patricia Meade,[1] Jennifer Berkman,[2] Paola de los Heros,[1] Erika Moreno,[1] Norma A. Bobadilla,[1] Norma Vázquez,[1] David H. Ellison,[2] and Gerardo Gamba[1]

[1]Molecular Physiology Unit, Instituto Nacional de Ciencias Médicas y Nutrición Salvador Zubirán, Instituto de Investigaciones Biomédicas, Universidad Nacional Autónoma de México, Tlalpan 14000, Mexico City, Mexico; and [2]Division of Nephrology and Hypertension, Department of Medicine, Oregon Health Sciences University, Portland, Oregon 97201

Sabath, Ernesto, Patricia Meade, Jennifer Berkman, Paola de los Heros, Erika Moreno, Norma A. Bobadilla, Norma Vázquez, David H. Ellison, and Gerardo Gamba. Pathophysiology of functional mutations of the thiazide-sensitive Na-Cl cotransporter in Gitelman disease. Am J Physiol Renal Physiol 287: F195–F203, 2004. First published April 6, 2004; 10.1152/ajprenal.00044.2004.—Most of the missense mutations that have been described in the human SLC12A3 gene encoding the thiazide-sensitive Na^+-Cl^- cotransporter (TSC, NCC, or NCCT), as the cause of Gitelman disease, block TSC function by interfering with normal protein processing and glycosylation. However, some mutations exhibit considerable activity. To investigate the pathogenesis of Gitelman disease mediated by such mutations and to gain insights into structure-function relationships on the cotransporter, five functional disease mutations were introduced into mouse TSC cDNA, and their expression was determined in Xenopus laevis oocytes. Western blot analysis revealed immunoreactive bands in all mutant TSCs that were undistinguishable from wild-type TSC. The activity profile was: wild-type TSC (100%) > G627V (66%) > R935Q (36%) ~ V995M (32%) > G610S (12%) > A585V (6%). Ion transport kinetics in all mutant clones were similar to wild-type TSC, except in G627V, in which a small but significant increase in affinity for extracellular Cl^- was observed. In addition, G627V and G610S exhibited a small increase in metolazone affinity. The surface expression of wild-type and mutant TSCs was performed by laser-scanning confocal microscopy. All mutants exhibited a significant reduction in surface expression compared with wild-type TSC, with a profile similar to that observed in functional expression analysis. Our data show that biochemical and functional properties of the mutant TSCs are similar to wild-type TSC but that the surface expression is reduced, suggesting that these mutations impair the insertion of a functional protein into the plasma membrane. The small increase in Cl^- and thiazide affinity in G610S and G627V suggests that the beginning of the COOH-terminal domain could be implicated in defining kinetic properties.

distal tubule; salt reabsorption; structure; Na-Cl cotransporter; diuretics

GITELMAN DISEASE IS AN AUTOSOMAL recessive hereditary disorder characterized by hypokalemic metabolic alkalosis, hypomagnesemia, salt wasting, low blood pressure, and hypocalciuria (23) (OMIM 600968), which is caused by inactivating mutations in the SLC12A3 gene that encode the thiazide-sensitive Na^+-Cl^- cotransporter (TSC) (31). To date, >100 different mutations in this gene, including nonsense, splice site, and missense mutations, have been described to be linked with Gitelman disease (25, 31). One of the major features of Gitelman disease is a reduction in arterial blood pressure, resulting, at least in part, from a decrease in extracellular fluid volume (8). Cruz et al. (8) observed in a large family with Gitelman disease that heterozygous subjects are able to maintain normal blood pressure by increasing dietary salt intake. In addition, loss of TSC downregulation that is normally induced by WNK1 and WNK4 kinases has been suggested to be involved in the pathogenesis of a salt-dependent form of human hypertension known as pseudohypoaldosteronism type II (39, 40). Thus TSC is one of the genes that are involved in setting arterial blood pressure levels and, in doing so, is a candidate gene in the genesis of primary hypertension.

TSC represents the major NaCl transport pathway in the apical membrane of the mammalian distal convoluted tubule (7, 14, 21, 29, 37) and also serves as the receptor for thiazide-type diuretics, which are the first line pharmacological therapy for hypertension (6). Despite the important role of TSC in cardiovascular and renal physiology, pharmacology, and pathophysiology, little is currently known about the structure-function relationships in this cotransporter. In this regard, naturally occurring mutations in Gitelman patients can help to reveal amino acid residues playing a key role in defining functional characteristics. Analysis at the physiological level has demonstrated that most of the point mutations occurring in patients with Gitelman disease result in a complete block of cotransporter activity (9, 22). Thus the contribution of these amino acid residues to define the functional properties of the cotransporter cannot be obtained because the protein is not expressed. During the course of our previous study (22), however, we noticed that some of the missense mutations exhibit partial function. De Jong et al. (9) also observed that some point mutations result in TSC proteins that are glycosylated and exhibit partial activity as metolazone-sensitive $^{22}Na^+$ uptake. Immunocytochemical analysis revealed that proteins harboring the functional mutations were equally present in the cytoplasm and plasma membrane. In the present study, we have now extended the functional and molecular characterization of TSC harboring "functional" mutations by performing a quantitative analysis comparing plasma membrane expression of wild-type and mutant TSC, as well as by defining the functional kinetic properties for ion transport and thiazide inhibition. Our observations expand the spectrum of mechanisms underlying Gitelman disease and suggest that the begin-

---

ning of the COOH-terminal domain could be implicated in defining affinity for extracellular Cl^- and thiazides.

METHODS

Xenopus laevis oocyte preparation. Oocytes were surgically harvested from anesthetized adult female *X. laevis* frogs under 0.17% tricaine and incubated for 1 h under vigorous shaking in frog Ringer-ND96 (mM: 96 NaCl, 2 KCl, 1.8 CaCl₂, 1 MgCl, and 5 HEPES/Tris, pH 7.4), supplemented with collagenase B (2 mg/ml). Then, oocytes were manually defolliculated and incubated overnight in ND96 at 18°C containing 2.5 mM sodium pyruvate and 5 mg/100 ml of gentamicin. The next day, mature oocytes (13) were injected with 50 nl of water with or without cRNA from wild-type or mutant TSC, at a concentration of 0.5 μg/μl (i.e., 25 ng cRNA/ooctye). After injection, oocytes were incubated for 4 days in ND96 with sodium pyruvate and gentamicin, and the day before the uptake experiments were performed oocytes were switched to a Cl^--free ND96 (mM: 96 Na^+ isethionate, 2 K^+ gluconate, 1.8 Ca^{2+} gluconate, 1.0 Mg^{2+}gluconate, 5 HEPES, and 2.5 sodium puruvate as well as 5 mg/100 ml gentamicin, pH 7.4) (17, 18).

In vitro rTSC cRNA translation. To prepare cRNA, all clones were digested at the 3'-end using *NotI* (Invitrogen), and cRNA was transcribed in vitro using a T7 RNA polymerase mMESSAGE kit (Ambion). Transcription product integrity was confirmed on agarose gels, and concentration was determined by absorbance reading at 260 nm (DU 640, Beckman, Fullerton, CA) and by densitometric analysis of the corresponding band in ethidium bromide-stained gels. cRNA was stored frozen in aliquots at −80°C until use.

Assessment of the Na^+-Cl^- cotransporter function. Functional analysis of the Na^+-Cl^- cotransporter was determined by assessing tracer $^{22}Na^+$ uptake (New England Nuclear) in groups of at least 15 oocytes. $^{22}Na^+$ uptake was measured using our usual protocol (27): a 30-min incubation period in an isotonic K^+- and Cl^--free medium (mM: 96 Na^+ gluconate, 6.0 Ca^{2+} gluconate, 1.0 Mg^{2+} gluconate, 5 HEPES/Tris, pH 7.4) with 1 mM ouabain, 100 μM bumetanide, and 100 μM amiloride, followed by a 60-min uptake in a K^+-free isotonic medium. The isotonic medium contained (in mM) 40 NaCl, 56 *N*-methyl-D-glucamine (NMDG)-Cl, 1.8 CaCl₂, 1 MgCl₂, 5 HEPES, pH 7.4, and 1 ouabain as well as 100 μM bumetanide, 100 μM amiloride, and 2.5 μCi $^{22}Na^+$.

To determine ion transport kinetics, experiments were performed by varying concentrations of Na^+ and Cl^- in the uptake medium (from 0 to 20 or 40 mM). To maintain osmolality and ionic strength, gluconate was used as a Cl^- substitute and NMDG as a Na^+ substitute. All kinetic experiments were obtained in duplicate. The dose-response for metolazone was assessed by exposing groups of cRNA-injected oocytes to concentrations varying from 10^{-9} to 10^{-4} M. The desired concentration of the diuretic was present in both the incubation and uptake periods.

All uptakes were performed at 32°C. At the end of the uptake period, oocytes were washed five times in ice-cold uptake solution without the isotope to remove extracellular fluid tracer. After the oocytes were dissolved in 10% SDS, tracer activity was determined for each oocyte by β-scintillation counting.

Western blotting. Western blotting was used to compare wild-type and mutant TSC protein in cRNA-injected oocytes following our standard protocol (22, 26). In brief, groups of 15 oocytes injected with water or cRNA were homogenized in 2 μl/oocyte of homogenization buffer, centrifuged twice at 100 *g* for 10 min at 4°C, and the supernatant was recollected. Oocyte protein (4 oocytes/lane) was heated in sample buffer containing 6% SDS, 15% glycerol, 0.3% bromophenol blue, 150 mM Tris, pH 7.6, and 2% β-mercaptoethanol and resolved by SDS-PAGE (7.5%). The proteins were transferred to a polyvinylene difluoride membrane (Amersham Pharmacia Biotech) at 100 V for 140 min in a buffer containing 25 mM Tris, 190 mM glycine, 0.1% SDS, and 20% (vol/vol) methanol. Prestained Rainbow

markers (Amersham) were used as molecular mass standards. Nonspecific binding sites were blocked for 1 h at room temperature in TBS (pH = 7.5) containing 0.4% blotting grade blocker nonfat dry milk (Bio-Rad), exposed overnight at 4°C to rabbit polyclonal TSC primary antibody diluted 1:1,000 in blocking buffer, TTBS 0.2% [either an antibody previously generated by ourselves (3) or one kindly provided by Dr. Mark Knepper (38)]. Membranes were washed for 40 min with TTBS changed every 10 min, then incubated for 60 min at room temperature with alkaline phosphatase-conjugated secondary (anti-rabbit) antibody (Bio-Rad) diluted 1:2,000 in blocking buffer and washed again. Bands were detected by using the Immun-Star Chemiluminescent Protein Detection System (Bio-Rad).

Assessment of rTSC expression in oocyte plasma membrane. The surface expression of wild-type TSC and mutants was measured by fluorescence using an enhanced green fluorescent protein-TSC fusion constructs (EGFP-TSC) following the strategy that we have previously reported (19, 39). In brief, oocytes were microinjected with water and TSC cRNA as the control and with EGFP-TSC wild-type or EGFP-TSC mutants. After 4 days of incubation, oocytes were monitored for EGFP fluorescence using a Zeiss laser-scanning confocal microscope (objective lens ×10, Nikon). The light from a 488-nm excitation wavelength and 515- to 565-nm emission was used to visualize GFP fluorescence. Plasma membrane fluorescence was quantified by determining the pixel intensity around the entire oocyte circumference using SigmaScan Pro image-analysis software.

Statistical analysis. Statistical significance is defined as two-tailed $P < 0.05$, and the results are presented as means ± SE. The significance of the differences between groups was tested by one-way ANOVA with multiple comparisons using the Bonferroni correction.

RESULTS

Functional expression of wild-type and mutant TSC. In preliminary experiments (2), 25 Gitelman mutations were introduced into the TSC by site-directed mutagenesis using the Quick Change kit from Stratagene. The products of site-directed mutagenesis were sequenced to confirm that additional mutations did not occur. As Fig. 1 shows, we observed in a Western blot from oocytes expressing wild-type and mutant TSCs, using a polyclonal antibody we generated previously (3), that some of the Gitelman mutants' TSCs produce proteins that are not fully glycosylated, whereas others generate proteins in which glycosylation patterns appear indistinguishable from wild-type (as shown by treating with endoglycosidase F). When expressed in *X. laevis* oocytes, Na^+ uptake rates relative to wild-type TSC were very different among the mutant clones. Five of these mutations were chosen for further functional
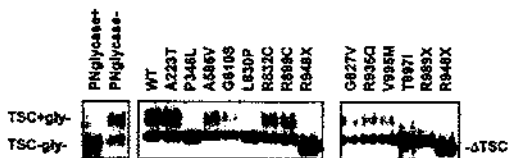
Fig. 1. Western blot analysis of oocytes expressing wild-type (WT) and mutant proteins. *Left*: effects of endoglycosidase F (PNglycase) in converting mature glycosylated thiazide-sensitive Na^+-Cl^- cotransporter protein (TSC+gly) to un- or core-glycosylated protein (TSC − gly). *Middle and right*: proteins that are misprocessed (P346L, L830P, R948X, T997I, R989X) exhibit faint or absent mature glycosylated products and resemble WT protein treated with PNglycase. Furthermore, the abundance of the un- or core-glycosylated band is increased among these mutants. In contrast, A223T, A585V, G610S, R832C, R899C, G627V, R935Q, and V995M generate proteins that exhibit mature glycosylated bands.
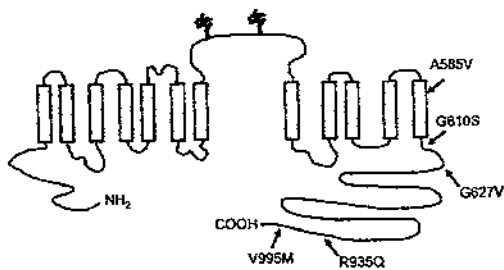
Fig. 2. Proposed TSC topological model that includes a central hydrophobic domain containing 12 putative transmembrane segments flanked by hydrophilic NH₂-terminal and COOH-terminal domains presumably located within the cell. There is a long hydrophilic extracellular glycosylated loop between transmembrane *segments 7* and *8*. Arrows, regions of the protein in which the mutations studied are located.

Fig. 3. Functional expression of WT and mutant mouse TSC in *Xenopus laevis* oocytes injected with water or with 25 ng of cRNA in vitro transcribed from corresponding cDNAs, as indicated. In all groups. $^{22}Na^+$ uptake was assessed in the presence of Na^+ and Cl^- (open bars) or in the presence of 10^{-4} metolazone (filled bars). Each bar represents a mean of 20 oocytes. $^{22}Na^+$ uptake was performed for 60 min. *Inset:* Western blot analysis of proteins extracted from oocytes used for functional analysis. Proteins extracted from 4 oocytes/lane were used. Immunodetection was performed using a rabbit polyclonal anti-rat TSC antibody provided by Dr. Mark Knepper (dilution 1:1,000). Antigen-antibody complexes were detected by autoradiography-enhanced chemiluminescence. The arbitrary units obtained in the densitometric analysis were 22.5 for WT TSC, 30.3. for G627V, 23.0 for R935Q, 24.2 for V995M, 30.6 for G610S, and 26.1 for A585V. *Significantly different from uptake in the water-injected control group ($P < 0.001$). **Significantly different from uptake in the same cRNA-injected group without metolazone ($P < 0.01$).

analysis. The localization of each mutation within the proposed TSC topology is shown in Fig. 2. The mutations are located in the putative intracellular COOH-terminal domain, except for A585V, which is located within transmembrane *segment 12*. Na^+ uptake rates relative to wild-type TSC of the mutant clones not selected for further study are shown in Table 1 of supplemental data. Figure 3 shows the results of a representative uptake experiment in which oocytes from the same frog were injected with either wild-type TSC or mTSC cRNA of each of the five Gitelman mutants. Tracer $^{22}Na^+$ uptake was assessed for 1 h under control conditions and in the presence of 10^{-4} M metolazone. We have shown previously that *X. laevis* oocytes do not exhibit endogenous thiazide-sensitive Na^+-Cl^- cotransport (17, 18). As shown in Fig. 3, the oocytes injected with wild-type TSC and a TSC mutation had a significant increase in $^{22}Na^+$ uptake compared with water-injected oocytes, and this effect was significantly reduced by metolazone; however, the activity level varied among mutants. As shown in Table 1, the activity profile was wild-type TSC > G627V > R935Q = V995M > G610S > A585V. It is worth noting that the two mutations with the lower activity are those located within or near the last membrane-spanning domain.

To compare $^{22}Na^+$ uptake among clones injected with different clones, we ensured that all groups were injected with 25 ng cRNA/oocyte. For this purpose, the cRNA concentration of all clones was measured by an absorbance reading at 260 nm and also by resolving cRNAs in 1% agarose/formaldehyde gels. The corresponding 4.4-kb band was quantified by densi-

Table 1. *Functional properties of TSC with or without Gitelman-type mutations*

Mutation	Activity	Na^+ K_m, mM	Cl^- K_m, mM	Metolazone (IC_{50})
Wild-type	100%	7.23±0.4	5.62±0.5	2×10^{-6}
G627V	66.5%	4.68±2.2	2.53±1.4*	1×10^{-7}
R935Q	36.5%	3.76±1.5	7.69±3.5	5×10^{-6}
V995M	32.5%	4.39±2.3	5.22±3.2	2×10^{-6}
G610S	12.7%	10.4±8.1	7.51±6.3	7×10^{-7}
A585V	6.2%	ND	ND	ND

Values are means ± SE. TSC, thiazide-sensitive Na^+-Cl^- cotransporter; ND, not detectable. *$P < 0.05$ vs. wild-type TSC.

tometric analysis. In addition, proteins extracted from the same batch of injected *X. laevis* oocytes shown in Fig. 3 were subjected to Western blot analysis to compare the TSC proteins produced between wild-type and mutant TSCs. The immunoblot (Fig. 3, *inset*) shows that protein produced in oocytes by wild-type TSC and mutant TSCs are very similar. This Western blot analysis was performed using a polyclonal anti-TSC antibody that was previously validated and kindly provided by Dr. Mark Knepper (38). With the use of this antibody, the glycosylation band is less apparent, even in wild-type TSC. Because the clones used in Fig. 3 are the same used in the immunoblot in Fig. 1, in which clear glycosylation bands were observed using the other antibody, it is likely that, for some reason, Dr. Knepper's antibody did not enable us to detect TSC glycosylation bands in proteins extracted from injected *X. laevis* oocytes. However, bands in the immunoblot were similar, and densitometric analysis revealed no significant difference among the TSC protein in the oocytes, while Fig. 3 showed that all clones induced TSC expression in oocytes. Therefore, the lower activity in mutant TSCs compared with wild-type does not seem to be associated with a defect in the production or an increase in the degradation rate.

Kinetics of ion transport and metolazone inhibition. One of the possible mechanisms for the reduction of TSC protein activity in mutant clones is that each particular mutation affects the affinity for ions or the intrinsic activity of the cotransporter. A dramatic reduction of the affinity for one or both ions could be responsible of a decrease in TSC activity, because the cotransporter will no longer be active in the presence of a 40 mM concentration of Na^+ or Cl^- that we currently used in the assay. Thus we assessed the kinetic properties of Na^+ and Cl^-

transport in all clones that exhibited enough expression as to measure uptakes with extracellular ion concentrations that will be below K_m values. Results from this series of experiments are shown in Figs. 4 and 5 and Table 1. The ion transport kinetics observed in wild-type TSC from the mouse are very similar to those previously observed for rat TSC (27). The Na^+ transport kinetics in Fig. 4 revealed that $^{22}Na^+$ uptake in all clones exhibited saturation curves that are compatible with Michaelis-Menten behavior. In all cases, a plateau was reached with an extracellular Na^+ concentration <20 mM, and we observed no significant differences in K_m values (Table 1). Cl^- transport kinetics are depicted in Fig. 5. All curves reached the plateau with extracellular Cl^- concentrations <10 mM, and K_m values were very similar, except in TSC harboring the G627V mutation, in which K_m was decreased to 2.5 ± 1.4 mM, a value significantly lower than the values of all other clones, including wild-type TSC. These observations suggest that the affinity for the cotransported ions is similar to wild-type TSC in all clones, except in G627V, where we observed an increased affinity for Cl^-. Thus because there is no decrease in the affinity for ions in mutant TSCs, a change in the functional properties of the cotransporter does not explain the reduced $^{22}Na^+$ uptake observed in the mutant clones.

In addition to ion transport kinetic analysis, we also assessed the dose response to the thiazide-type diuretic metolazone to determine the effect of functional missense mutations on the kinetics of thiazide inhibition of the cotransporter. The results of these experiments are shown in Fig. 6 and Table 1. TSC harboring the R935Q and V995M mutations exhibited an IC_{50} for metolazone inhibition of $^{22}Na^+$ uptake that was similar to that for wild-type TSC. In contrast, TSC with the G610S and G627V exhibited an IC_{50} that was shifted to the left by one-half and one order of magnitude, respectively.

Surface expression of wild-type and mutant EGFP-TSC constructs in X. laevis oocytes. Another potential mechanism that can account for a reduction in the activity of mutated clones is that mutations affect the insertion of normally functional protein into the plasma membrane. Thus, to quantitatively compare the plasma membrane expression of wild-type vs. mutant TSC, we assessed the surface expression by fluorescence under a confocal microscope using an EGFP-TSC fusion construct, identical to the one we have previously used to assess surface expression of rat TSC (19, 39). This analysis is performed in real time using live oocytes, and only the EGFP-TSC present in the plasma membrane generates fluorescence when EGFP protein is stimulated with light (19). Figure
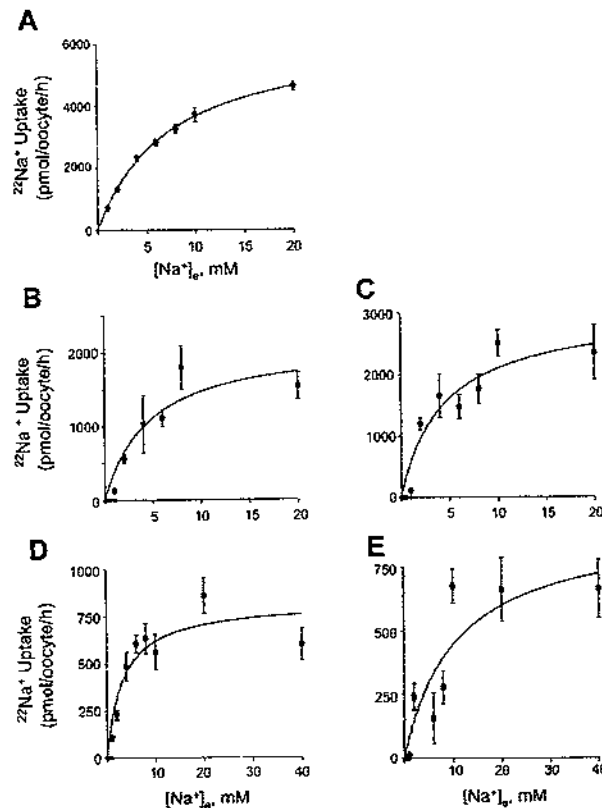
Fig. 4. Kinetic analysis of the Na^+ dependency of $^{22}Na^+$ uptake in WT or mutant TSC-injected oocytes. *A*: WT. *B*: G627V. *C*: R935Q. *D*: V995M. *E*: G610S. Uptake was performed for 30 min with a fixed concentration of Cl^- at 96 mM, with extracellular Na^+ concentration ([Na^+]_e) at 0, 1.0, 2.0, 4.0, 6.0, 8.0, 10, 20, and/or 40 mM. Uptake was also assessed in water-injected oocytes (data not shown), and the mean values for water groups were subtracted in corresponding cRNA groups. Each point represents the mean ± SE of 15 oocytes.

A

B

C
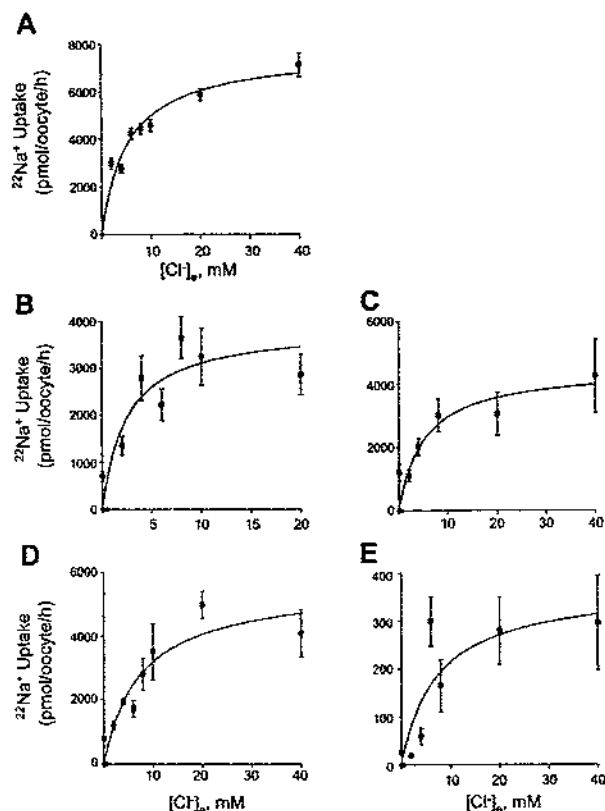
Fig. 5. Kinetic analysis of the Cl^- dependency of $^{22}Na^+$ uptake in WT or mutant TSC-injected oocytes. *A*: WT. *B*: G627V. *C*: R935Q. *D*: V995M. *E*: G610S. Uptake was performed for 30 min with a fixed concentration of Na^+ at 96 mM, with extracellular Cl^- concentration ($[Cl^-]_o$) at 0, 2.0, 4.0, 6.0, 8.0, 10, 20, and/or 40 mM. Uptake was also assessed in water-injected oocytes (data not shown), and the mean values for water groups were subtracted in corresponding cRNA groups. Each point represents the mean ± SE of 15 oocytes.

D

E

7*A* depicts a representative example of *X. laevis* oocytes injected with wild-type or mutant EGFP-TSC constructs, and Fig. 7*B* shows the results of densitometric analysis of 30 oocytes/group. Control oocytes injected with water showed no significant fluorescence at the emission and excitation wavelengths for EGFP. We have previously shown (19) surface colocalization of the EGFP-TSC fusion construct with the plasma membrane marker FM 4–64 fluorescence in all tested oocytes, indicating that EGFP-TSC fluorescence measured at equatorial confocal sections in oocytes is indicative of expression in plasma membrane. In addition, we also showed (19) that oocytes injected with wild-type EGFP-TSC cRNA exhibited an increased uptake of tracer $^{22}Na^+$ (4,977 ± 473 $pmol \cdot oocyte^{-1} \cdot h^{-1}$) that was reduced by 10^{-4} M metolazone (1,237 ± 314 $pmol \cdot oocyte^{-1} \cdot h^{-1}$, $P < 0.001$), indicating that the EGFP-TSC construct is located in the plasma membrane. As shown in Fig. 7, although a similar amount of wild-type and EGFP-TSC cRNA of each mutant was injected (25 ng/oocyte), fluorescence in oocyte plasma membrane was lower in mutant-injected oocytes. The analysis of 30 oocytes/group revealed that surface expression of the EGFP-TSC construct harboring mutations was significantly lower vs. the wild-type EGFP-TSC construct, with a profile similar to that observed in the reduc-
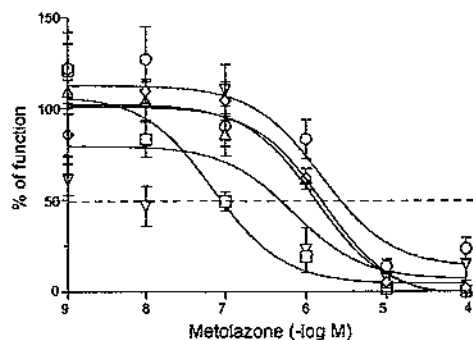
Fig. 6. Dose-dependent inhibition of $^{22}Na^+$ uptake by the thiazide-type diuretic metolazone in WT and mutant TSC-injected oocytes. Metolazone was tested at concentrations from 10^{-9} to 10^{-4} M. Injected cRNA was from WT (○), V995M (△), R935Q (◇), G610S (□), and G627V (▽). Uptake was performed for 60 min in uptake solution containing 96 mM NaCl. Uptake in the absence of metolazone was taken as 100%. Each point represents the mean ± SE of 15 oocytes.

A

WT   G627V

G610S   R935Q

V995M   A585V
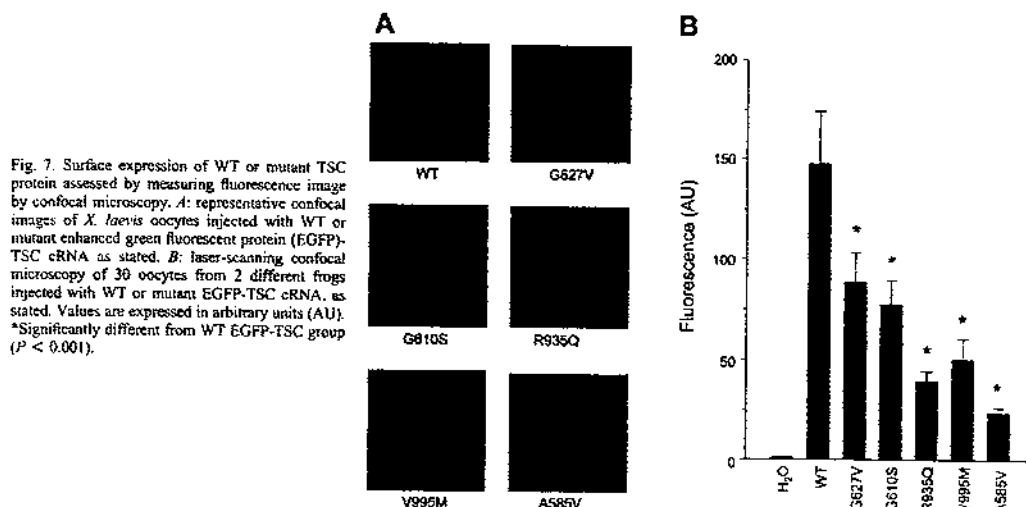
Fig. 7. Surface expression of WT or mutant TSC protein assessed by measuring fluorescence image by confocal microscopy. A: representative confocal images of X. laevis oocytes injected with WT or mutant enhanced green fluorescent protein (EGFP)-TSC cRNA as stated. B: laser-scanning confocal microscopy of 30 oocytes from 2 different frogs injected with WT or mutant EGFP-TSC cRNA, as stated. Values are expressed in arbitrary units (AU). *Significantly different from WT EGFP-TSC group (P < 0.001).

B

tion of transport activity, except for G610S, where confocal analysis revealed a percentage of surface expression (~50%) higher than the percentage of functional activity (~12%). This suggests that, in this particular clone, where the mutation is located in a residue very near to the end of transmembrane *domain 12*, both intrinsic activity and arrival to the plasma membrane are affected.

DISCUSSION

The present work describes the functional analysis of activity, ion transport kinetics, diuretic dose-response kinetics, and quantitative surface expression analysis of the thiazide-sensitive Na^+-Cl^- cotransporter harboring five different Gitelman-type mutations. The results revealed that these mutations result in TSC proteins that are similar to wild-type TSC by Western blot analysis and with similar functional transport properties but that exhibit different degrees of activity and arrival rate to the plasma membrane.

The functional characteristics of wild-type and mutant TSCs were assessed using the heterologous expression system in X. laevis oocytes. This expression system has shown to be an excellent tool for a robust and reproducible expression of TSC in our hands (17–19, 27, 36, 39) and other laboratories (9, 10, 22, 40), whereas TSC expression in transfected mammalian cells has not been successful in many laboratories, including our own. Thus previous studies using TSC cDNA in which Gitelman-type mutations were introduced have been performed using X. laevis oocytes (9, 22). Although expression in mammalian cells is preferred, the best results that have been obtained in stably transfected cells (Madin-Darby canine kidney cells) using wild-type TSC cDNA consisted of a small increase over background that was not >25% (11). This small increase in TSC expression would not be useful in determining the functional properties of mutant clones in which the activity is already lower than that using the wild-type cotransporter.

Studies by Kunchaparty et al. (22) were the first to analyze the functional consequences of several missense mutations

reported along TSC protein in kindreds with Gitelman disease. All mutations studied were shown to be functionally inactive, when expressed in X. laevis, owing to defective protein processing. It was observed that proteins were synthesized, but they were not properly glycosylated and were not expressed at the plasma membrane. Thus it was concluded that Gitelman mutations impair the function of cotransporter protein by interfering with protein processing. These conclusions are supported by results from Hoover et al. (19), who demonstrated that TSC is a glycoprotein and that both N-linked glycosylation residues (N404 and N424; Fig. 2) are required for the adequate processing of the cotransporter, because single-glycosylation TSC mutants N404Q or N424Q exhibited a significant reduction in functional activity of ~50% compared with wild-type TSC, whereas the double-mutant N404, 424Q resulted in a reduction of expression of ~95%. Most of the reduction in activity was explained by a decrease in the surface expression of the cotransporter. Thus as has been shown with other membrane proteins (1, 15, 24), glycosylation of TSC seems to be required for the proper folding and trafficking of the cotransporter to the plasma membrane.

During the course of previous experiments (22), we noticed that, while most of the Gitelman-type mutations result in nonglycosylated cotransporters, some missense mutations resulted in proteins that were indistinguishable from wild-type TSC by Western blot analysis. Interestingly, some of these "glycosylated" TSC mutants were observed in patients exhibiting a mild form of disease (Lifton R, personal communication), suggesting that the mutant cotransporter could be partially active. De Jong et al. (9) performed a partial characterization of four such functional missense TSC mutations from patients with Gitelman disease. They observed that mutant proteins were glycosylated in the injected X. laevis oocytes and that immunocytochemical analysis showed that mutants with some TSC activity exhibited immunostaining in both cytoplasm and the plasma membrane. The functional properties of the mutant TSCs, however, were not assessed. Thus they were

not able to define whether the studied missense mutations resulted in a defect of TSC insertion into the plasma membrane or in a defect in the functional properties of the cotransporter. In addition, all experiments by De Jong et al. were performed at room temperature, and thus a protein dysfunction associated with temperature was not ruled out. In the case of cystic fibrosis, for instance, the ΔF508 mutation leads to a temperature-dependent defect. When expressed in cells grown at 18°C, ΔF508 matures normally and is expressed at the plasma membrane. In contrast, when expressed in mammalian cells or in oocytes grown at higher temperatures, incomplete processing or insertion into the plasma membrane occurs (12).

In the present study, we have extended the analysis of functional missense mutations to include these possibilities. As shown in Fig. 8, there are at least five possible mechanisms by which mutations might reduce or abolish transporter activity. A mutation could *1*) impair protein synthesis, *2*) impair protein processing, *3*) impair the insertion of an otherwise functional protein into the plasma membrane, *4*) impair the functional properties of the cotransporter, and *5*) accelerate protein removal or degradation. Although mutations that introduce stop codons in the initial part of the protein, or those in which splicing is abolished resulting in nonsense proteins, have not been studied at the functional level, it is highly likely that the mechanism in these mutations relates to the first possiblity (Fig. 8), by which the synthesis of the complete protein is impaired (30, 33, 35). Our previous results are examples of mutations that belong to the second possibility (Fig. 8) because they impair protein processing (22). In the present work, we studied five Gitelman missense mutations that result in partial "functional" proteins. Western blot analysis using anti-TSC antibody revealed that all proteins were similar to wild-type TSC, suggesting that a defect in protein synthesis is not mainly responsible for the reduced activity in mutant TSCs. The functional analysis suggests that it is unlikely that a decrease in ion affinity is the mechanism responsible because Na^+ and Cl^- affinities were either normal or increased in mutant clones. Closeness of fits were reasonable in all clones, except in the one with the lower activity (G610S; Figs. 4*E* and 5*E*). In this clone, the observed K_m for Na^+ and Cl^- transport was slightly higher that in wild-type TSC, but the difference did not reach significance. However, we believe that, even in this clone, our results suggest that the reduced function of the cotransporter in

mutant TSCs is not due to a dramatic decrease in affinity for Na^+ or Cl^- which prevents the cotransporter from reaching V_{max} when extracellular ions concentrations are >20 mM. These observations suggested that a reduction in the number of cotransporter proteins in the plasma membrane or a decrease in the intrinsic activity of the cotransporter could be the reason for the reduced activity in mutant TSCs. Thus we assessed the surface expression of the EGFP-tagged wild-type and mutant proteins. In this analysis, we tagged the NH_2-terminal domain of wild-type mouse TSC, as well as all mutant clones, with EGFP and assessed surface EGFP-TSC by measuring the fluorescence emission under the confocal microscope. This strategy has been successfully used by us to assess the surface expression of TSC (19, 39) and several isoforms of the apical renal-specific bumetanide-sensitive Na^+-K^+-$2Cl^-$ cotransporter (26, 28), as well as by others to assess the surface expression of membrane proteins in *X. laevis* oocytes (4, 5, 16). The surface expression of all mutant proteins was significantly reduced (Fig. 7). In addition, the surface expression profile was similar to the functional profile, suggesting that reduction of transporter activity of mutant proteins is mainly caused by a decrease in the surface expression of the cotransporter. Thus our data suggest that mutations studied in the present work belong to the third possibility (Fig. 8), in which a missense mutation results in a cotransporter with normal functional properties but insertion into the plasma membrane is partially impaired. In this regard, we have recently shown (39, 40) that TSC insertion into the plasma membrane is an important regulatory control point, because mutations in a TSC-negative regulator, such as the WNK4 kinase in pseudohypoaldosteronism type II, result in a loss of inhibition of TSC activity due to uncontrolled insertion of TSC vesicles into the plasma membrane. Interestingly, missense mutations of other members of the electroneutral cotransporter family, such as the Na^+-K^+-$2Cl^-$ cotransporter in Bartter syndrome type 1 (32) and the KCC3 K^+-Cl^- cotransporter in the peripheral neuropathy associated with agenesis of the corpus callosum (Anderman's syndrome) (20), behave like the fourth possibility (Fig. 8), because the mutated proteins are normally produced and inserted into the plasma membrane, implying a defect in the functional properties or intrinsic activity of the cotransporter. These data taken together, the first four mechanisms proposed (Fig. 8) have been shown to be implicated in the molecular pathophysiology of hereditary syndromes associated with mutations in members of the SLC12 family.

The observations in the present study are also important in terms of the functional characterization of TSC and in providing some insights into structure-function relationships. The present study shows for the first time the analysis of the kinetic transport properties of mouse TSC. We have previously reported the major functional properties of the rat (17, 27) and flounder (28) isoforms of TSC, which exhibit several differences in ion transport kinetics and dose-response inhibition to thiazide diuretics. Here, we show that Na^+ and Cl^- transport and metolazone inhibitory kinetics in wild-type mouse TSC revealed K_m and IC_{50} values that are undistinguishable from those observed in rat TSC (27) and significantly different from those of flounder TSC (28). In addition, we observed that missense mutations G610S and G627V, which are located at the very beginning of the long COOH-terminal domain, increase the affinity for Cl^- and/or metolazone. As discussed
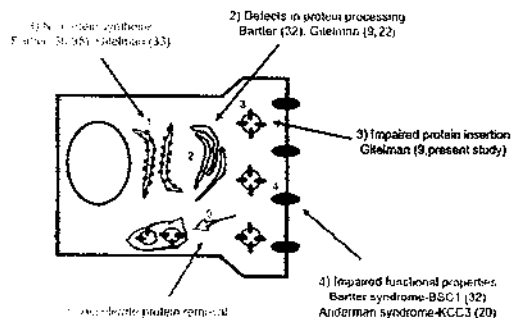

Fig. 8. Molecular mechanisms for the decreased activity of the electroneutral cotransporters associated with inherited syndromes.

above, this finding does not imply an important role for increased ion affinity in causing the clinical phenotype of Gitelman disease, because increased Cl^- affinity would not be expected to reduce TSC function in vivo. However, the results do suggest that this region of the protein is involved in defining the affinity for Cl^- and/or diuretics. Previous studies in which the binding of the tracer [^{3}H]metolazone was used to assess the thiazide receptor suggested that thiazide diuretics and Cl^- compete for the same site on the cotransporter (34). In this regard, we have shown that the affinity for thiazides is shifted to the left when dose-response curves are performed under low-extracellular Cl^- concentration (27, 36) and that the prevention of glycosylation in rat TSC increases the affinity for both extracellular Cl^- and thiazides (19). In the present study, we observed that the mutation G627V produces a slight but significant increase in Cl^- affinity, together with an increase in the affinity for thiazides, supporting the notion that affinity-modifying residue for Cl^- may also be involved in defining thiazide affinity. Further studies will be necessary to clarify this issue, but our results suggest that analysis of the functional properties of naturally occurring mutations can be useful in revealing the functional roles of individual amino acid residues, which will be helpful in beginning to understand the structure-function relationships among members of the cation Cl^- cotransporter gene family.

DISCLOSURES

Part of this work was presented at the 2002 Annual Meeting of the American Society of Nephrology (Philadelphia, PA) and is published as an abstract (*J Am Soc Nephrol* 13: 75A, 2002).

REFERENCES

1. Asano T, Takata K, Katagiri H, Ishihara H, Inukai K, Anai M, Hirano H, Yazaki Y, and Oka Y. The role of N-glycosylation in the targeting and stability of GLUT1 glucose transporter. *FEBS Lett* 324: 258–261, 1993.
2. Berkman J, Reilly RF, and Ellison DH. Mechanisms of thiazide-sensitive Na-Cl cotransporter dysfunction in Gitelman's syndrome (Abstract). *J Am Soc Nephrol* 10: 1261, 1999.
3. Bostanjoglo M, Reeves WB, Reilly RF, Velazquez H, Robertson N, Litwack G, Morsing P, Dorup J, Bachmann S, Ellison DH, and Bostonjoglo M. 11Beta-hydroxysteroid dehydrogenase, mineralocorticoid receptor, and thiazide-sensitive Na-Cl cotransporter expression by distal tubules. *J Am Soc Nephrol* 9: 1347–1358, 1998.
4. Chan KW, Sui JL, Vivaudou M, and Logothetis DE. Specific regions of heteromeric subunits involved in enhancement of G protein-gated K$^+$ channel activity. *J Biol Chem* 272: 6548–6555, 1997.
5. Chapell R, Bueno OF, Alvarez-Hernandez X, Robinson LC, and Leidenheimer NJ. Activation of protein kinase C induces gamma-aminobutyric acid type A receptor internalization in *Xenopus* oocytes. *J Biol Chem* 273: 32595–32601, 1998.
6. Chobanian AV, Bakris GL, Black HR, Cushman WC, Green LA, Izzo JL Jr, Jones DW, Materson BJ, Oparil S, Wright JT Jr, and Roccella EJ. The Seventh Report of the Joint National Committee on Prevention, Detection, Evaluation, and Treatment of High Blood Pressure: The JNC 7 Report. *JAMA* 289: 2560–2571, 2003.
7. Costanzo LS. Localization of diuretic action in microperfused rat distal tubules: Ca and Na transport. *Am J Physiol Renal Fluid Electrolyte Physiol* 248: F527–F535, 1985.
8. Cruz DN, Simon DB, Nelson-Williams C, Farhi A, Finberg K, Burleson L, Gill JR, and Lifton RP. Mutations in the Na-Cl cotransporter reduce blood pressure in humans. *Hypertension* 37: 1458–1464, 2001.
9. De Jong JC, Van Der Vliet WA, van den Heuvel LP, Willems PH, Knoers NV, and Bindels RJ. Functional expression of mutations in the human NaCl cotransporter: evidence for impaired routing mechanisms in Gitelman's syndrome. *J Am Soc Nephrol* 13: 1442–1448, 2002.
10. De Jong JC, Willems PH, Mooren FJ, van den Heuvel LP, Knoers NV, and Bindels RJ. The structural unit of the thiazide-sensitive NaCl cotransporter is a homodimer. *J Biol Chem* 278: 24302–24307, 2003.
11. De Jong JC, Willems PH, van den Heuvel LP, Knoers NV, and Bindels RJ. Functional expression of the human thiazide-sensitive NaCl cotransporter in Madin-Darby canine kidney cells. *J Am Soc Nephrol* 14: 2428–2435, 2003.
12. Denning GM, Anderson MP, Amara JF, Marshall J, Smith AE, and Welsh MJ. Processing of mutant cystic fibrosis transmembrane conductance regulator is temperature-sensitive. *Nature* 358: 761–764, 1992.
13. Dumont JN. Oogenesis in *Xenopus laevis* (Daudin). Stages of oocyte development in laboratory maintained animals. *J Morphol* 136: 153–180, 1970.
14. Ellison DH, Velazquez H, and Wright FS. Thiazide-sensitive sodium chloride cotransport in early distal tubule. *Am J Physiol Renal Fluid Electrolyte Physiol* 253: F546–F554, 1987.
15. Fishburn CS, Elazar Z, and Fuchs S. Differential glycosylation and intracellular trafficking for the long and short isoforms of the D$_2$ dopamine receptor. *J Biol Chem* 270: 29819–29824, 1995.
16. Flagg TP, Tate M, Merot J, and Welling PA. A mutation linked with Bartter's syndrome locks Kir1.1a (ROMK1) channels in a closed state. *J Gen Physiol* 114: 685–700, 1999.
17. Gamba G, Miyanoshita A, Lombardi M, Lytton J, Lee WS, Hediger MA, and Hebert SC. Molecular cloning, primary structure and characterization of two members of the mammalian electroneutral sodium-(potassium)-chloride cotransporter family expressed in kidney. *J Biol Chem* 269: 17713–17722, 1994.
18. Gamba G, Saltzberg SN, Lombardi M, Miyanoshita A, Lytton J, Hediger MA, Brenner BM, and Hebert SC. Primary structure and functional expression of a cDNA encoding the thiazide-sensitive, electroneutral sodium-chloride cotransporter. *Proc Natl Acad Sci USA* 90: 2749–2753, 1993.
19. Hoover RS, Poch E, Monroy A, Vazquez N, Nishio T, Gamba G, and Hebert SC. N-glycosylation at two sites critically alters thiazide binding and activity of the rat thiazide-sensitive Na$^+$:Cl$^-$ cotransporter. *J Am Soc Nephrol* 14: 271–282, 2003.
20. Howard HC, Mount DB, Rochefort D, Byun N, Dupre N, Lu J, Fan X, Song L, Riviere JB, Prevost C, Horst J, Simonati A, Lemcke B, Welch R, England R, Zhan FQ, Mercado A, Siesser WB, George AL Jr, McDonald MP, Bouchard JP, Mathieu J, Delpire E, and Rouleau GA. The K-Cl cotransporter KCC3 is mutant in a severe peripheral neuropathy associated with agenesis of the corpus callosum. *Nat Genet* 32: 384–392, 2002.
21. Kunau RT, Weller DR, and Webb HL. Clarification of the site of action of chlorothiazide in the rat nephron. *J Clin Invest* 56: 401–407, 1975.
22. Kunchaparty S, Palcso M, Berkman J, Velazquez H, Desir GV, Bernstein P, Reilly RF, and Ellison DH. Defective processing and expression of thiazide-sensitive Na-Cl cotransporter as a cause of Gitelman's syndrome. *Am J Physiol Renal Physiol* 277: F643–F649, 1999.
23. Kurtz I. Molecular pathogenesis of Bartter's and Gitelman's syndromes. *Kidney Int* 54: 1396–1410, 1998.
24. Landlot-Marticorena C and Reithmeier RAF. Asparagine-linked oligosaccharides are localized to single extracytosolic segments in multi-span membrane glycoproteins. *Biochem J* 302: 253–260, 1994.
25. Mastroianni N, Bettinelli A, Bianchetti M, Colussi G, de Fusco M, Sereni F, Ballabio A, and Casari G. Novel molecular variants of the Na-Cl cotransporter gene are responsible for Gitelman syndrome. *Am J Hum Genet* 59: 1019–1026, 1996.
26. Meade P, Hoover RS, Plata C, Vazquez N, Bobadilla NA, Gamba G, and Hebert SC. cAMP-dependent activation of the renal-specific Na$^+$-K$^+$-2Cl$^-$ cotransporter is mediated by regulation of cotransporter trafficking. *Am J Physiol Renal Physiol* 284: F1145–F1154, 2003.

27. Monroy A, Plata C, Hebert SC, and Gamba G. Characterization of the thiazide-sensitive Na⁺-Cl⁻ cotransporter: a new model for ions and diuretics interaction. *Am J Physiol Renal Physiol* 279: F161–F169, 2000.

28. Plata C, Meade P, Vazquez N, Hebert SC, and Gamba G. Functional properties of the apical Na⁺-K⁺-2Cl⁻ cotransporter isoforms. *J Biol Chem* 277: 11004–11012, 2002.

29. Plotkin MD, Kaplan MR, Verlander JM, Lee WS, Brown D, Poch E, Gullans SR, and Hebert SC. Localization of the thiazide sensitive Na-Cl cotransporter, rTSC1, in the rat kidney. *Kidney Int* 50: 174–183, 1996.

30. Simon DB, Karet FE, Hamdan JM, DI Pietro A, Sanjad SA, and Lifton RP. Bartter's syndrome, hypokalaemic alkalosis with hypercalciuria, is caused by mutations in the Na-K-2Cl cotransporter NKCC2. *Nat Genet* 13: 183–188, 1996.

31. Simon DB, Nelson-Williams C, Johnson-Bia M, Ellison D, Karet FE, Morey-Molina A, Vaara I, Iwata F, Cushner HM, Koolen M, Gainza FJ, Gitelman HJ, and Lifton RP. Gitelman's variant of Bartter's syndrome, inherited hypokalaemic alkalosis, is caused by mutations in the thiazide-sensitive Na-Cl cotransporter. *Nat Genet* 12: 24–30. 1996.

32. Starremans PG, Kersten FF, Knoers NV, van den Heuvel LP, and Bindels RJ. Mutations in the human Na-K-2Cl cotransporter (NKCC2) identified in Bartter syndrome type I consistently result in nonfunctional transporters. *J Am Soc Nephrol* 14: 1419–1426. 2003.

33. Syren ML, Tedeschi S, Cesareo L, Bellantuono R, Colussi G, Procaccio M, Ali A, Domenici R, Malberti F, Sprocati M, Sacco M, Miglietti N, Edefonti A, Sereni F, Casari G, Coviello DA, and Bettinelli A. Identification of fifteen novel mutations in the SLC12A3 gene encoding the Na-Cl cotransporter in Italian patients with Gitelman syndrome. *Hum Mutat* 20: 78, 2002.

34. Tran JM, Farrell MA, and Fanestil DD. Effect of ions on binding of the thiazide-type diuretic metolazone to kidney membrane. *Am J Physiol Renal Fluid Electrolyte Physiol* 258: F908–F915, 1990.

35. Vargas-Poussou R, Feldman D, Vollmer M, Konrad M, Kelly L, Van der Heuvel LPWJ, Tebouri L, Brandis M, Karolyi L, Hebert SC, Lemmink HH, Deschênes G, Hildebrandt F, Seyberth HW, Guay-Woodford LM, Knoers NVAM, and Antignac C. Novel molecular variants of the Na-K-2Cl cotransporter gene are responsible for atenatal Bartter syndrome. *Am J Hum Genet* 62: 1332–1340, 1998.

36. Vazquez N, Monroy A, Dorantes E, Munoz-Clares RA, and Gamba G. Functional differences between flounder and rat thiazide-sensitive Na-Cl cotransporter. *Am J Physiol Renal Physiol* 282: F599–F607, 2002.

37. Velazquez B, Good DW, and Wright FS. Mutual dependence of sodium and chloride absorption by renal distal tubule. *Am J Physiol Renal Fluid Electrolyte Physiol* 247: F904–F911, 1984.

38. Wang XY, Masilamani S, Nielsen J, Kwon TH, Brooks HL, Nielsen S, and Knepper MA. The renal thiazide-sensitive Na-Cl cotransporter as mediator of the aldosterone-escape phenomenon. *J Clin Invest* 108: 215–222, 2001.

39. Wilson FH, Kahle KT, Sabath E, Lalioti MD, Rapson AK, Hoover RS, Hebert SC, Gamba G, and Lifton RP. Molecular pathogenesis of inherited hypertension with hyperkalemia: the Na-Cl cotransporter is inhibited by wild-type but not mutant WNK4. *Proc Natl Acad Sci USA* 100: 680–684, 2003.

40. Yang CL, Angell J, Mitchell R, and Ellison DH. WNK kinases regulate thiazide-sensitive Na-Cl cotransport. *J Clin Invest* 111: 1039–1045, 2003.
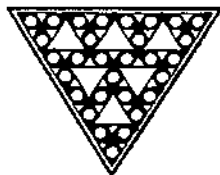
DISCUSIÓN

El cotransportador Na⁺-Cl⁻ sensible a tiazidas (CST) pertenece a la familia de transportadores cloro-catiónicos SLC12 y se localiza en la membrana apical de las células del túbulo distal de la neurona, en donde *constituye la principal vía de reabsorción de NaCl.*[1]

Este transportador ha sido identificado molecularmente y clonado a partir de diferentes especies; como el lenguado de invierno [29], el conejo [38], la rata, [37] el ratón [39] y el humano; [40,41] lo que ha permitido realizar diversos estudios para evaluar sus características estructurales y funcionales. Se ha comparado la estructura primaria de estos transportadores, [36] siendo las especies mamíferas las que guardan hasta un 90% de homología entre ellas, es decir, los CSTs de rata, ratón, conejo y humano son estructuralmente muy parecidos, mientras que el CST del lenguado de invierno solo muestra ~60% de homología cuando es comparado con los anteriores.

Investigaciones previas, han determinado diversas propiedades funcionales, farmacológicas y de regulación en el CST.

Vázquez y col. [45] analizaron las características funcionales del CST, de rata y del pez lenguado de invierno (CSTr y CSTfl). Los análisis cinéticos mostraron que estos transportadores presentan diferencias funcionales importantes, así como distinta sensibilidad a los diuréticos tipo tiazida y respuesta ante la osmolaridad extracelular. Como se mencionó el CST del lenguado de invierno (CSTfl) es el que presenta mayor diferencia en los aminoácidos que forman su estructura primaria. Las diferencias funcionales encontradas entre el CSTr y el CSTfl, pueden ser el resultado de estos cambios de aminoácidos en su secuencia.

Actualmente es de gran interés para varios grupos de investigación, los estudios de relación estructura función de los diferentes miembros de esta familia de transportadores cloro-catiónicos, donde el principal objetivo es determinar los dominios estructurales y/o aminoácidos puntuales involucrados en su función.

Consideramos que proteínas con estructuras primarias semejantes como el CSTr y el CSTfl, en donde se observan diferentes propiedades funcionales,

constituyen un excelente modelo de estudio, para investigar aspectos de relación estructura-función en este transportador.

En el presente trabajo reportamos la construcción de proteínas quiméricas y/o mutaciones puntuales entre el CSTr y el CSTfl, a través de las cuáles se determinaron dominios involucrados en la unión de Na^+, Cl^- y diurético al transportador.

Simultáneamente se evaluó el papel que juegan diferentes aminoácidos del CST sobre las propiedades funcionales del transportador; se estudió el efecto de la N-glucosilación sobre el CSTfl y el efecto de diversas mutaciones tipo Gitelman.

<u>OBJETIVO 1</u>

Comenzaremos por analizar el papel que juega la N-glucosilación sobre la función del CSTfl, con la finalidad de encontrar si este evento estaba involucrado en las diferencias funcionales encontradas entre este y el CSTr.

Desde la clonación del CSTfl [29], se describieron tres sitios consenso para N-glucosilación, localizados en el asa que une a la región transmembrana 7 con la región transmembrana 8 (TM 7-8). Los residuos asparagina involucrados en este evento fueron: N403, N414 y N432, siendo el residuo N403, un aminoácido conservado en los todas las secuencias disponibles del CST (ver figura 1 del artículo 1).

Para determinar el efecto de estos sitios sobre la función del CSTfl, fueron sustituidos los tres residuos de asparagina por glutamina a través de mutagénesis puntual. Se generaron mutantes simples, donde fue eliminado solo un sitio, mutantes dobles y una mutante triple que carecía de los tres sitios.

Nuestros resultados mostraron que la eliminación de un sitio de glucosilación e incluso la eliminación de dos sitios, no interfiere con la actividad del CSTfl. Sin embargo la eliminación de los tres sitios dio como resultado, una reducción significativa en la función del transportador (ver figura 3 del artículo 1). Con respecto a la sensibilidad al diurético, la eliminación de los sitios de glucosilación no tuvo ningún efecto (ver figura 4 del artículo 1). Previamente Hoover y col. [78] reportaron el efecto de la N-glucosilación sobre la función del CSTr. En este estudio, se reportaron dos sitios consenso para este evento sobre la estructura de este

transportador, en donde la eliminación de un solo sitio, redujo la función y la expresión sobre la superficie celular hasta un 50% y hasta un 90% con la eliminación de los dos sitios. La afinidad por el diurético tiazida se vio favorecida en estas mutantes de glucosilación del CSTr, en donde la eliminación de estos sitios, aumento la sensibilidad del transportador por el diurético.

Como se puede apreciar, el efecto que muestran estos transportadores ante la glucosilación es completamente diferente, mientras que, para el CSTr es necesaria la glucosilación para lograr una adecuada expresión sobre la superficie celular, para el CSTfl no es necesario este evento. El CSTr aumenta su sensibilidad por las tiazidas al no estar glucosilado, mientras que el CSTfl no muestra cambios significativos ante la misma situación. Brevemente mencionaremos que resultados similares encontramos en el CSB1/NKCC2, en donde la eliminación de los sitios de glucosilación no incrementó significativamente la afinidad de este transportador por la bumetanida (ver figura 6 del artículo 3).

OBJETIVO 2 Y 3

Para poder determinar los dominios estructurales involucrados en la función del CST, en un segundo paso generamos proteínas quiméricas entre el CSTr y el CSTfl.

Fueron generados sitios de restricción silenciosos para las enzimas NsiI, HpaI, MunI y SacII, en la secuencia de ambos transportadores, los que permitieron intercambiar fragmentos de la proteína (ver figura 5 del artículo 1).

La nomenclatura para las quimeras generadas, constó de cinco letras, en los que la posición de cada letra corresponde a uno de los 5 fragmentos en los que se dividió la proteína. Estos 5 fragmentos son: NH_2 (1), TM1-7 (2), asa conectora TM7-8 (3), TM8-12 (4) y región $COOH^-$ (5); siendo utilizadas las letras R o F para determinar si el fragmento pertenecía al CSTr o al CSTfl.

Con la generación de los sitios NsiI y HpaI, se logró la construcción de seis proteínas quiméricas; dos en las que se intercambio la región NH_2 (RFFFFF y FRRRR), dos quimeras en las que se intercambio el extremo $COOH^-$ (FFFFR y

4

RRRRF) y dos en donde las regiones TM del CSTr estaban flanqueadas por las regiones NH_2 y $COOH^-$ del CSTfl y viceversa (FRRRF y RFFFR).

Los sitios de restricción MunI y SacII permitieron la construcción de 4 quimeras adicionales, dos en las que se intercambio el asa conectora TM7-8 (RRFRR y FFRFF) y dos en las que además de intercambiar el asa conectora, también los sitios consenso para glucosilación fueron eliminados (RRFRR/G- y FFRFF/G-).

Cuatro cambios más fueron generados, en dos de ellos, los sitios para N-glucosilación presentes en el CSTr, fueron sustituidos por los sitios presentes en la secuencia del CSTfl y viceversa (CSTr-fl-G-like y CSTfl-r-G-like). Los otros dos cambios consistieron en construir quimeras en las que se intercambió el asa conectora TM7-8, permaneciendo las secuencias consenso para N-glucosilación del transportador nativo (RRFRR-r-G-like y FFRFF-fl-G-like).

Finalmente se construyeron cuatro quimeras más, en las cuales los segmentos TM1-7 y TM8-12 fueron intercambiados (RFRRR, FRFFF, RRRFR y FFFRF).

Los análisis cinéticos para determinar la afinidad del transporte de Na^+, mostraron que las quimeras formadas por las regiones TM del CSTr, guardaban un comportamiento similar al del transportador nativo (Km de 5.5 ± 1.0 mM), Por ejemplo, en la quimera FRRRR se observo un Km de 8.1 ± 1.1 mM. Mientras que la quimera RRFRR presento un Km de 5.0 ± 0.6 mM (ver figura 9 del artículo 1).

Un comportamiento similar mostraron las quimeras formadas por las regiones TM del CSTfl, en donde las quimeras RFFFR y FFRFF presentaron un Km para Na^+ de 28 ± 6.0 y de 87 ± 45 mM similar al del CSTfl nativo (30 ± 6.0 mM). En cuanto a su afinidad por el Cl^- estas mismas proteínas quiméricas mostraron valores semejantes a los del CSTfl nativo (17 ± 2.8 y 11 ± 4.1 mM vs 15 ± 2.0 respectivamente) (ver figura 6 del artículo 1).

La afinidad por el diurético fue similar entre los transportadores nativos y las quimeras en las cuales los dominios TM no fueron modificados.

En conclusión, nuestros primeros resultados *mostraron que son las regiones TM las involucradas en la afinidad por los iones y tiazidas;* mientras que las regiones NH_2, $COOH^-$, asa conectora TM7-8 y aminoácidos involucrados en la N-

glucosilación, no están involucradas en determinar las propiedades funcionales del CST.

Con base en los resultados mencionados, en un siguiente estudio evaluamos el papel que desempeñan las regiones TM sobre las propiedades funcionales del CST.

Como se mencionó anteriormente se construyeron cuatro quimeras en las que se intercambiaron las regiones TM1-7 y TM8-12 entre el CSTr y el CSTfl (RFRRR, FRFFF, RRRFR y FFFRF). Una de las cuatro quimeras no mostró actividad (FRFFF).

Los análisis funcionales de las quimeras RFRRR, RRRFR y FFFRF realizados en ovocitos de *Xenopus laevis*, mostraron datos importantes que permitieron determinar dominios involucrados en determinar la afinidad para iones y metolazona en el CST.

El IC_{50} para metolazona observado en las quimeras RFRRR y FFFRF (0.4 ± 0.002 y 0.6 ± 0.006 µM respectivamente) fue similar al del CSTr nativo (0.3 ± 0.005 µM) y diferente al que es observado en el CSTfl (12.5 ± 1.8 µM). Mientras que el IC_{50} observado en la quimera RRRFR fue semejante al del CSTfl nativo (ver figura 10 del artículo 1).

Estos resultados *sugieren que la afinidad para el diurético esta determinada por las regiones TM8-12 del CST.*

Los análisis cinéticos realizados para determinar la afinidad por Na^+, en las quimeras RFRRR, RRRFR y FFFRF (Km de 22 ± 2.8, 14.5 ± 0.7 y 43 ± 12.6 mM respectivamente), mostraron valores intermedios a los que presentan los transportadores nativos: CSTfl Km de 30 ± 6.0 mM y CSTr 5.5 ± 1.0 mM (ver figura 10 del artículo 1).

Las cinéticas de transporte para Cl^-, revelaron que las quimeras RFRRR y FFFRF (Km de 17 ± 4.6 y 12.8 ± 3.0 mM) presentan un comportamiento similar al del CSTfl nativo (Km de 15 ± 2.0 mM); mientras que la quimera RRRFR mostró un Km similar al de CSTr nativo (2.4 ± 0.7 vs 2.6 ± 0.6 mM respectivamente) (ver figura 10 del artículo 1).

6

Estos resultados sugieren que *la afinidad que muestra el CST por el Cl⁻ está determinada por las regiones TM1-7, mientras que la afinidad al Na⁺ esta determinada tanto por las regiones TM1-7como por las TM8-12* (ver figura 11 del artículo 1)*.*

OBJETIVO 4

Paralelamente a la construcción de quimeras, realizamos un estudio de Polimorfismos de Nucleótidos Individuales (SNPs) en el CST, con el objetivo de determinar aminoácidos específicos, involucrados en la función de este transportador.

Los SNPs se definen como un cambio en la secuencia de nucleótidos, que se presenta en al menos el 1% de la población y no es capaz de producir enfermedad.

Encontramos que existen reportados más de 200 SNPs a lo largo del gen SLC12A3 [90,91]. Solo algunos, están localizados en regiones exónicas y la sustitución no se refleja en un cambio del aminoácido (A122A, T465T, S628S, A714A, G876G).

En dos SNPs reportados, la sustitución mostró un aminoácido diferente; el SNP R863K y el G264A (ver figura 1 del artículo 2). En este estudio consideramos irrelevante el análisis del polimorfismo R863K, ya que es un residuo localizado en el extremo COOH⁻ de la proteína y como se mostró con la construcción de quimeras entre el CSTr y el CSTfl, este dominio no esta involucrado en determinar las propiedades funcionales del transportador; sumado a esto, el residuo Arginina (R) solamente se observa en la secuencia del CST de humano, mientras que el residuo Lisina (K), esta presente en todas las secuencias del CST por lo que se considero un cambio poco significativo.

Con base en lo anterior, enfocamos este estudio en el análisis del SNP G264A. El aminoácido Glicina 264 esta localizado en la TM4 y es un residuo altamente conservado no solo en las secuencias de CST, [29,37-41] sino en todos los miembros de la familia de transportadores SLC12 [36].

Los análisis en ovocitos de *Xenopus laevis*, mostraron que este polimorfismo disminuye la actividad del CST al 50% (ver figura 3 del artículo 2). Para explicar esta

reducción en la función, insertamos la proteína verde fluorescente (EGFP) tanto al transportador nativo, como en el SNP G264A. A través del análisis de microscopia confocal, se observaron cantidades similares de proteína en los ovocitos inyectados con el EGFP-CST y el EGFP-G264A. Por lo que la disminución en la función del CST-G264A no fue atribuida a una menor expresión de la proteína sobre la superficie celular (ver figura 4 del artículo 2).

Los análisis cinéticos para la afinidad por el transporte de Cl⁻, mostraron que *el SNP G264A disminuye drásticamente la Km para este ión cuando se compara con el CST nativo ⁻(Km 0.89 ± 0.2 vs 6.3 ± 1.1 mM).* Este polimorfismo no afectó la afinidad para Na^+ en el CST. (Km de 7.6 ± 1.6 y 5.7 ± 1.1 mM en el CST nativo y G264A respectivamente) (ver figura 5 del artículo 2).

También se determinó la afinidad a metolazona tanto en el CST nativo como en el SNP G264A. El IC_{50} para esta tiazida fue similar en ambos transportadores ($1X10^{-6}$ M) (ver figura 6 del artículo 2).

Los datos obtenidos en este estudio, mostrarón claramente como un único residuo incrementa significativamente la afinidad del transportador por el Cl⁻. Estos resultados concuerdan con los previamente descritos, en donde concluimos que son las regiones TM1-7 las que determinan la afinidad por Cl⁻ en el CST; ya que el SNP G264A se localiza en la región TM4. Estos resultados son semejantes a los reportados por Insenring y Forbush, quienes demostraron que es la región TM4 la involucrada en la afinidad a Cl⁻ en el CSB2/NKCC1.[54]

En un siguiente análisis, evaluamos el papel de la región TM4 del CST, con la finalidad de encontrar otros residuos involucrados en su función. Esta región esta formada por 22 residuos acídicos, de los cuales 3 aminoácidos adicionales al G264, son altamente conservados en todos los miembros de la familia, estos residuos corresponden a la Aspargina 258, Arginina 261 y Glicina 278 (ver figura 8 del artículo 2).

Para determinar si estos residuos influyen sobre las propiedades funcionales del transportador, a través de mutagénesis puntual se realizaron sustituciones de estos, por aminoácidos con características parecidas.

El análisis funcional en ovocitos de *Xenopus laevis*, mostró que la sustitución N258Q y R261L disminuyen significativamente la función del CST (~50%), mientras que la sustitución G278A resulta en un transportador no funcional (ver figura 9 del artículo 2). La reducción en la función del transportador, no fue asociada con menor expresión de éste sobre la superficie celular, ya que el análisis de microscopia confocal, no mostró cambios significativos entre EGFP-N258Q, EGFP-R261L y EGFP-CST nativo (ver figura 10 del artículo 2).

Se realizaron análisis cinéticos para determinar si el transporte de iones, se modificaba ante las sustituciones N258Q y R261L. Sin embargo las cinéticas para el transporte de Na^+ fueron similares entre estos cambios y el transportador nativo.

En cuanto a la afinidad por el Cl^- extracelular, la sustitución N258Q, incremento significativamente la afinidad por este ión (3.2 ± 0.7 mM) en comparación con el CST nativo (6.3 ± 1.1 mM). Un ligero aumento en la afinidad a Cl^- se observó en la sustitución R261L, aunque este incremento no fue estadísticamente significativo (3.2 ± 1.6 mM).

Nuestros resultados concluyen nuevamente que la afinidad para Cl^- en el CST esta determinada por los dominios TM1-7, donde la región TM4 juega un papel importante.

OBJETIVO 5

AMINOÁCIDOS INVOLUCRADOS EN EL TRÁFICO DE CST A LA MEMBRANA CELULAR.

Otros aspectos de relación estructura-función en el CST fueron evaluados. Determinamos aminoácidos puntuales involucrados en el tráfico de esta proteína a la membrana celular y en su regulación.

El análisis de mutaciones que suceden espontáneamente en el CST, permitió detectar residuos responsables del tráfico de esta proteína a la membrana, una vez que ha sido sintetizada adecuadamente.

Hasta el momento más de 100 mutaciones en el gen SLC12A han sido reportadas, cuando estas suceden, producen una enfermedad conocida como Síndrome de Gitelman.[61]

Un porcentaje considerable de mutaciones-Gitelman, ocasionan bloqueo total de la función del CST, [39,75] por lo tanto, el papel que juegan estos aminoácidos sobre la función del transportador no puede ser evaluado, debido a la nula expresión de la proteína sobre la superficie celular. Kunchaparty y col.[39] analizaron varias mutaciones-Gitelman, encontrando nula actividad del transportador mutado, que fue asociado a un estado de glucosilación deficiente. Berkman y col.[92] analizaron 25 mutaciones más, a través de un análisis de Western blot observaron que algunas de ellas, se glucosilaban adecuadamente originando un transportador funcional. Consideramos que el estudio de estos residuos es de gran importancia, ya que pueden revelar aminoácidos involucrados en las propiedades funcionales del CST.

Para el siguiente estudio realizado, elegimos 5 mutaciones-Gitelman que si se glucosilan; G627V, R935Q, V995M, G610S y A585V; todas ellas localizadas en el extremo $COOH^-$ del CST, excepto A585V, que se encontró en la TM12 (ver figura 1 y 2 del artículo 4).

El análisis funcional en ovocitos de Xenopus laevis, mostró que las 5 mutaciones disminuyeron significativamente la función del CST. El porcentaje de función fue: CST nativo 100%, G627V 66.5%, R935Q 36.5%, V995M 32.5%, G610S 12.7% y A585V 6.21% (ver figura 3 del artículo 4).

Se realizó un nuevo análisis de Western blot para estas mutaciones, donde se corroboró la adecuada glucosilación de las 5 proteínas.

Los análisis cinéticos para el transporte de Na^+ y Cl^- fueron realizados en cada una de estas mutaciones-Gitelman. Los análisis cinéticos revelaron constantes de afinidad similares para ambos iones, tanto en las mutantes como en el CST nativo, excepto G627V que mostró mayor afinidad por Cl^- (Km Cl^- = 5.62 ± 0.5 y 2.53 ± 1.4 mM, en CST y G627V respectivamente) (ver figura 4 y 5 del artículo 4).

En cuanto a la afinidad por la tiazida, esta no se vio alterada en las mutaciones R935Q y V995M, que mostraron el mismo IC_{50} que el CST nativo ($2X10^{-6}$, $5X10^{-6}$ y $2X10^{-6}$ M respectivamente). Las mutaciones G610S y G627V aumentaron la afinidad del transportador por el diurético ($7X10^{-7}$ y $1X10^{-7}$ M respectivamente) (ver figura 6 del artículo 4).

Como se puede observar, no se apreciaron marcadas diferencias en cuanto a la afinidad por iones y/o tiazida entre el CST nativo y las mutantes-Gitelman. Sin embargo la función del CST mutado se redujo drásticamente. Para determinar esta disminución en la función, se insertó la proteína verde fluorescente (EGFP) en las 5 mutantes. Las construcciones EGFP-mutante y EGFP-CST la cuál se menciono anteriormente en el texto, fueron inyectadas en ovocitos de *Xenopus laevis*. El análisis de microscopia confocal reveló menor cantidad de proteína en la membrana de los ovocitos inyectados con las construcciones EGFP-mutantes (ver figura 7 del artículo 4).

Previos estudios de Hoover y col. [78] demostraron que la glucosilación es un evento necesario para la adecuada llegada del CSTr a la membrana celular. Así mismo, nuestro estudio de las mutaciones-Gitelman reveló que para el adecuado tráfico del CST a la membrana celular se requiere, tanto de un estado de glucosilación adecuado así como de aminoácidos puntuales que determinen esta función. *Concluimos que los aminoácidos G627, R935, V995, G610 y A585 son críticos para el tráfico del CST a la membrana celular.*

VIII. AMINOÁCIDOS PUNTUALES INVOLUCRADOS EN LA REGULACIÓN DE LA FUNCIÓN DEL CST

Durante la realización de mi proyecto doctoral colaboré en otros estudios donde el principal objetivo fue determinar los mecanismos involucrados en la regulación del CST. En este trabajo reportamos la fosforilación de aminoácidos específicos que determinan la funcionalidad de este transportador. De manera muy general a continuación describo los antecedentes, objetivos y resultados mas relevantes de este estudio.

ANTECEDENTES

Numerosos estudios han sugerido que la actividad de los miembros de la familia SLC12A esta regulada por procesos de fosforilación y defosforilación.

Se ha observado que la fosforilación activa al CSB/NKCC e inhibe a los KCCs, mientras que la defosforilación activa a los transportadores de K-Cl e inhibe la función del CSB/NKCC. Con estas observaciones se ha propuesto que estos transportadores comparten una vía de señalización común, ya que los estímulos que activan a una rama de la familia inhiben a la otra y viceversa. Por ejemplo la disminución del volumen celular, las concentraciones bajas de Cl$^-$ intracelular y la presencia de inhibidores de las proteínas fosfatasas inhiben a los transportadores KCCs, estimulando el transporte en los CSB/NKCC. Un efecto contrario se observa ante el aumento del volumen celular, las concentraciones intracelulares altas de Cl$^-$ y la presencia de proteínas fosfatasas. [79,80]

Estudios recientes de relación estructura-función han reportado aminoácidos específicos involucrados en eventos de fosforilación/defosforilación en el CSB2/NKCC1, estos aminoácidos corresponden a Treoninas localizadas en el extremo aminoterminal del transportador.

En 1992 Lytle y Forbush [81] realizaron estudios en túbulos de glándulas rectales de tiburón, mostraron que al agregar AMPc, estas células disminuyen su tamaño y a través de ensayos de [^{3}H] benzometanida (derivado de la bumetanida marcado radiactivamente) observaron un incremento en la unión del diurético a

las membranas celulares, lo que fue asociado como un aumento en la función del transportador. Los análisis de inmunoprecipitación realizados con anticuerpos monoclonales dirigidos a CSB2/NKCC1, revelaron que la activación de este transportador estaba asociada con la fosforilación del mismo.

En 1994 Xu y col. [19] señalaron que los residuos 184 al 194 localizados en el extremo aminoterminal del CSB2/NKCC1 (FGHNTIDAVP) estaban involucrados con la fosforilación de este transportador. En el 2002 Darman y Forbush [83] observaron la fosforilación en tres residuos del CSB2/NKCC1, estas observaciones fueron hechas después de someter a células de la glándula rectal del tiburón que expresan a este transportador a una estimulación máxima con caliculina A (agente que previene la actividad de la fosfolipasa 1 y en consecuencia la defosforilación del transportador). Los residuos involucrados fueron a las Treoninas 184, 189 y 202 de CSB2/NKCC1, localizadas en el extremo aminoterminal de la proteína.

Para conocer la relevancia de estos residuos sobre la función del transportador, las treoninas fueron eliminadas a través de mutagénesis puntual y expresadas en células HEK-293 para su estudio.

Los estudios revelaron que la treonina 189 fue la más importante para la función de CSB2/NKCC1, ya que al ser sustituida por otro residuo (Alanina), la función del transportador se inhibió completamente, sugiriendo que la fosforilación en este residuo es necesaria para alcanzar un estado constitutivamente activo.

La eliminación de las treoninas 184 y 202 no tuvo efecto sobre la función del transportador. [84]

Posteriormente, este mismo grupo de investigación realizó estudios in vivo de la fosforilación del CSB2/NKCC1. Utilizaron fosfoanticuerpos específicos para este transportador denominados R5.

Los fosfoanticuerpos R5 fueron dirigidos a un péptido del extremo aminoterminal que incluía a las tres Treoninas ya estudiadas. Los resultados mostraron que la fosforilación del CSB2/NKCC1 corresponde con la activación del transportador. Recientemente se han reportado numerosos estudios que involucran la asociación de otras proteínas como SPAK (cinasa rica en prolinas y alaninas

relacionada con cinasas Ste20) y OSR1 (cinasa de respuesta a estrés oxidativo. 1) en la regulación del CSB2/NKCC1, así como en otros miembros de esta familia de transportadores cloro-catiónicos. [86, 87]

OBJETIVOS

1.- Estudiar aminoácidos involucrados en la regulación del CST.

1.a. Generar las mutaciones T53A, T58A y S71A sobre la secuencia nativa del CST.
1.b. Determinar las propiedades funcionales de las clonas construidas en el punto 1.a.
2.a. Determinar el efecto que tiene la concentración de Cloro intracelular $[Cl^-]_i$ sobre la regulación del CST.

RESULTADOS

Como ya se menciono anteriormente, estudios de relación estructura-función han reportado aminoácidos específicos involucrados en eventos de fosforilación/defosforilación en algunos miembros de la familia SLC12.

En estos estudios se ha reportado que los aminoácidos T184 y T189 ambos localizados en el extremo aminoterminal de la proteína, están asociados con la activación del CSB2/NKCC1. [83] Sumado es conocido que el CSB2/NKCC1 es regulado por la concentración de cloro intracelular $[Cl-]_i$ [103], al parecer la concentración de este ión propicia la fosforilación de los residuos de treonina descritos previamente.

Poco se conoce de aminoácidos involucrados en la regulación del CST, por lo que el objetivo de este trabajo, fue estudiar el papel que juegan ciertos residuos sobre la actividad de este transportador, así como el papel que juega la concentración de Cloro intracelular $[Cl^-]_i$ sobre la regulación de esta proteína.

Durante la realización de este estudio en un primer paso determinamos sí la disminución de $[Cl^-]_i$ tenía un efecto sobre la actividad del CST, como recordaremos, la $[Cl^-]_i$ determina la activación del CSB2/NKCC1.[103]

Para la realización de este estudio utilizamos dos estrategias experimentales. La primera consistió en la microinyección de ovocitos de *X. laevis* con el cRNA del CST y con agua. Los ovocitos fueron incubados por 16 horas en una solución

hipotónica libre de Cl^-. El fundamento de este protocolo estuvo basado en diferentes observaciones de otro grupo de investigación, en las cuáles se ha demostrado que el estrés hipotónico (170 mon$_M$/kg H_2O) induce la disminución en la $[Cl^-]_i$ en distintos tipos de células, [83,84] además se ha observado que el estrés hipotónico también origina la abertura de canales de Cl- en los ovocitos de *X. laevis*, promoviendo la salida de este ión de la célula. [102]

La segunda maniobra utilizada consistió en microinyectar ovocitos de *X. laevis* con el cRNA del CST solo, o junto con el cRNA del cotransportador K^+:Cl^- (KCC2). Se consideró de utilidad el KCC2 ya que es un transportador que permite la constantemente salida de los iones K^+ y Cl^- de la célula, además de que es el único de los KCCs que presenta actividad en condiciones isotónicas . [36,101]

Los ensayos de expresión funcional realizados en los ovocitos microinyectados con los diferentes cRNAs y con agua, mostraron que estos últimos no expresan actividad de transporte para Na^+-Cl^-.

Los ovocitos inyectados con el CST y sometidos a estrés hipotónico, aumentaron significativamente su función, en comparación con los ovocitos inyectados con el CST pero que fueron incubados en condiciones isotónicas.

Resultados similares se observaron en los ovocitos inyectados con CST-KCC2, estos incrementaron significativamente su función en comparación con los ovocitos que únicamente habían sido inyectados con el CST (ver figura 1 y 2 del artículo 5).

Estos resultados mostraron claramente que la regulación de la función del CST depende de la $[Cl^-]_i$.

Nuestro siguiente objetivo en este trabajo fue determinar si la disminución de la $[Cl^-]_i$ se relacionaba con la fosforilación del CST.

Como ya se mencionó, en el CSB2/NKCC1, la $[Cl^-]_i$ está involucrada en la fosforilación de los residuos Treonina, localizados en el extremo NH_2 de la proteína. Previamente se mostró la fosforilación de CSB2/NKCC1 en los residuos T184 y T189, a través de fosfo-anticuerpos denominados R5. [84]

En el CST, se encuentran sitios consenso para fosforilación, dentro de los cuáles las Treoninas T53 y T58 son aminoácidos conservados entre este transportador y el CSB2/NKCC1. Por lo que se especuló que la fosforilación del CST pudiera ser en estos residuos.[83, 100] (ver figura 3 A del artículo 5)

Para determinar la fosforilación del CST, no contamos con fosfo-anticuerpos que permitan reconocer al transportador fosforilado, por lo que utilizamos los fosfo-anticuerpos R5.

Inicialmente estos fosfo-anticuerpos no fueron capaces de reconocer al CST fosforilado, ya que la secuencia de residuos que reconoce el péptido R5 en CSB2/NKCC1 es diferente a su homologa en el CST.

El péptido R5 reconoce 16 residuos del CSB2/NKCC1. Analizando las secuencias de estos dos transportadores se encontraron 4 aminoácidos diferentes entre el CST y el CSB2/NKCC1.

A través de mutagénesis puntual se sustituyo el residuo Tirosina (Tyr 56) por un residuo Histidina (originando la sustitución Y56H), el cuál es un aminoácido conservado entre el CST y el CSB2/NKCC1.

Con la sola sustitución Y56H, el fosfo-anticuerpo fue capaz de reconocer una banda de 120 kDa que equivale al peso del CST.

Ante este hallazgo se inyectaron ovocitos de *Xenopus laevis* con el cRNA del CST y del CST junto con el KCC2. (ver figura 3 B del artículo 5)

El grupo de ovocitos inyectado con el CST fue incubado todo la noche en una solución hipotónica libre en Cl⁻, al igual que un grupo de ovocitos inyectados con CST-KCC2, mientras que un tercer grupo de ovocitos inyectados con CST-KCC2 se mantuvo en condiciones isotónicas. Análisis de Western blot mostraron que los fosfo-anticuerpos R5 incrementaron significativamente la detección del CST en los ovocitos en los cuales la $[Cl^-]_i$ había sido disminuida en comparación con los que habían sido mantenidos en condiciones isotónicas. (ver figura 3 C del artículo 5)

Simultáneamente se realizaron 3 sustituciones adicionales a la Y56H en el CST, es decir se genero un CST mutante en el cuál, 4 residuos diferentes en este transportador fueron cambiados por los residuos del CSB2/NKCC1. Como

resultado de estas sustituciones se genero una secuencia en el CST idéntica a la secuencia que reconoce el péptido R5 en el CSB2/NKCC1. Las sustituciones fueron las siguientes: L49Y, I59M y V61A.

El CST que contenía las 4 sustituciones (CST-4M), también fue detectado por los fosfo-anticuerpos R5. La detección aumento significativamente en ovocitos en los cuales la $[Cl^-]_i$ había sido disminuida. (ver figura 3 D del artículo 5)

Para determinar si la mayor expresión del CST observada en los ovocitos expuestos a estrés hipotónico o a la depleción de Cl^- ocasionada por KCC2, era producto de una mayor síntesis de proteína, se realizaron análisis de Western blot con anticuerpos dirigidos contra el CST. En los análisis no se observaron diferencias de cantidad de proteína entre los ovocitos en los cuales la $[Cl^-]_i$ había sido disminuida y los ovocitos que habían sido incubados en condiciones isotónicas.

Nuestros estudios mostraron que la actividad del CST esta asociada con la fosforilación de los residuos Thr^{53} y Thr^{58}, en donde el nivel de fosforilación está incrementado por la disminución de la $[Cl^-]_i$.

Para analizar el papel que juegan las treoninas T53 y T58 sobre la fosforilación del CST, estos residuos fueron sustituidos por residuos de Alanina.

Además de las 2 Treoninas involucradas con la fosforilación del transportador, se detecto un sitio consenso adicional en el extremo NH_2 del CST. Este sitio corresponde a un residuo Serina localizado en la posición 71, el cual también fue sustituido por un residuo Alanina para evaluar su posible participación sobre la fosforilación del CST.

Se generaron 3 mutantes simples en las cuales se eliminó un sitio de fosforilación en el CST (T53A, T58A y S71A), 3 mutantes dobles, en las cuáles fueron eliminados dos sitios (T53-58A, T58-S71A y T53-S71A) y una mutante triple que carecía de los tres sitios (T53-T58-S71A).

Se inyectaron ovocitos de *X. laevis* con los cRNAs tanto del CST nativo como de cada una de las mutantes de fosforilación. A través de análisis de expresión funcional, se observó que la mutante triple redujo el 100% la función del CST.

Las mutantes simples disminuyeron en diferentes porcentajes la función del CST. La mutante T53A disminuyó 27% la función del CST, mientras que la mutante S71A disminuyó 75% la función del transportador. La mutante T58A redujo el 100% de la función del CST. (ver figura 6 del artículo 5)

En cuanto al efecto de las dobles mutantes, en los 3 casos la función del CST fue significativamente reducida en comparación con el CST nativo y con las mutantes simples T53A y S71A.

Nuevamente se inyectaron ovocitos de *X. laevis* con los cRNAs del CST nativo y de cada una de las mutantes de fosforilación más el KCC2.

Todos los grupos de ovocitos fueron expuestos a estrés hipotónico.

A través de análisis de expresión funcional, se observó que la actividad fue incrementada significativamente tanto en el CST nativo como en las mutantes simples y dobles de fosforilación, sin observarse actividad en la triple mutante. (ver figura 7 del artículo 5) Estas observaciones sugieren que la función del CST puede ser disminuida e incluso abolida por la ausencia de algún sitio de fosforilación en condiciones basales. La función disminuida en las mutantes de fosforilación puede ser parcialmente restituida ante condiciones de estrés hipotónico.

En conclusión, en este estudio mostramos que la actividad del CST aumenta significativamente cuando se disminuye la $[Cl^-]_i$, así como también mostramos que los residuos T53, T58 y S71 son aminoácidos específicos involucrados en la fosforilación de este transportador.

The Na⁺:Cl⁻ Cotransporter Is Activated and Phosphorylated at the Amino-terminal Domain upon Intracellular Chloride Depletion*

Diana Pacheco-Alvarez[‡1], Pedro San Cristóbal[‡1], Patricia Meade[‡], Erika Moreno[‡¶], Norma Vazquez[‡], Eva Muñoz[§], Abigail Díaz[‡], María Eugenia Juárez[‡], Ignacio Giménez[§2], and Gerardo Gamba[‡3]

From the ‡Molecular Physiology Unit, Instituto Nacional de Ciencias Médicas y Nutrición Salvador Zubirán, Instituto de Investigaciones Biomédicas, Universidad Nacional Autónoma de México, Tlalpan 14000, Mexico City, Mexico, ¶Instituto de Ciencias de la Salud, Universidad Autónoma del Estado de Hidalgo, Pachuca, Hidalgo 42160, Mexico, and §Department of Pharmacology and Physiology, Facultad de Medicina, Universidad de Zaragoza, Zaragoza 50009, Spain

The renal Na⁺:Cl⁻ cotransporter rNCC is mutated in human disease, is the therapeutic target of thiazide-type diuretics, and is clearly involved in arterial blood pressure regulation. rNCC belongs to an electroneutral cation-coupled chloride cotransporter family (SLC12A) that has two major branches with inverse physiological functions and regulation: sodium-driven cotransporters (NCC and NKCC1/2) that mediate cellular Cl⁻ influx are activated by phosphorylation, whereas potassium-driven cotransporters (KCCs) that mediate cellular Cl⁻ efflux are activated by dephosphorylation. A cluster of three threonine residues at the amino-terminal domain has been implicated in the regulation of NKCC1/2 by intracellular chloride, cell volume, vasopressin, and WNK/STE-20 kinases. Nothing is known, however, about rNCC regulatory mechanisms. By using rNCC heterologous expression in Xenopus laevis oocytes, here we show that two independent intracellular chloride-depleting strategies increased rNCC activity by 3-fold. The effect of both strategies was synergistic and dose-dependent. Confocal microscopy of enhanced green fluorescent protein-tagged rNCC showed no changes in rNCC cell surface expression, whereas immunoblot analysis, using the R5-anti-NKCC1-phosphoantibody, revealed increased phosphorylation of rNCC amino-terminal domain threonine residues Thr⁵³ and Thr⁵⁸. Elimination of these threonines together with serine residue Ser⁷¹ completely prevented rNCC response to intracellular chloride depletion. We conclude that rNCC is activated by a mechanism that involves amino-terminal domain phosphorylation.

The renal Na⁺:Cl⁻ cotransporter (NCC⁴ or TSC, gene symbol SLC12A3, locus identification number 6559) that is expressed at the apical membrane of the mammalian distal convoluted tubule represents the major salt transport pathway in this segment of the nephron (1–4). Its essential role in preserving the extracellular fluid volume and blood pressure has been established by the identification of inactivating mutations of the SLC12A3 gene as the cause of Gitelman's disease (5, 6), an inherited disorder featuring arterial hypotension, renal salt wasting, hypokalemic metabolic alkalosis, hypocalciuria, and hypomagnesemia. In addition, a defect in NCC regulation by serine/threonine kinases WNK1 and WNK4 has been implicated in the pathogenesis of a salt-dependent form of human hypertension known as pseudohypoaldosteronism type II (PHAII) (7, 8), which features marked sensitivity to hydrochlorothiazide and a clinical picture that is a mirror image of Gitelman's disease (9). NCC is the pharmacological target of thiazide-type diuretics that are currently recommended by the Joint National Committee VII for the detection, evaluation, and treatment of high blood pressure as the first line treatment of arterial hypertension either as the unique drug or in combination with other antihypertensive agents (10). Despite the importance of NCC for cardiovascular and renal physiology, pharmacology, and pathophysiology, little is known about the mechanisms by which NCC activity is regulated.

NCC belongs to the superfamily of electroneutral cation-coupled chloride cotransporters (SLC12) from which seven members have been identified at both the functional and molecular level. NCC, together with two isoforms of the Na⁺:K⁺:2Cl⁻ cotransporter, NKCC1 and NKCC2, compose the sodium-driven branch (NKCCs), and four isoforms of the K⁺:Cl⁻ cotransporter compose the potassium-driven branch (KCCs). Because these cotransporters are involved in the regulation of cell volume and/or in clamping the intracellular chloride concentration $[Cl^-]_i$, it has been proposed that their activity is regulated by changes in cell volume and/or $[Cl^-]_i$ by means of phosphorylation/dephosphorylation pathways (for

---

review, see Refs. 11–15). Several lines of evidence suggest that phosphorylation activates NKCCs and inhibits KCCs cotransporters, whereas dephosphorylation inhibits NKCCs and activates KCCs cotransporters. For instance, cell shrinkage, low intracellular chloride concentration, and protein phosphatase inhibitors activate NKCC1. Studies in this last cotransporter led to the identification of three amino-terminal threonine residues that become phosphorylated under such stimulatory conditions (16, 17). These threonine residues participate also in the stimulation of NKCC1 and NKCC2 by serine/threonine kinase WNK3 (18, 19) or WNK1–WNK4/STE20 kinases pathways (20, 21) as well as NKCC2 by vasopressin in thick ascending limb cells (22). Little is known, however, about NCC regulation. We have shown that rNCC is partially inhibited by cell swelling (23) or WNK4 (7) and is remarkably activated by WNK3 (19), suggesting that, like NKCC1 and NKCC2, NCC could be regulated by cell volume, $[Cl^-]_i$, or WNK kinases, at least in part through phosphorylation of the conserved amino-terminal domain threonine residues. Here we show that rNCC activity and amino-terminal domain phosphorylation is increased by $[Cl^-]_i$ depletion strategies. rNCC activation is completely prevented when the amino-terminal domain threonine residues Thr[53] and Thr[58] and serine residue Ser[71] are eliminated, suggesting that these amino acid residues are absolutely required for such regulation.

EXPERIMENTAL PROCEDURES

Clones and Mutagenesis—We used the rat NCC and human KCC2 cDNAs that we cloned previously from rat kidney and human brain, respectively (24, 25). All site directed mutations were introduced by using the QuikChange site directed mutagenesis system (Stratagene). Automatic DNA sequencing was used to confirm all mutations. All primers used for mutagenesis were custom made (Sigma).

Assessment of the Na$^+$:Cl$^-$ Cotransporter Function—rNCC activity was assessed by functional expression in *Xenopus laevis* oocytes following our protocols published previously (23, 26). Oocytes injected with water or rNCC cRNA (10 ng/oocyte) were exposed to two different conditions that promote a decrease in the $[Cl^-]_i$:low Cl$^-$ hypotonic stress and/or coinjection with the K$^+$:Cl$^-$ cotransporter KCC2 cRNA (10 ng/oocyte). After injection, oocytes were maintained during 4 days in isotonic ND96 (96 mM NaCl, 2 mM KCl, 1.8 mM CaCl$_2$, 1.0 mM MgCl$_2$, and 5.0 mM HEPES/Tris, pH 7.4). The night before the uptake assay, oocytes were incubated in two different osmolar conditions: isotonic (ND96, ~210 mosm/kg H$_2$O) or low Cl$^-$ hypotonic stress (79 mM Na$^+$ isethionate, 2 mM K$^+$-gluconate, 1.8 mM Ca^{2+} gluconate, 1.0 mM Mg^{2+}-gluconate, 5 mM HEPES, ~170 mosm/kg H$_2$O, pH 7.4). Then, tracer ^{22}Na$^+$ uptake (PerkinElmer Life Sciences) was assessed in oocytes exposed to isotonicity using our usual isotonic uptake solution (40 mM NaCl, 56 mM N-methyl-D-glucamine-chloride, 1.8 mM CaCl$_2$, 1.0 mM MgCl$_2$, 5.0 mM HEPES, pH 7.4, 210 mosm/kg H$_2$O) containing 1 mM ouabain, 0.1 mM amiloride, and 0.1 mM bumetanide plus 2 μCi of ^{22}Na$^+$ per mL. In contrast, uptake in oocytes exposed to low Cl$^-$ hypotonic stress was assessed in a similar hypotonic uptake medium (40 mM NaCl, 38 mM N-methyl-D-glucamine-chloride, 1.8 mM CaCl$_2$, 1.0 mM MgCl$_2$,

5.0 mM HEPES, pH 7.4, 170 mosm/kg H$_2$O) with the same drugs and tracer ^{22}Na$^+$. Thus, ^{22}Na$^+$ uptake in oocytes injected with water, rNCC cRNA alone, rNCC + KCC2 cRNA, or any rNCC mutant with or without KCC2 cRNA was assessed under both regular isotonic and Cl$^-$-free hypotonic protocols. Tracer activity was determined for each oocyte dissolved in 10% SDS by β-scintillation counting.

Western Blotting—Western blot was used to compare the amount of NCC protein in cRNA-injected oocytes exposed to the intracellular chloride depletion maneuvers described above. Immunoblots were performed using a rabbit polyclonal anti-NCC antibody kindly provided by Mark Knepper, National Institutes of Health, (27) following our previously published protocol (28). In brief, groups of 15 oocytes exposed to each maneuver were homogenized in 4 μl/oocyte of homogenization buffer, centrifuged twice at 100 × g for 10 min at 4 °C, and supernatant was recollected. Oocyte protein (equivalent to one oocyte per lane) was heated in sample buffer containing 6% SDS, 15% glycerol, 0.3% bromphenol blue, 150 mM Tris, pH 7.6, and 2% β-mercaptoethanol, resolved by SDS-PAGE (7.5%). Proteins were transferred to a polyvinylidene difluoride membrane and exposed overnight at 4 °C to the rabbit polyclonal anti-NCC antibody diluted 1:1500 in blocking buffer, TTBS (2.24 g/liter Tris-base, 8 g/liter NaCl, 0.1% Tween, pH 7.6) 0.2%. Membranes were washed and incubated with horseradish peroxidase-conjugated secondary (anti-rabbit) antibody (Alpha Diagnostic Intl.) diluted 1:2000 in blocking buffer and washed again. Bands were detected by using ECL plus Western blotting detection system (Amersham Biosciences).

Assessment of the rNCC Expression at the Oocytes Plasma Membrane—Surface expression of wild type or mutant NCC (see below) was determined with confocal microscopy by assessing the surface fluorescence in *Xenopus* oocytes using an amino terminus enhanced green fluorescent protein (EGFP)-NCC fusion construct that we have validated previously (7, 19, 28–30). In this construct, the EGFP was fused in frame to the amino-terminal domain of NCC. *Xenopus* oocytes were microinjected with water as control or with EGFP-wild type-rNCC or EGFP-mutant-rNCC cRNA. Four days later, oocytes were monitored for EGFP fluorescence in the surface of the oocytes using a Zeiss laser scanning confocal microscope (objective lens ×10, Nikon). Excitation and emission wavelengths used to visualize EGFP fluorescence were 488 and 515–565 nm, respectively. For densitometry analysis, the plasma membrane fluorescence was quantified by determining the pixel intensity around the entire oocytes circumference using SigmaScan Pro image analysis software. Western blot was performed in proteins extracted from the EGFP-NCC-injected oocytes following the procedures described above.

NCC Phospho-antibody Studies—We used the previously characterized R5 antibody (17) that was raised to detect phosphorylation of residues Thr[212] and Thr[217] in human NKCC1 (shark Thr[184] and Thr[189]), a generous gift from B. Forbush, Yale University. R5-antibody is also useful to detect phosphorylation of corresponding residues Thr[99] and Thr[104] in rabbit NKCC2 (31). Through sequence comparison and mutation analysis (see Fig. 3 in "Results and Discussion"), we found that for rNCC to

be recognizable by the R5 antibody at least tyrosine at position 56 in rat NCC must be converted to the histidine found in NKCCs. Therefore, using custom primers we constructed an rNCC single mutant Y56H-NCC or a quadruple mutant L49Y-Y56H-I59M-V61A, this latter containing all significant differences between NCC and NKCC2. For functional analysis oocytes injected with appropriate cRNA constructs were incubated in the same experimental solutions and for the same time as those described above. At the end of the incubation period, 4 oocytes per group were homogenized in 100 μl of ice-cold antiphosphatase solution (150 mM NaCl, 30 mM NaF, 5.0 mM EDTA, 15 mM Na_2HPO_4, 15 mM pyrophosphate, 20 mM HEPES, pH 7.2) with 1% Triton X-100 and a protease inhibitor mixture. Then, homogenate was cleared by centrifugation, and supernatants were subjected to Western blotting. The equivalent to 6 μl of lysate was loaded per lane. The analysis was repeated four times, and functional expression was assessed in parallel for each experiment.

To test for the specificity of R5 antibody signal with NCC samples, we carried out alkaline phosphatase treatment of oocyte homogenates. Briefly, after 16-h incubation in ND96 or Cl^--free solutions, oocytes were lysed in AlkPhos solution (50 mM Tris, pH 8.0, 1 mM EDTA, 100 mM NaCl, 2 mM $MgCl_2$, 1% Triton, 0.2% SDS) to which protease inhibitors and calyculin A were added to avoid protein degradation and PP1-mediated dephosphorylation. Then, homogenates were split in two, and 5 units of phosphatase alkaline were added to one of the samples. Homogenates were incubated for 1 h at 37 °C. The dephosphorylation reaction was terminated by adding the same volume of 2x sample buffer. 12 μl of this solution were loaded per lane and was subjected to SDS-PAGE electrophoresis and Western blotting with R5 antibody.

In Vitro cRNA Translation—To prepare cRNA for microinjection, each of the wild-type or mutant cDNA was digested at the 3' end using NotI or NheI from New England Biolabs (Carlsbad, CA), and cRNA was transcribed *in vitro* using the T7 RNA polymerase mMESSAGE mMACHINE™ (Ambion) transcription system. cRNA product integrity was confirmed on agarose gels, and concentration was determined by absorbance reading at 260 nm (DU 640, Beckman Coulter, Fullerton, CA). cRNA was stored frozen in aliquots at −80 °C until used.

Data Analysis—All results presented are based in a minimum of three different experiments with at least 10 oocytes per group in each experiment. Statistical significance is defined as two-tailed, with $p < 0.05$, and the results are presented as mean ± S.E. The significance of the differences between groups was tested by one-way analysis of variance with multiple comparisons using Bonferroni's correction.

RESULTS AND DISCUSSION

NCC Activity Is Increased by Intracellular Chloride Depletion Maneuvers—Because the regulatory mechanisms controlling electroneutral cotransporters in their native tissues and in transfected cells seem to operate in response to intracellular chloride concentration or to correct changes in intracellular chloride concentration (11), the present study tested such mechanisms of regulation for NCC. We used two different experimental strategies to induce a depletion of $[Cl^-]_i$. The first
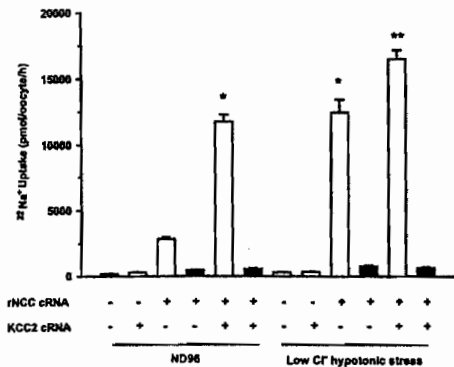
FIGURE 1. **Effect of intracellular chloride depletion protocols upon rNCC activity.** *X. laevis* oocytes were injected with water or 0.2 μg/μl of rNCC cRNA alone or together with 0.2 μg/μl of KCC2 cRNA, as stated. After 4 days of incubation in regular ND96, oocytes were incubated for 16 h in either regular ND96 (210 mosm/kg H_2O) or a Cl^--free hypotonic medium (170 mosm/kg H_2O), as stated. In the next day $^{22}Na^+$ uptake was assessed in the absence (*open bars*) or presence (*closed bars*) of 100 μM metolazone in uptake media containing 40 mM NaCl with similar osmolarity to which oocytes were exposed the night before (see "Experimental Procedures"). This figure shows combined results from five different experiments with the mean ± S.E. of 50 oocytes for each group. *, significantly different from the uptake observed in the control group of rNCC-injected oocytes incubated in ND96. **, significantly different from each strategy alone.

protocol was to compare the activity of rNCC in *X. laevis* oocytes injected with rNCC cRNA alone or together with of K^+:Cl^- cotransporter KCC2 cRNA. We chose KCC2 because it is the K^+:Cl^- cotransporter isoform that is significantly active in isotonic conditions when expressed in *X. laevis* oocytes (11, 25), thus maintaining a continuous K^+:Cl^- efflux over the incubation days before the uptake assays were performed. A similar approach was used in HEK-293 cells by Gillen and Forbush (32) that analyzed the regulation of NKCC1 activity by intracellular chloride depletion induced by cotransfecting the cells with KCC1. The second protocol was the "low Cl^- hypotonic stress" in which rNCC-injected oocytes were incubated in a Cl^--free, slightly hypotonic medium (170 mosm/kg H_2O) for several hours before the uptake assay. Low Cl^- hypotonic stress is known to induce a decrease in $[Cl^-]_i$ in several cells (16, 17), including oocytes from *Rana pipens* (33). In addition, low Cl^- hypotonic stress in *X. laevis* oocytes induces the opening of Cl^- channels that promote Cl^- efflux (34).

Fig. 1 depicts the effect of each protocol separately, or together, upon tracer $^{22}Na^+$ uptake in H_2O- or rNCC-injected oocytes. As we have shown previously (1, 23, 30), $^{22}Na^+$ uptake in water-injected oocytes was very small and not thiazide sensitive, indicating that *X. laevis* oocytes do not express endogenous activity of a Na^+:Cl^- cotransporter. As shown in Fig. 1, the minimum uptake observed in water-injected oocytes was not affected by KCC2 cRNA injection or by low Cl^- hypotonic stress. $^{22}Na^+$ uptake in rNCC-injected oocytes overnight in regular ND96 was 2840 ± 154 pmol oocyte^{-1} h^{-1}. In contrast, $^{22}Na^+$ uptake in oocytes coinjected with rNCC and
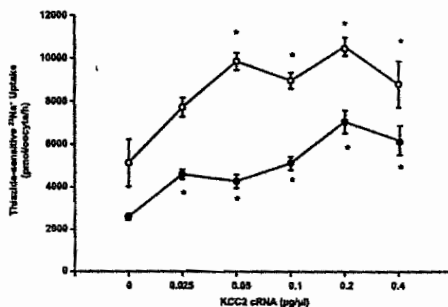
Regulation of rNCC by Chloride and Phosphorylation

FIGURE 2. **Dose-dependent effect of KCC2 cRNA upon NCC activity in oocytes.** Thiazide sensitive ^{22}Na$^+$ uptake in oocytes injected with rNCC cRNA exposed to regular isotonic conditions (*closed circles*) or to low Cl$^-$ hypotonic stress (*open circles*) the night before uptake experiments were performed. Oocytes were coinjected with increased concentration of KCC2 cRNA as stated. The figure shows combined results from three different experiments. *, $p < 0.05$ versus corresponding group not coinjected with KCC2 cRNA.

KCC2 cRNA and that were incubated in similar isotonic conditions was $11,757 \pm 514$ pmol oocyte^{-1} h^{-1} ($p < 0.001$). In oocytes that were injected with rNCC alone but were exposed to low Cl$^-$ hypotonic stress, ^{22}Na$^+$ uptake was $12,449 \pm 974$ pmol oocyte^{-1} h^{-1} ($p < 0.001$). Combination of both experimental protocols resulted in synergistic effect because ^{22}Na$^+$ uptake in rNCC + KCC2 cRNA-injected oocytes incubated overnight in the Cl$^-$-free hypotonic medium was $16,469 \pm 669$ pmol oocyte^{-1} h^{-1} ($p < 0.001$). As shown in Fig. 2, in oocytes incubated in isotonic conditions or exposed to low Cl$^-$ hypotonic stress, the effect of KCC2 cRNA coinjection upon rNCC activity was dose-dependent. Increased amount of KCC2 cRNA injected was associated with increased activity of rNCC. Oocytes exposed to low Cl$^-$ hypotonic stress exhibited higher basal activity and reached the plateau phase at lower KCC2 cRNA concentrations. Thus, promoting intracellular chloride depletion by two different strategies resulted in increased ^{22}Na$^+$ uptake by the renal Na$^+$:Cl$^-$ cotransporter. The increased uptake could be caused by the augmented driving force by the intracellular chloride depletion. Alternatively, as has been shown to occur with NKCC1, NCC can also be regulated by chloride-sensitive mechanisms. Therefore, we analyzed whether the intracellular chloride depletion maneuvers modulate the phosphorylation status of the conserved NCC amino-terminal domain threonines that in NKCC1 have been shown to be involved in its regulation by intracellular chloride (16).

Effect of Intracellular Chloride Depletion Protocols upon rNCC Phosphorylation—Data with kinase/phosphatase pharmacological inhibitors suggest that members of the *SLC12A* family of cotransporters are regulated by phosphorylation/dephosphorylation pathways. Phosphorylation induced by cell shrinkage, low intracellular Cl$^-$, and protein phosphatase inhibitors stimulates NKCCs and inhibits KCCs, whereas dephosphorylation induced by cell swelling, high intracellular Cl$^-$, and protein phosphatases stimulates KCCs and inhibits NKCCs (11, 13, 14, 33, 34). However, direct phosphorylation

has only been demonstrated so far for NKCC1 and NKCC2 (17, 22, 35). By using R5 antibody, a phospho-antibody that recognizes the phosphorylation of two amino-terminal domain threonine residues in NKCC1 (human sequence, Thr^{212}, Thr^{217}; shark, Thr^{184}, Thr^{189}) (17), it has been shown that activation of NKCC1 by low Cl$^-$ hypotonic stress, cell shrinkage, or coexpression with the WNK3 kinase is associated with phosphorylation of these conserved threonine residues (17–19, 36, 37). R5 antibody recognizes phosphorylation of NKCC1 across species (shark *versus* human) or isoforms (NKCC1 and NKCC2 (17, 22)) despite small amino acid divergences within the sequence used to raise the antibody (see alignment in Fig. 3A in which the 16 amino acid residues from human NKCC1 that were used to raise the R5-phosphoantibody (17) are indicated). In the close relative NCC, the two phosphoacceptor residues corresponding to Thr^{53} and Thr^{58} in rNCC are conserved. Because NCC retains the potential phosphoacceptor sites in this region of the amino-terminal domain, it was speculated previously that NCC could also be regulated by phosphorylation of these threonines (16, 22). As shown in Fig. 3B, however, the R5-phosphoantibody is not readily able to detect the wild-type rNCC under any experimental conditions either because these threonines are not phosphorylated in rNCC or because the epitope for R5 is somewhat altered, reducing its affinity for the antibody. This latter explanation is favored by the fact that in some instances we can observe a very faint band in wild-type NCC under low chloride conditions. Thus, we analyzed the sequence divergence among NKCCs and NCC (Fig. 3A) and introduced mutations in rNCC accordingly to render it recognizable by R5 antibody. We found (Fig. 3B) that this can be accomplished by simply replacing tyrosine Tyr^{56} by histidine (rNCC-Y56H in Fig. 3A), which is the major nonconservative change between NKCCs and NCC in the R5–16-amino acid residues peptide. R5 recognizes a band of 120 kDa corresponding to NCC only in the protein bearing the Y56H substitution, which is not observed in samples from wild-type NCC injected oocytes. More importantly, incubating the oocytes in Cl$^-$-free solution overnight or coinjecting Y56H-NCC with KCC2, conditions that remarkable increased transport activity (Figs. 1 and 2), caused a parallel stimulation of R5 signal in samples from Y56H-injected oocytes. We also made a quadruple mutant bearing all substitutions corresponding to sequence differences between NCC and NKCC2 (*Rat NCC-4M* in Fig. 3A: L49Y-Y56H-I59M-V61A). As shown in Fig. 3B, the quadruple mutant rNCC-4 M was also detected by R5-antibody, and the signal was increased after exposing oocytes to intracellular chloride depletion maneuvers. To answer the question of whether increased signal in oocytes exposed to Cl$^-$ hypotonic stress or coinjected with KCC2 was caused by increased amount of NCC protein, extracts from oocytes were analyzed by Western blot with polyclonal anti-NCC antisera. As shown in Fig. 3C, no difference in the amount of NCC was observed in proteins extracted from NCC-injected oocytes in control conditions when compared with those either exposed to Cl$^-$ hypotonic stress or coinjected with KCC2 or both. In addition, to answer the question of whether what we observed with R5 antibody is actual phosphorylation of NCC, we treated the oocyte lysates with alkaline phosphatase. As shown in Fig. 3D, the R5 signal disappeared or
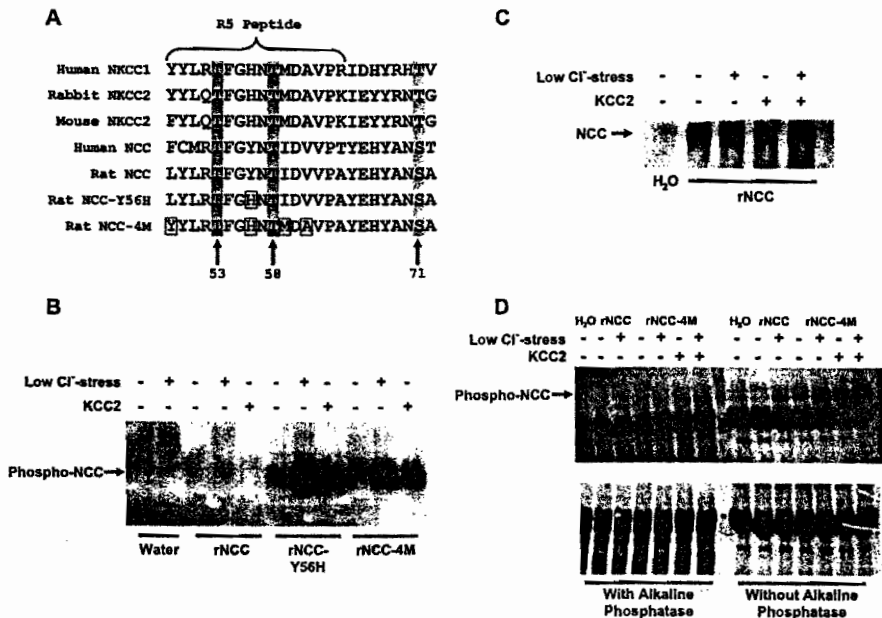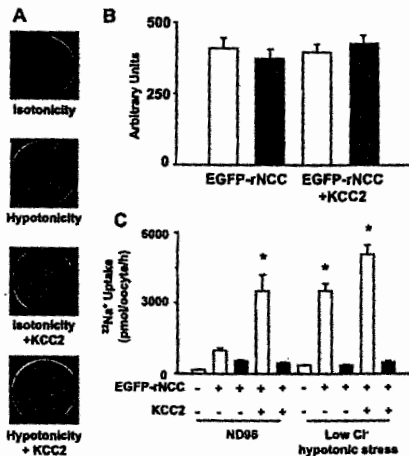
FIGURE 3. **Effect of intracellular chloride depletion protocols upon rNCC phosphorylation.** *A,* sequence alignment of an amino-terminal domain fragment of human NKCC1, rabbit and human NKCC2, human and rat NCC, and mutant rNCC, as stated. The proposed phosphorylation sites are highlighted by *gray boxes.* The mutated residues in NCC-Y56H and NCC-4 M are *outlined in black.* The *arrows* show the putative phosphorylation sites. *B,* a representative immunoblot analysis of proteins extracted from *X. laevis* oocytes injected with water, wild-type rNCC cRNA, the mutant rNCC-Y56H cRNA, or the mutant rNCC-4M cRNA at 0.2 μg/μl using the R5-phosphoantibody raised against the 16-residue phosphorylated peptide of NKCC1 shown in A. The band corresponding to phosphorylated NCC is shown as phospho-NCC. *C,* a representative Western blot of proteins extracted from rNCC-injected oocytes using polyclonal anti-NCC antibody (27). *D,* a representative immunoblot analysis of proteins extracted from *X. laevis* oocytes injected with water, wild-type rNCC cRNA, or the mutant rNCC-4 M cRNA at 0.2 μg/μl using the R5-phosphoantibody. The immunoblot was performed in control conditions or after exposing proteins to alkaline phosphatase as described under "Experimental Procedures" and is shown in the *upper panel.* The corresponding Coomassie Blue image is shown in the *lower panel.* For immunoblots in *B, C,* and *D,* proteins were extracted from oocytes in control conditions or either exposed to low chloride hypotonic stress or coinjected with KCC2 cRNA or subjected to both maneuvers together. Similar results were observed in five different experiments.

was greatly reduced after this treatment. As shown in Fig. 4, functional expression analysis revealed that single substitution of the tyrosine 56 for histidine (rNCC-Y56H) or the quadruple substitution (rNCC-4M) did not affect either the basal activity of rNCC or its activation by the coinjection with KCC2 or low Cl⁻ hypotonic stress.

Our results in the present study show that activity of rNCC in basal conditions is associated with phosphorylation of the amino-terminal domain threonine residues Thr⁵³ and Thr⁵⁸. The phosphorylation level was significantly increased by intracellular chloride depletion strategies that simultaneously increased the cotransporter activity. These observations suggest that increased uptake by NCC is not only a consequence of the augmented driving force by the intracellular chloride depletion. Supporting this conclusion, we have observed that protein phosphatase inhibition is coupled with increased activity of rNCC. Incubation of rNCC-injected *X. laevis* oocytes with the protein phosphatase 1 and 2A inhibitor calyculin A (100 nM) resulted in significant increase in rNCC-mediated ²²Na⁺

uptake from a value of 3961 ± 209 pmol oocyte⁻¹ h⁻¹ in the rNCC control group in the absence of calyculin A to a value of 5888 ± 310 pmol oocyte⁻¹ h⁻¹ in its presence ($n = 45$; $p < 0.001$). Taken together, our results demonstrate that, as for NKCCs, the activity of NCC correlates with phosphorylation of NH₂-terminus threonine residues at position 53 and 58.

Effect of Intracellular Chloride Depletion Protocols upon rNCC Surface Expression—Increased activity of rNCC by coinjection of KCC2 or low Cl⁻ hypotonic stress could be caused by the activation of cotransporter units that are already in the plasma membrane or by an increase in the amount of transporter units that reach the plasma membrane. To analyze these possibilities, we assessed in *X. laevis* oocytes the surface expression of the EGFP-rNCC construct that we have validated previously (29). We have shown that EGFP-rNCC fluorescence in the oocytes surface co-localizes with the F-404 specific plasma membrane dye and that oocytes injected with EGFP-rNCC exhibit significant thiazide sensitive ²²Na⁺ uptake, indicating the EGFP-NCC fluorescence is located in the plasma mem-

FIGURE 5. **Effect of intracellular chloride depletion protocols upon EGFP-rNCC surface expression.** Oocytes were injected with water or 25 ng of wild-type EGFP-rNCC cRNA with or without 10 ng/oocyte of KCC2 cRNA. Four days later oocytes were incubated overnight in either isotonic ND96 or Cl⁻-free hypotonic medium. The next day, the surface fluorescence of the oocytes was visualized through a laser scanning confocal microscope, and activity was assessed by tracer ^{22}Na$^+$ uptake assay as described under "Experimental Procedures." A shows a representative confocal image of each group, as stated. B, fluorescence intensity is expressed as mean ± S.E. of 30 oocytes from three different experiments exposed to isotonicity (*open bars*) or hypotonicity (*closed bars*) with or without coinjection with KCC2 cRNA, as stated. C, ^{22}Na$^+$ uptake was assessed in the absence (*open bars*) or presence (*closed bars*) of 100 μM metolazone in the uptake medium. Each bar represents the mean ± S.E. of 30 oocytes from three different experiments. *, significantly different from the uptake observed in the EGFP-rNCC control group.
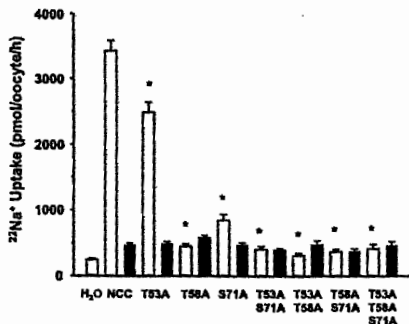
FIGURE 6. **Effect of elimination of Thr^{53}, Thr^{58}, and/or Ser^{71} of rNCC upon the rNCC basal function.** ^{22}Na$^+$ uptake in oocytes injected with wild-type or mutant rNCC, as stated, in the absence (*open bars*) or presence (*closed bars*) of 100 μM metolazone. Each bar shows the mean ± S.E. of 25–40 oocytes from three to five different experiments. *, significantly different from the uptake observed in wild type rNCC, $p < 0.01$.

neither functional in basal conditions nor activated by the intracellular Cl⁻ depletion strategies. In contrast, as long as one of the three phosphorylation sites is present, rNCC
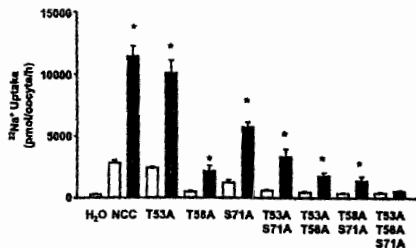
FIGURE 7. **Effect of elimination of Thr^{53}, Thr^{58}, and/or Ser^{71} of rNCC upon rNCC activation by intracellular chloride depletion protocols.** *Open bars* represent ^{22}Na$^+$ uptake in control oocytes, *e.g.* oocytes injected with rNCC cRNA or mutant rNCC cRNA and incubated the night before the uptake assay in isotonic ND96. *Black bars* represent rNCC or mutant NCC cRNA-injected oocytes exposed to low Cl⁻ hypotonic stress and coinjected with KCC2 cRNA. *, significantly different from the uptake observed in the corresponding control. Each bar represents at least the mean ± S.E. of 20 oocytes from three different frogs.

could be non-functional in basal conditions but still be activated by intracellular chloride depletion.

Effect of Replacing Thr^{53}, Thr^{58}, and Ser^{71} upon EGFP-rNCC Surface and Functional Expression—Because elimination of the three phosphorylation sites in the amino-terminal domain alone or in combination resulted in a significant reduction of the cotransporter basal activity, we wanted to know the effect of these mutations upon surface expression of the cotransporter. Thus we introduced the triple mutation T53-T58-S71A into the EGFP-rNCC cDNA. *X. laevis* oocytes were injected with 25 ng of each clone cRNA, and 4 days later the surface fluorescence intensity was assessed under confocal microscopy. Then, the same oocytes were used for functional analysis by assessing the thiazide sensitive ^{22}Na$^+$ uptake. As shown in Fig. 8, the surface expression of the triple mutant EGFP-rNCC was similar to wild-type EGFP-rNCC, whereas the functional expression was completely abolished. As a positive control, in the same experiment a group of oocytes was injected with 25 ng of cRNA transcribed from the EGFP-rNCC double mutant N404,424Q, in which both N-glycosylation sites of EGFP-rNCC were eliminated. As we have reported previously (29), elimination of the N-glycosylation sites resulted in a cotransporter in which the surface expression, and thus its activity, is seriously reduced. The observation that elimination of phosphorylation sites resulted in reduction of the cotransporter activity without affecting the surface expression is consistent with the results in Fig. 5 in which activation of rNCC by intracellular chloride depletion was not associated with surface expression changes. Taken together, the results of the present study show for the first time that the renal Na$^+$:Cl⁻ cotransporter is regulated by intracellular chloride concentration through phosphorylation of the amino-terminal domain and that the mechanism seems to be caused by an increased turnover rate of the cotransporter rather than by an increase in its expression in the plasma membrane.

In the present study we used the heterologous expression system in *X. laevis* oocytes to assess the regulation of NCC by intracellular chloride depletion. This expression system has
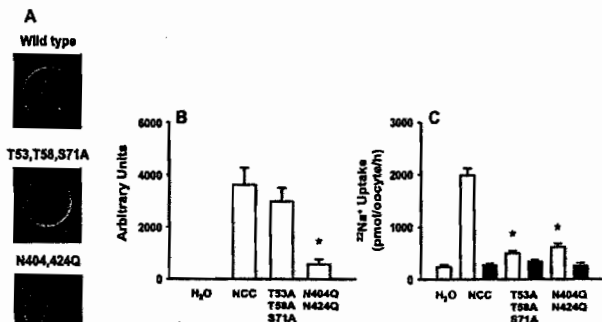
FIGURE 8. Effect of elimination of phosphorylation sites in the amino-terminal domain of EGFP-rNCC upon surface and functional expression. *A*, representative confocal image of each group, as stated. *B*, fluorescence intensity is expressed as mean ± S.E. of 20 oocytes from two different experiments. *C*, functional expression assessed by $^{22}Na^+$ uptake assay in the absence (*open bars*) or presence (*closed bars*) of 100 μM metolazone. Oocytes were injected with the wild-type or mutant EGFP-rNCC cRNA as stated. Functional expression assays were performed with the same oocytes that were used for fluorescence analysis in *B*. The EGFP-N404,424Q rNCC mutant, in which the two N-glycosylation sites have been eliminated, was used as control and was described previously (29). *, significantly different from wild-type EGFP-rNCC.

shown to be an excellent tool for a robust and reproducible expression of NCC in our hands (1, 7, 19, 23, 24, 29, 35) and in other laboratories (8, 36–38). In contrast, NCC expression in transfected mammalian cells has not been successful in many laboratories, including our own. In this regard, however, the prediction conducted using *X. laevis* oocytes by two different groups (7, 8) indicating that WNK4 down-regulates the surface expression (and thus activity) of NCC has recently been confirmed by assessing surface expression of NCC in renal epithelial cells transfected with NCC and WNK4 cDNA (39).

Because of the gradient of accompanying cation, the Na$^+$-couple chloride cotransporters NKCCs mediate Cl$^-$ influx, whereas K$^+$-coupled chloride cotransporters KCCs mediate Cl$^-$ efflux. Because intracellular concentration of Na$^+$ and K$^+$ are quickly restored by Na$^+$:K$^+$:ATPase, what the activity of electroneutral cation chloride cotransporters seems to modulate is the [Cl$^-$]$_i$. For instance, in most cells, [Cl$^-$]$_i$, and thus cell volume, is maintained by coordinated activity of NKCC1 and KCC1. It has been demonstrated in duck red blood cells that activity of these cotransporters is regulated by [Cl$^-$]$_i$ in such a way that low [Cl$^-$]$_i$ activates NKCC1 and inhibits KCC1, whereas high [Cl$^-$]$_i$ activates KCC1 and inactivates NKCC1 (40, 41). In neurons, intracellular chloride concentration is defined by the ratio of NKCC1/KCC2, and these in turn define the type of response to neurotransmitters such as γ-aminobutyric acid that acts by opening Cl$^-$ channels in postsynaptic membranes. The excitatory effect of γ-aminobutyric acid in the prenatal period is caused by an increased NKCC1/KCC2 ratio, which results in increased [Cl$^-$]$_i$, whereas the inhibitory effect of γ-aminobutyric acid in the postnatal period can be explained by decreased NKCC1/KCC2 ratio that results in decreased [Cl$^-$]$_i$ (42–45). It has been clearly shown that modulation of NKCC1 by [Cl$^-$]$_i$ is mediated, at least in part, by phosphorylation of the amino-terminal domain threonine residues shown

in Fig. 3 (17, 46). In addition, recent studies have shown that electroneutral cation chloride cotransporters are regulated also through phosphorylation of the amino-terminal domain by members of two serine/threonine kinase families known as WNK and STE20 (18–20, 47, 48). First it was shown that STE-20-related kinases such as SPAK or OSR1 mediate functional activation of NKCC1 (47, 49) by a process in which phosphorylation of the amino-terminal domain threonine residues is implicated. Later, Vitari *et al.* (20) observed that WNK1 and WNK4 seem to activate SPAK and OSR1, which in turns phosphorylated the amino-terminal domain of NKCC1. At the functional level, Gagnon *et al.* (48) also showed that WNK4 is able to increase the activity of NKCC1 only in the presence of SPAK or OSR1.

Distorted modulation of NCC activity by WNK1 and WNK4 is implicated in the pathophysiology of arterial hypertension in patients with PHAII (7, 8). WNK4 inhibits the activity of NCC, and the PHAII-type mutations prevent this inhibition, thus releasing NCC, which by its increasing activity produces arterial hypertension. This hypothesis can explain the exquisite sensitivity to thiazide-type diuretics in PHAII patients (9). WNK1 seems to produce PHAII by its ability to regulate WNK4 activity (8, 50, 51). We have recently shown that WNK3, another member of the WNK family, is a powerful activator of NCC as well as NKCC1 and NKCC2 (18, 19). The activation of NKCC1 and NKCC2 induced by WNK3 is also associated with increased phosphorylation of the amino-terminal domain threonine residues shown in Fig. 3 (18, 19). In the present study we show that NCC activity is modulated by [Cl$^-$]$_i$ and that phosphorylation of the amino-terminal domain threonine residues Thr^{53} and Thr^{58}, and probably Ser^{71}, is implicated, suggesting that modulation of NKCCs by [Cl$^-$]$_i$ and WNKs could be mediated by a common pathway. Supporting this possibility, it has been suggested that activity of WNK kinases is modulated by intracellular chloride. Xu *et al.* (52) identified WNK1 at the molecular level and observed that its activity was remarkably increased in the presence of NaCl. Then, Lenertz *et al.* (51) showed that WNK1 is activated by NaCl and other osmotic challenges in a variety of cell lines, including distal convoluted kidney tubule cells, although it is not affected by short or long exposure to several hormones and by agents that modulate cell proliferation, suggesting that the major regulator of WNK kinases is cell ion strength, volume, and/or intracellular ion concentrations. In this regard, Moriguchi *et al.* (21) have recently shown in HEK-293 cells that both WNK1 and SPAK/OSR1 kinases activity is increased when cells were exposed to low Cl$^-$ hypotonic stress, suggesting that WNK1 behaves as an activator of SPAK/OSR1 in response to a decrease in the [Cl$^-$]$_i$.

Supporting the observations in the present study, Moriguchi *et al.* (21) also observed in HEK-293 cells transfected with T7-tagged mouse NCC that the amino-terminal domain of NCC can be phosphorylated *in vitro* by the WNK1/SPAK/OSR1 pathway and that the phosphorylation level increases when cells are incubated under low Cl^- hypotonic stress and decreases when the residues Thr[53], Thr[58], and Ser[71] are eliminated. Thus, taking all these observations together it is reasonable to speculate that $[Cl^-]_i$ probably regulates WNKs and STE20 kinase activity that in turn modulates electroneutral cotransporters function.

In summary, we present evidence that rNCC can be activated by intracellular chloride depletion strategies such as co-expression with the K^+:Cl^- cotransporter KCC2 and/or exposure to low Cl^- hypotonic stress. The rNCC activation is associated with increased phosphorylation of the threonine residues 53 and 58 at the amino-terminal domain without changing the surface expression of the cotransporter. In addition, substituting Thr[53], Thr[58], and Ser[71] residues with alanine renders rNCC inactive in basal conditions and insensitive to intracellular chloride depletion, indicating that in addition to Thr[53], Thr[58], the serine at the position 71 is also critical for rNCC regulation.

REFERENCES

1. Gamba, G., Saltzberg, S. N., Lombardi, M., Miyanoshita, A., Lytton, J., Hediger, M. A., Brenner, B. M., and Hebert, S. C. (1993) *Proc. Natl. Acad. Sci. U. S. A.* **90**, 2749–2753
2. Ellison, D. H., Velazquez, H., and Wright, F. S. (1987) *Am. J. Physiol.* **253**, F546–F554
3. Plotkin, M. D., Kaplan, M. R., Verlander, J. M., Lee, W.-S., Brown, D., Poch, E., Gullans, S. R., and Hebert, S. C. (1996) *Kidney Int.* **50**, 174–183
4. Costanzo, L. S. (1985) *Am. J. Physiol.* **248**, F527–F535
5. Simon, D. B., Nelson-Williams, C., Johnson-Bia, M., Ellison, D., Karet, F. E., Morey-Molina, A., Vaara, I., Iwata, F., Cushner, H. M., Koolen, M., Gainza, F. J., Gitelman, H. J., and Lifton, R. P. (1996) *Nat. Genet.* **12**, 24–30
6. Mastroianni, N., Bettinelli, A., Bianchetti, M., Colussi, G., de Fusco, M., Sereni, F., Ballabio, A., and Casari, G. (1996) *Am. J. Hum. Genet.* **59**, 1019–1026
7. Wilson, F. H., Kahle, K. T., Sabath, E., Lalioti, M. D., Rapson, A. K., Hoover, R. S., Hebert, S. C., Gamba, G., and Lifton, R. P. (2003) *Proc. Natl. Acad. Sci. U. S. A.* **100**, 680–684
8. Yang, C. L., Angell, J., Mitchell, R., and Ellison, D. H. (2003) *J. Clin. Investig.* **111**, 1039–1045
9. Mayan, H., Vered, I., Mouallem, M., Tzadok-Witkon, M., Pauzner, R., and Farfel, Z. (2002) *J. Clin. Endocrinol. Metab.* **87**, 3248–3254
10. Chobanian, A. V., Bakris, G. L., Black, H. R., Cushman, W. C., Green, L. A., Izzo, J. L., Jr., Jones, D. W., Materson, B. J., Oparil, S., Wright, J. T., Jr., and Roccella, E. J. (2003) *JAMA* **289**, 2560–2571
11. Gamba, G. (2005) *Physiol. Rev.* **85**, 423–493
12. Hebert, S. C., Mount, D. B., and Gamba, G. (2004) *Eur. J. Physiol.* **447**, 580–593
13. Flatman, P. W. (2002) *Biochim. Biophys. Acta* **1566**, 140–151
14. Adragna, N. C., Fulvio, M. D., and Lauf, P. K. (2004) *J. Membr. Biol.* **201**, 109–137
15. Lauf, P. K., and Adragna, N. C. (2000) *Cell Physiol. Biochem.* **10**, 341–354
16. Darman, R. B., and Forbush, B. (2002) *J. Biol. Chem.* **277**, 37542–37550
17. Flemmer, A. W., Gimenez, I., Dowd, B. F., Darman, R. B., and Forbush, B. (2002) *J. Biol. Chem.* **277**, 37551–37558
18. Kahle, K. T., Rinehart, J., De Los, H. P., Louvi, A., Meade, P., Vazquez, N.,

19. Hebert, S. C., Gamba, G., Gimenez, I., and Lifton, R. P. (2005) *Proc. Natl. Acad. Sci. U. S. A.* **102**, 16783–16788
19. Rinehart, J., Kahle, K. T., De Los, H. P., Vazquez, N., Meade, P., Wilson, F. H., Hebert, S. C., Gimenez, I., Gamba, G., and Lifton, R. P. (2005) *Proc. Natl. Acad. Sci. U. S. A.* **102**, 16777–16782
20. Vitari, A. C., Deak, M., Morrice, N. A., and Alessi, D. R. (2005) *Biochem. J.* **391**, 17–24
21. Moriguchi, T., Urushiyama, S., Hisamoto, N., Iemura, S., Uchida, S., Natsume, T., Matsumoto, K., and Shibuya, H. (2005) *J. Biol. Chem.* **280**, 42685–42693
22. Gimenez, I., and Forbush, B. (2003) *J. Biol. Chem.* **278**, 26946–26951
23. Monroy, A., Plata, C., Hebert, S. C., and Gamba, G. (2000) *Am. J. Physiol.* **279**, F161–F169
24. Gamba, G., Miyanoshita, A., Lombardi, M., Lytton, J., Lee, W. S., Hediger, M. A., and Hebert, S. C. (1994) *J. Biol. Chem.* **269**, 17713–17722
25. Song, L., Mercado, A., Vazquez, N., Xie, Q., Desai, R., George, A. L., Gamba, G., and Mount, D. B. (2002) *Brain Res.* **103**, 91–105
26. Plata, C., Meade, P., Vazquez, N., Hebert, S. C., and Gamba, G. (2002) *J. Biol. Chem.* **277**, 11004–11012
27. Wang, X. Y., Masilamani, S., Nielsen, J., Kwon, T. H., Brooks, H. L., Nielsen, S., and Knepper, M. A. (2001) *J. Clin. Investig.* **108**, 215–222
28. Sabath, E., Meade, P., Berkman, J., De Los, H. P., Moreno, E., Bobadilla, N. A., Vazquez, N., Ellison, D. H., and Gamba, G. (2004) *Am. J. Physiol.* **287**, F195–F203
29. Hoover, R. S., Poch, E., Monroy, A., Vazquez, N., Nishio, T., Gamba, G., and Hebert, S. C. (2003) *J. Am. Soc. Nephrol.* **14**, 271–282
30. Moreno, E., Tovar-Palacio, C., De Los, H. P., Guzman, B., Bobadilla, N. A., Vazquez, N., Riccardi, D., Poch, E., and Gamba, G. (2004) *J. Biol. Chem.* **279**, 16553–16560
31. Gimenez, I., and Forbush, B. (2005) *Am. J. Physiol.* **289**, F1341–F1345
32. Gillen, C. M., and Forbush, B., III (1999) *Am. J. Physiol.* **276**, C328–C336
33. Keicher, E., and Meech, R. (1994) *J. Physiol. (Lond.)* **475**, 45–57
34. Ackerman, M. J., Wickman, K. D., and Clapham, D. E. (1994) *J. Gen. Physiol.* **103**, 153–179
35. Vazquez, N., Monroy, A., Dorantes, E., Munoz-Clares, R. A., and Gamba, G. (2002) *Am. J. Physiol.* **282**, F599–F607
36. Kunchaparty, S., Palcso, M., Berkman, J., Velázquez, H., Desir, G. V., Bernstein, P., Reilly, R. F., and Ellison, D. H. (1999) *Am. J. Physiol.* **277**, F643–F649
37. De Jong, J. C., Willems, P. H., Mooren, F. J., van den Heuvel, L. P., Knoers, N. V., and Bindels, R. J. (2003) *J. Biol. Chem.* **278**, 24302–24307
38. De Jong, J. C., Van Der Vliet, W. A., van den Heuvel, L. P., Willems, P. H., Knoers, N. V., and Bindels, R. J. (2002) *J. Am. Soc. Nephrol.* **13**, 1442–1448
39. Cai, H., Cebotaru, V., Wang, Y. H., Zhang, X. M., Cebotaru, L., Guggino, S. E., and Guggino, W. B. (2006) *Kidney Int.* **69**, 2162–2170
40. Lytle, C., and Forbush, B., III (1996) *Am. J. Physiol.* **270**, C437–C448
41. Lytle, C., and McManus, T. (2002) *Am. J. Physiol.* **283**, C1422–C1431
42. Lu, J., Karadsheh, M., and Delpire, E. (1999) *J. Neurobiol.* **39**, 558–568
43. Rivera, C., Voipio, J., Payne, J. A., Ruusuvuori, E., Lahtinen, H., Lamsa, K., Pirvola, U., Saarma, M., and Kaila, K. (1999) *Nature* **397**, 251–255
44. Delpire, E. (2000) *News Physiol. Sci.* **15**, 309–312
45. Mercado, A., Mount, D. B., and Gamba, G. (2004) *Neurochem. Res.* **29**, 17–25
46. Darman, R. B., Flemmer, A., and Forbush, B. (2001) *J. Biol. Chem.* **276**, 34359–34362
47. Dowd, B. F., and Forbush, B. (2003) *J. Biol. Chem.* **278**, 27347–27353
48. Gagnon, K. B., England, R., and Delpire, E. (2006) *Am. J. Physiol.* **290**, C134–C142
49. Piechotta, K., Garbarini, N., England, R., and Delpire, E. (2003) *J. Biol. Chem.* **278**, 52848–52856
50. Subramanya, A. R., Yang, C. L., Zhu, X., and Ellison, D. H. (2006) *Am. J. Physiol.* **290**, F619–F624
51. Lenertz, L. Y., Lee, B. H., Min, X., Xu, B. E., Wedin, K., Earnest, S., Goldsmith, E. J., and Cobb, M. H. (2005) *J. Biol. Chem.* **280**, 26653–26658
52. Xu, B., English, J. M., Wilsbacher, J. L., Stippec, S., Goldsmith, E. J., and Cobb, M. H. (2000) *J. Biol. Chem.* **275**, 16795–16801

IX. BIBLIOGRAFIA

1. Gamba G. Biología Molecular de la reabsorción renal de sodio. Rev. Invst. Clin. 44, 545-562. 1992.

2. Copen B M and Stanton B A. Renal Physiology. 1997.

3. Guyton A and Hall J. Textbook of Medical Physiology. W B Saunders Company. 349-365. 1996.

4. Drucker Colín. Fisiología Médica, Manual Moderno. 193-196, 226-229. 2005.

5. Hebert S C. Handbook of Physiology: Renal Physiology. Windhager E E. 875-925. 1992.

6. Berry C A and Rector F C. Mechanism of proximal NaCl reabsorption in the proximal tubule of the mammalian kidney. Sem Nephrol. 11:86-97. 1991.

7. Rector F C. Sodium, bicarbonate and chloride absorption by proximal tubule. Am J Physiol. (Renal Fluid Electrolyte Physiol) 244:F461- F471. 1993.

8. Schafer J A. Mechanism coupling the absorption of solutes and water in the proximal tubule. Kidney Int. 25: 708-716. 1984.

9. Berry C A and Rector F C. Renal transport of glucose, aminoacids, sodium, chloride and water. The Kidney. Edited by Brenner B M and Rector F J. Philadelphia: W.B. Saundres Company. 245-282. 1991.

10. Biemesderfer D, Rutherford P A, Nagy T, Pizzonia J H, Abu-Alfa A K. Monoclonal antibodies for high- resolution localization of NH3 in the adult and neonatal rat kidney. Am J Physiol. 273: F289-299.1997.

11. Greger R. Ion mechanism in thick ascending limb of Helen's loop of mammalian nephron. Physiol Rev. 65:760-97. 1985.

12. Gamba G. Electroneutral chloride-coupled co-transporters. Curr Opin. Nephrol Hypertens. 9:535-540. 2000.

13. Reeves W B, Winters C J, Andreoli T E. Chloride channels in the loop of Henle. Annu Rev Physiol 63:631-645. 2001.

14. Giebisch G. Physiological roles of renal potassium Channels. Semin Nephrol. 19:458-471. 1999.

15. Ellison D H, Velazquez H, Wright F S. Thiazide-sensitive sodium chloride cotransport in early distal tubule. Am J Physiol. 253:F546-F554. 1987.

16. Rose B D. Diuretics. Kidney Int. 39:336-352. 1991.

17. Verlander J M; Tran T M; Zhang L; Kaplan M R; Hebert S C. Estradiol enhances thiazide-sensitive NaCl cotransporter density in the apical plasma membrane of the distal convoluted tubule in ovariectomized rats. J.Clin.invest. 1661-1669. 1998.

18. htto://archive.uwcm.ac.uk/uwcm/mg/hgmd0.html

19. Xu J-C; Lytle C; Zhu T T; Payne J A; Benz Jr.E; Forbush III B. Molecular cloning and functional expression of the bumetanide-sensitive Na-K-Cl cotransporter. Proc Natl Acad Sci USA 91:2201-2205. 1994

20. Renfro J.L., (1975). Water and ion transport by the urinary bladder of the teleost Pseudopleuronectus americanus. Am.J.Physiol *228*, 52-61.

21. Renfro J L (1978). Interdependence of active Na+ and Cl- transport by the isolated urinary bladder of the teleosot, pseudopleronectes americanus. J.Exp.Zool. *199*, 383-390.

22. Stokes J B, Lee I, D'Amico M. Sodium Chloride absorption by the urinary bladder of the winter flounder. A thiazide-sensitive, electrically neutral transport system. *J Clin invest* 1984; 74:7-16. 1984

23. Kunau R T, Weller D R, and Webb H L (1975). Clarification of the site of action of chlorothiazide in the rat nephron. J.Clin.invest. *56*, 410-407.

24. Beaumont K, Vaughn D A, and Fanestil D D (1988). Thiazide diuretic receptors in rat kidney: Identification with [^{3}H]metolazone. Proc.Natl.Acad.Sci.USA *85*, 2311-2314.

25. Kim G-H; Masilamani S; Turner R; Mitchell C; Wade J B; Knepper M. The thiazide-sensitive Na-Cl cotransporter is an aldosterone-induced protein. Proc.Natl.Acad.Sci.USA. 95:14552-14557.1998

26. Costanzo L S (1985). Localization of diuretic action in microperfused rat distal tubules: Ca and Na transport. Am.J.Physiol.(Renal Fluid Electrolyte Physiol.) *248*, F527-F535.

27. Friedman P A and Gesek F A (1993). Mechanism of action of thiazide diuretics on sodium and calcium transport by distal convoluted tubules. In Diuretics IV: Chemestry, Pharmacology and Clinical Applications. Puschett J B and Greenberg A, eds. (New York: Elsevier Scientific Publications), pp. 319-327.

28. Feskanich D, Willett W C, Stampfer M J, and Colditz G A (1997). A prospective study of thiazide use and fractures in women. Osteoporosis Int. *7*, 79-84.

29. Gamba G, Saltzberg SN, Lombardi M, Miyanoshita A, Lytton J, Hediger M A et al. Primary structure and functional expression of a cDNA encoding the thiazide-sensitive, electroneutral sodium-chloride cotransporter. *Proc Natl Acad Sci USA* 1993; 90:2749-2753.

30. Lahlou B. Excretion renale chez un poisson euryhalin, le flet (Platichthys flesus L.): Caracteristiques de L'urine normale en eau douce et en eau de mer et effets des changements de milieu. Comp. Biochem. Physiol. 20 :925-938.1967.

31. Lahlou B, Hernderson IW, Saweyer WH. Renal adaptations by Opsanus tau, a euryhaline aglomerular teleost, to dilute media. Am. J. Physiol 216:1266-1272.1969.

32. Lagler KF. Bardach JE, Miller RR. Icthyology, New York, New York Wiley, 1962.

33. Tran JM, Farrel MA, Fanestil DD. Effect of ions on binding of the thiazide-type diuretic metolazone to kidney membrane. Am. J. Physiol. 258:F908-F915, 1990.

34. The Seventh Repot of the joint National Committee on the Prevention, Detection, Evaluation and Treatment of High Blood Pressure. JAMA. 289:2560-2572.2003.

35. Kyte J. and Doollite RF. A simple method for displaying the hidropathic character of a protein. J. Mol. Biol. 157:105-132. 1982.

36. Gamba G. Physiol.Rev. 85:423-429.2005.

37. Gamba G, Miyanoshita A, Lombardi M, Lytton J, Lee WS, Hediger MA et al. Molecular cloning, primary structure and characterization of two members of the mammalian electroneutral sodium-(potassium)-chloride cotransporter family expressed in kidney. *J Biol Chem* 1994; 296:17713-17722.

38. Velazquez,H.; Naray-Fejes-Toth,A.; Silva,T.; Andujar,E.; Reilly,R.F.; Desir,G.V.; Ellison,D.H.. Rabbit distal convoluted tubule coexpresses NaCl cotransporter and 11 beta-hydroxysteroid dehydrogenase II mRNA. Kindney Int. 54:464-472, 1998.

39. Schultheis P J, Lorenz P, Meneton J, Nieman T M, Riddle M, FlagellaJ, Duffy T, Shull G E. Phenotype resembling Gitelman´s syndrome in mice lacking the

apical Na+Cl- cotransporter of the distal convoluted tubule. J. Biol. Chem. 273:29150-29155.1998.

40. Mastroianni N, DeFusco M, Zollo M, Arrigo G, Zuffardi O, Bettinelli A, Ballabio A, Casari G. Molecular cloning, expression pattern, and chromosomal localization of the human Na-Cl thiazide-sensitive cotransporter (SLC12A3). Genomics 35:486-493.1996.

41. Simon D B, Nelson-Williams C, Johnson-Bia M, Ellison D, Karet F E, Morey-Molina A, Vaara I, Iwata F, Cushner H M, Koolen M, Gainza F J, Gitelman H J, Lifton R P. Gitelman's variant of Bartter's syndrome, inherited hypokalaemic alkalosis, is caused by mutations in the thiazide-sensitive Na-Cl cotransporter. Nature Genet. 12:24-30.1996.

42. Obermuller N; Bernstein P; Velázquez H; Reilly R; Moser D; Ellison D H; Bachman S. Expression of the thiazide-sensitive Na-Cl cotransporter in rat and human kidney. Am J Physiol. 269: F900-F910.1995.

43. Gitelman, HJ, Graham JB, Welt LG. A new familial disorder characterized by hypokalemia and hypomagnesemia. Trans. Assoc. Am. Phys. 79,221-235. 1966.

44. Monroy,A.; Plata,C.; Hebert,S.C.; Gamba,G. Characterization of the thiazide-sensitive Na(+)-Cl(-) cotransporter: a new model for ions and diuretics interaction. Am J Renal Physiol 279:F161-169. 2000.

45. Vazquez,N.; Monroy,A.; Dorantes,E.; Munoz-Clares,R.A.; Gamba,G. Functional differences between flounder and rat thiazide-sensitive Na- Cl cotransporter. Am J Renal Physiol 282:F599-F607. 2002.

46. Rubin A A; Roth F E; Taylor R M; Rosenkilde H. Pharmocology of diazoxide, an antihypertensive, nondiuretic benzothiadiazine. J Pharmacol Exp Ther. 136:344-351. 1962.

47. Eknoyan G. A history of diuretics. In: Diuretic Agents: Clinical Physiology and Pharmacology. Edited by Seldin and Giebish G. San Diego Ca. Academic.1997. p3-28.

48. Zeidel M L. Special diuretics. In: Diuretic Agents: Clinical Physiology and Pharmacology. Edited by Seldin and Giebish G. San Diego Ca. Academic.1997. p.113-134.

49. Wilkinson,D.J.; Post,M.A.; Venglarik,C.; Chang,D.; Dawson,D.C. Mercury blockade of thiazide-sensitive NaCl cotransport in flounder urinary bladder. Toxicol Appl Pharmacol. 123:170-176. 1993.

50. Jacoby,S.C.; Gagnon,E.; Caron,L.; Chang,J.; Isenring,P. Inhibition of Na(+)-K(+)-2Cl(-) cotransport by mercury. Am J Physiol Cell Physiol. 277:C684-C692. 1999.

51. Isenring P; Forbush III B. on and bumetanide binding by the Na-K-Cl cotransporter. Importance of transmembrane domains. J.Biol.Chem. 272: 24556-24562. 1997.

52. Payne J A; Xu J-C; Haas M; Lytle C Y; Ward D; Forbush III B. Primary structure, functional expression, and chromosomal localization of the bumetanide-sensitive Na-K-Cl cotransporter in human colon. J.Biol.Chem. 270: 17977-17985. 1995.

53. Isenring P; Jacoby S C; Forbush III B. The role of transmembrane domain 2 in cation transport by the Na-K-Cl cotransporter. Proc.Natl.Acad.Sci.USA. 95: 7179-7184, 1998.

54. Isenring,P.; Forbush,B. on transport and ligand binding by the Na-K-Cl cotransporter, structure-function studies. Comp Biochem Physiol A Physiol. 130: 487-497. 2001.

55. Sandberg M, Riquier AD, Pihakaski K, McDonough A, Mounsbach A. AGII provokes acute trafficking of distal tubule Na+-Cl-cotransporter to apical membrane. Am.J. Physiol. Renal Physiol. 293:F662-F669.2007.

56. Plata C; Meade P; Hall A E; Welch RC; Vazquez N; Hebert,S.C.; Gamba,G. Alternatively spliced isoform of the apical Na-K-Cl cotransporter gene encodes a furosemide sensitive Na-Cl cotransporter. Am J Physiol Renal Physiol. 280: F574-F582. 2001.

57. Payne J A; Forbush III B. Alternatively spliced isoforms of the putative renal Na-K-Cl cotransporter are differentially distributed within the rabbit kidney. Proc.Natl.Acad.Sci.USA. 91:4544-4548, 1994.

58. Gagnon E, Bergeron MJ, Brunet GM, Daigle ND, Simard CF, Isenring P. Molecular Mechanism of Cl transport by the renal Na-K-Cl cotransporter. Identification of an intracellular locus that may form part of a high affinity Cl-binding site. J Biol Chem. 279: 5648-5654. 2003.

59. Gimenez I, Forbush,B. The residues determinig differences in ion affinities among the alternative splice variants F,A, and B of the mammalian renal Na-K-Cl cotransporter (NKCC2). J Biol Chem. 282: 6540-6547. 2007.

60. Tovar-Palacio,C.; Bobadilla,N.A.; Cortes,P.; Plata,C.; De Los,Heros P.; Vazquez,N.; Gamba,G. on and Diuretic Specificity of Chimeric Proteins Between Apical Na+:K+:2Cl- and Na+:Cl- Cotransporters. Am J Physiol Renal Physiol. 287: F570-F577.2004.

61. Gitelman H J; Graham J B; Welt L G. A new family disorder characterized by hypokalemia and hypomagnesemia. Trans Assoc Am Physicians. 79: 221-235. 1966.

62. Mastroianni N; Bettinelli A; Bianchetti M; Colussi G; de Fusco M; Sereni F; Ballabio A; Casari G. Novel molecular variants of the Na-Cl cotransporter gene are responsible for Gitelman síndrome. Am.J.Hum.Genet. 59:1019-1026. 1996.

63. Lemmink,H.H.; Knoers,N.V.; Karolyi,L.; van Dijk,H.; Niaudet,P.; Antignac,C.; Guay-Woodford,L.M.; Goodyer,P.R.; Carel,J.C.; Hermes,A.; Seyberth,H.W.; Monnens,L.A.; van den Heuvel,L.P. Novel mutations in the thiazide-sensitive NaCl cotransporter gene in patients with Gitelman syndrome with predominant localization to the C-terminal domain. Kidney Int. 54: 720-730. 1998.

64. Lin,S.H.; Cheng,N.L.; Hsu,Y.J.; Halperin,M.L. Intrafamilial phenotype variability in patients with Gitelman syndrome having the same mutations in their thiazide-sensitive sodium/chloride cotransporter. Am J Kidney Dis. 43:304-312. 2004.

65. Maki,N.; Komatsuda,A.; Wakui,H.; Ohtani,H.; Kigawa,A.; Aiba,N.; Hamai,K.; Motegi,M.; Yamaguchi,A.; Imai,H.; Sawada,K.I. Four novel mutations in the thiazide-sensitive Na-Cl co-transporter gene in Japanese patients with Gitelman's síndrome. Nephrol Dial Transplant. 1-6. 2004.

66. Melander,O.; Orho-Melander,M.; Bengtsson,K.; Lindblad,U.; Rastam,L.; Groop,L.; Hulthen,U.L. Genetic variants of thiazide-sensitive NaCl-cotransporter in Gitelman's syndrome and primary hypertension. Hypertension 36: 389-394. 2000.

67. Monkawa,T.; Kurihara,I.; Kobayashi,K.; Hayashi,M.; Saruta,T. Novel mutations in thiazide-sensitive Na-Cl cotransporter gene of patients with Gitelman's syndrome. J Am Soc Nephrol 11:65-70. 2000.

68. Pantanetti,P.; Arnaldi,G.; Balercia,G.; Mantero,F.; Giacchetti,G. Severe hypomagnesaemia-induced hypocalcaemia in a patient with Gitelman's síndrome. Clin Endocrinol. 56:413-418. 2002.

69. Reissinger,A.; Ludwig,M.; Utsch,B.; Promse,A.; Baulmann,J.; Weisser,B.; Vetter,H.; Kramer,H.J.; Bokemeyer,D. Novel NCCT gene mutations as a cause of Gitelman's syndrome and a systematic review of mutant and polymorphic NCCT alleles. Kidney Blood Pres Res 25:354-362. 2002.

70. Syren,M.L.; Tedeschi,S.; Cesareo,L.; Bellantuono,R.; Colussi,G.; Procaccio,M.; Ali,A.; Domenici,R.; Malberti,F.; Sprocati,M.; Sacco,M.; Miglietti,N.; Edefonti,A.; Sereni,F.; Casari,G.; Coviello,D.A.; Bettinelli,A. Identification of fifteen novel mutations in the SLC12A3 gene encoding the

Na-Cl Co-transporter in Italian patients with Gitelman síndrome. Hum Mutat. 20:78. 2002.

71. Tajima,T.; Kobayashi,Y.; Abe,S.; Takahashi,M.; Konno,M.; Nakae,J.; Okuhara,K.; Satoh,K.; Ishikawa,T.; Imai,T.; Fujieda,K. Two novel mutations of thiazide-sensitive Na-Cl cotrans porter (TSC) gene in two sporadic Japanese patients with Gitelman syndrome. Endocr J 49:91-96. 2002.

72. Takeuchi,K.; Kure,S.; Kato,T.; Taniyama,Y.; Takahashi,N.; Ikeda,Y.; Abe,T.; Narisawa,K.; Muramatsu,Y.; Abe,K. Association of a mutation in thiazide-sensitive Na-Cl cotransporter with familial Gitelman's síndrome. J Clin Endocrinol Metab 81:4496-4499. 1996.

73. Yahata,K.; Tanaka,I.; Kotani,M.; Mukoyama,M.; Ogawa,Y.; Goto,M.; Nakagawa,M.; Sugawara,A.; Tanaka,K.; Shimatsu,A.; Nakao,K. Identification of a novel R642C mutation in Na/Cl cotransporter with Gitelman's syndrome. Am J Kidney Dis. 34:845-853. 1999.

74. Yoo,T.H.; Lee,S.H.; Yoon,K.; Baek,H.; Chung,J.H.; Lee,T.; Ihm,C.; Kim,M. Identification of novel mutations in Na-Cl cotransporter gene in a Korean patient with atypical Gitelman's syndrome. Am J Kidney Dis. 42:E11-E-16. 2003.

75. De Jong,J.C.; Willems,P.H.; Mooren,F.J.; van den Heuvel,L.P.; Knoers,N.V.; Bindels,R.J. The structural unit of the thiazide-sensitive NaCl cotransporter is a homodimer. J Biol Chem 278:24302-24307. 2003.

76. De Jong,J.C.; Willems,P.H.; van den Heuvel,L.P.; Knoers,N.V.; Bindels,R.J. Functional Expression of the Human Thiazide-Sensitive NaCl Cotransporter in Madin-Darby Canine Kidney Cells. J Am Soc Nephrol. 13:1442-1448. 2002.

77. Landlot-Marticorena C; Reithmeier R A F. Asparagine-linked oligosaccharides are localized to single extracytosolic segments in multi-span membrane glycoproteins. Biochem J 302 (Pt I): 253-260. 1994.

78. Hoover,R.S.; Poch,E.; Monroy,A.; Vazquez,N.; Nishio,T.; Gamba,G.; Hebert,S.C. N-Glycosylation at Two Sites Critically Alters Thiazide Binding and Activity of the Rat Thiazide-sensitive Na(+):Cl(-) Cotransporter. J Am Soc Nephrol. 14:271-282. 2003.

79. Flatman,P.W. Regulation of Na-K-2Cl cotransport by phosphorylation and protein-protein interactions. Biochim Biophys Acta 1566: 140-151.2002.

80. Lytle C. A volume sensitive protein kinase regulates the Na-K-2Cl cotransporter in duck red blood cells. Am J Physiol Cell Physiol. 274:C1002-C1010. 1998.

81. Lytle C; Forbush III B. The Na-K-Cl cotransport protein of shark rectal gland. II Regulation by direct phosphorylation. J.Biol.Chem. 267: 25438-25443. 1992.

82. Harrison-Bernard LM, Navar LG, Ho MM, Vinson GP, el-Dahr SS. Inmunohistochemical localization of AGII AT1 receptor in adult rat kidney using a monoclonal antibody. Am.J. Physiol. Renal Physiol. 273:F170-F177.1997.

83. Darman,R.B.; Forbush,B. A regulatory locus of phosphorylation in the N terminus of the Na-K-Cl cotransporter, NKCC1. J Biol Chem. 277: 37542-37550. 2002.

84. Flemmer,A.W.; Gimenez,I.; Dowd,B.F.; Darman,R.B.; Forbush,B. Activation of the Na-K-Cl otransporter NKCC1 detected with a phospho-specific antibody. J Biol Chem. 277:37551-37558. 2002.

85. Blakely P, Vaughn DA, and Fanestil DD. Amylin, calcitonin gene-related peptide, and adrenomedullin: effects on thiazide receptor and calcium. *Am J Physiol Renal Fluid Electrolyte Physiol* 272: F410–F415, 1997.

86. Ushiro,H.; Tsutsumi,T.; Suzuki,K.; Kayahara,T.; Nakano,K. Molecular cloning and characterization of a novel Ste20-related protein kinase enriched in neurons and transporting epithelia. Arch Biochem Biophys. 355: 233-240.1998.

87. Tamari,M.; Daigo,Y.; Nakamura,Y. solation and characterization of a novel serine threonine kinase gene on chromosome 3p22-21.3 J.Hum.Genet. 44:116-120. 1999.

88. Farman N.Steroid receptors: distribution along the nephron. Sem.Nephrol. 12-17. 1992.

89. Velazquez H, Bartiss A, Bernstein P, and Ellison D H. Adrenal steroids stimulate thiazide-sensitive NaCl transport by rat renal distal tubules. Am.J.Physiol.(Renal Fluid Electrolyte Physiol.) *270,* F211-F219. 1996.

90. lpgws.nci.nih.gov/cgi-bin.

91. GeneViewer.cgi;ncbi,nlm.nih.gov/SNP

92. Berkman J; Reilly RF; Ellison,D.H. Mechanisms of thiazide-sensitive Na-Cl cotransporter dysfunction in Gitelman's syndrome. J Am Soc.Nephrol. 10:1261,1999.

93. Chen Z, Vaughn D A, Blakley P, and Fanestil D D. (Adrenocortical steroids increase renal thiazide diuretic receptor density and response. J.Am.Soc.Nephrol. *5*, 1361-1368. 1994.

94. Chen Z, Vaughn D A, Beaumont K, and Fanestil D D. Effects of diuretic treatment and of dietary sodium on renal binding of ^{3}H-metolazone. J.Am.Soc.Nephrol. *1*, 91-98.1990.

95. Hir M L, Kaissling B, and Dubach U C. Distal tubular segments of the rabbit kidney after adaptation to altered Na- and K-intake. II. Changes in Na-K-ATPase activity. Cell Tissue Res. *224*, 493-504. 1982.

96. Kaissling B and Hir M L. Distal tubular segments of the rabbit kidney after adaptation to altered Na- and K-intake. I Structural changes. Cell Tissue Res. *224*, 469-492.1982.

97. Wilson,F.H.; Disse-Nicodeme,S.; Choate,K.A.; Ishikawa,K.; Nelson-Williams,C.; Desitter,I.; Gunel,M.; Milford,D.V.; Lipkin,G.W.; Achard,J.M.; Feely,M.P.; Dussol,B.; Berland,Y.; Unwin,R.J.; Mayan,H.; Simon,D.B.; Farfel,Z.; Jeunemaitre,X.; Lifton,R.P. Human hypertension caused by mutations in WNK kinases. Sience. 293:1107-1112. 2001.

98. Scherzer P, Wald H, and Popovtzer M M . Enhanced glomerular filtration and Na+-K+-ATPase with furosemide administration. Am.J.Physiol.(Renal Fluid Electrolyte Physiol.) *252*, F910-F915.1987.

99. Ellison D H, Velazquez H, and Wright F S. Adaptation of the distal convoluted tubule of the rat. Structural and functional effects of dietary salt intake and chronic diuretic infusion. J.Clin.invest. *83*, 113-126. 1989

100. Gimenez,I.; Forbush,B. Short-term stimulation of the renal Na-K-Cl cotransporter (NKCC2) by vasopressin involves phosphorylation and membrane translocation of the protein. J.Biol.Chem. 278: 26946-26951. 2003.

101. Song,L.; Mercado,A.; Vazquez,N.; Xie,Q.; Desai,R.; George,A.L.; Gamba,G.; Mount,D.B. Molecular, functional, and genomic characterization of human KCC2, the neuronal K-Cl cotransporter. Brain Res. 103:91-105. 2002.

102.	Ackerman M J; Wickman K D; Clapham D E. Hypotonicity activates a native chloride current in *Xenopus* oocytes. J.Gen.Physiol. 103:153-179. 1994.

103.	Lytle,C.; McManus,T. Coordinate modulation of Na-K-2Cl cotransport and K-Cl cotransport by cell volume and chloride. Am.J.Physiol Cell Physiol. 283:C1422-C1431. 2002.